MODELING AND INVERSION IN WEAKLY ANISOTROPIC MEDIA

Dissertation

zur Erlangung des Doktorgrades
der Naturwissenschaften im Fachbereich
Geowissenschaften
der Universität Hamburg

vorgelegt von

SVETLANA M. GOLOVNINA

aus St-Petersburg, Russland

Hamburg
2004

Als Dissertation angenommen vom Fachbereich Geowissenschaften
der Universität Hamburg

auf Grund der Gutachten

von Prof. Dr. D. Gajewski

and Prof. Dr. B. M. Kashtan

Hamburg, den 28. April 2004

Prof. Dr. H. Schleicher
Dekan
des Fachbereiches Geowissenschaften

Contents

Abstract

Approximation of weakly anisotropic media allows to simplify solutions of modeling and inversion in anisotropic media. Perturbation methods are commonly used tools for describing wave propagation in weakly anisotropic media. An anisotropic medium is replaced by an isotropic background medium where wave propagation can be treated easily and, then, the correction for the effects of anisotropy are computed by perturbation techniques.

To minimize errors which are inherent in any perturbation method the background isotropic medium should be chosen to be as close as possible to the true anisotropic medium. To obtain the isotropic background media, formulae for a sectorially best-fitting isotropic medium are derived and their application is illustrated by examples of media with transversely isotropic and orthorombic symmetries.

For modeling in weakly anisotropic media a quasi-isotropic (QI) approach is considered. Seismograms obtained by the QI approach are compared with seismograms resulting from the standard anisotropic ray method and finite-difference numerical forward modeling. The comparison shows that the QI approach is sufficiently accurate in media with 1–5% anisotropy.

I develop a 3D finite-difference (FD) perturbation method for the robust and efficient qP-wave traveltime computation in anisotropic media which is important in many modeling and inversion applications. I suggest to apply this method using isotropic and ellipsoidally anisotropic background media. The ellipsoidally anisotropic background media allow to improve the accuracy of the traveltime computations.

The approximation of weakly anisotropic media allows to obtain linear relations between perturbations of the elastic parameters of the weakly anisotropic medium with respect to an isotropic background medium and corresponding traveltime perturbations. The relations are inherently linear for qP-wave traveltimes, and can be linearized for qS-wave traveltimes using the qS-wave polarization vectors. The qS-wave polarization vectors are available from a seismic experiment as well as traveltimes. On the basis of these linear relations the same linear tomographic inversion scheme for qP- as well as for qS-wave data is developed. The joint inversion of qP- and qS-waves allows to determine the full elastic tensor of the weakly anisotropic medium. The inversion procedure was tested using synthetic noise-free and noisy data obtained for homogeneous and layered models.

Zusammenfassung

Mit der Annahme schwacher Anisotropie vereinfachen sich die Lösungen der Modellierung und Inversion anisotroper Medien. Üblicherweise werden Perturbation-Methoden zur Beschreibung der Wellen-Ausbreitung in schwach anisotropen Medien verwendet, ein anisotropes Medium wird ersetzt durch ein isotropes Hintergrundmodell. Hier lässt sich die Wellenausbreitung leicht behandeln und die anisotropen Effekte werden mit Hilfe der Perturbations-Methode berechnet.

Um die jeder Perturbations-Methode anhaftenden Fehler zu minimieren, sollte das gewählte isotrope Hintergrundmedium dem korrektem anisotropen Medium so ähnlich wie möglich sein. Zur Bestimmung des optimalen isotropen Mediums wurden Formeln für sektoriell best angepasste isotrope Medien entwickelt. Deren Anwendung wurde anhand von Modellen mit transversal isotropen und orthorombischen Symmetrien gezeigt.

Für das Modellieren in schwach anisotropen Medien wurde ein quasi-isotroper (QI) Ansatz verwendet. Die mit Hilfe dieses Ansatzes erhaltenen Seismogramme wurden mit Seismogrammen verglichen, die durch Standart-Strahl-Methoden und Finite-Differenzen Vorwärtsmethoden bestimmt worden sind. Dieser Vergleich hat eine ausreichende Genauigkeit für Medien mit 1–5% Anisotropie ergeben.

Ich habe eine 3D Finite-Differenzen (FD) Perturbations-Methode für die stabile und effektive Bestimmung von Laufzeiten in anisotropen Medien entwickelt. Laufzeiten werden für eine Vielzahl von Anwendungen, z.B. Modellieren und Inversion, benötigt. Für die Laufzeitberechnung kann sowohl ein isotropes als auch ein ellipsoides anisotropes Hintergrundmodell angenommen werden. Letzteres erhöht die Genauigkeit der Laufzeitbestimmung.

Die Annahme schwacher Anisotropie erlaubt die Verwendung eines linearen Zusammenhanges zwischen der Perturbation der elastischen Parameter in Bezug auf das isotrope Hintergrundmedium und die dazugehörigen Laufzeit-Perturbationen. Es besteht ein linearer Zusammenhang für die qP-Wellen-Laufzeiten. Der Zusammenhang für qS-Wellen lässt sich unter Zuhilfenahme der qS-Polarisations Vektoren ebenfalls linearisieren. Die qS-Polarisationsvektoren sind ebenso wie die Laufzeiten aus dem seismischen Experiment bekannt. Aufgrund dieses linearen Zusammenhanges kann der gleiche tomografische Inversions Algorithmus für beide Wellentypen verwendet werden. Durch die gemeinsame Inversion der qP- und qS-Wellen kann der gesamte elastische Tensor für schach ansiotrope Medien berechnet werden. Die Inversionsmethode wurde sowohl an verrauschten als auch an rauschfreien synthetischen Daten für homogene und geschichtete Modelle erfolgreich angewendet.

Introduction

In geophysics, anisotropy is a common phenomenon. Due to its nature, seismic anisotropy can provide important quantitative information about structure, lithology of rocks and possible deformation processes in sedimentary rocks. However, until the 80s, anisotropy was mostly considered in the context of crystals. The fact that no crystals with weak anisotropy exist was a strong argument against considering anisotropic media in geophysics. Anisotropy is also almost always a 3D phenomenon. Therefore, observations, data processing or inversions must be performed in 3D models. But limited acquisition and lower computer resources did not allow 3-D applications. Recently, due to more intense acquisitions (3D, 4D), better equipment and new survey methodologies, the quality of the observed data is improved considerably. More powerful computers and adaptable workstation interfaces for aiding interpretation make good use of anisotropy these days. Therefore, seismic anisotropy is now a part of geophysical expertise.

There are other reasons for the long neglect of anisotropy. Equations describing isotropic media are simpler than those for anisotropic media, and their application is more direct. Any computations (of rays, traveltimes, seismograms and so on) for inhomogeneous anisotropic media of arbitrary symmetry are much more complicated and computationally expensive than for isotropic media. Therefore, any approximation which allows to simplify or to perform faster computations of rays or some of their parameters is desired.

The approximation of weakly anisotropic media is best suited to seismic anisotropy. Thomsen (1986) has summarized a large number of laboratory measurements and has pointed out that in most cases of interest to geophysicists the anisotropy is weak. Perturbation methods are commonly used tools for describing wave propagation in weakly anisotropic media. The anisotropic medium is replaced by an isotropic background medium where wave propagation can be treated easily and the correction for the effects of anisotropy are computed by perturbation techniques. This allows to simplify the calculation of rays, traveltimes, polarization vectors, seismograms and solution of inversion problem in weakly anisotropic media. The topic of my thesis is to consider modeling and inversion in weakly anisotropic media.

I consider the quasi-isotropic (QI) approach which allows to perform computations of seismic waves in weakly anisotropic media. The QI approach was proposed by Kravtsov (1968) to avoid difficulties with the standard ray method for anisotropic media in the isotropic limit when the velocities of the two quasi-shear waves are close to each other. It is based on a combination of the perturbation method and the kinematic and dynamic ray-tracing differential equations for an isotropic background medium. Pšenčík and Dellinger

(2001) and Zillmer et al. (1998) showed that the QI approach spans the gap between the ray methods for isotropic and anisotropic media. It allows to compute wavefields in isotropic regions as well as in regions of weak anisotropy.

In my study I test how well the QI approach works for anisotropic media with different strength of anisotropy. I consider anisotropic media with anisotropies from 5% to 11%. Such strength of anisotropy is considered as weak for seismic media (see e.g., Thomsen, 1986). I derive expressions for the calculation of zeroeth- and additional first-order terms of the QI approximation for qP- and qS-waves. The expressions are applicable to inhomogeneous media of arbitrary but weak anisotropy. All calculations partly repeat the calculations performed by several authors (see e.g. Zillmer et al., 1998; Pšenčík, 1998). Resulting equations presented in my work contain only derivatives of all quantities with respect to Cartesian coordinates. This allows nearly directly to obtain analytical solutions for qP- and qS-waves in the case of homogeneous weakly anisotropic media. Analysis of these analytical solutions reveals advantages and drawbacks of the QI approach. Using these analytical solutions the quality of the QI approximation is investigated. The seismograms computed from these analytical solutions for weakly anisotropic media were compared with seismograms computed by the standard anisotropic ray theory and by a 3-D seismic forward modeling algorithm which is based on a pseudo-spectral method (Kosloff and Baysal, 1982; Tessmer, 1995).

To minimize errors which are inherent in any perturbation method the background isotropic medium should be chosen to be as close as possible to the true anisotropic medium, with respect to the physical properties to be investigated. Formulae for the best-fitting isotropic background medium were suggested by Fedorov (1968). I modified the formulae for the best-fitting isotropic medium to enable us to select the isotropic background medium in such way that it gives the best fit to the anisotropic medium considered not over all possible directions, but only for the direction of interest or a region surrounding the direction of interest.

The inversion problem in anisotropic media of arbitrary symmetry is an extremely complicated task. The approximation of weakly anisotropic media allows to simplify its solution. There are two main groups of approaches to solve the inversion problem. One group of approaches is based on tomography, where observations are directly transformed into the elastic parameters of the media. In another group of approaches, the inversion problem is solved in two steps: First, a reference velocity model of the medium is constructed by solving the kinematic problem. Then, on the basis of the reference model the migration is carried out.

To perform the migration robust and efficient methods for the traveltime computation are important. For example, for Kirchhoff type of migration, computation of a large number of diffraction stack surfaces is required. Therefore, to perform a Kirchhoff migration in arbitrary anisotropic media, an approach which allows fast traveltime computations is needed. For the fast traveltime computations in arbitrary anisotropic media, I suggest to use a finite-difference (FD) perturbation method. The concept of the 2-D FD perturbation method was suggested by Ettrich and Gajewski (1998). They used the FD perturbation method to compute qP-wave traveltimes in a 2-D isotropic and weakly anisotropic media with transversely isotropic symmetry. I develop a 3-D extension of the FD perturbation

method and implement it for anisotropic models with arbitrary types of symmetry. My implementation is also restricted to qP-waves.

In this method, the anisotropic medium is considered as a perturbed medium and approximated by a simpler background medium. I use two types of background media. In the case of strong anisotropy, ellipsoidally anisotropic media are used as background media, while in the case of weak anisotropy isotropic media are used. Traveltimes in the unperturbed background medium are computed with a FD eikonal solver which is fast and accurate in both isotropic and ellipsoidally anisotropic media. Traveltimes in the perturbed anisotropic medium are obtained by adding corrections to the traveltimes of the background medium according to the perturbation equations.

The inversion problem based on ray tomography is significantly non-linear and complicated in the general case of anisotropy. Any computations (of rays, traveltimes, polarization vectors etc.) in anisotropic media required for the forward modeling are much more complicated and computationally expensive than for isotropic media. The anisotropic ray theory yields non-linear relations between the elastic parameters and the traveltimes of waves propagating in the anisotropic medium. The approximation of weakly anisotropic media allows to simplify the solution of the forward modeling and, what is more important, leads to the linear relations between the elastic parameters and the traveltimes of waves. The relations are inherently linear for qP-wave traveltimes, and can be linearized for the qS-wave traveltimes by using additionally the observations of qS-wave polarization vectors.

I develop a traveltime inversion procedure for the determination of the elastic parameters of a weakly anisotropic medium based on observations of the qS-wave polarization vectors. The observations of qS-wave polarization vectors are available from experiments as well as the traveltime observations. If the observed qS-wave polarization vectors are introduced into the inversion, the tomographic relations for qS-waves linearize and are formally identical to those for qP-waves. I perform the inversion procedure for homogeneous anisotropic and layered models using synthetic data. Because the traveltimes of both qP- and qS-waves are jointly inverted, the whole elastic tensor of the weakly anisotropic medium can be determined.

After this introduction in **chapter 1**, I give a short review of the subject of seismic anisotropy. The definition of the elasticity tensor and the consideration of its main properties are followed by short descriptions of the basic features of waves propagating in anisotropic media. Then, in **chapter 2**, the quality of the QI approximation used for modeling in weakly anisotropic media is investigated. **Chapter 3** contains the resulting formulae obtained for the sectorially best-fitting isotropic background medium. It is followed by **chapter 4** where I develop a 3-D extension of the FD perturbation method and implement it for anisotropic models with arbitrary types of symmetry. In the last **chapter 5**, I develop a traveltime inversion procedure for the determination of the elastic parameters of an weakly anisotropic medium. Finally, I summarize the most important results.

Chapter 1

Review of elastic anisotropy

Motivation

Anisotropy refers to the directional dependence of elastic properties of media. The seismic anisotropy appears due to a fine-scale layering of sedimentary rocks or the presence of oriented micro-cracks or fractures in the rocks, preferred orientations of non-spherical grains or anisotropic minerals. In general, the seismic anisotropy can be considered as ordered heterogeneity on the small scale, which appears as seismic anisotropy on the large scale (Thomsen, 2002). The seismic wavelength allows to define the large and small scales. Whenever the seismic wavelengths are large compared to the scale of the ordered heterogeneities, they obey the laws of anisotropic wave propagation.

The layered structure of the sedimentary rocks is obviously established by the force of gravity. It is the vertical direction which is preferred. Particular fabric of rocks can also be established by the gradient of temperature in the cooling magma or the distortions caused by metamorphic flow. The stress inside of the rock mass is one more source of seismic anisotropy. This means that due to its nature, seismic anisotropy can provide important quantitative information about structure, lithology of rocks and possible deformation processes in sedimentary rocks. Estimation of anisotropy can help to provide an elastic model that can be used in migration and inversion of seismic data.

The subject of seismic anisotropy has a long history. Until the 80s, anisotropy was mostly considered in the context of crystals. The fact that no crystals with weak anisotropy exist was a strong argument against considering weakly anisotropic media. There are other reasons for the long neglect of anisotropy. Equations describing isotropic media are simpler than those for anisotropic media, and their application is more direct. Anisotropy is also almost always a 3D phenomenon. Therefore, observations, data processing or inversions must be performed in 3D models. But limited acquisition and lower computer resources did not allow 3-D applications.

Recently, due to more intense acquisitions (3D, 4D), better equipment and new survey methodologies, the quality of the observed data is improved considerably. More powerful computers and adaptable workstation interfaces for aiding interpretation make good use of anisotropy these days. Therefore, seismic anisotropy is now a part of geophysical expertise.

Anisotropic media are usually specified by the elasticity tensor introduced in physics of crystals (see e.g. Fedorov, 1968; Helbig, 1994). In this chapter, the definition of the elasticity tensor and the consideration of its main properties are followed by short de-

scriptions of the basic features of seismic waves propagating in anisotropic media. Then, several approximations used in anisotropic models are shortly reviewed.

Elasticity tensor

The properties of the anisotropic medium are described by a tensor of the elastic parameters. The tensor is introduced in the following way. A linear elastic material is defined as one in which each component of stress σ_{ik} depends linearly upon every component of strain ϵ_{lm}. Each directional indices takes the values 1, 2, 3 corresponding directions x, y, z in Cartesian coordinates.

$$\sigma_{ik} = c_{iklm}\epsilon_{lm}, \qquad i,k,l,m = 1,2,3 \tag{1.1}$$

where c_{iklm} is the tensor of elastic parameters (or elasticity tensor) which completely characterizes the elastic properties of the medium. In (1.1) summation over repeated indices is supposed. The elasticity tensor has four indices, two corresponding to the indices of stress, σ_{ik}, and two to the indices of strain, ϵ_{lm}. Both stress and strain are symmetric. The fourth order tensor c_{iklm} possesses the following symmetry:

$$c_{iklm} = c_{kilm} = c_{kiml} = c_{lmik}.$$

The elasticity tensor c_{iklm} has at most 21 independent moduli (components or parameters). By choosing of a special coordinate system three of the 21 components can always be set equal to zero. Therefore, the number of components is reduced to 18. This coordinate system is called the principal coordinate system (see e.g., Červený, 2001; Thomsen, 2002).

For convenience of writing and simplifying the conceptual discussion, the fourth order tensor c_{iklm} can also be represented by a symmetric 6×6 matrix $C_{\alpha\beta}$ according to the Voigt recipe:

$$\begin{aligned} C_{\alpha\beta} = c_{iklm}: \qquad & (ik) \rightarrow \alpha \quad \text{and} \quad (lm) \rightarrow \beta: \\ & (11) \rightarrow 1; \quad (22) \rightarrow 2; \quad (33) \rightarrow 3; \\ & (23) = (32) \rightarrow 4; \quad (13) = (31) \rightarrow 5; \quad (12) = (21) \rightarrow 6. \end{aligned} \tag{1.2}$$

Note that the matrix $C_{\alpha\beta}$ is not a tensor, therefore, it can not be used in matrix algebra.

Every so often instead of the elasticity tensor c_{iklm}, a density-normalized elasticity tensor is used:

$$a_{iklm} = \frac{1}{\rho}\, c_{iklm}, \tag{1.3}$$

where ρ is the density of the medium. The components of a_{iklm} are measured in km^2/sec^2. The 6×6 matrix corresponding to the tensor a_{iklm} is denoted as $A_{\alpha\beta}$. In the majority of numerical examples presented in my thesis, anisotropic media are specified by the matrices $A_{\alpha\beta}$ of the density-normalized elastic moduli.

The number of the different (independent) moduli varies with respect to the class of symmetry of the elastic medium. An anisotropic medium with triclinic symmetry has the maximal number of independent elastic parameters. In the principal coordinate system this medium is defined by 18 different elastic moduli. For comparison, any isotropic medium is defined only by two independent moduli.

The simplest case of an anisotropic medium is a medium with hexagonal symmetry (see e.g. Thomsen, 2002, page 1-23), also termed, transversely isotropic (TI) symmetry. The TI medium is defined by five elastic moduli. In general, the elasticity tensor has more then five non-zero components, but only five are independent. The TI medium has one distinct direction (or axis of symmetry), while the other directions are equivalent to each other. The TI medium with vertical axis of symmetry is referred to as VTI medium, the one with horizontal axis of symmetry as HTI medium. The TI symmetry describes shales and thin-bed sequences and, therefore, it is the most frequently used in practical (field) geophysics. It should be noted that in exploration geophysics, the TI medium is alternatively characterized by the P- and S-wave vertical velocities plus three dimensionless parameters of anisotropy, introduced by Thomsen (1986).

Orthorombic symmetry can be described as the most realistic symmetry (see e.g. Thomsen, 2002, page 1-25). This symmetry corresponds, e.g., to sedimentary beds containing vertical fractures. Elastic properties of the orthorombic medium are described by nine independent elastic moduli. Only little exploration data have been analyzed in these terms. However, that situation has been changing. With wide-azimuth 3D surveys becoming more common, the need will soon arise for dealing with this situation (see e.g. Mensch and Farra, 1999; Tsvankin, 1997; Grechka et al., 1999).

It should be noted that the matrices $C_{\alpha\beta}$ (and the tensors c_{iklm}) have the simple forms shown only in the principal coordinate system of elastic media. If a medium is considered in any coordinate system rotated with respect to its principal coordinate system, the number of non-zero parameters of the matrix $C_{\alpha\beta}$ (and the tensor c_{iklm}) increases. For example, in the case of TI symmetry, this happens when none of the axes of the coordinate system is directed along the symmetry axis of the TI medium. The orthorombic medium has three mutually orthogonal symmetry axes. All components of the matrix $C_{\alpha\beta}$ of the orthorombic medium can be non-zero, if the axes of the coordinate system are not aligned with these symmetry axes. To obtain the elastic moduli in the rotated coordinate system, the elasticity tensor c_{iklm} specified in the principal coordinate system is converted using the corresponding rotation matrix. Note that the matrix $C_{\alpha\beta}$ can not simply be transfered by rotation, since it is not a tensor.

Elastic plane waves in homogeneous anisotropic media

In this section I shortly describe the most important differences of plane elastic waves propagating in homogeneous isotropic and anisotropic media. To discuss plane waves propagating in elastic media, the following 3×3 matrix $\mathbf{\Lambda}$ is introduced (see e.g Fedorov, 1968; Helbig, 1994):

$$\Lambda_{im} = a_{iklm} n_k \, n_l \tag{1.4}$$

with the density normalized elasticity tensor a_{iklm} and the wavefront normal $\mathbf{n}$. The matrix $\mathbf{\Lambda}$ is called the Christoffel matrix. Equation (1.4) indicates that to each direction of the wavefront normal $\mathbf{n}$ a particular matrix $\mathbf{\Lambda}$ corresponds. Since $\mathbf{\Lambda}$ is a symmetric, positive definite matrix, its eigenvalues are positive and its eigenvectors are mutually orthogonal.

The three eigenvalues and eigenvectors of the Christoffel matrix $\mathbf{\Lambda}$ determine three phase velocities, v_1, v_2, v_3, and three polarization vectors, $\mathbf{A}_{qP}$, $\mathbf{A}_{qS1}$, $\mathbf{A}_{qS2}$, of *three waves propagating in a homogeneous anisotropic medium: one quasi-longitudinal (qP) wave and*

two quasi-shear (qS) waves. The word "quasi" is used, since generally the polarization directions of these waves are not exactly aligned along or exactly perpendicular to the direction of wavefront propagation $\mathbf{n}$. The polarization vectors, $\mathbf{A}_{qP}$, $\mathbf{A}_{qS1}$ and $\mathbf{A}_{qS2}$ correspond to the same phase normal $\mathbf{n}$, and they are mutually orthogonal. In real anisotropic media the phase velocity v_1 of the quasi-longitudinal wave is always larger than the phase velocities v_2 and v_3 of the quasi-shear waves. For the phase velocities of the quasi-shear waves the condition $v_2 \geq v_3$ is fulfilled.

For comparison, in an isotropic medium we have $v_1 > v_2 = v_3$. Since two eigenvalues of the matrix $\mathbf{\Lambda}$ for isotropic medium coincide, only two plane waves can propagate: one longitudinal (P) and one shear (S) wave. The polarization vector of the P-wave coincides with the wavefront normal $\mathbf{n}$, whereas the S-wave polarization vector is only known to be situated in the plane perpendicular to the wavefront normal $\mathbf{n}$. The S-wave polarization vector is specified by the source.

Therefore, *because only one shear wave propagates in isotropic media, and two relevant quasi-shear waves in anisotropic media, we speak of shear waves splitting in anisotropic media.*

In anisotropic media, two types of velocity vectors are considered: phase and ray (or group) velocity vectors. The phase velocity vector is perpendicular to the wavefront, whereas the ray (or group) velocity vector is parallel to the energy flux. In the isotropic case (no dispersion) both phase and ray (or group) velocity vectors coincide and are perpendicular to the wavefront of the plane wave. In an anisotropic medium, *the phase and ray vectors have different directions and different magnitudes*. This means that in an anisotropic medium the energy flux is not perpendicular to the wavefront. Since, rays are defined as trajectories along which the high-frequency part of seismic energy flows, *the rays are not perpendicular to the wavefronts in anisotropic media.*

Figure 1.1 shows a schematical wavefront and ray in homogeneous isotropic *(a)* and anisotropic media *(b)* generated by a point source. The vector $\mathbf{n}$ is the wavefront normal, and $\mathbf{m}$ is a unit vector in the direction of the ray. Since the wavefront in the isotropic homogeneous medium is a circle, both vectors coincide. In the anisotropic medium the wavefronts have more complex shapes. Therefore, the directions of the vectors $\mathbf{n}$ and $\mathbf{m}$ are different.

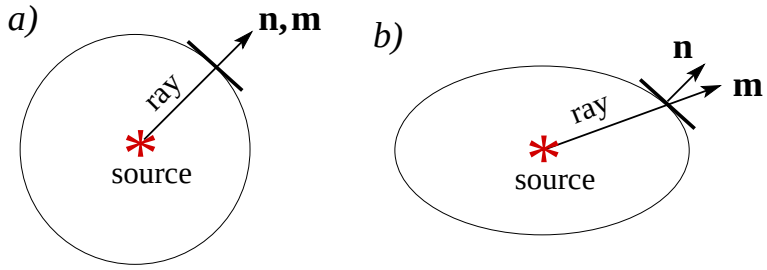

Figure 1.1: Scheme of wavefront and ray in homogeneous isotropic *(a)* and anisotropic *(b)* media from a point source. The vector $\mathbf{n}$ is the wavefront normal, and $\mathbf{m}$ is a unit vector in the direction of the ray. Since the wavefront in the isotropic medium is a circle, both vectors coincide. In the anisotropic medium the wavefront has a complex shape. Therefore, the directions of the vectors $\mathbf{n}$ and $\mathbf{m}$ are different.

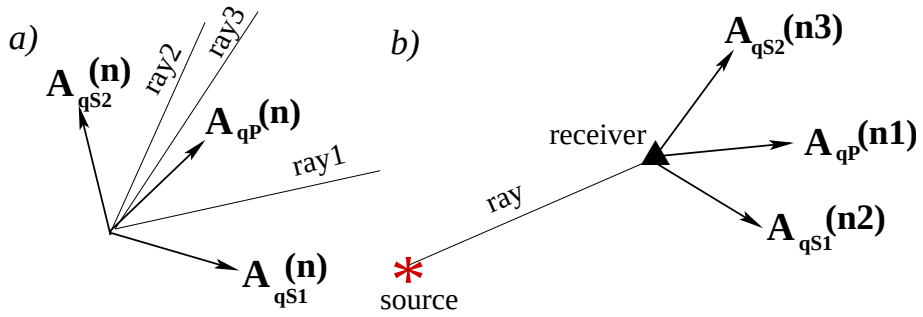

Figure 1.2: Features of wave propagation in homogeneous anisotropic media. *(a)* Polarization vectors of three waves corresponding to the same wavefront normal **n**, but different rays. All three vectors, $\mathbf{A}_{qP}$, $\mathbf{A}_{qS1}$ and $\mathbf{A}_{qS2}$, are mutually orthogonal to each other. The directions of the wavefront normal **n** and the qP-wave polarization vector, $\mathbf{A}_{\mathbf{qP}}$, do not coincide. *(b)* Three waves from a source are recorded at a receiver. All rays are straight lines connecting the source and the receiver. The waves correspond to the different wavefront normals, **n1**, **n2** and **n3**, and their polarization vectors are not mutually orthogonal to each other.

In a homogeneous anisotropic medium, a ray is a straight line connecting a source and a receiver. If the polarization vectors, $\mathbf{A}_{qP}$, $\mathbf{A}_{qS1}$ and $\mathbf{A}_{qS2}$, correspond to the same wavefront normal **n**, they are mutually orthogonal to each other, but each wave propagates along its own individual ray (see Fig.1.2*a*). To obtain all three waves (qP- and two qS-waves) at the same receiver (Fig.1.2*b*, black triangle), for each wave we need to find the wavefront normal that provides the ray velocity vector along the source-receiver line. *The qP- and qS-waves at the receiver correspond to the different wavefront normals (***n1***, ***n2*** and ***n3****). Therefore, their polarization vectors are not mutually orthogonal to each other.*

I want to mention one more feature of qS-wave propagation in anisotropic media. For certain specific directions of propagation, the phase velocity vectors of both qS-waves coincide. Such directions are called *singular directions of quasi-shear waves*. The behavior of qS-waves in the vicinity of singular directions is particularly complicated.

Weakly anisotropic media

Any computations (of rays, traveltimes, seismograms and so on) for inhomogeneous anisotropic media of arbitrary symmetry are much more complicated and computationally expensive than for isotropic media. Therefore, any approximation which allows to simplify or to perform faster computations of rays or some of their parameters is desired. I mention three approximations which are used in my thesis: elliptically anisotropic media, weak anisotropy and factorized anisotropic inhomogeneous (FAI) media.

The concept of FAI medium not only considerably reduces the number of data describing the inhomogeneous anisotropic structure, but also simplifies the ray tracing system (see e.g., Shearer and Chapman, 1988; Červený, 1989). Particularly dramatic simplification is obtained for the perturbation of the delay time between two split quasi-shear waves, if the background medium is isotropic (see Červený and Simões-Filho, 1991).

Although the occurrence of elliptically anisotropic media in nature is vanishingly rare (see Thomsen, 1986, Fig. 4), these media are useful as background media in the perturbation approach. They allow to consider stronger anisotropy without loosing the computa-

tional speed, since traveltime computation for these media using the eikonal equation is fast and accurate (see e.g., Ettrich, 1998; Ettrich et al., 2001; Soukina et al., 2003).

Thomsen (1986) has summarized a large number of laboratory measurements and has pointed out that in most cases of interest to geophysicists the anisotropy is weak. Therefore, approximation of weakly anisotropic media is best suited to seismic anisotropy. Perturbation methods are commonly used tools for describing wave propagation in weakly anisotropic media. The anisotropic medium is replaced by an isotropic background medium where wave propagation can be treated easily and the correction for the effects of anisotropy is computed by perturbation techniques.

The perturbation method allows to compute approximate phase velocities, polarization vectors and traveltimes in anisotropic media for qP- as well as for qS-waves. More details are given in Jech and Pšenčík (1989) or Farra (2001). A quasi-isotropic (QI) approach can be used to compute seismograms for weakly anisotropic media (see e.g. Kravtsov, 1968; Zillmer et al., 1998; Pšenčík and Dellinger, 2001). This approach is based on a combination of the perturbation method and the kinematic and dynamic ray-tracing differential equations for an isotropic background medium.

The most useful application of weakly anisotropic approximation is in solving inverse problems for anisotropic structures, since it allows to obtain linear relations between traveltimes and the perturbation of elastic parameters with respect to the elastic parameters of the isotropic background medium. The relations are inherently linear for qP-wave traveltimes and can also be linearized for qS-wave traveltimes. See e.g. Jech and Pšenčík (1992); Pratt and Chapman (1992).

Chapter 2

The quasi-isotropic approximation

Any computations (of rays, traveltimes, seismograms and so on) for inhomogeneous anisotropic media of arbitrary symmetry are much more complicated and computationally expensive than for isotropic media. Therefore, any approximation which allows to simplify or to perform faster computations of rays or some of their parameters is desired. In this chapter I consider quasi-isotropic (QI) approximation which allows to perform modeling in weakly anisotropic medium.

The QI approximation was proposed by Kravtsov (1968) to avoid difficulties with the standard ray method for anisotropic media in the isotropic limit when the velocities of the two quasi-shear waves are close to each other. The QI approach spans the gap between the ray methods for isotropic and anisotropic media. It can be used in isotropic regions and in regions of weak anisotropy.

The QI approach is based on the kinematic and dynamic ray-tracing differential equations for an isotropic background medium. The asymptotic solution of the elastodynamic equation is searched as an expansion with respect to two small parameters of the same order: the parameter used in the standard ray method, $1/(i\omega)$, and the parameter ε characterizing the deviation of a weakly anisotropic medium from the isotropic background medium. The parameter ε appears, because the elasticity tensor c_{iklm} of a weakly anisotropic medium is introduced as a sum of an isotropic part $c^{(0)}_{iklm}$ and a small anisotropic deviation of first order.

The goal of this chapter is to investigate how well the QI approach actually performs in weakly anisotropic media. For this purpose, at first the theory of the QI approach is considered. The QI approach yields a recurrent system of differential equations. This system is similar to the recurrent system appearing in the standard isotropic ray theory, but it includes terms containing the parameter ε. In the presented work only two equations of the recurrent system are used. The first equation is obtained due to collecting the terms without any small parameters and the terms with the combination of two small parameters $i\omega\varepsilon$. The second equation contains the terms with the small parameter $1/i\omega$ or ε. These two equations allow to obtain so-called zeroth-order and first-order additional components of the solution for qP-wave as well as for qS-waves. All calculations partly repeat the calculations performed by several authors (see e.g. Zillmer et al., 1998; Pšenčík, 1998). Resulting equations presented in my work contain only derivatives of all quantities with respect to Cartesian coordinates. I obtain analytical solutions for qP- and qS-waves

in the case of homogeneous weakly anisotropic media. Analysis of these analytical solutions reveals advantages and drawbacks of the QI approach.

Then, to illustrate the derived equations, numerical VSP experiments are carried out. Seismograms for several homogeneous models with different strengths and types of symmetry of anisotropic medium are calculated using the zeroth- and first-order QI approximation. These seismograms are compared with seismograms computed by the standard anisotropic ray theory (ART) and by a 3D seismic forward modeling algorithm which is based on a pseudo-spectral method (Kosloff and Baysal, 1982; Tessmer, 1995). The seismograms obtained by the last-named method are considered as exact seismograms. The actual program is derived from a modeling code for general material anisotropy described in Tessmer (1995). Also, for comparison, seismograms obtained by the standard isotropic ray theory (IRT) will be presented.

2.1 QI approach for inhomogeneous weakly anisotropic media

The equation of motion for an inhomogeneous anisotropic medium for a fixed frequency ω is given by

$$\frac{\partial}{\partial x_k}\left[c_{iklm}(\mathbf{x})\frac{\partial u_l}{\partial x_m}(\omega,\mathbf{x})\right] - (i\omega)^2\rho(\mathbf{x})u_i(\omega,\mathbf{x}) = 0, \tag{2.1}$$

with the elasticity tensor c_{iklm}, density ρ, displacement vector $\mathbf{u}$ and the vector of space coordinates $\mathbf{x}$. Summation from 1 to 3 with respect to repeated lower subscripts is carried out. Please note that the symbol i denotes the usual index for the lower subscripts, but the imaginary unit for other cases. The elasticity tensor of a weakly anisotropic medium is considered in the following form

$$c_{iklm} = c^{(0)}_{iklm}(\mathbf{x}) + \varepsilon c^{(1)}_{iklm}(\mathbf{x}), \tag{2.2}$$

where $c^{(0)}_{iklm}$ is an elasticity tensor of an isotropic background medium defined by

$$c^{(0)}_{iklm}(\mathbf{x}) = \lambda(\mathbf{x})\delta_{ik}\delta_{lm} + \mu(\mathbf{x})(\delta_{il}\delta_{km} + \delta_{im}\delta_{kl}) \tag{2.3}$$

with the Lamé parameters λ and μ, and δ_{ik} is the Kronecker symbol. The second term in (2.2) describes deviations of the elastic parameters of the anisotropic medium c_{iklm} from isotropy. The small parameter ε is introduced by the perturbation theory. Note that instead $\varepsilon c^{(1)}_{iklm}(\mathbf{x})$ the notation Δc_{iklm} is also used in literature (and in this thesis). Here I use $\varepsilon c^{(1)}_{iklm}(\mathbf{x})$ to show explicitly the small parameter ε. This allows to fix an relation between the two parameters used in the QI approximation. In the QI approach it is assumed that ε is of the order

$$\varepsilon \sim \frac{1}{\omega}.$$

The solution of the equation of motion (2.1) is sought in the form of the ray series:

$$u_j(\omega,\mathbf{x}) = e^{-i\omega\tau(\mathbf{x})}\sum_{n=0}^{\infty}\frac{U^{(n)}_j(\mathbf{x})}{(i\omega)^n}. \tag{2.4}$$

Here, i is the imaginary unit, the scalar real-valued function $\tau(\mathbf{x})$ is the eikonal or phase function and the vectorial, generally complex-valued functions $U_j^{(n)}(\mathbf{x})$ are the amplitude coefficients of the ray series.

To determine the phase function and amplitude coefficients, the ansatz (2.4) and the elasticity tensor (2.2) are substituted into equation (2.1). Collecting the terms of zeroth- and first-order leads to the following recurrent system

$$(\lambda+\mu)(\mathbf{p},\mathbf{U}^{(0)})p_i+(\mu p_j p_j-\rho)U_i^{(0)}=0 \tag{2.5a}$$

$$\begin{aligned}(\lambda+\mu)(\mathbf{p},\mathbf{U}^{(1)})p_i+(\mu p_j p_j-\rho)U_i^{(1)} &= -i\omega\varepsilon c_{iklm}^{(1)}p_k p_m U_l^{(0)}+\\ &+\frac{\partial\lambda}{\partial x_i}(\mathbf{p},\mathbf{U}^{(0)})+\frac{\partial\mu}{\partial x_l}p_l U_i^{(0)}+\frac{\partial\mu}{\partial x_l}U_l^{(0)}p_i+(\lambda+\mu)\frac{\partial U_l^{(0)}}{\partial x_l}p_i+\\ &+2\mu\frac{\partial U_i^{(0)}}{\partial x_m}p_m+(\lambda+\mu)\frac{\partial U_l^{(0)}}{\partial x_i}p_l+\lambda\frac{\partial p_i}{\partial x_l}U_l^{(0)}+\mu\frac{\partial p_m}{\partial x_m}U_i^{(0)}+\mu\frac{\partial p_l}{\partial x_i}U_l^{(0)},\end{aligned} \tag{2.5b}$$

with the slowness vector defined as

$$p_k=\frac{\partial\tau}{\partial x_k},\quad\text{and}\quad(\mathbf{p},\mathbf{U}) \tag{2.6}$$

denotes the scalar product of $\mathbf{p}$ and $\mathbf{U}$. Note that the equation (2.5a) of the recurrent system is identical with the corresponding equation from the standard isotropic ray theory. But the second equation (2.5b) of the recurrent system has an additional term $-i\omega\varepsilon c_{iklm}^{(1)}\,p_k\,p_m\,U_l^{(0)}$ on the right-hand side.

The vectorial equation (2.5a) yields the eikonal equations for the determination of the phase functions $\tau(\mathbf{x})$ of P- and S-waves propagating in the isotropic background medium defined by $c_{iklm}^{(0)}$ (see e.g. Červený, 2001). The eikonal equations have the form

$$\frac{\partial\tau}{\partial x_k}\frac{\partial\tau}{\partial x_k}=\frac{1}{v_p^2},\qquad\frac{\partial\tau}{\partial x_k}\frac{\partial\tau}{\partial x_k}=\frac{1}{v_s^2},$$

with

$$v_p=\sqrt{\frac{\lambda+2\mu}{\rho}}\quad\text{and}\quad v_s=\sqrt{\frac{\mu}{\rho}}. \tag{2.7}$$

The equation (2.5a) also specifies the orientation of the polarization of the waves in the zeroth-order QI approximation. It indicates that the polarization of qP-waves in the zeroth-order QI approximation coincides with the P-wave polarization in the background isotropic medium. The polarization of qS-waves in the zeroth-order QI approximation are confined to the plane perpendicular to the ray in the the background isotropic medium.

To continue the consideration of the recurrent system (2.5) it is necessary to introduce an orthogonal vectorial basis. Here we will work with the vectorial ray-centered basis connected with the ray in the isotropic background medium. This basis is extremely useful for many applications in isotropic media. The basis consists of three mutually orthogonal unit vectors $\mathbf{e}^{(1)}$, $\mathbf{e}^{(2)}$ and $\mathbf{e}^{(3)}$. The vector $\mathbf{e}^{(1)}$ is tangent to the ray in the isotropic background medium. Since the ray and slowness directions coincide for isotropic media, the vector $\mathbf{e}^{(1)}$ is determined as follows

$$\mathbf{e}^{(1)}=v\,\mathbf{p},$$

where v is either the P- or the S-wave velocity in the isotropic background medium. The remaining two vectors $\mathbf{e}^{(2)}$ and $\mathbf{e}^{(3)}$ are situated in the plane perpendicular to the ray. They can be chosen arbitrarily at any point on the ray. From that point the base vectors $\mathbf{e}^{(2)}$ and $\mathbf{e}^{(3)}$ change along the ray according to the differential equation (see, e.g., Popov and Pšenčík, 1978):

$$\frac{d\mathbf{e}^{(K)}}{d\tau} = \left(\mathbf{e}^{(K)}, \operatorname{grad} v\right) \mathbf{e}^{(1)}, \qquad K = 2, 3. \tag{2.8}$$

Again, the symbol v denotes either P- or S-wave velocity in the isotropic background medium.

Please, note that sometimes in the geophysical literature the vectors $\mathbf{e}^{(1)}$, $\mathbf{e}^{(2)}$ and $\mathbf{e}^{(3)}$ are labeled in an alternative order. The vector tangent to the ray is denoted by $\mathbf{e}^{(3)}$, and the two vectors situated in the plane perpendicular to the ray are denoted by $\mathbf{e}^{(1)}$ and $\mathbf{e}^{(2)}$.

In the vectorial basis, the vector amplitude coefficients $\mathbf{U}^{(n)}$ of the ray series (2.4) can be expressed as follows

$$\mathbf{U}^{(n)} = a_1^{(n)}\mathbf{e}^{(1)} + a_2^{(n)}\mathbf{e}^{(2)} + a_3^{(n)}\mathbf{e}^{(3)}, \qquad n = 0, 1, 2 \ldots, \tag{2.9}$$

where $a_1^{(n)}$, $a_2^{(n)}$ and $a_3^{(n)}$ are called scalar amplitudes. According to the terminology of the ray method for isotropic media, the following notations are used: For qP-waves, the component along $\mathbf{e}^{(1)}$ is called the principal component and along $\mathbf{e}^{(2)}$ or $\mathbf{e}^{(3)}$ are the additional components. For qS-waves, the principal components are directed along $\mathbf{e}^{(2)}$ or $\mathbf{e}^{(3)}$ and the additional component along $\mathbf{e}^{(1)}$.

Taking into account equation (2.9) and the P- and S-wave velocities from (2.7) leads to two possible solutions of equation (2.5a) for $n = 0$:

$$\text{for the } qP\text{-wave:} \qquad \mathbf{U}^{(0)} = a_{1p}^{(0)}\mathbf{e}^{(1)} \tag{2.10}$$

$$\text{for the } qS\text{-waves:} \qquad \mathbf{U}^{(0)} = a_{2s}^{(0)}\mathbf{e}^{(2)} + a_{3s}^{(0)}\mathbf{e}^{(3)}. \tag{2.11}$$

Here, for convenience, the characters p and s are used in the lower indices to point out the type of wave. Note that in the zeroth-order QI approximation only the principal components of qP- and qS-waves are non-zero. To obtain the scalar amplitudes from a_{1p}, a_{2s} and a_{3s} the second equation (2.5b) of the recurrent system should be used.

In the subsequent discussions, the quasi-compressional and quasi-shear waves will be considered separately. Also for the sake of convenience, the index "(0)" in the solutions (2.10) and (2.11) will be omitted.

2.1.1 qP-wave

According to equation (2.9), the vectorial amplitude coefficient of the first-order ($n = 1$) QI approximation for a qP-wave may be written as:

$$\mathbf{U}^{(1)} = b_{1p}\,\mathbf{e}^{(1)} + b_{2p}\,\mathbf{e}^{(2)} + b_{3p}\,\mathbf{e}^{(3)}. \tag{2.12}$$

Here for convenience, b_{1p}, b_{2p} and b_{3p} are used instead of $a_1^{(1)}$, $a_2^{(1)}$ and $a_3^{(1)}$. The character p is used in the lower indices to point out the type of wave.

Inserting equations (2.10) and (2.12) into the second equation of the recurrent system (2.5b) and taking into account the P-wave velocity (2.7) lead to the transport equation:

$$-i\omega\varepsilon c^{(1)}_{iklm}\frac{a^2_{1p}}{v^2}e^{(1)}_k e^{(1)}_m e^{(1)}_l e^{(1)}_i + \frac{\partial}{\partial\tau}\left(a^2_{1p}\rho\right) + \frac{a^2_{1p}\rho}{J}\frac{\partial J}{\partial\tau} = 0. \tag{2.13}$$

(As already mentioned, the index "(0)" is omitted: a_{1p} is used instead of $a^{(0)}_{1p}$.) The transport equation (2.13) can be used to determine the scalar amplitude a_{1p}. The symbol J denotes Jacobian for transformation from ray coordinates (τ, α, β) to Cartesian coordinates (x_1, x_2, x_3):

$$J = \frac{\partial(x_1, x_2, x_3)}{\partial(\tau, \alpha, \beta)}. \tag{2.14}$$

Note that the transport equation (2.13) is obtained as a condition of solvability of equation (2.5b): After inserting equations (2.10) and (2.12) into into (2.5b), the left part of equation (2.5b) becomes orthogonal to the base vector $\mathbf{e}^{(1)}$. Therefore, the right part of the equation (2.5b) must also be orthogonal to $\mathbf{e}^{(1)}$. This means that the right part of equation (2.5b) equals zero, when it is multiplied by $\mathbf{e}^{(1)}$. (For more details see Zillmer et al., 1998).

The solution of the transport equation (2.13) is

$$a_{1p} = \frac{\psi_p(\alpha,\beta)}{\sqrt{\rho(\tau)J(\tau)}}\exp\left\{\frac{i\omega}{2}\int\limits_0^{\tau_p}\varepsilon c^{(1)}_{iklm}\frac{1}{\rho}p_k p_m e^{(1)}_l e^{(1)}_i d\tau'\right\}. \tag{2.15}$$

The integral over the traveltime calculated along the P-wave ray path in the isotropic background medium yields the traveltime correction with respect to the isotropic traveltime τ_p. Further in this chapter, the ray path in the isotropic background medium will also be called reference ray. The function $\psi_p(\alpha, \beta)$ depends on the type of source considered and is constant along the ray. The Jacobian $J(\tau)$ can be obtained by solving the dynamic ray-tracing system for the isotropic background medium. Thus, the solution (2.15) for the qP-wave consists of two terms: the P-wave amplitude from the isotropic background medium and the term defining the additional traveltime shift caused by the anisotropy. Due to the last-named term the scalar amplitude a_{1p} in (2.15) depends on the frequency. Note also that in the zeroth-order QI approximation of a qP-wave the perturbation of the elastic parameters, $\varepsilon c^{(1)}_{iklm}$, affects only the traveltime.

To find the scalar amplitude b_{2p} and b_{3p}, the expansion (2.12) is substituted into equation (2.5b). Then, the resulting equation is multiplied by the base vector $\mathbf{e}^{(2)}$ to obtain b_{2p} and by the base vector $\mathbf{e}^{(3)}$ to obtain b_{3p}. Some algebra leads to the following solutions for the scalar amplitudes b_{2p} and b_{3p}

$$\begin{aligned} b_{2p} = {} & i\omega\varepsilon c^{(1)}_{iklm}e^{(1)}_k e^{(1)}_m e^{(1)}_l e^{(2)}_i \frac{a_{1p}}{\lambda+\mu} - \frac{\partial\lambda}{\partial x_i}e^{(2)}_i\frac{v_p a_{1p}}{\lambda+\mu} \\ & + \frac{\partial v_p}{\partial x_i}e^{(2)}_i\frac{\lambda+3\mu}{\lambda+\mu}a_{1p} - \frac{\partial a_{1p}}{\partial x_i}e^{(2)}_i v_p, \end{aligned} \tag{2.16}$$

$$\begin{aligned} b_{3p} = {} & i\omega\varepsilon c^{(1)}_{iklm}e^{(1)}_k e^{(1)}_m e^{(1)}_l e^{(3)}_i \frac{a_{1p}}{\lambda+\mu} - \frac{\partial\lambda}{\partial x_i}e^{(3)}_i\frac{v_p a_{1p}}{\lambda+\mu} \\ & + \frac{\partial v_p}{\partial x_i}e^{(3)}_i\frac{\lambda+3\mu}{\lambda+\mu}a_{1p} - \frac{\partial a_{1p}}{\partial x_i}e^{(3)}_i v_p, \end{aligned}$$

where the scalar amplitude a_{1p} was already obtained by equation (2.15). Note the scalar amplitudes of the additional components of the qP wave defined by (2.16) coincide with the corresponding scalar amplitudes of additional components of the standard ray method in isotropic media (see e.g. Kucher and Kashtan, 1999), with the exception of the terms:

$$i\omega\varepsilon c^{(1)}_{iklm} e^{(1)}_k e^{(1)}_m e^{(1)}_l e^{(2)}_i \frac{a_{1p}}{\lambda+\mu} \quad \text{and} \quad i\omega\varepsilon c^{(1)}_{iklm} e^{(1)}_k e^{(1)}_m e^{(1)}_l e^{(3)}_i \frac{a_{1p}}{\lambda+\mu}.$$

These terms appear due to the small perturbations of elastic parameters $\varepsilon c^{(1)}_{iklm}$.

The equations for the additional components of qP waves were already obtained by Pšenčík (1998), see his equation (32). In his work these equations include derivatives with respect to Cartesian coordinates as well as derivatives with respect to ray-centered coordinates. For the calculation of the latter derivatives a special procedure is required. Eisner and Pšenčík (1996) suggested to compute them approximately from neighboring rays by substituting the derivatives by finite-differences. These authors are unaware of an application of this procedure to anisotropic media.

In practice, before considering complex models, the more simple homogeneous case should be analyzed. It is of interest to obtain QI approximation expressions for qP-wave in homogeneous weakly anisotropic media. Analytical expression for qP-wave for this limiting case can be obtained from equations (2.16). Section 2.2 is devoted to consider homogeneous weakly anisotropic media.

To determine the scalar amplitude b_{1p} along the base vector $\mathbf{e}^{(1)}$ in equation (2.12), a second-order equation of the recurrent system needs to be taken into account. The contribution from the term b_{1p} is also the first-order, but the consideration of this equation is a significantly more complex task. It was outside the scope of my work. In principal, the results obtained from the first two equations of the recurrent system allow already to appreciate the profit of the first-order terms,

The final solution obtained in the presented work for qP-wave is:

$$\mathbf{U}^{(0+1A)}_{qP} = a_{1p}\,\mathbf{e}^{(1)} + \frac{1}{i\omega}\left(b_{2p}\,\mathbf{e}^{(2)} + b_{3p}\,\mathbf{e}^{(3)}\right). \tag{2.17}$$

The solution $\mathbf{U}^{(0+1A)}_{qP}$ includes the zeroth-order QI approximation and two terms along $\mathbf{e}^{(2)}$ and $\mathbf{e}^{(3)}$ from the first-order QI approximation. The scalar amplitudes a_{1p}, b_{2p} and b_{3p} are calculated by equations (2.15) and (2.16).

According to the notations used in the ray method for isotropic media, the component $a_{1p}\,\mathbf{e}^{(1)}$ is called the zeroth-order principal component (0). The two first-order components along $\mathbf{e}^{(2)}$ and $\mathbf{e}^{(3)}$ are called the first-order additional components (1A). To indicate the composition of (2.17), the index $(0+1A)$ is used.

2.1.2 qS-waves

Now I consider the more interesting case of quasi-shear waves. qS-waves are stronger affected by anisotropy than qP-waves. Also, splitting of shear-waves is a principal feature that takes place in anisotropic media. Therefore, my prime interest is in this section to investigate how the QI approach describes the qS-wave propagation.

The zeroth-order QI approximation for qS-waves is given by (2.11). The scalar amplitudes a_{2s} and a_{3s} (the index "(0)" is again omitted) can be sought from equation (2.5b).

According to equation (2.9) the vectorial amplitude coefficient $\mathbf{U}^{(1)}$ of the first-order QI approximation for the qS-waves may be written as:

$$\mathbf{U}^{(1)} = b_{1s}\,\mathbf{e}^{(1)} + b_{2s}\,\mathbf{e}^{(2)} + b_{3s}\,\mathbf{e}^{(3)}, \tag{2.18}$$

where, for convenience, b_{1s}, b_{2s} and b_{3s} are used instead of $a_1^{(1)}$, $a_2^{(1)}$ and $a_3^{(1)}$. The characters s is used in the lower indexes to point out the type of wave.

As in the case of the qP-wave, $\mathbf{U}^{(1)}$ is inserted into the left part of equation (2.5b). Then, taking into account the S-wave velocity (2.7) in the background isotropic medium, we find that the left part of (2.5b) has only a component along the base vector $\mathbf{e}^{(1)}$. This means that the right part of this equation should also have only the component along $\mathbf{e}^{(1)}$. In other words, the right part of (2.5b) is orthogonal to the vector $\mathbf{e}^{(2)}$ as well as to the vector $\mathbf{e}^{(3)}$. Therefore, the following system of two equations are obtained as conditions of solvability of the equation (2.5b):

$$\begin{aligned}
&-i\omega\varepsilon c^{(1)}_{iklm}p_k p_m U^{(0)}_l e^{(2)}_i + \frac{\partial\lambda}{\partial x_i}(\mathbf{p},\mathbf{U}^{(0)})e^{(2)}_i + \frac{\partial\mu}{\partial x_l}p_l U^{(0)}_i e^{(2)}_i + \frac{\partial\mu}{\partial x_l}U^{(0)}_l p_i e^{(2)}_i + \\
&\quad +(\lambda+\mu)\frac{\partial U^{(0)}_l}{\partial x_l}p_i e^{(2)}_i + 2\mu\frac{\partial U^{(0)}_i}{\partial x_m}p_m e^{(2)}_i + (\lambda+\mu)\frac{\partial U^{(0)}_l}{\partial x_i}p_l e^{(2)}_i + \\
&\quad +\lambda\frac{\partial p_i}{\partial x_l}U^{(0)}_l e^{(2)}_i + \mu\frac{\partial p_m}{\partial x_m}U^{(0)}_i e^{(2)}_i + \mu\frac{\partial p_l}{\partial x_i}U^{(0)}_l e^{(2)}_i = 0 \\
&-i\omega\varepsilon c^{(1)}_{iklm}p_k p_m U^{(0)}_l e^{(3)}_i + \frac{\partial\lambda}{\partial x_i}(\mathbf{p},\mathbf{U}^{(0)})e^{(3)}_i + \frac{\partial\mu}{\partial x_l}p_l U^{(0)}_i e^{(3)}_i + \frac{\partial\mu}{\partial x_l}U^{(0)}_l p_i e^{(3)}_i + \\
&\quad +(\lambda+\mu)\frac{\partial U^{(0)}_l}{\partial x_l}p_i e^{(3)}_i + 2\mu\frac{\partial U^{(0)}_i}{\partial x_m}p_m e^{(3)}_i + (\lambda+\mu)\frac{\partial U^{(0)}_l}{\partial x_i}p_l e^{(3)}_i + \\
&\quad +\lambda\frac{\partial p_i}{\partial x_l}U^{(0)}_l e^{(3)}_i + \mu\frac{\partial p_m}{\partial x_m}U^{(0)}_i e^{(3)}_i + \mu\frac{\partial p_l}{\partial x_i}U^{(0)}_l e^{(3)}_i = 0
\end{aligned} \tag{2.19}$$

From this system, the scalar amplitudes a_{2s} and a_{3s} for the solution (2.11) can not be obtained directly. After substituting $\mathbf{U}^{(0)}$ from (2.11) into the system (2.19) and taking into account properties of the basis $\mathbf{e}^{(1)}$, $\mathbf{e}^{(2)}$ and $\mathbf{e}^{(3)}$ from the appendix A at the end of this chapter, a system of two transport equations is obtained:

$$\begin{aligned}
&-i\omega\varepsilon c^{(1)}_{iklm}p_k p_m e^{(2)}_l e^{(2)}_i a^2_{2s} - i\omega\varepsilon c^{(1)}_{iklm}p_k p_m e^{(3)}_l e^{(2)}_i a_{3s}a_{2s} + \frac{\partial}{\partial\tau}\Big(\rho a^2_{2s}J\Big) = 0 \\
&-i\omega\varepsilon c^{(1)}_{iklm}p_k p_m e^{(2)}_l e^{(3)}_i a_{2s}a_{3s} - i\omega\varepsilon c^{(1)}_{iklm}p_k p_m e^{(3)}_l e^{(3)}_i a^2_{3s} + \frac{\partial}{\partial\tau}\Big(\rho a^2_{3s}J\Big) = 0.
\end{aligned} \tag{2.20}$$

With the following notations

$$\begin{aligned}
B_{22} &= \varepsilon c^{(1)}_{iklm}p_k p_m e^{(2)}_l e^{(2)}_i, \quad B_{23} = \varepsilon c^{(1)}_{iklm}p_k p_m e^{(3)}_l e^{(2)}_i, \\
B_{32} &= \varepsilon c^{(1)}_{iklm}p_k p_m e^{(2)}_l e^{(3)}_i, \quad B_{33} = \varepsilon c^{(1)}_{iklm}p_k p_m e^{(3)}_l e^{(3)}_i,
\end{aligned} \tag{2.21}$$

$$X_2^2 = \rho a^2_{2s}J, \quad X_3^2 = \rho a^2_{3s}J \tag{2.22}$$

the system (2.20) can be rewritten in the form of two coupled linear differential equations for X_2 and X_3:

$$\frac{\partial}{\partial\tau}\begin{pmatrix}X_2\\X_3\end{pmatrix} = \frac{i\omega}{2}\,\mathbf{B}\begin{pmatrix}X_2\\X_3\end{pmatrix}, \tag{2.23}$$

where the symmetric 2×2 matrix

$$\mathbf{B} = \begin{pmatrix} B_{22} & B_{23} \\ B_{23} & B_{33} \end{pmatrix} \tag{2.24}$$

is the so-called weak anisotropy matrix (see Jech and Pšenčík, 1989; Červený, 2001). Thus, the conditions of solvability of the equation (2.5b) lead to the two coupled linear differential equations for a_{2s} and a_{3s}. If the matrix $\mathbf{B}$ is known along the ray, then we can solve the coupled equations (2.23) and determine the scalar amplitudes a_{2s} and a_{3s} for each frequency ω. Similarly to the case of qP-waves, we can see that the scalar amplitudes a_{2s} and a_{3s} are frequency-dependent in the QI approximation. The system (2.23) will be examined in more detail in subsection 2.1.3.

To find the first-order scalar amplitudes from (2.18), equation (2.5b) is used. After substituting $\mathbf{U}^{(0)}$ from (2.11) and $\mathbf{U}^{(1)}$ from (2.18), equation (2.5b) takes the form:

$$\begin{aligned}
(\lambda+\mu)(\mathbf{p},[b_{1s}\mathbf{e}^{(1)}+b_{2s}\mathbf{e}^{(2)}+b_{3s}\mathbf{e}^{(3)}])\,p_i = \\
= -i\omega\varepsilon c^{(1)}_{iklm}p_k p_m[a_{2s}e^{(2)}_l + a_{3s}e^{(3)}_l] + \frac{\partial\lambda}{\partial x_i}(\mathbf{p},[a_{2s}\mathbf{e}^{(2)}+a_{3s}\mathbf{e}^{(3)}]) + \\
\frac{\partial\mu}{\partial x_l}p_l[a_{2s}e^{(2)}_i + a_{3s}e^{(3)}_i] + \frac{\partial\mu}{\partial x_l}[a_{2s}e^{(2)}_l + a_{3s}e^{(3)}_l]p_i + (\lambda+\mu)\frac{\partial[a_{2s}e^{(2)}_l + a_{3s}e^{(3)}_l]}{\partial x_l}p_i + \\
+2\mu\frac{\partial[a_{2s}e^{(2)}_i + a_{3s}e^{(3)}_i]}{\partial x_m}p_m + (\lambda+\mu)\frac{\partial[a_{2s}e^{(2)}_l + a_{3s}e^{(3)}_l]}{\partial x_i}p_l + \lambda\frac{\partial p_i}{\partial x_l}[a_{2s}e^{(2)}_l + a_{3s}e^{(3)}_l] + \\
\mu\frac{\partial p_m}{\partial x_m}[a_{2s}e^{(2)}_i + a_{3s}e^{(3)}_i] + \mu\frac{\partial p_l}{\partial x_i}[a_{2s}e^{(2)}_l + a_{3s}e^{(3)}_l].
\end{aligned} \tag{2.25}$$

Since the slowness vector $\mathbf{p}$ is orthogonal to the base vector $\mathbf{e}^{(2)}$ and $\mathbf{e}^{(3)}$, the following equation applies for the left side of equation (2.25):

$$(\lambda+\mu)(\mathbf{p},[b_{1s}\mathbf{e}^{(1)}+b_{2s}\mathbf{e}^{(2)}+b_{3s}\mathbf{e}^{(3)}])\,p_i = (\lambda+\mu)\frac{b_{1s}}{v_s}\,p_i.$$

This means that equation (2.25) allows to find only the scalar amplitude b_{1s} along the base vector $\mathbf{e}^{(1)}$. Multiplying (2.25) by $e^{(1)}_i$, after some algebra, we obtain for b_{1s}:

$$b_{1s} = -\frac{i\omega\varepsilon}{(\lambda+\mu)}c^{(1)}_{iklm}e^{(1)}_k e^{(1)}_m e^{(1)}_i\,U^{(0)}_l + \frac{v_s\,U^{(0)}_l}{(\lambda+\mu)}\frac{\partial\mu}{\partial x_l} + v_s\frac{\partial U^{(0)}_l}{\partial x_l} + \frac{2\mu}{(\lambda+\mu)}\,U^{(0)}_l\,\frac{\partial v_s}{\partial x_l}, \tag{2.26}$$

where $U^{(0)}_l$ is defined by (2.11).

To determine the scalar amplitudes b_{2s} and b_{3s} from (2.18), the second-order equation of the recurrent system needs to be taken into account. The contributions from the terms b_{2s} and b_{3s} are the first-order, but the consideration of this equation is significantly more complex task. It was outside the scope of my work. In principal, the results obtained from the first two equations of the recurrent system allow already to appreciate the profit from the first-order terms,

The solution of the recurrent system (2.5) for qS-waves obtained in the presented work are written as follows:

$$\mathbf{U}^{(0+1A)}_{qS} = a_{2s}\,\mathbf{e}^{(2)} + a_{3s}\,\mathbf{e}^{(3)} + \frac{1}{i\omega}b_{1s}\,\mathbf{e}^{(1)} \tag{2.27}$$

The solution $\mathbf{U}_{qS}^{(0+1A)}$ includes the zeroth-order QI approximation terms and the first-order term along the base vector $\mathbf{e}^{(1)}$ from the first-order QI approximation. The scalar amplitudes a_{2s}, a_{3s} can be calculated by solving the coupled system (2.23), and b_{1s} is obtained from equation (2.26).

According to the terminology used in the ray method for isotropic media, the component $a_{2s}\,\mathbf{e}^{(2)}+a_{3s}\,\mathbf{e}^{(3)}$ is called the principal component (0). The first-order component along $\mathbf{e}^{(1)}$ is called the additional component (1A). To indicate the composition of (2.27), the index $(0+1A)$ is used.

The expression for the additional component of qS-waves was already obtained by Pšenčík (1998), his equation (42). Similar to the case of the qP-wave, his equation includes derivatives with respect to the Cartesian coordinates as well as with respect to the ray-centered coordinates. Equation (2.26) derived here includes only derivatives with respect to the Cartesian coordinates.

It is interesting to obtain the QI approximation expression for qS-waves in the more simple homogeneous case. Equation (2.26) allows nearly directly to obtain an analytical equation for qS-wave in this limiting case. Section 2.2 is devoted to the consideration of homogeneous weakly anisotropic media.

2.1.3 Investigation of the coupled system of linear differential equations for the qS-waves

To define the zeroth-order scalar amplitudes a_{2s} and a_{3s}, the system of two coupled linear differential equations (2.23) needs to be solved. In this section the system (2.23) will be investigated. For convenience, we rewrite this system in the form

$$\begin{aligned}\frac{dX_2(\tau)}{d\tau} &= \frac{i\omega}{2}\Big[B_{22}X_2(\tau)+B_{23}X_3(\tau)\Big]\\ \frac{dX_3(\tau)}{d\tau} &= \frac{i\omega}{2}\Big[B_{32}X_2(\tau)+B_{33}X_3(\tau)\Big],\end{aligned} \tag{2.28}$$

where the notations (2.21) and (2.22) are used.

In the plane perpendicular to $\mathbf{e}^{(1)}$, the base vectors $\mathbf{e}^{(2)}$ and $\mathbf{e}^{(3)}$ may be taken arbitrarily at any point on the ray. From that point they have to satisfy the differential equation (2.8). Therefore, it is possible, for instance, to choose the base vectors in such way that the matrix element

$$B_{23}=0 \qquad \text{at an initial point} \quad \tau=0. \tag{2.29}$$

The values of $X_2(0)$ and $X_3(0)$ at the initial point with $\tau=0$ are used as initial conditions for solving the system (2.28). The values of $X_2(0)$ and $X_3(0)$ are determined by the type of source.

Now a vector $\begin{pmatrix}Y_2\\Y_3\end{pmatrix}$ is introduced instead of the vector $\begin{pmatrix}X_2\\X_3\end{pmatrix}$ by rotation through an angle γ:

$$\begin{aligned}X_2(\tau) &= Y_2(\tau)\cos\gamma+Y_3(\tau)\sin\gamma\\ X_3(\tau) &= -Y_2(\tau)\sin\gamma+Y_3(\tau)\cos\gamma.\end{aligned} \tag{2.30}$$

With $Y_2(\tau)$ and $Y_3(\tau)$ the coupled system (2.28) is written in the form:

$$\frac{dY_2}{d\tau} = \frac{i\omega}{2}\Big\{Y_2\Big(B_{22}\cos^2\gamma + B_{33}\sin^2\gamma - 2B_{23}\cos\gamma\sin\gamma\Big) + \\ +Y_3\Big((B_{22}-B_{33})\cos\gamma\sin\gamma + B_{23}\cos 2\gamma\Big)\Big\} - Y_3\frac{d\gamma}{d\tau}$$

$$\frac{dY_3}{d\tau} = \frac{i\omega}{2}\Big\{Y_3\Big(B_{22}\sin^2\gamma + B_{33}\cos^2\gamma + 2B_{23}\cos\gamma\sin\gamma\Big) + \\ +Y_2\Big((B_{22}-B_{33})\cos\gamma\sin\gamma + B_{23}\cos 2\gamma\Big)\Big\} + Y_2\frac{d\gamma}{d\tau}.$$

If the angle γ is chosen to satisfy the condition

$$(B_{22}-B_{33})\cos\gamma\sin\gamma + B_{23}\cos 2\gamma = 0, \tag{2.31}$$

the following system is obtained

$$\begin{aligned}\frac{dY_2}{d\tau} &= \frac{i\omega}{2}Y_2\Big(B_{22}\cos^2\gamma + B_{33}\sin^2\gamma - 2B_{23}\cos\gamma\sin\gamma\Big) - Y_3\frac{d\gamma}{d\tau} \\ \frac{dY_3}{d\tau} &= \frac{i\omega}{2}Y_3\Big(B_{22}\sin^2\gamma + B_{33}\cos^2\gamma + 2B_{23}\cos\gamma\sin\gamma\Big) + Y_2\frac{d\gamma}{d\tau}.\end{aligned} \tag{2.32}$$

Because all elements of the weak anisotropy matrix $\mathbf{B}$ are known along the ray in the isotropic background medium, the angle γ can be determined according to equation (2.31). With the notations

$$\begin{aligned}\lambda_2(\tau) &\equiv B_{22}\cos^2\gamma + B_{33}\sin^2\gamma - 2B_{23}\cos\gamma\sin\gamma \\ \lambda_3(\tau) &\equiv B_{22}\sin^2\gamma + B_{33}\cos^2\gamma + 2B_{23}\cos\gamma\sin\gamma\end{aligned} \tag{2.33}$$

the system (2.32) takes the form

$$\frac{d}{d\tau}\begin{pmatrix}Y_2\\Y_3\end{pmatrix} = \begin{pmatrix}\frac{i\omega}{2}\lambda_2 & -\frac{d\gamma}{d\tau}\\ \frac{d\gamma}{d\tau} & \frac{i\omega}{2}\lambda_3\end{pmatrix}\begin{pmatrix}Y_2\\Y_3\end{pmatrix}, \tag{2.34}$$

where the coupling term $\dfrac{\partial\gamma}{\partial\tau}$ obtained from the condition (2.31) is

$$\frac{d\gamma}{d\tau} = \frac{(B_{33}-B_{22})\,\dfrac{\partial B_{23}}{\partial\tau} - B_{23}\left(\dfrac{\partial B_{33}}{\partial\tau} - \dfrac{\partial B_{22}}{\partial\tau}\right)}{(B_{33}-B_{22})^2 + 4B_{23}^2}.$$

The initial conditions for the coupled equations (2.34) can be obtained as follows: At an initial point with $\tau = 0$ the base vectors are chosen such that $B_{23} = 0$, the condition (2.31) for $\tau = 0$ appears as

$$\Big(B_{22}[\tau=0] - B_{33}[\tau=0]\Big)\cos\gamma[\tau=0]\,\sin\gamma[\tau=0] = 0,$$

from which it follows that the angle γ is

$$\gamma[\tau=0] = \frac{\pi}{2}\,k, \qquad k = 0, 1, \ldots \tag{2.35}$$

Therefore, according to (2.35) the initial conditions for (2.34) can be determined from X_2 and X_3 at $\tau = 0$. From (2.30), we get

$$Y_2(0) = X_2(0), \qquad Y_3(0) = X_3(0) \qquad \text{for} \quad \gamma[\tau = 0] = 0.$$

Thus, we have obtained the initial conditions for $Y_2(\tau)$ and $Y_3(\tau)$.

With $Y_2(\tau)$ and $Y_3(\tau)$ the zeroth-order QI approximation for qS-waves, $\mathbf{U}^{(0)}$, from (2.11) can be written as

$$\mathbf{U}^{(0)} = \frac{1}{\sqrt{\rho J}}\Big(Y_2 \underbrace{\{\mathbf{e}^{(2)}\cos\gamma - \mathbf{e}^{(3)}\sin\gamma\}}_{\mathbf{g}^{(2)}} + Y_3 \underbrace{\{\mathbf{e}^{(2)}\sin\gamma + \mathbf{e}^{(3)}\cos\gamma\}}_{\mathbf{g}^{(3)}}\Big). \tag{2.36}$$

The two mutually orthogonal vectors obtained by the rotation of the base vectors $\mathbf{e}^{(2)}$ and $\mathbf{e}^{(3)}$ through the angle γ under condition (2.31) are denoted as $\mathbf{g}^{(2)}$ and $\mathbf{g}^{(3)}$:

$$\mathbf{g}^{(2)} = \mathbf{e}^{(2)}\cos\gamma - \mathbf{e}^{(3)}\sin\gamma; \qquad \mathbf{g}^{(3)} = \mathbf{e}^{(2)}\sin\gamma + \mathbf{e}^{(3)}\cos\gamma. \tag{2.37}$$

Equation (2.36) presents the wave field in terms of two interacting linearly polarized S-waves. The vectors $\mathbf{g}^{(2)}$ and $\mathbf{g}^{(3)}$ describe the polarization vectors for these two S-waves. The weak anisotropy matrix $\mathbf{B}^{\mathrm{g}}$, expressed in terms of the vectors $\mathbf{g}^{(2)}$ and $\mathbf{g}^{(3)}$ is diagonal (see e.g Červený, 2001):

$$B^{\mathrm{g}}_{JN} = \varepsilon c^{(1)}_{iklm}\, p_i\, p_m\, \mathrm{g}^{(J)}_k\, \mathrm{g}^{(N)}_l, \quad J, N = 2, 3.$$

The coupling term $\dfrac{d\gamma}{d\tau}$ of the system (2.34) describes the rate of the change of the angle γ along the ray in the background isotropic medium. Or, in other words, it describes the rotation of the polarization vectors $\mathbf{g}^{(2)}$ and $\mathbf{g}^{(3)}$ along the ray with respect to the base vectors $\mathbf{e}^{(2)}$ and $\mathbf{e}^{(3)}$ as the anisotropy of the medium changes from one point on the reference ray to another. According to equation (2.8) the base vectors $\mathbf{e}^{(2)}$ and $\mathbf{e}^{(3)}$ rotate along the ray due to the inhomogeneity of the isotropic background medium. Usually, the description of a seismic wave contains an amplitude term multiplied by the exponential term. In the zeroth-order QI approximation, we can not derive such type of expression for for the qS-waves. Because of the rotation of the vectors $\mathbf{g}^{(2)}$ and $\mathbf{g}^{(3)}$ and the frequency dependence of system (2.34), we can not obtain the individual exponential term for $Y_2(\tau)$ and $Y_3(\tau)$. Therefore, in the strict sense, the solution of the system (2.34) is not a simple superposition of two qS-waves. The superposition following from (2.34) depends on frequency and local properties of the inhomogeneous anisotropic medium considered. This interaction of the two waves is usually called coupling of qS-waves.

There are situations when the system (2.34) decouples and its solution is represented in the form of two decoupled qS waves. In the case of a homogeneous weakly anisotropic medium, the weak anisotropy matrix $\mathbf{B}$ is constant along the whole ray, therefore, $\dfrac{\partial\gamma}{\partial\tau} = 0$. As a result, the two equations of the system (2.34) can be solved separately. The solution of each equation represents a linearly polarized qS-wave.

In the case of wave propagation within a symmetry plane of an inhomogeneous weakly anisotropic medium, we also obtain $\dfrac{\partial\gamma}{\partial\tau} = 0$ and, as a result, two decoupled qS-waves. For example, this situation appears in a model where the elastic parameters depend only

on the z-coordinate, but for each values of z the elastic parameters define a transversely isotropic medium with the symmetry axis along the Z-direction. Thus, in this type of model each plane which contains the symmetry axis is a symmetry plane where qS-waves decouple.

If it is assumed that not only the perturbations $\varepsilon c^{(1)}_{iklm}$ are small, but the derivatives $\frac{\partial c^{(1)}_{iklm}}{\partial x_j}$ are also small, it follows that $\frac{d\gamma}{d\tau} << 1$. Therefore, in the system (2.34) the contributions from $Y_2\frac{d\gamma}{d\tau}$ and $Y_3\frac{d\gamma}{d\tau}$ are negligible.

If two qS waves decouple, the solution of the system (2.34) can be given in the following form:

$$\begin{aligned} Y_2(\tau) &= Y_2(0)\exp\left\{\frac{i\omega}{2}\int_0^\tau \lambda_2(t)dt\right\} \\ Y_3(\tau) &= Y_3(0)\exp\left\{\frac{i\omega}{2}\int_0^\tau \lambda_3(t)dt\right\}, \end{aligned} \tag{2.38}$$

where both integrals are calculated along the S-wave ray path in the background isotropic medium.

I would like to note that with a change in variables (Zillmer et al., 1998)

$$\begin{pmatrix} Y_2 \\ Y_3 \end{pmatrix} \equiv \begin{pmatrix} Z_2 \exp\frac{i\omega}{2}\int_0^\tau \lambda_2 dt \\ Z_3 \exp\frac{i\omega}{2}\int_0^\tau \lambda_3 dt \end{pmatrix}$$

we transform the system (2.34) and obtain

$$\frac{\partial}{\partial\tau}\begin{pmatrix} Z_2 \\ Z_3 \end{pmatrix} = \frac{\partial\gamma}{\partial\tau}\begin{pmatrix} 0 & -\exp\left\{\frac{i\omega}{2}\int_0^\tau(\lambda_3-\lambda_2)dt\right\} \\ \exp\left\{\frac{-i\omega}{2}\int_0^\tau(\lambda_3-\lambda_2)dt\right\} & 0 \end{pmatrix}\begin{pmatrix} Z_2 \\ Z_3 \end{pmatrix} \tag{2.39}$$

This system of two integral-differential equations is equivalent to the system (2.34) and describes the coupling between two qS waves in weakly anisotropic media. The system (2.39) was obtained by Coates and Chapman (1990) using an approach based on a scattering integral. Note that the equations of Coates and Chapman are a specification of a more general system whose applicability is much broader than the equations (2.39).

2.2 QI approximation for a homogeneous weakly anisotropic media

Since the study of anisotropic media is a very complicated problem, it is desirable to consider the cases where analytical expressions describing the waves propagating in anisotropic media are available.

The zeroth- and first-order QI approximations for qP- and qS-waves obtained in the previous section are valid in inhomogeneous weakly anisotropic media. To apply these

equations to the calculation of qP- and qS-waves the two coupled equations (2.11) have to be solved and all derivatives in the expression for the scalar amplitudes (2.16) and (2.26) are need to be computed. In the case of an inhomogeneous weakly anisotropic medium all calculations can only be carried out numerically. Obviously these calculations are complex and require special numerical procedures (see e.g. Eisner and Pšenčík, 1996). But in the case of a homogeneous weakly anisotropic medium the equations simplify and, therefore, allow to easily compute the qP- and qS-waves. Because the system (2.11) decouples, it can be solved analytically. Furthermore, in a homogeneous weakly anisotropic medium, the derivatives in (2.16) and (2.26) are equal to zero or can be calculated analytically.

In this section the analytical expressions for the zeroth- and first-order QI approximations for qP- and qS-waves are derived. Also, to reveal advantages and drawbacks of the QI approach, an analysis of these analytical solutions is carried out.

2.2.1 qP-wave

In the previous section the following equation for qP wave was obtained:

$$\mathbf{U}_{qP}^{(0+1A)} = a_{1p}\,\mathbf{e}^{(1)} + \frac{1}{i\omega}\left(b_{2p}\,\mathbf{e}^{(2)} + b_{3p}\,\mathbf{e}^{(3)}\right). \tag{2.40}$$

This equation includes the zeroth-order principal component and two first-order additional components. For homogeneous weakly anisotropic media, the equations (2.15) and (2.16) for the scalar amplitudes a_{1p}, b_{2p} and b_{3p} can be simplified. For the zeroth-order scalar amplitude a_{1p} equation (2.15) leads to

$$a_{1p} = \frac{\psi_p(\alpha,\beta)}{\sqrt{\rho \overline{J}}} \exp\left\{\frac{i\omega}{2\rho}\varepsilon c_{iklm}^{(1)} p_k p_m e_l^{(1)} e_i^{(1)} \tau_p\right\}, \tag{2.41}$$

where τ_p is traveltime of the P wave in the background isotropic medium. The traveltime τ_p appears instead of the integral along the reference ray path in (2.15).

Since the background isotropic medium for the homogeneous weakly anisotropic medium is also homogeneous, the derivatives $\dfrac{\partial \lambda}{\partial x_i}$ and $\dfrac{\partial v_p}{\partial x_i}$ in (2.16) are equal to zero. Therefore, for the first-order scalar amplitudes b_{2p} and b_{3p} we get

$$\begin{aligned} b_{2p} &= \frac{i\omega}{v_p^2 - v_s^2}\varepsilon c_{iklm}^{(1)} e_k^{(1)} e_m^{(1)} e_l^{(1)} e_i^{(2)}\,\frac{a_{1p}}{\rho} - v_p \frac{\partial a_{1p}}{\partial x_i}\, e_i^{(2)}, \\ b_{3p} &= \frac{i\omega}{v_p^2 - v_s^2}\varepsilon c_{iklm}^{(1)} e_k^{(1)} e_m^{(1)} e_l^{(1)} e_i^{(3)}\,\frac{a_{1p}}{\rho} - v_p \frac{\partial a_{1p}}{\partial x_i}\, e_i^{(3)}. \end{aligned} \tag{2.42}$$

Note that the first terms of equations (2.42) can be obtained in the perturbation theory considering plane waves as first-order corrections to the polarization vector in the plane perpendicular to the ray in the background isotropic medium (see Jech and Pšenčík, 1989; Farra, 2001). But the second terms are connected to the curvature of the wavefront resulting from a point source and, therefore, can not be derived using perturbation theory, because the derivative $\dfrac{\partial a_{1p}}{\partial x_i}$ is equal to zero for the plane waves. For point sources, the values of a_{1p} change along the wavefront, therefore, the derivative $\dfrac{\partial a_{1p}}{\partial x_i} \neq 0$.

To calculate $\frac{\partial a_{1p}}{\partial x_i}\, e_i^{(2)}$ and $\frac{\partial a_{1p}}{\partial x_i}\, e_i^{(3)}$ the following relations are used:

$$e_k^{(1)} = \frac{x_k}{R}, \qquad R = v_p \tau_p, \qquad \frac{\partial x_\alpha}{\partial x_\beta} = \delta_{\alpha\beta}. \tag{2.43}$$

(No summation over p-index is performed. Here v_p and τ_p are velocity and traveltime of P-wave in the isotropic background medium.) Taking into account equations (2.43) and the symmetry of $c_{iklm}^{(1)}$ we can perform the following calculations:

$$\frac{\partial a_{1p}}{\partial x_j} e_j^{(2)} = a_{1p} \frac{i\varepsilon\omega}{2} \frac{\tau_p}{\rho v_p^2} \frac{\partial}{\partial x_j} \left[c_{iklm}^{(1)} x_k x_m x_l x_i \right] e_j^{(2)} \frac{1}{R^4} =$$

$$= \frac{i\varepsilon\omega}{2} \frac{a_{1p}\tau_p}{R\rho v_p^2} \left[c_{ijlm}^{(1)} e_m^{(1)} e_l^{(1)} e_i^{(1)} + c_{iklj}^{(1)} e_k^{(1)} e_l^{(1)} e_i^{(1)} + c_{ikjm}^{(1)} e_k^{(1)} e_m^{(1)} e_i^{(1)} + c_{jklm}^{(1)} e_k^{(1)} e_m^{(1)} e_l^{(1)} \right] e_j^{(2)} =$$

$$= \frac{i\varepsilon\omega}{2} \frac{a_{1p}\tau_p}{R\rho v_p^2} 4 c_{ijlm}^{(1)} e_m^{(1)} e_l^{(1)} e_i^{(1)} e_j^{(2)} = i\varepsilon\omega \frac{2a_{1p}}{\rho v_p^3} c_{ijlm}^{(1)} e_m^{(1)} e_l^{(1)} e_i^{(1)} e_j^{(2)}.$$

In this calculation the derivatives

$$\frac{\partial}{\partial x_i} \left[\frac{\psi_p(\alpha,\beta)}{\sqrt{\rho J}} \right]$$

are not taken into account, because, they depend on the type of the point source, therefore, a special consideration is needed. This consideration was outside the scope of my work.

The substitution of the calculated $\frac{\partial a_{1p}}{\partial x_j}\, e_j^{(2)}$ into the first equation of (2.42) leads to:

$$b_{2p} = \frac{2v_s^2 - v_p^2}{v_p^2(v_p^2 - v_s^2)}\, i\omega\varepsilon c_{iklm}^{(1)} e_k^{(1)} e_m^{(1)} e_l^{(1)} e_i^{(2)} \frac{a_{1p}}{\rho}. \tag{2.44}$$

In a similar manner the scalar amplitude b_{3p} can be obtained:

$$b_{3p} = \frac{2v_s^2 - v_p^2}{v_p^2(v_p^2 - v_s^2)}\, i\omega\varepsilon c_{iklm}^{(1)} e_k^{(1)} e_m^{(1)} e_l^{(1)} e_i^{(3)} \frac{a_{1p}}{\rho}. \tag{2.45}$$

As a result, for the qP-wave propagating in a homogeneous weakly anisotropic medium, the zeroth-order and additional terms of the first-order QI approximation lead to the following expression:

$$\mathbf{U}_{qP}^{(0+1A)} = \left[\mathbf{e}^{(1)} + \frac{\varepsilon c_{iklm}^{(1)}}{\rho} e_k^{(1)} e_m^{(1)} e_l^{(1)} e_i^{(2)} \frac{2v_s^2 - v_p^2}{v_p^2(v_p^2 - v_s^2)} \mathbf{e}^{(2)} + \right. \tag{2.46}$$

$$\left. + \frac{\varepsilon c_{iklm}^{(1)}}{\rho} e_k^{(1)} e_m^{(1)} e_l^{(1)} e_i^{(3)} \frac{2v_s^2 - v_p^2}{v_p^2(v_p^2 - v_s^2)} \mathbf{e}^{(3)} \right] \frac{\psi_p(\alpha,\beta)}{\sqrt{\rho J}} \exp\left\{ \frac{i\omega}{2\rho} \varepsilon c_{iklm}^{(1)} p_k p_m e_l^{(1)} e_i^{(1)} \tau_p \right\}.$$

According to equation (2.46), the additional terms are responsible for the deviation of the polarization vector from $\mathbf{e}^{(1)}$. Thus, this deviation yields a polarization vector which has also components in the plane perpendicular to the reference ray. These components are of the order of ε.

Note that the additional first-order components in the perturbation theory coincide with the corresponding components of equation (2.46) with the exception of a factor. In

perturbation theory, this factor is $\dfrac{1}{v_p^2 - v_s^2}$ (see, e.g., Jech and Pšenčík, 1989; Farra, 2001). However, the QI approximation leads to the factor $\dfrac{2v_s^2 - v_p^2}{v_p^2(v_p^2 - v_s^2)}$, which is smaller than the factor obtained by the perturbation theory. The difference appears due to the second terms in equations (2.42). The terms are connected to the curvature of the wavefront resulting from a point source considered in the QI theory and, therefore, are missing in the the perturbation theory considering plane waves.

2.2.2 qS-waves

In the previous section the following equation for qS waves was obtained (see equations 2.22, 2.27 and 2.30):

$$\mathbf{U}_{qS}^{(0+1A)} = \frac{Y_2(\tau)}{\sqrt{\rho J}}\Big(\cos\gamma\mathbf{e}^{(2)} - \sin\gamma\mathbf{e}^{(3)}\Big) + \frac{Y_3(\tau)}{\sqrt{\rho J}}\Big(\sin\gamma\mathbf{e}^{(2)} + \cos\gamma\mathbf{e}^{(3)}\Big) + \frac{1}{i\omega}\, b_{1s}\,\mathbf{e}^{(1)} \quad (2.47)$$

This equation includes the zeroth-order principal components and first-order additional component. $Y_2(\tau)$ and $Y_3(\tau)$ are obtained from the system (2.34) and the first-order scalar amplitude b_{1s} from equation (2.26). For homogeneous weakly anisotropic media, the system (2.34) decouples and its solutions are given by:

$$\begin{aligned} Y_2(\tau) &= Y_2(0)\exp\left\{\frac{i\omega}{2}\lambda_2\,\tau_s\right\} \\ Y_3(\tau) &= Y_3(0)\exp\left\{\frac{i\omega}{2}\lambda_3\,\tau_s\right\}, \end{aligned} \quad (2.48)$$

where λ_2 and λ_3 are defined by equation (2.33). The traveltime of the S-wave in the background isotropic medium, τ_s, appears instead of the integral along the ray path in (2.38). The functions $Y_2(0)$ and $Y_3(0)$ are defined by initial conditions at $\tau = 0$. They depend on the type of source under consideration.

For homogeneous weakly anisotropic media, the first-order scalar amplitude b_{1s} contains only two terms:

$$b_{1s} = -\frac{i\omega\varepsilon}{(\lambda+\mu)} c_{iklm}^{(1)} e_k^{(1)} e_m^{(1)} e_i^{(1)}\, U_l^{(0)} + v_s \frac{\partial U_\alpha^{(0)}}{\partial x_\alpha}, \quad (2.49)$$

with the zeroth-order principal term $\mathbf{U}^{(0)}$

$$\mathbf{U}^{(0)} = \frac{Y_2}{\sqrt{\rho J}}\Big(\cos\gamma\mathbf{e}^{(2)} - \sin\gamma\mathbf{e}^{(3)}\Big) + \frac{Y_3}{\sqrt{\rho J}}\Big(\sin\gamma\mathbf{e}^{(2)} + \cos\gamma\mathbf{e}^{(3)}\Big)$$

and the angle γ follows from the condition (2.31). As in the case of a qP-wave, equation (2.49) includes an additional first-order term which does not appear in the perturbation theory working with plane waves. The second term in equation (2.49) depends on the curvature of the wavefront. Since the wave front curvature of plane waves is infinite, the derivative $\dfrac{\partial U_\alpha^{(0)}}{\partial x_\alpha} = 0$. The QI approach assumes that the wave field is generated by a point source, therefore, the derivative $\dfrac{\partial U_\alpha^{(0)}}{\partial x_\alpha} \neq 0$.

To compute the derivative $\dfrac{\partial U_\alpha^{(0)}}{\partial x_\alpha}$, the base vectors $\mathbf{e}^{(1)}$, $\mathbf{e}^{(2)}$ and $\mathbf{e}^{(3)}$ are specified using the inclination angle θ and the azimuth angle φ. These two angles describe the ray direction in the isotropic background medium. This ray direction coincides with the base vector $\mathbf{e}^{(1)}$:

$$\mathbf{e}^{(1)} = \begin{pmatrix} \sin\theta\cos\varphi \\ \sin\theta\sin\varphi \\ \cos\theta \end{pmatrix} \tag{2.50}$$

The two mutually orthogonal vectors $\mathbf{e}^{(2)}$ and $\mathbf{e}^{(3)}$ are chosen in the plane perpendicular to the reference ray as

$$\mathbf{e}^{(2)} = \begin{pmatrix} \cos\theta\cos\varphi \\ \cos\theta\sin\varphi \\ -\sin\theta \end{pmatrix}, \qquad \mathbf{e}^{(3)} = \begin{pmatrix} -\sin\varphi \\ \cos\varphi \\ 0. \end{pmatrix}. \tag{2.51}$$

Using these base vectors the derivative $\dfrac{\partial U_\alpha^{(0)}}{\partial x_\alpha}$ can be calculated as follows:

$$\frac{\partial U_\alpha^{(0)}}{\partial x_\alpha} = \frac{\partial}{\partial x_\alpha}\left[\frac{Y_2(0)}{\sqrt{\rho J}}\Big(\cos\gamma\, e_\alpha^{(2)} - \sin\gamma\, e_\alpha^{(3)}\Big)\,\exp\left\{\frac{i\omega}{2\rho}\lambda_2\tau_s\right\}\right.$$

$$\left. + \frac{Y_3(0)}{\sqrt{\rho J}}\Big(\sin\gamma\, e_\alpha^{(2)} + \cos\gamma\, e_\alpha^{(3)}\Big)\,\exp\left\{\frac{i\omega}{2\rho}\lambda_3\tau_s\right\}\right].$$

Taking into account the angle γ from (2.31)

$$\gamma = \frac{1}{2}\arctan\left\{\frac{2B_{23}}{B_{33}-B_{22}}\right\},$$

and λ_2 and λ_3 from (2.33), we can calculate the derivatives $\dfrac{\partial\lambda_2}{\partial x_\alpha}$, $\dfrac{\partial\lambda_3}{\partial x_\alpha}$, and $\dfrac{\partial\gamma}{\partial x_\alpha}$. The calculations of these derivatives are organized into differentiation of the elements of the weak anisotropic matrix $\mathbf{B}$ from (2.24) with respect to the space coordinates x_α. All these calculations are cumbersome, therefore, they are given in the appendix B at the end of this chapter. Resulting from these calculations, the derivative $\dfrac{\partial U_\alpha^{(0)}}{\partial x_\alpha}$ can be written as

$$\frac{\partial U_\alpha^{(0)}}{\partial x_\alpha} = \frac{Y_2(0)}{\sqrt{\rho J}}\frac{1}{R\sin\theta}\,\exp\left\{\frac{i\omega}{2}\lambda_2\tau_s\right\}\left(\frac{\mathcal{H}_2}{(\lambda_3-\lambda_2)^2} + \frac{i\omega}{2\rho}\,\frac{\tau_s\mathcal{N}_2}{\lambda_3-\lambda_2}\right) \tag{2.52}$$

$$+\frac{Y_3(0)}{\sqrt{\rho J}}\frac{1}{R\sin\theta}\,\exp\left\{\frac{i\omega}{2}\lambda_3\tau_s\right\}\left(\frac{\mathcal{H}_3}{(\lambda_3-\lambda_2)^2} + \frac{i\omega}{2\rho}\,\frac{\tau_s\mathcal{N}_3}{\lambda_3-\lambda_2}\right), \tag{2.53}$$

where

$$\mathcal{H}_2 = -\sin\gamma\, D_2 + \cos\gamma\,\cos\theta\,(\lambda_3-\lambda_2)^2 - \cos\gamma\, D_3,$$

$$\mathcal{H}_3 = \cos\gamma\, D_2 + \sin\gamma\,\cos\theta\,(\lambda_3-\lambda_2)^2 - \sin\gamma\, D_3,$$

$$\mathcal{N}_2 = \cos\gamma\,(-\lambda_2 P_2 + Q_2) - \sin\gamma\,(-\lambda_2 P_3 + Q_3)$$

$$\mathcal{N}_3 = \sin\gamma\,(\lambda_3 P_2 + Q_2) + \cos\gamma\,(\lambda_3 P_3 + Q_3),$$

with

$$\begin{aligned}
D_2 &= -B_{23}\Big(S_2^{(33)} - S_2^{(22)}\Big) + \Big(B_{33} - B_{22}\Big)S_2^{(23)} \\
D_3 &= -B_{23}\Big(S_3^{(33)} - S_3^{(22)}\Big) + \Big(B_{33} - B_{22}\Big)S_3^{(23)} \\
P_2 &= S_2^{(22)} + S_2^{(33)} \\
P_3 &= S_3^{(22)} + S_3^{(33)} \\
Q_2 &= B_{22}S_2^{(33)} + B_{33}S_2^{(22)} - 2B_{23}S_2^{(23)} \\
Q_3 &= B_{22}S_3^{(33)} + B_{33}S_3^{(22)} - 2B_{23}S_3^{(23)}
\end{aligned}$$

and

$$\begin{aligned}
S_2^{(22)} &= \frac{2\,\sin\theta}{v_s^2}\Big(\varepsilon c_{iklm}^{(1)} e_i^{(2)} e_k^{(2)} e_l^{(2)} e_m^{(1)} - \varepsilon c_{iklm}^{(1)} e_i^{(2)} e_k^{(1)} e_l^{(1)} e_m^{(1)}\Big) \\
S_3^{(22)} &= \frac{2\,\sin\theta}{v_s^2}\,\varepsilon c_{iklm}^{(1)} e_i^{(2)} e_k^{(3)} e_l^{(2)} e_m^{(1)} + \frac{2\cos\theta}{v_s^2}\,\varepsilon c_{iklm}^{(1)} e_i^{(2)} e_k^{(1)} e_l^{(3)} e_m^{(1)} \\
S_2^{(33)} &= \frac{2\,\sin\theta}{v_s^2}\,\varepsilon c_{iklm}^{(1)} e_i^{(3)} e_k^{(2)} e_l^{(3)} e_m^{(1)} \\
S_3^{(33)} &= \frac{2\,\sin\theta}{v_s^2}\Big(\varepsilon c_{iklm}^{(1)} e_i^{(3)} e_k^{(3)} e_l^{(3)} e_m^{(1)} - \varepsilon c_{iklm}^{(1)} e_i^{(3)} e_k^{(1)} e_l^{(1)} e_m^{(1)}\Big) - \frac{2\cos\theta}{v_s^2}\,\varepsilon c_{iklm}^{(1)} e_i^{(3)} e_k^{(1)} e_l^{(2)} e_m^{(1)} \\
S_2^{(23)} &= \frac{\sin\theta}{v_s^2}\Big(\varepsilon c_{iklm}^{(1)} e_i^{(3)} e_k^{(2)} e_l^{(2)} e_m^{(1)} + \varepsilon c_{iklm} e_i^{(3)} e_k^{(1)} e_l^{(2)} e_m^{(2)} - \varepsilon c_{iklm}^{(1)} e_i^{(3)} e_k^{(1)} e_l^{(1)} e_m^{(1)}\Big) \\
S_3^{(23)} &= \frac{\sin\theta}{v_s^2}\Big(\varepsilon c_{iklm}^{(1)} e_i^{(3)} e_k^{(3)} e_l^{(2)} e_m^{(1)} + \varepsilon c_{iklm} e_i^{(3)} e_k^{(1)} e_l^{(2)} e_m^{(3)} - \varepsilon c_{iklm}^{(1)} e_i^{(1)} e_k^{(1)} e_l^{(2)} e_m^{(1)}\Big) \\
&\quad + \frac{\cos\theta}{v_s^2}\Big(\varepsilon c_{iklm}^{(1)} e_i^{(3)} e_k^{(1)} e_l^{(3)} e_m^{(1)} - \varepsilon c_{iklm}^{(1)} e_i^{(2)} e_k^{(1)} e_l^{(2)} e_m^{(1)}\Big).
\end{aligned}$$

Note that in equation (2.52) I have not taken into account the derivatives

$$\frac{\partial}{\partial x_\alpha}\left(\frac{Y_2(0)}{\sqrt{\rho J}}\right) \quad \text{and} \quad \frac{\partial}{\partial x_\alpha}\left(\frac{Y_3(0)}{\sqrt{\rho J}}\right).$$

They depend on the type of source considered. Consideration of the sources is a special topic which is outside the scope of my work.

After substituting (2.52) into (2.47) we get for qS waves

$$\begin{aligned}\mathbf{U}_{qS}^{(0+1A)} = &\left[\mathbf{g}^{(2)} + \left(- \frac{\varepsilon c_{iklm}^{(1)} e_i^{(1)} e_k^{(1)} e_l^{(1)} \mathrm{g}_m^{(2)}}{\lambda + \mu} + \frac{1}{\sin\theta} \frac{1}{(\lambda_3 - \lambda_2)} \frac{\mathcal{N}_2}{2\rho} \right.\right. \\ &\left.\left. + \frac{1}{i\omega} \frac{1}{R \sin\theta} \frac{v_s \mathcal{H}_2}{(\lambda_3 - \lambda_2)^2} \right) \mathbf{e}^{(1)} \right] \times \frac{Y_2(0)}{\sqrt{\rho J}} \exp\left\{ \frac{i\omega}{2\rho} \lambda_2 \tau_s \right\} \\ &+ \left[\mathbf{g}^{(3)} + \left(- \frac{\varepsilon c_{iklm}^{(1)} e_i^{(1)} e_k^{(1)} e_l^{(1)} \mathrm{g}_m^{(3)}}{\lambda + \mu} + \frac{1}{\sin\theta} \frac{1}{(\lambda_3 - \lambda_2)} \frac{\mathcal{N}_3}{2\rho} \right.\right. \\ &\left.\left. + \frac{1}{i\omega} \frac{1}{R \sin\theta} \frac{v_s \mathcal{H}_3}{(\lambda_3 - \lambda_2)^2} \right) \mathbf{e}^{(1)} \right] \times \frac{Y_3(0)}{\sqrt{\rho J}} \exp\left\{ \frac{i\omega}{2\rho} \lambda_3 \tau_s \right\}. \end{aligned} \tag{2.54}$$

According to equation (2.54), the QI isotropic approximation $\mathbf{U}_{qS}^{(0+1A)}$ represents a superposition of two qS-waves. The first two lines correspond to one qS-wave, and the last two lines to a second qS-wave. From (2.54) we can also conclude that in homogeneous weakly anisotropic media, the first-order additional term causes the deviation of the polarization vectors from the vectors $\mathbf{g}^{(2)}$ and $\mathbf{g}^{(3)}$ describing two linearly polarized S-waves in the background isotropic medium. Furthermore, the additional first-order term causes the frequency dependence due to the factor $\frac{1}{i\omega}$. It means that in the time domain, the signal form is distorted.

Equation (2.54) also allows to recognize a drawback of the QI approach. Two terms in (2.54) are proportional to the factor $\frac{1}{\lambda_3 - \lambda_2}$. Therefore, these terms become infinite in the regions where $(\lambda_3 - \lambda_2) \to 0$. This happens if the two qS-waves propagate with nearly the same velocities. It should be noted that the order of $\mathcal{N}_2$ and $\mathcal{N}_3$ is ε^2, whereas the order of λ_2 and λ_3 is ε. Therefore, one can write

$$\frac{\mathcal{N}_2}{\lambda_3 - \lambda_2} = \frac{\varepsilon^2 \hat{\mathcal{N}}_2}{\varepsilon(\hat{\lambda}_3 - \hat{\lambda}_2)}, \tag{2.55}$$

To indicate the order of terms $\mathcal{N}_2$ and $\lambda_3 - \lambda_2$ in equation (2.55), the parameter ε is separated from them. The symbols with " $\hat{}$ " denote the corresponding magnitudes of $\mathcal{N}_2$, λ_2 or λ_3 without the parameter ε. For the regions where two qS-waves propagate with nearly the same velocities, the value of (2.55) is finite only if $\varepsilon \sim (\hat{\lambda}_3 - \hat{\lambda}_2)$. This is true only for an infinitely weak anisotropic media. For finite values of ε, which correspond to a moderate or weak anisotropy, the factor (2.55) tends to infinity as the qS-waves approach regions with $(\lambda_3 - \lambda_2) \to 0$. In the case of homogeneous anisotropic media, these regions appear around so-called singular directions. In these directions wavefronts of the two qS waves cross each other, or are tangent to each other. Farra (2001) investigated the perturbation method and found similar problems in singular directions. This shows that for any weak or moderate anisotropy the QI approximation method, as well as the perturbation theory, produce distorted results. The ray theory for anisotropic media also fails in the singular direction. But in contrast to the anisotropic ray theory, in the QI approach this manifests only in the first-order approximation. In principle, the values of (2.55) can be used to identify the singular directions.

The terms with the factors $\frac{\mathcal{H}_2}{(\lambda_3-\lambda_2)^2}$ and $\frac{\mathcal{H}_3}{(\lambda_3-\lambda_2)^2}$ do not exhibit such a dramatical behavior, because these factors are compensated by the factor $\frac{1}{i\omega R}$ which is in the order of $\frac{\varepsilon}{R}$.

Also note that the behavior associated with factor $\frac{1}{\sin\theta}$ is caused by the choice of the coordinate system, not by the QI approach.

2.3 Numerical tests of the quality of the QI solution

To apply the QI approach to weakly anisotropic media one has to know how reliable this approximation is. Therefore, this section is concerned with validating the results obtained by the QI approach.

Pšenčík and Dellinger (2001) presented numerical results obtained by the zeroth-order approximation of the QI approach for qS-waves in inhomogeneous weakly anisotropic media. As models they considered vertically inhomogeneous weakly anisotropic HTI (transversely isotropic with a horizontal axis of symmetry) media, with the symmetry axis of the HTI anisotropy rotated by 45° from the plane defined by the source-receiver offsets of the VSP. Their two models differed only in the strength of anisotropy: 0.02–0.1% (very weak anisotropic model) and 1–4% (weak anisotropic model). For each model, Pšenčík and Dellinger compared results obtained by the zeroth-order approximation of the QI approach with the zeroth-order of the ray methods for anisotropic and isotropic media. As a "reality check", they used the seismograms computed by a non-ray algorithm, the anisotropic reflectivity modeling program "Anivec" (Mallick and Frazer, 1990). The comparisons showed that for both models the zeroth-order QI approach represents a link between the ray method for isotropic and anisotropic media. The QI approach produced correct results for the very weak anisotropic model as well as for the weak anisotropic model, whereas the standard anisotropic ray theory failed to describe the amplitudes of the qS-waves in the very weak anisotropic model.

Following Pšenčík and Dellinger (2001), in this section, I compare results obtained by the QI approach with the results obtained by ray and non-ray methods. Homogeneous weakly anisotropic media with different types of symmetry (transversely isotropic and orthorombic) and different strength of anisotropy (5%, 8.3%) are considered. For all models, I also compute the zeroth-order as well as the first-order approximation of the QI approach.

The equations for homogeneous weakly anisotropic media obtained in the previous section can be directly used to compute traveltimes, polarizations and seismograms for waves propagating in homogeneous weakly anisotropic media. For validation purposes, the seismograms obtained by the QI approach are compared with seismograms computed by other methods. I computed seismograms using standard ray theory for anisotropic (ART) as well as for isotropic (IRT) media. The seismograms obtained by the ray method for anisotropic media are used for comparison with the seismograms obtained by the QI approach. Also, traveltimes and qS-wave polarization vectors obtained the QI approach and the standard ray theory for anisotropic media are analyzed. The ray method for

isotropic media is applied to compute the seismograms in the background isotropic medium required in the QI approach.

Because the ART method fails to produce correct results for the singular regions of anisotropic media, I also computed seismograms by a numerical forward modeling algorithm using a pseudo-spectral method (Kosloff and Baysal, 1982; Tessmer, 1995). The actual program is derived from a modeling code for general material anisotropy described in Tessmer (1995). These seismograms are considered as exact. They allow to investigate the behavior of the QI approach also in the singular directions.

2.3.1 Implementation of the QI approach

To implement the QI approach, I begin by defining a background isotropic medium, obtaining the necessary isotropic P- and S-wave velocities, v_p and v_s, using equations for the best fitting isotropic medium derived by Fedorov (1968). They were obtained by minimizing the norm of differences between the elastic coefficients of the anisotropic and the isotropic medium (see the appendix at the end of the chapter 4 on page 86). A ray connecting the source and receiver is calculated in the background isotropic medium. The geometrical spreading of the S- or P-wave in the isotropic medium is calculated along this ray.

In the homogeneous case all these calculations are simple, because, the ray is a straight line and the geometrical spreading is $\frac{1}{R}$, where R is the distance between the source and the receiver along the straight line.

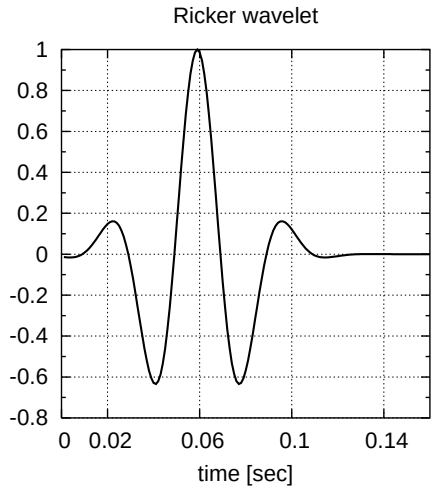

Figure 2.1: The Ricker wavelet used for all numerical examples. The dominant frequency of this wavelet is about 25 Hz

When a unit force is used as a source, the ray method for isotropic media leads to the following equations for S- and P-waves:

$$\mathbf{u}^{(P)} = \frac{\left(\mathbf{f},\mathbf{e}^{(1)}\right)\,\mathbf{e}^{(1)}}{4\pi v_p^2 R}\,\Phi\left(t-\frac{R}{v_p}\right) \tag{2.56}$$

$$\mathbf{u}^{(S)} = \frac{\mathbf{f}-\left(\mathbf{f},\mathbf{e}^{(1)}\right)\,\mathbf{e}^{(1)}}{4\pi v_s^2 R}\,\Phi\left(t-\frac{R}{v_s}\right), \tag{2.57}$$

where $\mathbf{f}$ is a unit vector defining the unit force; $\mathbf{e}^{(1)}$ is the unit vector along the ray, see equations (2.6) and (2.8); the source time function Φ, a Ricker wavelet, is shown in Figure 2.1. The dominant frequency of this wavelet is 25 Hz. The equations (2.56) and (2.57) are used to compute the seismograms in the isotropic background medium.

The next step is the determination of the QI amplitudes of zeroth- and first-order for the qP- and two the qS-waves using equations (2.15), (2.16), (2.26) and the system of two equations (2.23). Due to the frequency dependence of all these equations, the QI amplitudes have to be determined for each frequency within the frequency band of the source time function. In the homogeneous case, the simpler equations (2.46) and (2.54) are used.

Finally, Fourier transformation into the time domain is performed to obtain seismograms. To estimate the contributions of the zeroth- and first-order terms, two types of seismograms are computed: seismograms for which the terms of both order are taken into account and seismograms for which only the zeroth-order terms are considered.

2.3.2 Ray theory for homogeneous anisotropic media

Traveltimes, polarization vectors and seismograms obtained by the standard ray theory for anisotropic media are compared with the QI approach results. For a unit force $\mathbf{f}$ in a homogeneous anisotropic medium, the anisotropic ray theory leads to the following expression for each wave (see, e.g., Petrashen et al., 1984, pp.154–155):

$$\mathbf{u}^{(K)} = I_0^{(K)}(\mathbf{f},\, \mathbf{A}^{(K)})\; \mathbf{A}^{(K)} \Phi \left(t - \tau^{(K)}(\mathbf{x})\right), \qquad K = 1, 2, 3 \tag{2.58}$$

where the index K enumerates the three waves propagating in the anisotropic medium; $\mathbf{A}^{(K)}$ is the polarization vector of the Kth-wave; the source time function Φ is shown in Figure 2.1, and the intensity $I_0^{(K)}$ of the K-wave is defined as

$$I_0^{(K)} = \frac{1}{4\pi\rho\, v_K^{3/2} |\boldsymbol{\xi}_K|^{1/2} L_K},$$

with the density ρ, the geometrical spreading L_K, the ray velocity $\boldsymbol{\xi}_K$ and the phase velocity v_K of the Kth-wave.

2.3.3 The non-ray solutions

The non-ray solutions (considered as exact) for the comparisons are calculated with a numerical forward modeling algorithm which is based on the Fourier (or pseudo-spectral) method (Kosloff and Baysal, 1982). The actual program which is used for the calculations was derived from a modeling code for general material anisotropy described in Tessmer (1995). The program computes the full wave field on a 3-D grid and, therefore accounts for all wave types. The method does not allow to compute waves separately, therefore, all comparisons are carried out using seismograms at the receiver positions. For modeling also the Ricker wavelet shown in Figure 2.1 was used.

2.3.4 Scheme of numerical experiments

For the following investigation with different media, the vertical seismic profile (VSP) configuration is used (see Figure 2.2). The source, a tilted or vertical unit force, is situated at the point S. There are four wells denoted as well 1, well 2, well 3 and well 4 in Figure 2.2. All wells have the same distance from the source. All wells are parallel to the Z-axis. In each well 26 receivers are uniformly distributed with a spacing of 32 m, and receiver depths ranging from 0 m to 800 m. Three-component receivers record the X-, Y- and Z-components of the wave field. The effects of the free surface are neglected throughout. All calculated seismograms will be shown without scaling between the components, so true relative amplitudes can be seen.

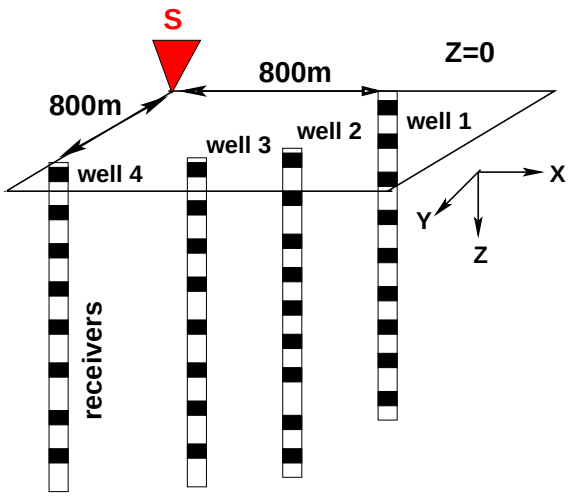

Figure 2.2: A schematic illustration of the VSP configuration used for all numerical experiments in this section.

2.3.5 VTI medium

First, a homogeneous transversely isotropic medium with the symmetry axis parallel to the Z-axis (VTI) is considered. The density normalized elastic parameters are $A_{11} = 13.59$, $A_{33} = 12.23$, $A_{44} = 3.06$, $A_{66} = 3.4$ and $A_{13} = 6.12$ km^2/s^2 (Thomsen parameters $\varepsilon = 0.056$, $\gamma = 0.056$ and $\delta = 0.001$). The deviation from isotropy is 5%. The source, a tilted unit force

$$\mathbf{f} = (\sin\theta\cos\varphi, \sin\theta\sin\varphi, \cos\theta) \tag{2.59}$$

with $\theta = 45°$ and $\varphi = 45°$, generates all types of waves propagating in a VTI medium: qP, qSV and SH waves. Figure 2.3 shows the phase velocities of the two qS-waves with respect to the angle θ between the Z-axis and the wavefront normal. The VTI medium considered has two singularities: The two phase velocity curves are tangent to each other (kiss singularity) at $\theta = 0°$ and cross each other (intersection singularity) at $\theta \approx 59°$. The kiss singularity is located outside of the aperture of the numerical experiment (see Fig. 2.2), but the intersection singularity is within the aperture.

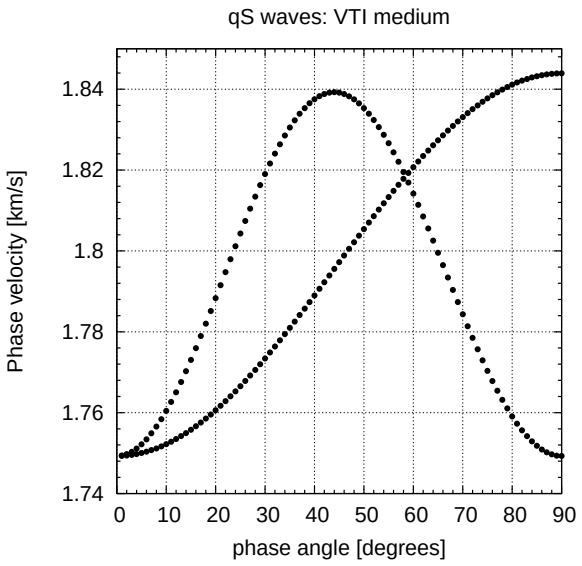

Figure 2.3: Phase velocities of qSV- and SH waves propagating in the VTI medium with respect to the phase angle θ. The angle $\theta = 0°$ corresponds to the Z-direction. The curves cross each other at $\theta \approx 59°$ and are tangent to each other at $\theta = 0°$. In the numerical VSP experiment an angle interval from $\theta = 45°$ to $90°$ is considered.

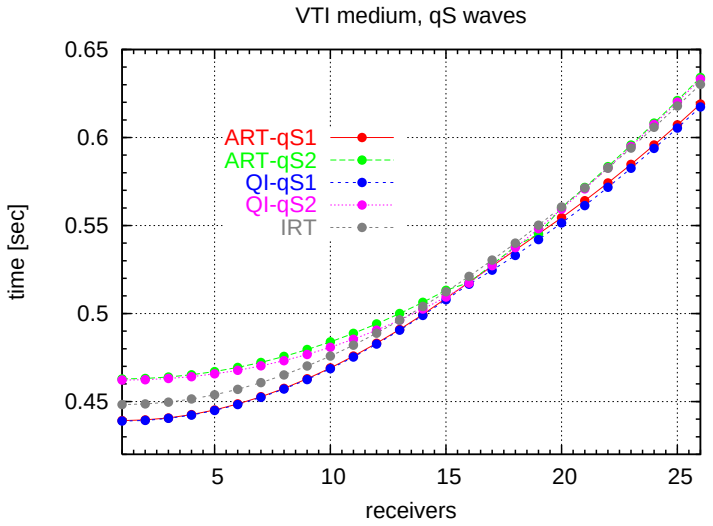

Figure 2.4: Traveltime curves of qS-waves propagating in a VTI medium calculated by the ART method (red and green), by the QI approach (blue and pink) and the IRT method for the background isotropic medium (gray). Note that the ART method fails to compute traveltimes for the fast qS-wave at the receivers 14 to 19.

The P and S velocities of the background medium are 3.6 and 1.81 km/s respectively. Traveltimes from the source position to the receiver positions (see Fig. 2.2) are computed using three methods. Since, all wells are situated at the same distance from the source and the VTI medium possesses rotational symmetry, the traveltimes curve for all wells are identical (amplitudes, however, are not identical for different azimuth due to the different source conditions). In Figure 2.4 the traveltime curves of the qS-waves computed by the ray theory for anisotropic media (throughout my thesis I use the abbreviation ART for the ray theory for anisotropic media) are given by red and green lines, the traveltimes from the QI approach — by blue and pink lines, and the traveltime curve in the background isotropic medium computed by the ray method for isotropic media is shown by the gray line. The ART and QI traveltime curves are very close.

The ART method fails to compute traveltimes for the fast qS-wave at the receivers 14 to 19. These six receivers are close to the singular direction where the two qS wavefronts are close to each other. At the receivers 1–14 the first wave is the SH-wave, but at receivers 15–26 it is the qSV-wave. For the former receiver group the slow wave is the qSV-wave, but it is the SH-wave for the latter group of receivers. (Please note that for the first receiver the phase angle θ is 90°.)

Figures 2.5 (well 2) and 2.6 (well 4) show three-component (X,Y,Z) seismograms obtained by numerical forward modeling (black), the ART method (red) and seismograms in the background isotropic medium (green). The ART seismograms agree very well with the exact seismograms with exceptions at receivers 14 and 16 near the singularity at $\theta = 59°$, where the ART method fails.

My goal was to validate the QI approach. Therefore, Figures 2.7 (well 2) and 2.8 (well 4) compare three-component seismograms obtained by numerical forward modeling (black) and the zeroth-order QI approach (blue). For comparison, also the seismograms for

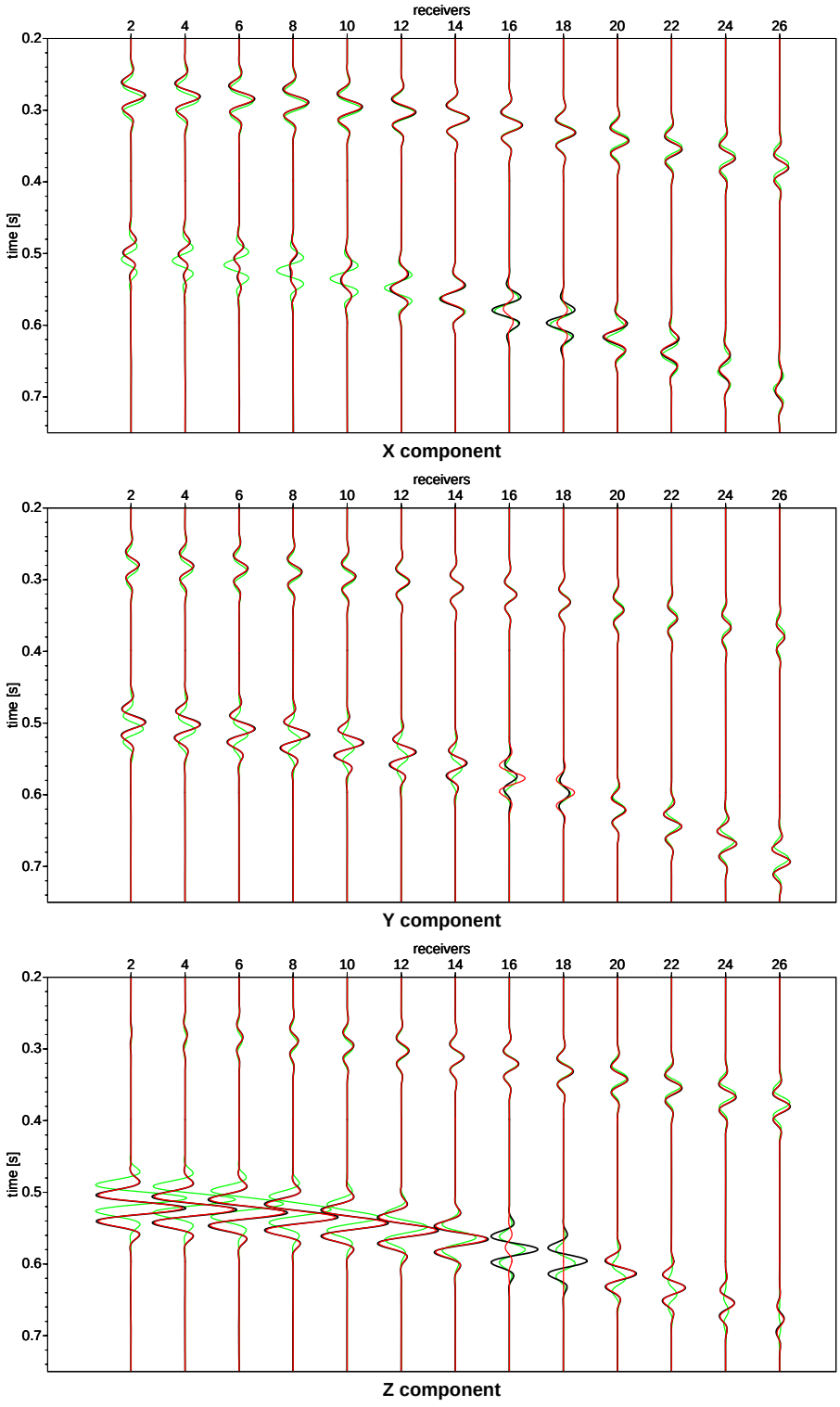

Figure 2.5: VTI medium, well 2. Synthetic seismograms calculated by the ART method (red) and numerical forward modeling (black). The seismograms for the background isotropic medium computed by the IRT method are shown by green lines. Only seismograms for even-numbered receivers are displayed. Red and black lines correlate well with the exception of traces 16 and 18 which are close to the singular direction. (See also the traveltime curves in Fig. 2.4.)

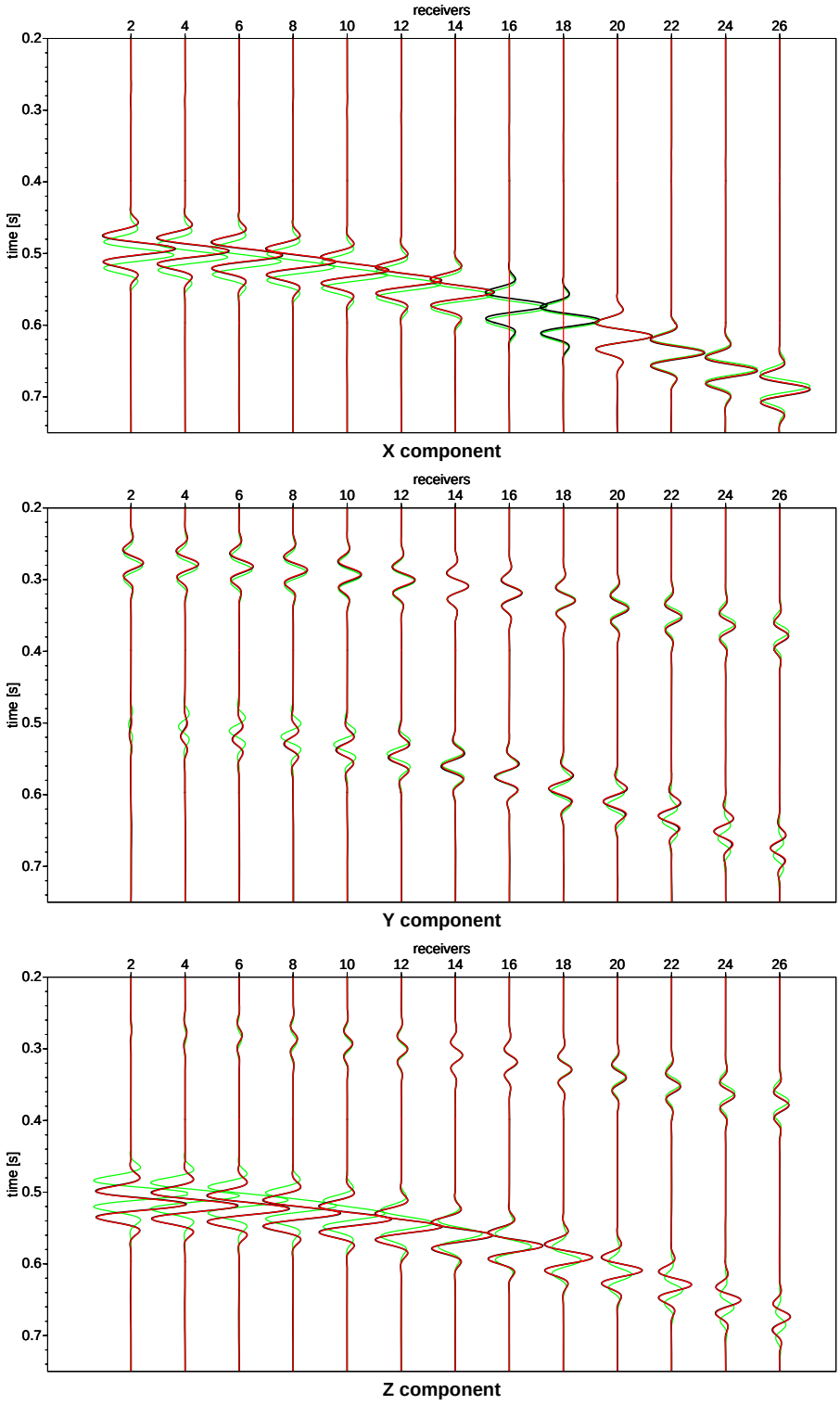

Figure 2.6: VTI medium, well 4. Synthetic seismograms calculated by the ART method (red) and numerical forward modeling (black). The seismograms for the background isotropic medium computed by the IRT method are shown by green lines. Only seismograms for even-numbered receivers are displayed. Red and black lines correlate well with the exception of traces 16 and 18 which are close to the singular direction. (See also traveltime curves in Fig. 2.4.)

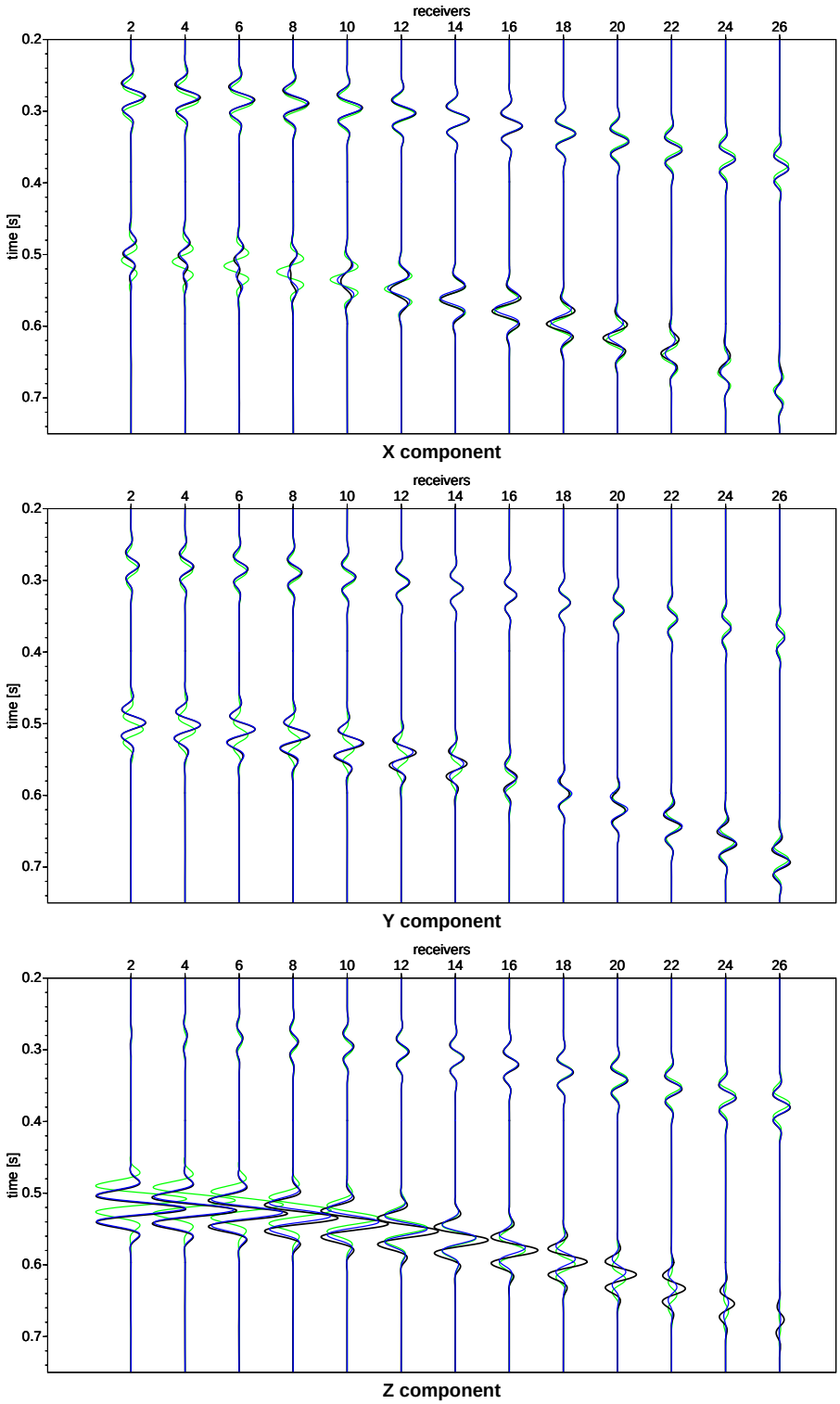

Figure 2.7: VTI medium, well 2. Synthetic seismograms calculated by the QI approach (blue) and numerical forward modeling (black). The seismograms for the background isotropic medium computed by the IRT method are given by green color. The QI seismograms agree well with the exact (black) seismograms on the X- and Y-components, which contain mainly the SH-wave. The Z-component which contains only the qS-wave attenuates faster with depth than the exact seismograms. Only seismograms for even-numbered receivers are shown. (See also traveltime curves in Fig. 2.4.)

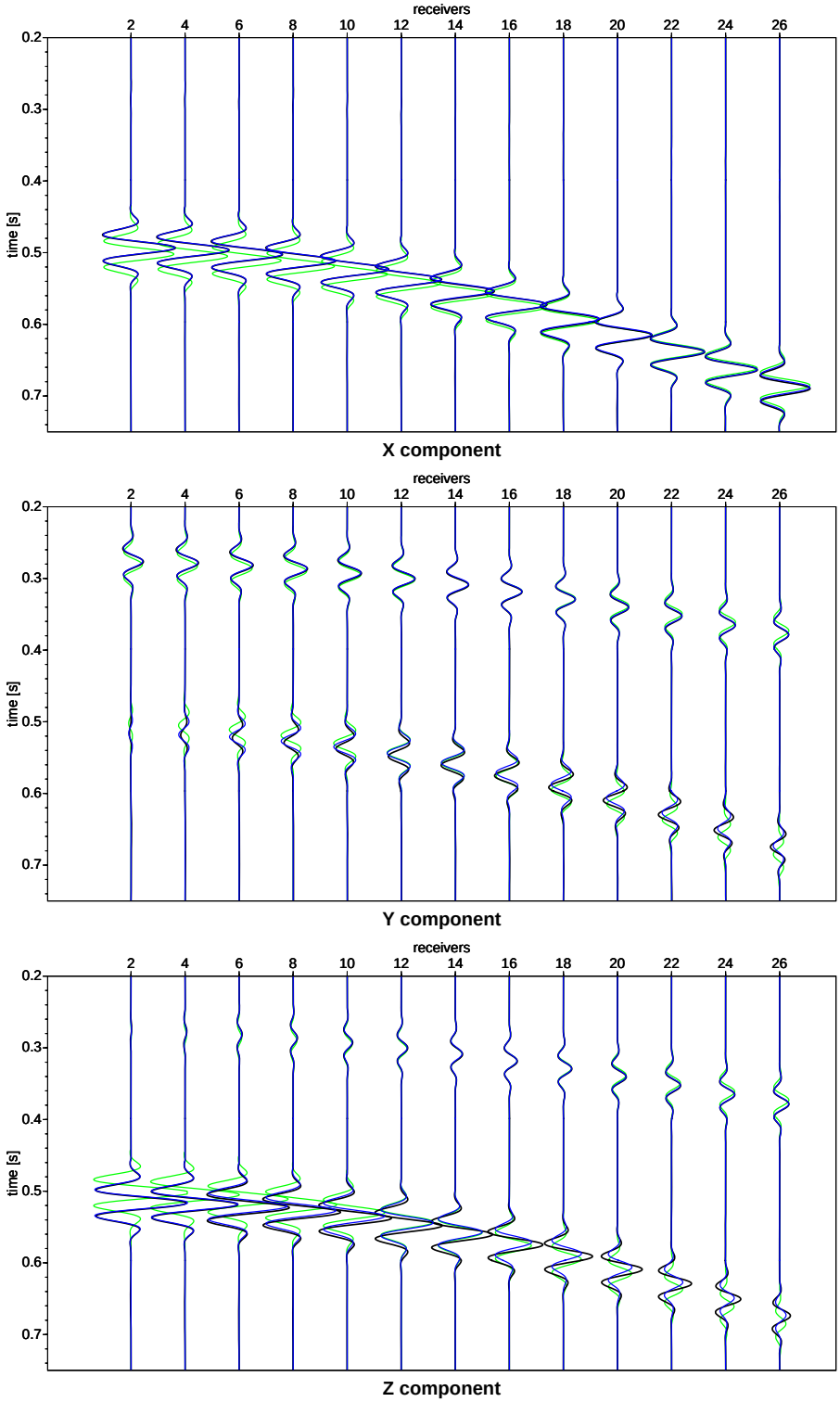

Figure 2.8: VTI medium, well 4. Synthetic seismograms calculated by the QI approach (blue) and numerical forward modeling (black). The seismograms for the background isotropic medium computed by the IRT method are given by green color. The QI seismograms agree well with the exact (black) seismograms on the X- and Y-components. The X-component contains only the SH-wave. The Z-component which contains only the qS-wave attenuates faster with depth than the exact seismograms. Only seismograms for even-numbered receivers are shown. (See also traveltime curves in Fig. 2.4.)

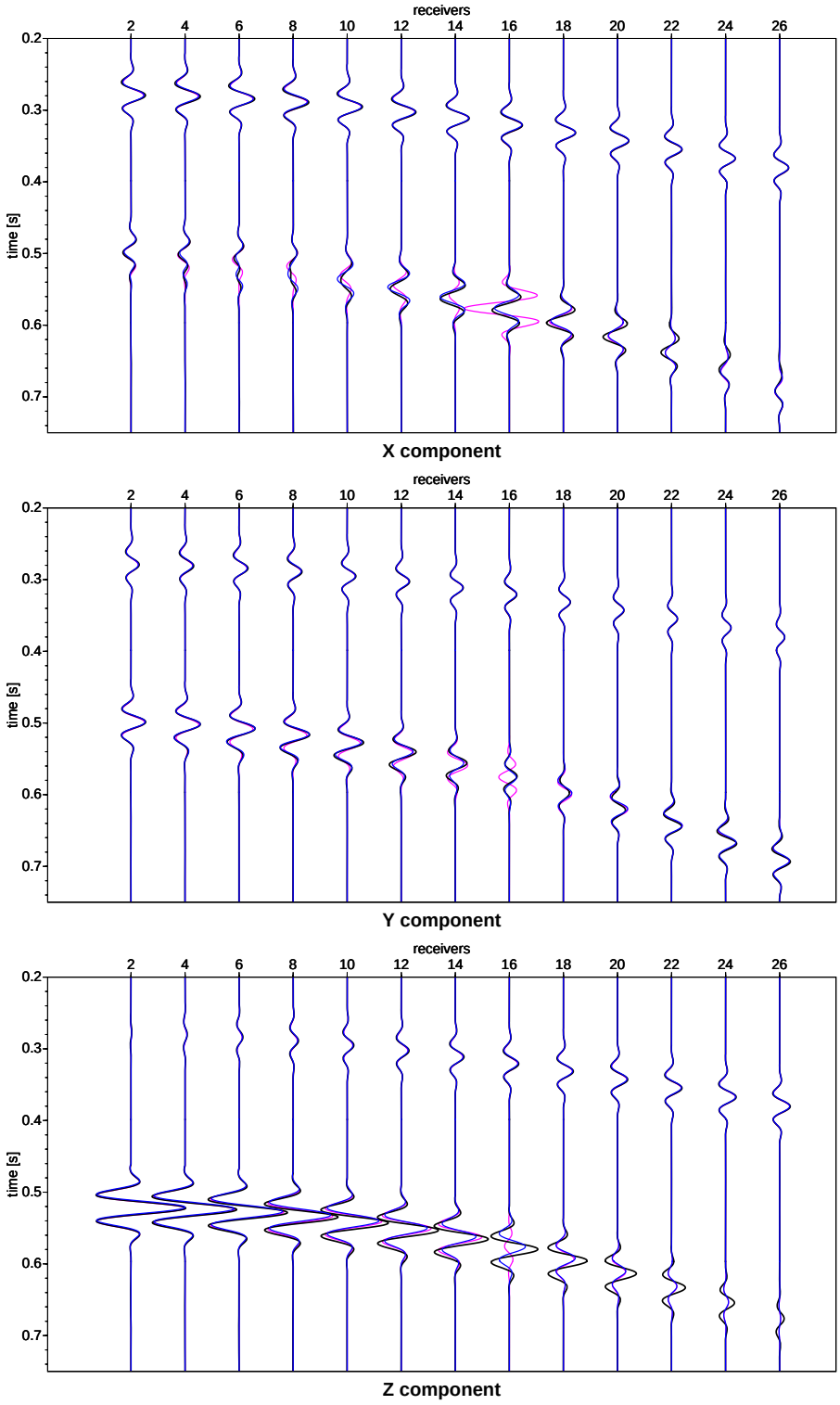

Figure 2.9: VTI medium, well 2. Synthetic seismograms calculated by numerical forward modeling (black), by the zeroth-order (blue) and by the zeroth- and first-order (pink) QI approach. Blue and pink seismograms are barely distinguishable for most receivers except the receivers 14–20. These receivers are situated near the singularity, where the first-order additional terms of the QI approximation go to infinity. (See also traveltime curves in Fig. 2.4.)

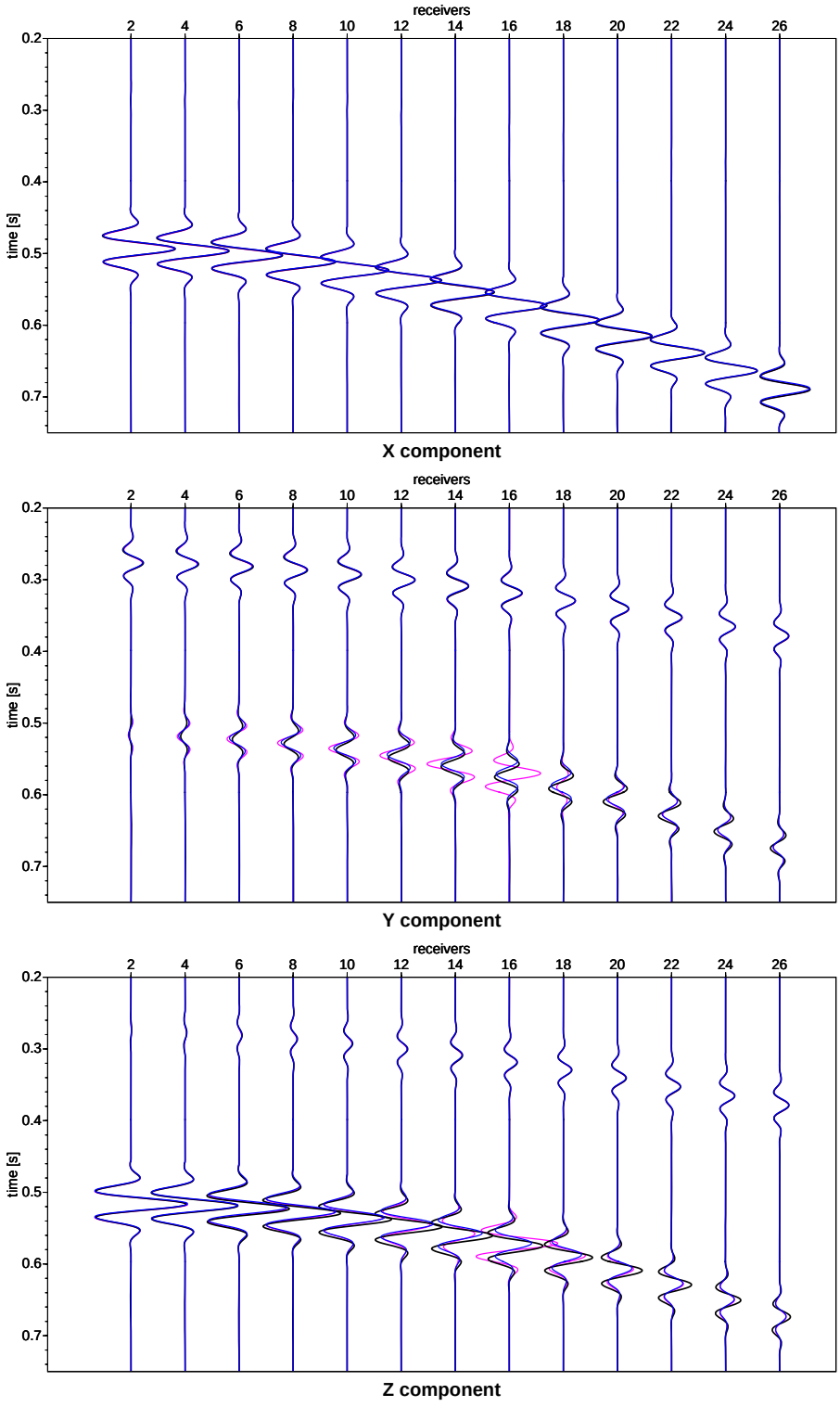

Figure 2.10: VTI medium, well 4. Synthetic seismograms calculated by numerical forward modeling (black), by the zeroth-order (blue) and by the zeroth- and first-order (pink) QI approach. Blue and pink seismograms coincide for most receivers except the receivers 14–20. These receivers are situated near the singularity, where the first-order additional terms of the QI approximation go to infinity. (See also traveltime curves in Fig. 2.4.)

the background isotropic medium are presented (green). One can see that the QI approach yields a good approximation for the qP-wave. The black and blue seismograms of the qP-wave coincide very well. The QI approximation also leads to a good approximation for the SH-wave. The Y- and X-components for well 2 containing mainly SH-waves agree well with the exact (black) seismograms. For the qSV-wave the approximation is worse. The Z-component of the seismograms contain only the qSV-wave. For both wells the Z-component of the exact and QI seismograms do not correlate so well. The zeroth-order QI approach yields a qSV-wave which attenuates faster with depth, then the qSV-waves of the exact seismograms (black).

How much does the QI solution improve, if the additional terms of the first-order approximation are taken into account? On Figures 2.9 and 2.10 the seismograms computed by the numerical forward modeling (black), the zeroth-order QI approach (blue) and the zeroth- and first-order QI approach (pink) are shown. One can see that taking into account the additional first-order terms only slightly improves the QI seismograms. The pink and blue seismograms are barely distinguishable for most receivers except the receivers 14–20. These receivers are situated near the singularity, where the additional first-order terms go to infinity due to the factor $\dfrac{1}{\lambda_3 - \lambda_2}$ (see eq. (2.55) and discussion on the page 36).

2.3.6 Orthorombic medium

The next model considered is a homogeneous orthorombic medium used by Farra (2001). The density normalized elastic parameters are (in km^2/s^2)

$$A_{ik} = \begin{pmatrix} 10.8 & 2.2 & 1.9 & 0. & 0. & 0. \\ & 11.3 & 1.7 & 0. & 0. & 0 \\ & & 8.5 & 0. & 0. & 0. \\ & & & 3.6 & 0. & 0. \\ & & & & 3.9 & 0. \\ & & & & & 4.3 \end{pmatrix} \tag{2.60}$$

The deviation from isotropy is 8.3%. Figure 2.11 shows phase velocities of the two qS-waves with respect to the phase angles: the inclination angle θ for the XZ- and YZ-plane and the azimuth angle φ for the XY-plane. The orthorombic medium considered has a singularity around $\theta \approx 35^\circ$ where the two phase velocity surfaces cross each other.

The P- and S-wave velocities of the background medium are 3.17 and 2.0 km/s respectively. The source is the same tilted force (2.59) as in the previous example. It generates all types of waves propagating in the orthorombic medium. As for the previous VTI model, the traveltimes from the source to the receiver positions (see Fig. 2.2) are computed using three methods. In Figure 2.12 the traveltime curves of qS-waves computed by the ART method are given by red and green lines, by the QI approach by blue and pink lines, and the traveltime curve in the background isotropic medium is shown by the gray color. The ART and QI traveltimes of the slow qS-waves are very close for all four wells: the red and blue curves are barely distinguishable. But in the case of the fast qS-waves, the QI approach produces slightly smaller traveltimes in comparison to the corresponding ART traveltimes. Please note that the traveltime curves of the fast and slow qS-waves approach each other at the lower receivers in the wells 1 and 4. This happens because these receivers are near the singularity, see Figure 2.11.

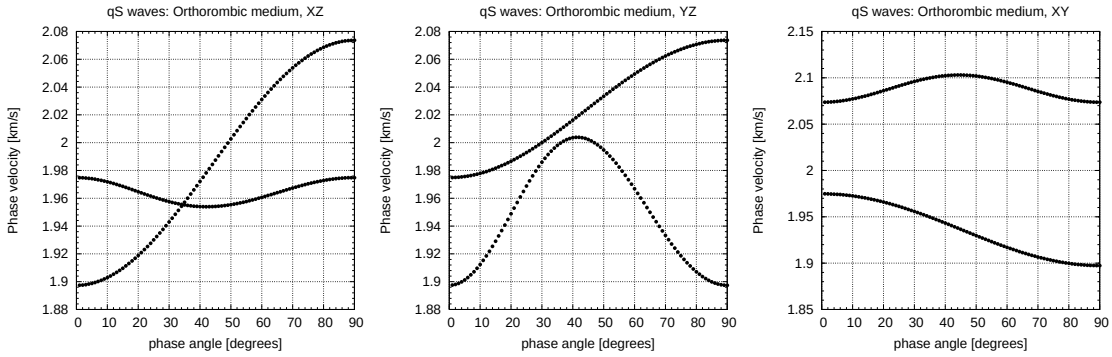

Figure 2.11: Phase velocities of qS-waves propagating in an orthorombic medium considered in the XZ-, YZ- and XY-planes. The angle $\theta = 0°$ corresponds to the Z-direction. The phase velocity curves cross each other or are close to each other at $\theta \approx 35°$.

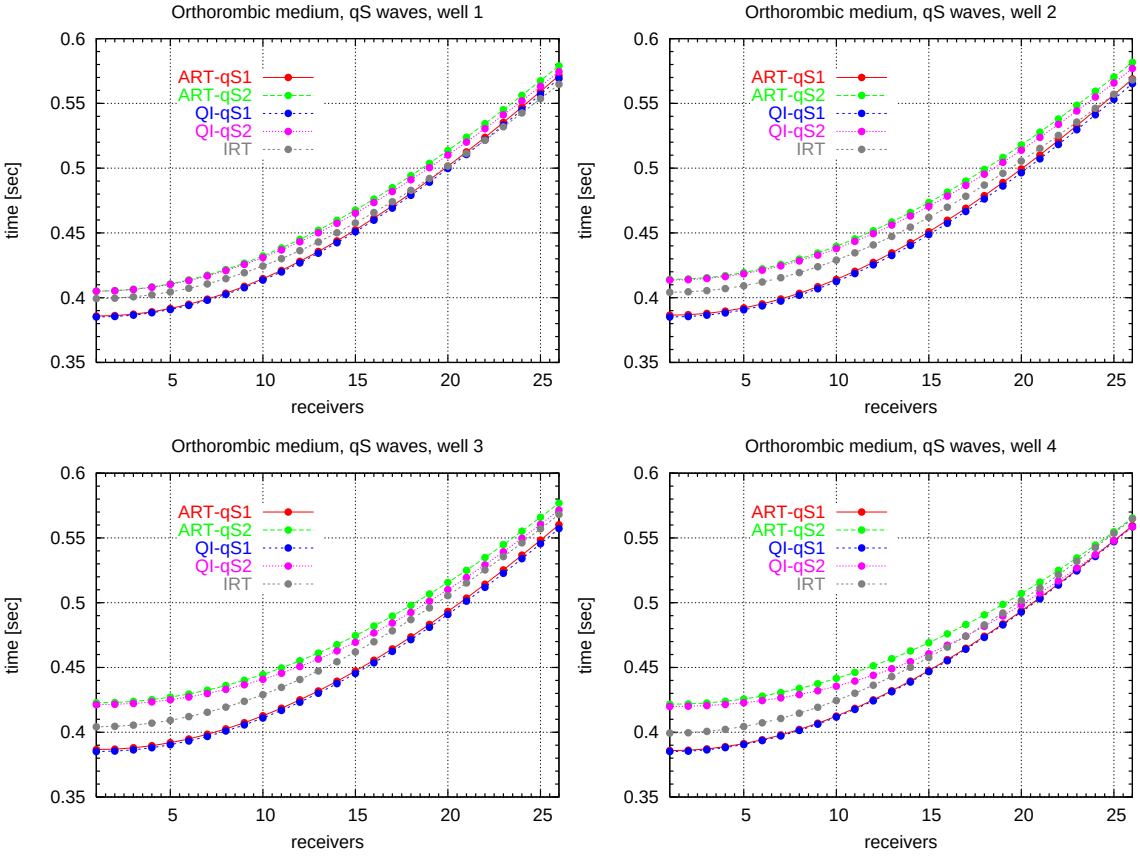

Figure 2.12: Traveltime curves of the qS-waves in an orthorombic medium for all four wells calculated by the ART method (red and green), by the QI approach (blue and pink) and the IRT method for the background isotropic medium (gray).

Figure 2.13 shows a map of the angular deviation between the qS-wave exact polarization vectors and the zeroth-order approximated polarization vectors as a function of the ray angles θ and φ. The angles θ and φ define the ray direction. The regions with strong deviations (dark color) correspond to singular regions of the orthorombic medium.

Now I will compare the seismograms. The ART seismograms and seismograms com-

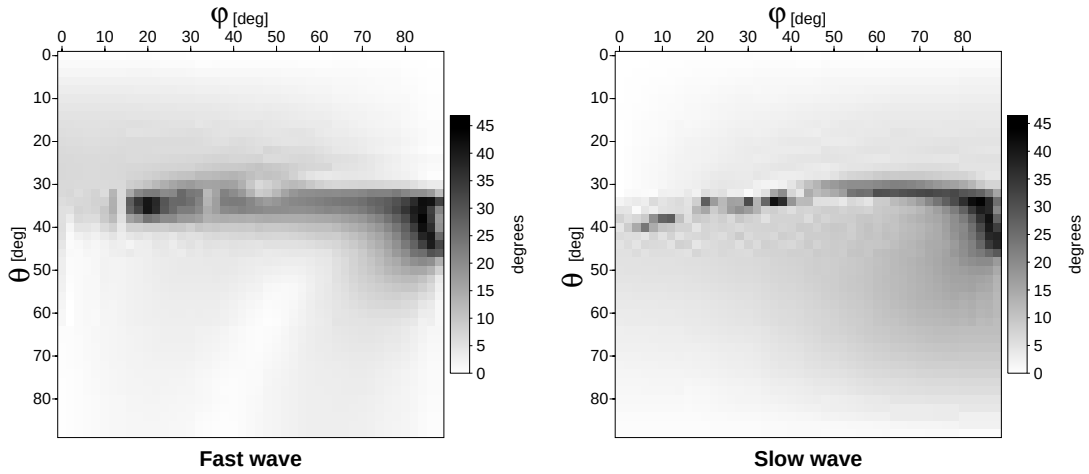

Figure 2.13: A map of angular deviation between the qS-wave polarization vectors in an orthorombic medium obtained by the zeroth-order QI approximation and the corresponding polarization vectors obtained by the ART method. The inclination angle θ and azimuth angle φ define the ray direction. The regions with strong deviations (dark color) correspond to singular regions of the orthorombic medium.

puted by numerical forward modeling coincide almost perfectly, therefore, I do not present figures with this comparison. I compare the seismograms computed by the zeroth- and first-order QI approach with the numerical forward modeling seismograms considered as exact seismograms. In Figures 2.14 and 2.15 the seismograms for wells 1 and 4 computed by numerical forward modeling (black), zeroth-order QI approach (blue) and zeroth- and first-order QI approach (pink) are shown. For well 1 the QI and exact seismograms agree well: black and blue lines are close to each other. The Z-components of the exact and QI seismograms differ significantly. For well 4, the QI approach is even worse. As for the previous VTI model, taking into account the first-order additional terms of the QI approximation does not improve the seismograms significantly: the pink seismograms practically coincide with the blue ones. The first-order terms introduce an additional problem. Since the lower receivers are close to the singularity area, amplitudes of seismograms at these receivers tend to go to infinity due to the factor $\dfrac{1}{\lambda_3 - \lambda_2}$ (see eq. (2.55) and discussion on the page 36).

2.4 Conclusions

Expressions for the calculation of zeroth- and additional first-order (0+1A) terms of the QI approximation have been derived. The equations are applicable to inhomogeneous media of arbitrary but weak anisotropy. All derivatives in the equations are derivatives only with respect to Cartesian coordinates. The analytical QI solutions for qP- and qS-waves in homogeneous weakly anisotropic media were obtained. Analysis of these analytical solutions reveals drawbacks of the QI approximation. Particularly, in the singular directions the QI approximation method produces distorted results. But in contrast to the anisotropic ray theory, in the QI approach this manifests only in the first- and higher-order

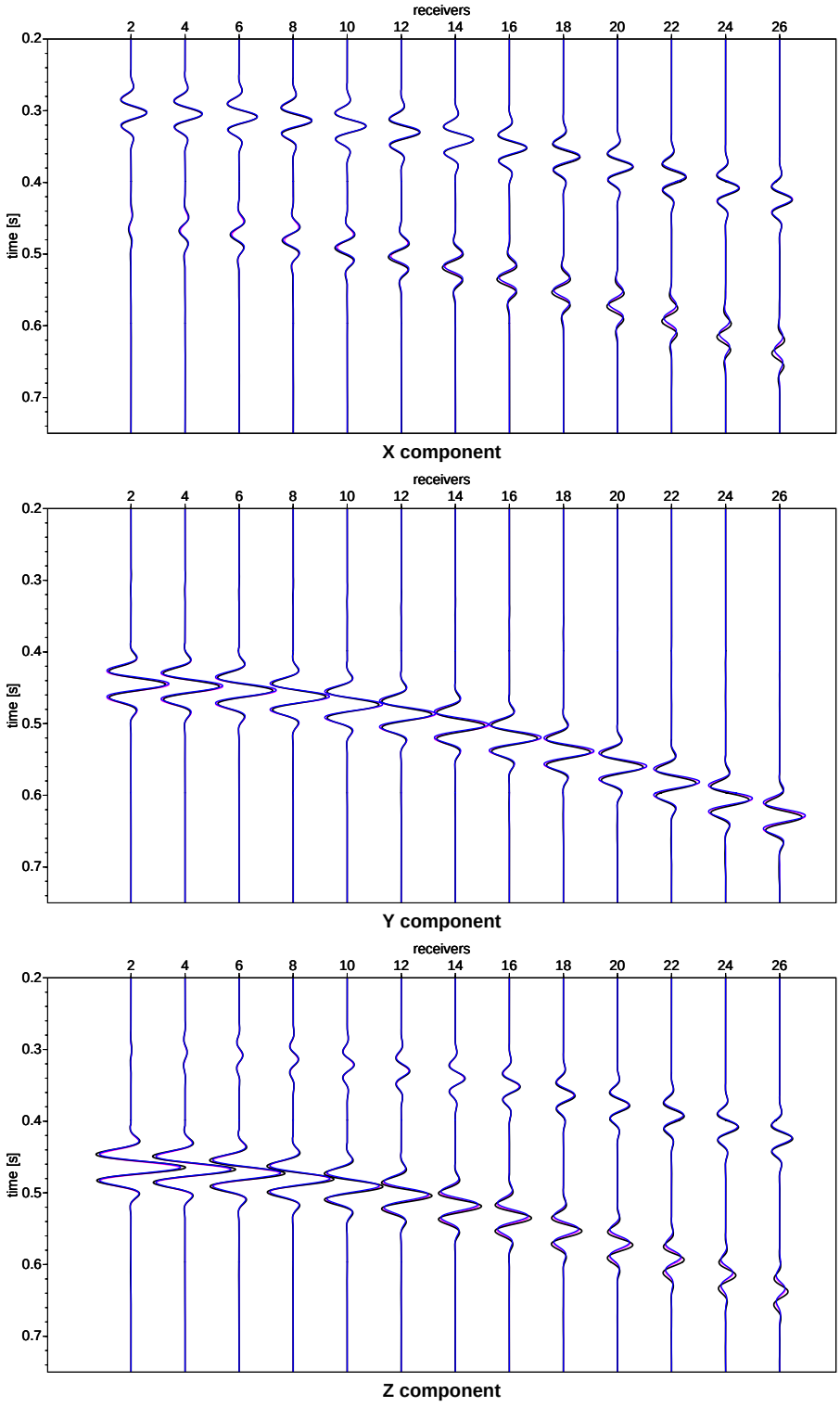

Figure 2.14: Orthorombic medium, well 1. Synthetic seismograms calculated by numerical forward modeling (black), by zeroth-order (blue) and by zeroth- and first-order (pink) QI approach. Only seismograms for even-numbered receivers are shown. All of these seismograms practically coincide with each other. (See also traveltime curves in Fig. 2.12.)

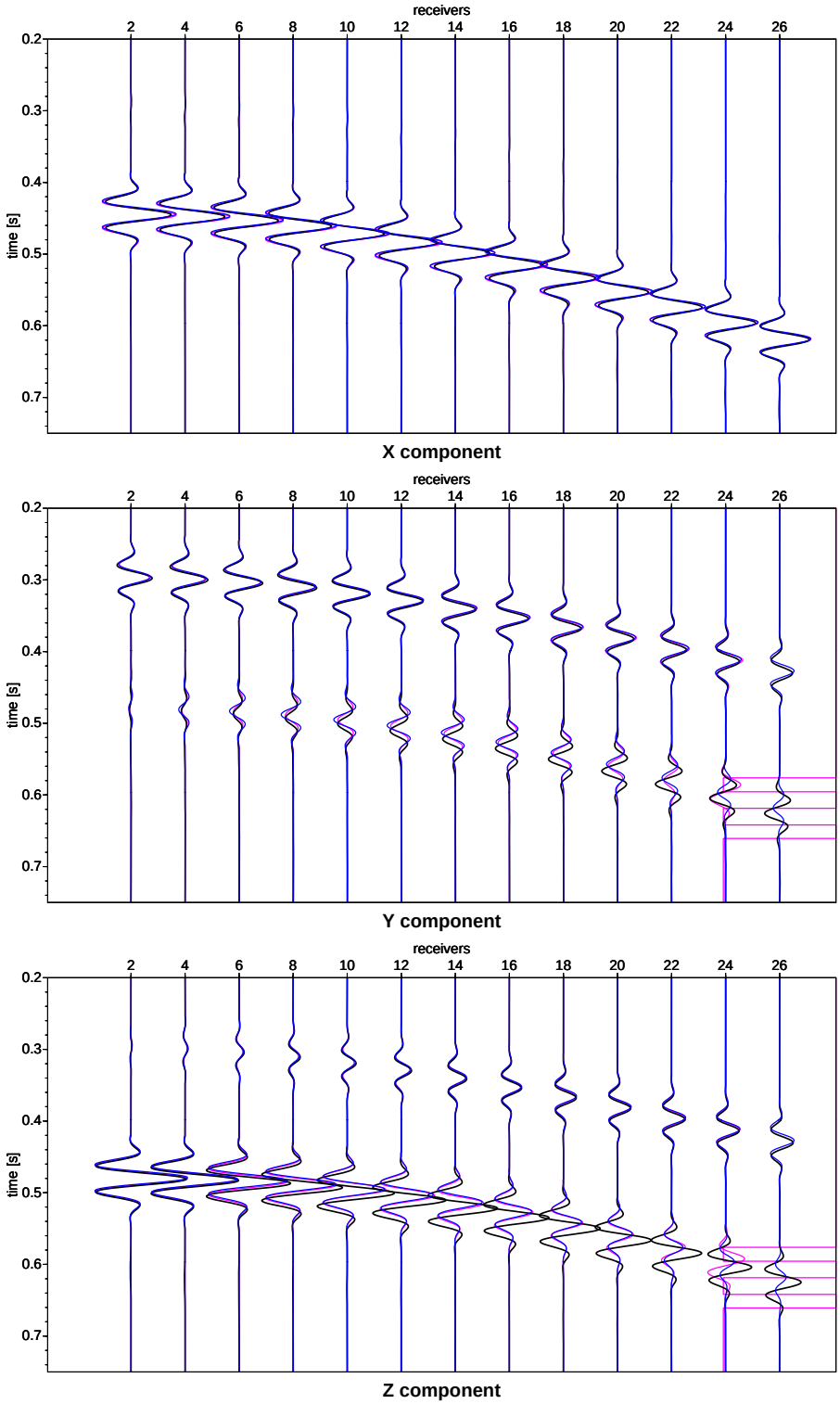

Figure 2.15: Orthorombic medium, well 4. Synthetic seismograms calculated by numerical forward modeling (black), by zeroth-order (blue) and by zeroth- and first-order (pink) QI approximation. Taking into account the first-order additional terms does not improve the QI seismograms significantly. The pink seismograms practically coincide with the blue one with the exception of the lower receivers. These receivers are close to the singularity, where the first-order additional terms of the QI approximation go to infinity (see amplitudes of the pink seismograms for the traces 24 and 26). Only seismograms for even-numbered receivers are shown. (See also traveltime curves in Fig. 2.12.)

approximations.

To test the QI approach, seismograms for a numerical VSP experiment were computed using the (0+1A) terms of the QI approximation and compared with seismograms obtained by ray tracing and by numerical forward modeling. The seismograms obtained by the latter method were considered as exact seismograms. As models homogeneous weakly anisotropic media with different types of symmetry (VTI, orthorombic) and strength of anisotropy (5%, 8.3%) were used.

For a qP-wave propagating in a homogeneous weakly anisotropic medium, taking into account the additional first-order terms causes only a deviation of the polarization vectors from a base vector $\mathbf{e}^{(1)}$ tangent to the reference ray. The newly obtained polarization vector of the qP-wave also possesses a component in the plane perpendicular to the reference ray. The contribution of this component to the full wavefield is of order ε. The equations for additional terms of the qP-wave obtained by the QI approach and by the perturbation theory are identical with one exception: The perturbation theory yields a factor $\dfrac{1}{v_p^2 - v_s^2}$, whereas the QI approach leads to the factor $\dfrac{2v_s^2 - v_p^2}{v_p^2(v_p^2 - v_s^2)}$. The difference appears as the QI approach takes into account the curvature of the wavefront (i.e., point source situation).

For two qS-waves propagating in a weakly anisotropic medium the zeroth-order QI approximation is regular everywhere. Therefore, it is expected to yield regular results also for singular regions. But the quality of the zeroth-order QI solution for singular regions is lower. Deviations of the polarization vectors of qS-waves obtained by the zeroth-order QI approximation from the exact ones can range up to 45°. For non-singular regions, however, the deviations vary from 1° to about $10 - 20°$, depending on the type and strength of anisotropy. Taking into account the additional first-order terms slightly improves the QI solution, but introduces an additional problem. In a singular region where the velocities of the two qS-waves are identical or very close to each other, the amplitudes of the seismograms go to infinity due to the factor $\dfrac{1}{\lambda_3 - \lambda_2}$ (see page 36). The standard ray theory fails to give any result in the singular region already in the zeroth-order approximation, but the QI approximation fails only in the first and higher-order approximations.

Appendix A

The vectorial basis $\mathbf{e}^{(M)}$, $(M = 1, 2, 3)$ of the ray-centered coordinate system proved to be extremely useful in the ray method for isotropic media. The basis consists of a unit vector $\mathbf{e}^{(1)}$ tangent to the ray (parallel to the slowness vector) and two mutually perpendicular unit vectors $\mathbf{e}^{(2)}$ and $\mathbf{e}^{(3)}$ situated in the plane perpendicular to the ray. The vectors $\mathbf{e}^{(2)}$ and $\mathbf{e}^{(3)}$ change along the ray according to the equation (see, e.g., Popov and Pšenčík, 1978)

$$\frac{d\mathbf{e}^{(K)}}{d\tau} = \left(\mathbf{e}^{(K)}, \operatorname{grad} v\right) \mathbf{e}^{(1)}, \qquad K = 2, 3 \tag{2.61}$$

with the velocity v of a P- or S-wave. The vectors $\mathbf{e}^{(2)}$ and $\mathbf{e}^{(3)}$ determine the S-wave polarization in isotropic medium. Properties of these base vectors are used for the calculations presented in this chapter. I derived several useful relations:

$$e_l^{(1)} = \frac{1}{v}\frac{\partial x_l}{\partial \tau}, \qquad \frac{\partial e_l^{(1)}}{\partial x_l} = \frac{1}{v}\frac{1}{J}\frac{\partial J}{\partial \tau} - \frac{1}{v^2}\frac{\partial v}{\partial \tau}, \qquad \frac{\partial e_l^{(1)}}{\partial \tau} e_l^{(1)} = 0,$$

$$\frac{\partial}{\partial x_p}\left(\frac{1}{J}\frac{\partial x_p}{\partial \tau}\right) = 0, \qquad \frac{\partial e_l^{(1)}}{\partial \tau} e_l^{(K)} = -\operatorname{grad} v\, e_l^{(K)}, \qquad K = 2, 3,$$

where the symbol J denotes the Jacobian of the transformation from ray coordinates (τ, α, β) to Cartesian coordinates (x_1, x_2, x_3),

$$J \equiv \left|\frac{\partial(x_1, x_2, x_3)}{\partial(\tau, \alpha, \beta)}\right|.$$

Appendix B

• Choice of the base vectors $\mathbf{e}^{(1)}$, $\mathbf{e}^{(2)}$ and $\mathbf{e}^{(3)}$

The base vector of the ray coordinates may be specified by the inclination and azimuth angles θ and φ defining the direction of a ray in the isotropic background medium. These two angles and the traveltime τ along the ray are considered as the ray coordinates. Vector $\mathbf{e}^{(1)}$ is a unit vector tangent to the ray in the background isotropic medium. Vectors $\mathbf{e}^{(2)}$ and $\mathbf{e}^{(3)}$ are situated in the plane perpendicular to the ray.

$$\mathbf{e}^{(1)} = \begin{pmatrix} \sin\theta\cos\varphi \\ \sin\theta\sin\varphi \\ \cos\theta \end{pmatrix}, \qquad \mathbf{e}^{(2)} = \begin{pmatrix} \cos\theta\cos\varphi \\ \cos\theta\sin\varphi \\ -\sin\theta \end{pmatrix}, \qquad \mathbf{e}^{(3)} = \begin{pmatrix} -\sin\varphi \\ \cos\varphi \\ 0. \end{pmatrix}.$$

The derivatives of the base vectors with respect to θ and φ are

$$\frac{\partial \mathbf{e}^{(1)}}{\partial \theta} = \mathbf{e}^{(2)}, \qquad \frac{\partial \mathbf{e}^{(2)}}{\partial \theta} = -\mathbf{e}^{(1)}, \qquad \frac{\partial \mathbf{e}^{(3)}}{\partial \theta} = 0,$$

$$\frac{\partial \mathbf{e}^{(1)}}{\partial \varphi} = \sin\theta\, \mathbf{e}^{(3)}, \qquad \frac{\partial \mathbf{e}^{(2)}}{\partial \varphi} = \cos\theta\, \mathbf{e}^{(3)}, \qquad \frac{\partial \mathbf{e}^{(3)}}{\partial \varphi} = -\sin\theta\, \mathbf{e}^{(1)} - \cos\theta\, \mathbf{e}^{(2)}.$$

For a homogeneous medium the rays are straight lines. Therefore, the base vectors do not depend on the ray coordinate τ. In this case, the derivatives of the base vectors with

respect to the spatial coordinates x_i have the form

$$\frac{\partial \mathbf{e}^{(1)}}{\partial x_j} = \mathbf{e}^{(2)}\frac{\partial \theta}{\partial x_j} + \mathbf{e}^{(3)}\sin\theta\,\frac{\partial \varphi}{\partial x_j},$$
$$\frac{\partial \mathbf{e}^{(2)}}{\partial x_j} = -\mathbf{e}^{(1)}\frac{\partial \theta}{\partial x_j} + \mathbf{e}^{(3)}\cos\theta\,\frac{\partial \varphi}{\partial x_j},$$
$$\frac{\partial \mathbf{e}^{(3)}}{\partial x_j} = \Big(-\sin\theta\,\mathbf{e}^{(1)} - \cos\theta\,\mathbf{e}^{(2)}\Big)\frac{\partial \varphi}{\partial x_j}.$$

Using $R = \tau v$ and $\mathbf{x} = R\,\mathbf{e}^{(1)}$ we get

$$\operatorname{div}\mathbf{e}^{(1)} = \frac{2}{R}, \qquad \operatorname{div}\mathbf{e}^{(2)} = \frac{\cos\theta}{R\,\sin\theta}, \qquad \operatorname{div}\mathbf{e}^{(3)} = 0.$$

For calculations the following derivatives are also useful:

$$\frac{\partial \theta}{\partial x_i} = \frac{1}{R}\,e_i^{(2)}; \qquad \frac{\partial \varphi}{\partial x_i} = \frac{1}{R\sin\theta}\,e_i^{(3)}; \qquad \frac{\partial R}{\partial x_i} = e_i^{(1)}.$$

- **The derivatives $\dfrac{\partial B_{22}}{\partial x_\alpha}$, $\dfrac{\partial B_{33}}{\partial x_\alpha}$ and $\dfrac{\partial B_{23}}{\partial x_\alpha}$**

The weak anisotropy matrix $\mathbf{B}$ is defined by equation (2.24). For a homogeneous anisotropic medium $\varepsilon c^{(1)}_{iklm}$ and the velocity of the background isotropic medium v_p do not depend on the space coordinates x_α, therefore, only the components of the base vectors $\mathbf{e}^{(1)}$, $\mathbf{e}^{(2)}$ and $\mathbf{e}^{(3)}$ have to be differentiated. For the calculation, equations from the previous section are used.

$$\frac{\partial B_{22}}{\partial x_\alpha} = \frac{1}{v_s^2}\,\frac{\partial}{\partial x_\alpha}\Big(\varepsilon c^{(1)}_{iklm} e_k^{(1)} e_m^{(1)} e_l^{(2)} e_i^{(2)}\Big) =$$

$$= \frac{1}{v_s^2}\Bigg\{\varepsilon c^{(1)}_{iklm}\Big[\frac{\partial e_k^{(1)}}{\partial\theta}\frac{\partial\theta}{\partial x_\alpha} + \frac{\partial e_k^{(1)}}{\partial\varphi}\frac{\partial\varphi}{\partial x_\alpha}\Big] e_m^{(1)} e_l^{(2)} e_i^{(2)} + \varepsilon c^{(1)}_{iklm} e_k^{(1)}\Big[\frac{\partial e_m^{(1)}}{\partial\theta}\frac{\partial\theta}{\partial x_\alpha} + \frac{\partial e_m^{(1)}}{\partial\varphi}\frac{\partial\varphi}{\partial x_\alpha}\Big] e_l^{(2)} e_i^{(2)}$$

$$+ \varepsilon c^{(1)}_{iklm} e_k^{(1)} e_m^{(1)}\Big[\frac{\partial e_l^{(2)}}{\partial\theta}\frac{\partial\theta}{\partial x_\alpha} + \frac{\partial e_l^{(2)}}{\partial\varphi}\frac{\partial\varphi}{\partial x_\alpha}\Big] e_i^{(2)} + \varepsilon c^{(1)}_{iklm} e_k^{(1)} e_m^{(1)} e_l^{(2)}\Big[\frac{\partial e_i^{(2)}}{\partial\theta}\frac{\partial\theta}{\partial x_\alpha} + \frac{\partial e_i^{(2)}}{\partial\varphi}\frac{\partial\varphi}{\partial x_\alpha}\Big]\Bigg\} =$$

$$= \frac{1}{v_s^2}\Bigg\{\frac{2}{R}\,\varepsilon c^{(1)}_{iklm} e_i^{(2)} e_k^{(2)} e_l^{(2)} e_m^{(1)}\, e_\alpha^{(2)} - \frac{2}{R}\,\varepsilon c^{(1)}_{iklm} e_i^{(2)} e_k^{(1)} e_l^{(1)} e_m^{(1)}\, e_\alpha^{(2)}$$

$$+ \frac{2}{R}\,\varepsilon c^{(1)}_{iklm} e_i^{(2)} e_k^{(3)} e_l^{(2)} e_m^{(1)}\, e_\alpha^{(3)} + 2\frac{\cos\theta}{R\sin\theta}\,\varepsilon c^{(1)}_{iklm} e_i^{(2)} e_k^{(1)} e_l^{(3)} e_m^{(1)}\, e_\alpha^{(3)}\Bigg\}.$$

With the following notations

$$S_2^{(22)} = \frac{2\,\sin\theta}{v_s^2}\Big(\varepsilon c^{(1)}_{iklm} e_i^{(2)} e_k^{(2)} e_l^{(2)} e_m^{(1)} - \varepsilon c^{(1)}_{iklm} e_i^{(2)} e_k^{(1)} e_l^{(1)} e_m^{(1)}\Big)$$

$$S_3^{(22)} = \frac{2\,\sin\theta}{v_s^2}\,\varepsilon c^{(1)}_{iklm} e_i^{(2)} e_k^{(3)} e_l^{(2)} e_m^{(1)} + \frac{2\cos\theta}{v_s^2}\,\varepsilon c^{(1)}_{iklm} e_i^{(2)} e_k^{(1)} e_l^{(3)} e_m^{(1)}$$

one gets

$$\frac{\partial B_{22}}{\partial x_\alpha} = \frac{1}{R\sin\theta}\left(S_2^{(22)}\, e_\alpha^{(2)} + S_3^{(22)}\, e_\alpha^{(3)}\right). \tag{2.62}$$

The derivative $\dfrac{\partial B_{33}}{\partial x_\alpha}$ can be calculated in a similar way:

$$\frac{\partial B_{33}}{\partial x_\alpha} = \frac{1}{v_s^2}\frac{\partial}{\partial x_\alpha}\left(\varepsilon c_{iklm}^{(1)} e_k^{(1)} e_m^{(1)} e_l^{(3)} e_i^{(3)}\right) =$$

$$= \frac{1}{v_s^2}\left\{\frac{2}{R}\,\varepsilon c_{iklm}^{(1)} e_i^{(3)} e_k^{(2)} e_l^{(3)} e_m^{(1)}\, e_\alpha^{(2)} + \frac{2}{R}\,\varepsilon c_{iklm}^{(1)} e_i^{(3)} e_k^{(3)} e_l^{(3)} e_m^{(1)}\, e_\alpha^{(3)} - \right.$$

$$\left. -\frac{2}{R}\,\varepsilon c_{iklm}^{(1)} e_i^{(3)} e_k^{(1)} e_l^{(1)} e_m^{(1)}\, e_\alpha^{(3)} - 2\,\frac{\cos\theta}{R\sin\theta}\,\varepsilon c_{iklm}^{(1)} e_i^{(3)} e_k^{(1)} e_l^{(2)} e_m^{(1)}\, e_\alpha^{(3)}\right\},$$

and with the notations

$$S_2^{(33)} = \frac{2\,\sin\theta}{v_s^2}\,\varepsilon c_{iklm}^{(1)} e_i^{(3)} e_k^{(2)} e_l^{(3)} e_m^{(1)}$$

$$S_3^{(33)} = \frac{2\,\sin\theta}{v_s^2}\left(\varepsilon c_{iklm}^{(1)} e_i^{(3)} e_k^{(3)} e_l^{(3)} e_m^{(1)} - \varepsilon c_{iklm}^{(1)} e_i^{(3)} e_k^{(1)} e_l^{(1)} e_m^{(1)}\right) - \frac{2\cos\theta}{v_s^2}\,\varepsilon c_{iklm}^{(1)} e_i^{(3)} e_k^{(1)} e_l^{(2)} e_m^{(1)}$$

the derivative can be written as

$$\frac{\partial B_{33}}{\partial x_\alpha} = \frac{1}{R\sin\theta}\left(S_2^{(33)}\, e_\alpha^{(2)} + S_3^{(33)}\, e_\alpha^{(3)}\right). \tag{2.63}$$

Since, the matrix $\mathbf{B}$ is symmetric, the condition $\dfrac{\partial B_{23}}{\partial x_\alpha} = \dfrac{\partial B_{32}}{\partial x_\alpha}$ is true.

$$\frac{\partial B_{23}}{\partial x_\alpha} = \frac{1}{v_s^2}\frac{\partial}{\partial x_\alpha}\left(\varepsilon c_{iklm}^{(1)} e_k^{(1)} e_m^{(1)} e_l^{(2)} e_i^{(3)}\right) =$$

$$= \frac{1}{v_s^2}\left\{\frac{1}{R}\,\varepsilon c_{iklm}^{(1)} e_i^{(3)} e_k^{(2)} e_l^{(2)} e_m^{(1)}\, e_\alpha^{(2)} + \frac{1}{R}\,\varepsilon c_{iklm} e_i^{(3)} e_k^{(1)} e_l^{(2)} e_m^{(2)}\, e_\alpha^{(2)} - \right.$$

$$\frac{1}{R}\,\varepsilon c_{iklm}^{(1)} e_i^{(3)} e_k^{(1)} e_l^{(1)} e_m^{(1)}\, e_\alpha^{(2)} + + \frac{1}{R}\,\varepsilon c_{iklm}^{(1)} e_i^{(3)} e_k^{(3)} e_l^{(2)} e_m^{(1)}\, e_\alpha^{(3)} +$$

$$+\frac{1}{R}\,\varepsilon c_{iklm} e_i^{(3)} e_k^{(1)} e_l^{(2)} e_m^{(3)}\, e_\alpha^{(3)} + \frac{\cos\theta}{R\sin\theta}\,\varepsilon c_{iklm}^{(1)} e_i^{(3)} e_k^{(1)} e_l^{(3)} e_m^{(1)}\, e_\alpha^{(3)} -$$

$$\left. -\frac{1}{R}\,\varepsilon c_{iklm}^{(1)} e_i^{(1)} e_k^{(1)} e_l^{(2)} e_m^{(1)}\, e_\alpha^{(3)} - \frac{\cos\theta}{R\sin\theta}\varepsilon c_{iklm}^{(1)} e_i^{(2)} e_k^{(1)} e_l^{(2)} e_m^{(1)}\, e_\alpha^{(3)}\right\}.$$

Using the notations

$$S_2^{(23)} = \frac{\sin\theta}{v_s^2}\left(\varepsilon c_{iklm}^{(1)} e_i^{(3)} e_k^{(2)} e_l^{(2)} e_m^{(1)} + \varepsilon c_{iklm} e_i^{(3)} e_k^{(1)} e_l^{(2)} e_m^{(2)} - \varepsilon c_{iklm}^{(1)} e_i^{(3)} e_k^{(1)} e_l^{(1)} e_m^{(1)}\right)$$

$$S_3^{(23)} = \frac{\sin\theta}{v_s^2}\left(\varepsilon c_{iklm}^{(1)} e_i^{(3)} e_k^{(3)} e_l^{(2)} e_m^{(1)} + \varepsilon c_{iklm} e_i^{(3)} e_k^{(1)} e_l^{(2)} e_m^{(3)} - \varepsilon c_{iklm}^{(1)} e_i^{(1)} e_k^{(1)} e_l^{(2)} e_m^{(1)}\right)$$

$$+\frac{\cos\theta}{v_s^2}\left(\varepsilon c_{iklm}^{(1)} e_i^{(3)} e_k^{(1)} e_l^{(3)} e_m^{(1)} - \varepsilon c_{iklm}^{(1)} e_i^{(2)} e_k^{(1)} e_l^{(2)} e_m^{(1)}\right)$$

one gets:

$$\frac{\partial B_{23}}{\partial x_\alpha} = \frac{1}{R\sin\theta}\left(S_2^{(23)}\, e_\alpha^{(2)} + S_3^{(23)}\, e_\alpha^{(3)}\right) \tag{2.64}$$

- **Derivatives $\dfrac{\partial\lambda_2}{\partial x_\alpha}$ and $\dfrac{\partial\lambda_3}{\partial x_\alpha}$**

λ_2 and λ_3 are eigenvalues of the weak anisotropy matrix $\mathbf{B}$ from (2.24). It is known that (see e.g. Zillmer et al., 1998)

$$\begin{aligned}\lambda_2 &= \frac{1}{2}(B_{22}+B_{33}) - \frac{1}{2}\sqrt{(B_{22}+B_{33})^2 - 4(B_{22}B_{33}-B_{23}^2)} \\ \lambda_3 &= \frac{1}{2}(B_{22}+B_{33}) + \frac{1}{2}\sqrt{(B_{22}+B_{33})^2 - 4(B_{22}B_{33}-B_{23}^2)}.\end{aligned}$$

The derivatives of λ_2 and λ_3 with respect to the space coordinates x_i are

$$\begin{aligned}\frac{\partial\lambda_2}{\partial x_\alpha} &= \frac{1}{\lambda_3-\lambda_2}\left\{-\lambda_2\left(\frac{\partial B_{22}}{\partial x_\alpha}+\frac{\partial B_{33}}{\partial x_\alpha}\right)+\left(\frac{\partial B_{22}}{\partial x_\alpha}B_{33}+\frac{\partial B_{33}}{\partial x_\alpha}B_{22}-2B_{23}\frac{\partial B_{23}}{\partial x_\alpha}\right)\right\} \\ \frac{\partial\lambda_3}{\partial x_\alpha} &= \frac{1}{\lambda_3-\lambda_2}\left\{\lambda_3\left(\frac{\partial B_{22}}{\partial x_\alpha}+\frac{\partial B_{33}}{\partial x_\alpha}\right)+\left(\frac{\partial B_{22}}{\partial x_\alpha}B_{33}+\frac{\partial B_{33}}{\partial x_\alpha}B_{22}-2B_{23}\frac{\partial B_{23}}{\partial x_\alpha}\right)\right\}\end{aligned}$$

If equations (2.62), (2.63) and (2.64) are taken into account, the derivatives can be rewritten in the short way

$$\begin{aligned}\frac{\partial\lambda_2}{\partial x_\alpha} &= \frac{1}{R\sin\theta}\,\frac{1}{\lambda_3-\lambda_2}\left\{(-\lambda_2P_2+Q_2)\,e_\alpha^{(2)}+(-\lambda_2P_3+Q_3)\,e_\alpha^{(3)}\right\} \\ \frac{\partial\lambda_3}{\partial x_\alpha} &= \frac{1}{R\sin\theta}\,\frac{1}{\lambda_3-\lambda_2}\left\{(\lambda_3P_2+Q_2)\,e_\alpha^{(2)}+(\lambda_3P_3+Q_3)\,e_\alpha^{(3)}\right\},\end{aligned}$$

where the following notations are used:

$$\begin{aligned}P_2 &= S_2^{(22)}+S_2^{(33)}, \\ P_3 &= S_3^{(22)}+S_3^{(33)}, \\ Q_2 &= B_{22}\,S_2^{(33)}+B_{33}\,S_2^{(22)}-2B_{23}\,S_2^{(23)}, \\ Q_3 &= B_{22}\,S_3^{(33)}+B_{33}\,S_3^{(22)}-2B_{23}\,S_3^{(23)}.\end{aligned}$$

- **Derivatives $\dfrac{\partial\gamma}{\partial x_\alpha}$**

To calculate the derivatives $\dfrac{\partial\gamma}{\partial x_\alpha}$ we use the definition of the angle γ from equation (2.31). According (2.31) we need to calculate

$$\frac{\partial\gamma}{\partial x_\alpha} = \frac{\partial}{\partial x_\alpha}\left[\frac{1}{2}\arctan\left\{\frac{2B_{23}}{B_{33}-B_{22}}\right\}\right] =$$

$$= \frac{1}{(\lambda_3-\lambda_2)^2}\left\{\frac{\partial B_{23}}{\partial x_\alpha}\Big(B_{33}-B_{22}\Big)-B_{23}\Big(\frac{\partial B_{33}}{\partial x_\alpha}-\frac{\partial B_{22}}{\partial x_\alpha}\Big)\right\}$$

If equations (2.62), (2.63) and (2.64) are taken into account, the derivatives can be rewritten as

$$\frac{\partial\gamma}{\partial x_\alpha} = \frac{1}{R\sin\theta}\,\frac{1}{(\lambda_3-\lambda_2)^2}\left\{D_2\,e^{(2)}+D_3\,e^{(3)}\right\},$$

where the following notations are used:

$$\begin{aligned} D_2 &= -B_{23}\Big(S_2^{(33)} - S_2^{(22)}\Big) + \Big(B_{33} - B_{22}\Big)S_2^{(23)} \\ D_3 &= -B_{23}\Big(S_3^{(33)} - S_3^{(22)}\Big) + \Big(B_{33} - B_{22}\Big)S_3^{(23)}. \end{aligned}$$

Chapter 3

Sectorially best-fitting isotropic medium

Perturbation methods are commonly used tools for describing wave propagation in weakly anisotropic media. The anisotropic medium is replaced by an isotropic background medium where wave propagation can be treated more easily and the correction for the effects of anisotropy is computed by perturbation techniques. To minimize errors which are inherent in the perturbation methods, the background (i.e. reference) medium should be chosen to be as close as possible to the true anisotropic medium. Formulae for the best-fitting isotropic background medium were suggested by Fedorov (1968). The parameters of the best-fitting isotropic medium are obtained by minimizing the sum of the squares of differences between the components of the Christoffel matrices of the anisotropic, Λ_{il}, and the isotropic, $\Lambda_{il}^{(0)}$, background medium. In doing so the average is taken over the whole unit sphere to eliminate the dependence of the Christoffel matrices on the direction of the wavefront normal $\mathbf{n}$. This can be written as

$$\frac{1}{4\pi}\int_{\varphi=0}^{2\pi}\int_{\theta=0}^{\pi}\sum_{i,l=1}^{3}\left[\Lambda_{il}-\Lambda_{il}^{(0)}\right]^2\sin\theta\,d\theta\,d\varphi=\min,$$

where θ and φ are inclination and azimuth angles.

Let us assume that we are interested only in one particular direction. I call this direction the direction of interest, e.g., the vertical direction which is most important in seismic exploration. In this case it is better to select the isotopic background medium in such a way that it gives the best fit to the anisotropic medium considered not over all possible directions, but only for the direction of interest or a region surrounding the direction of interest. It was my motivation to modify the formulae for the best-fitting isotropic medium to enable us to choose the sectorially best-fitting isotropic medium. To derive the formulae for the sectorially best-fitting isotropic medium, I use Fedorov's technique, but restrict the averaging to a sector (or cone) around the direction of interest. The sector is specified by the range of the inclination (θ) and azimuth (φ) angles: from θ_1 till θ_2 and from φ_1 till φ_2. This chapter contains the resulting formulae obtained for the sectorially best-fitting isotropic reference medium. To illustrate the formulae several numerical tests were carried out.

3.1 Formulae for sectorially best-fitting isotropic medium

Following Fedorov (1968) I search the parameters of the best-fitting isotropic medium for a given anisotropic medium that provides the minimum of the following equation:

$$\frac{1}{\Omega}\int_{\varphi_1}^{\varphi_2}\int_{\theta_1}^{\theta_2}\sum_{i,l=1}^{3}\left[\Lambda_{il}-\Lambda_{il}^{(0)}\right]^2\sin\theta\,d\theta\,d\varphi=\min, \tag{3.1}$$

Here $\Omega=-(\varphi_2-\varphi_1)\,(\cos\theta_2-\cos\theta_1)$ is the solid angle, Λ_{il} and $\Lambda_{il}^{(0)}$ are the Christoffel matrices of the anisotropic medium considered and the best-fitting isotropic medium for a wavefront normal $\mathbf{n}$. The phase angles θ_1, θ_2 and φ_1, φ_2 specify the sector. The Christoffel matrices are

$$\begin{aligned}\Lambda_{il} &= c_{iklm}\,n_k\,n_m,\\ \Lambda_{il}^{(0)} &= (\lambda+\mu)\,n_i n_l+\mu\,\delta_{il}\end{aligned} \tag{3.2}$$

where c_{iklm} are the elastic parameters of the anisotropic medium, and λ and μ are the Lamé parameters of the best-fitting isotropic medium to be found. The necessary conditions for a minimum of equation (3.1) are of the form

$$\begin{aligned}&\frac{\partial}{\partial\lambda}\left(\frac{1}{\Omega}\int_{\varphi_1}^{\varphi_2}\int_{\theta_1}^{\theta_2}\sum_{i,l=1}^{3}\left[\Lambda_{il}-\Lambda_{il}^{(0)}\right]^2\sin\theta\,d\theta\,d\varphi\right)=0,\\ &\frac{\partial}{\partial\mu}\left(\frac{1}{\Omega}\int_{\varphi_1}^{\varphi_2}\int_{\theta_1}^{\theta_2}\sum_{i,l=1}^{3}\left[\Lambda_{il}-\Lambda_{il}^{(0)}\right]^2\sin\theta\,d\theta\,d\varphi\right)=0.\end{aligned} \tag{3.3}$$

After substitution the equations

$$\begin{aligned}\left[\Lambda_{il}-\Lambda_{il}^{(0)}\right]^2 &= \Lambda_{il}^2-2\Lambda_{il}\Lambda_{il}^{(0)}+\left(\Lambda_{il}^{(0)}\right)^2\\ \left(\Lambda_{il}^{(0)}\right)^2 &= 6\mu^2+\lambda^2+4\lambda\mu\\ -2\Lambda_{il}\Lambda_{il}^{(0)} &= -2(\lambda+\mu)\,c_{iklm}\,n_k\,n_m\,n_i\,n_l-2\mu\,c_{ikim}\,n_k\,n_m\end{aligned}$$

the system (3.3) can be written as

$$\begin{aligned}&\frac{1}{\Omega}\int_{\varphi_1}^{\varphi_2}\int_{\theta_1}^{\theta_2}c_{iklm}n_k n_m n_i n_l\,\sin\theta\,d\theta\,d\varphi=\lambda+2\mu,\\ &\frac{1}{\Omega}\int_{\varphi_1}^{\varphi_2}\int_{\theta_1}^{\theta_2}c_{iklm}n_k n_m n_i n_l\,\sin\theta\,d\theta\,d\varphi+\frac{1}{\Omega}\int_{\varphi_1}^{\varphi_2}\int_{\theta_1}^{\theta_2}c_{ikim}n_k n_m\,\sin\theta\,d\theta\,d\varphi=6\mu+2\lambda.\end{aligned} \tag{3.4}$$

In terms of P- and S-wave velocities, $V_p^2 = \dfrac{\lambda + 2\mu}{\rho}$ and $V_s^2 = \dfrac{\mu}{\rho}$, the last system takes the form

$$\begin{aligned} V_p^2 &= \frac{1}{\Omega} \int_{\varphi_1}^{\varphi_2} \int_{\theta_1}^{\theta_2} \frac{1}{\rho}\, c_{iklm}\, n_k\, n_m\, n_i\, n_l\, \sin\theta\, d\theta\, d\varphi \\ V_s^2 &= \frac{1}{2\,\Omega} \int_{\varphi_1}^{\varphi_2} \int_{\theta_1}^{\theta_2} \frac{1}{\rho}\, c_{ikim}\, n_k\, n_m\, \sin\theta\, d\theta\, d\varphi - \frac{1}{2} V_p^2. \end{aligned} \tag{3.5}$$

With the normal $\mathbf{n}$ specified by the phase angles θ and φ,

$$\mathbf{n} = (\sin\theta\, \cos\varphi,\ \sin\theta\, \sin\varphi,\ \cos\theta),$$

the integrals in equations (3.5) are easily calculated in the following way: First, the integral from the first equation of system (3.5) is expanded:

$$\begin{aligned} &\frac{1}{\Omega} \int_{\varphi_1}^{\varphi_2} \int_{\theta_1}^{\theta_2} \sum_{i,k,l,m=1}^{3} c_{iklm}\, n_k\, n_m\, n_i\, n_l \sin\theta\, d\theta\, d\varphi \\ &= \frac{1}{\Omega} \int_{\varphi_1}^{\varphi_2} \int_{\theta_1}^{\theta_2} \sin\theta\, d\theta\, d\varphi \Big\{ C_{11} n_1^4 + (C_{12} + 2C_{66}) 2 n_1^2 n_2^2 + (C_{13} + 2C_{55}) 2 n_1^2 n_3^2 \\ &+ (C_{14} + 2C_{56}) 4 n_1^2 n_2 n_3 + C_{15} 4 n_1^3 n_3 + C_{16} 4 n_1^3 n_2 + C_{22} n_2^4 + (C_{23} + 2C_{44}) 2 n_2^2 n_3^2 \\ &+ C_{24} 4 n_2^3 n_3 + (C_{25} + 2C_{46}) 4 n_1 n_2^2 n_3 + C_{26} 4 n_1 n_2^3 + C_{33} n_3^4 + C_{34} 4 n_2 n_3^3 \\ &+ C_{35} 4 n_1 n_3^3 + (C_{36} + 2C_{45}) 4 n_1 n_2 n_3^2 \Big\} \end{aligned}$$

Here the tensor of the elastic parameters c_{iklm} is rewritten using Voigt notation in the form of a symmetric 6×6 matrix $C_{\alpha\beta}$. As a result we get for V_p^2

$$\begin{aligned} V_p^2 = \frac{1}{\Omega}\frac{1}{\rho} \Big(& C_{11}\, I_1 + (C_{12} + 2C_{66})\, I_2 + (C_{13} + 2C_{55})\, I_3 + (C_{14} + 2C_{56})\, I_4 + C_{15}\, I_5 \\ & + C_{16}\, I_6 + C_{22}\, I_7 + (C_{23} + 2C_{44})\, I_8 + C_{24}\, I_9 + (C_{25} + 2C_{46})\, I_{10} \\ & + C_{26}\, I_{11} + C_{33}\, I_{12} + C_{34}\, I_{13} + C_{35}\, I_{14} + (C_{36} + 2C_{45})\, I_{15} \Big), \end{aligned} \tag{3.6}$$

where

$$\begin{aligned} I_1 &= A \left[\frac{3}{8} (\varphi_2 - \varphi_1) + \frac{1}{4} (\sin 2\varphi_2 - \sin 2\varphi_1) + \frac{1}{32} (\sin 4\varphi_2 - \sin 4\varphi_1) \right], \\ I_2 &= A \left[\frac{1}{4} (\varphi_2 - \varphi_1) - \frac{1}{16} (\sin 4\varphi_2 - \sin 4\varphi_1) \right], \\ I_3 &= C \left[\varphi_2 - \varphi_1 + \frac{1}{2} (\sin 2\varphi_2 - \sin 2\varphi_1) \right], \qquad I_4 = \frac{4}{3} B \Big[-\cos^3\varphi_2 + \cos^3\varphi_1 \Big], \end{aligned}$$

$$
\begin{aligned}
I_5 &= 4B\left[\sin\varphi_2 - \sin\varphi_1 - \frac{1}{3}(\sin^3\varphi_2 - \sin^3\varphi_1)\right],\\
I_6 &= A\Big[-\cos^4\varphi_2 + \cos^4\varphi_1\Big],\\
I_7 &= A\left[\frac{3}{8}(\varphi_2-\varphi_1) - \frac{1}{4}(\sin 2\varphi_2 - \sin 2\varphi_1) + \frac{1}{32}(\sin 4\varphi_2 - \sin 4\varphi_1)\right],\\
I_8 &= C\left[\varphi_2 - \varphi_1 - \frac{1}{2}(\sin 2\varphi_2 - \sin 2\varphi_1)\right],\\
I_9 &= 4B\left[-\cos\varphi_2 + \cos\varphi_1 + \frac{1}{3}(\cos^3\varphi_2 - \cos^3\varphi_1)\right],\\
I_{10} &= \frac{4}{3}B\Big[\sin^3\varphi_2 - \sin^3\varphi_1\Big], \qquad I_{11} = A\Big[\sin^4\varphi_2 - \sin^4\varphi_1\Big],\\
I_{12} &= E\Big[\varphi_2 - \varphi_1\Big]; \qquad I_{13} = 4D\Big[-\cos\varphi_2 + \cos\varphi_1\Big],\\
I_{14} &= 4D\Big[\sin\varphi_2 - \sin\varphi_1\Big], \qquad I_{15} = 2C\Big[\sin^2\varphi_2 - \sin^2\varphi_1\Big],
\end{aligned}
\tag{3.7}
$$

with

$$
\begin{aligned}
A &= -\frac{1}{5}(\sin^4\theta_2\cos\theta_2 - \sin^4\theta_1\cos\theta_1) - \frac{4}{5}(\cos\theta_2 - \cos\theta_1) + \frac{4}{15}(\cos^3\theta_2 - \cos^3\theta_1),\\
B &= \frac{1}{5}(\sin^5\theta_2 - \sin^5\theta_1); \quad C = -\frac{1}{3}(\cos^3\theta_2 - \cos^3\theta_1) + \frac{1}{5}(\cos^5\theta_2 - \cos^5\theta_1),\\
D &= \frac{1}{3}(\sin^3\theta_2 - \sin^3\theta_1) - \frac{1}{5}(\sin^5\theta_2 - \sin^5\theta_1), \qquad E = -\frac{1}{5}(\cos^5\theta_2 - \cos^5\theta_1).
\end{aligned}
\tag{3.8}
$$

The integral from the second equation of system (3.5) are expanded similarly:

$$
\begin{aligned}
&\frac{1}{\Omega}\int_{\varphi_1}^{\varphi_2}\int_{\theta_1}^{\theta_2} c_{ikim}\, n_k\, n_m\, \sin\theta\, d\theta\, d\varphi\\
&= \frac{1}{\Omega}\int_{\varphi_1}^{\varphi_2}\int_{\theta_1}^{\theta_2} \sin\theta\, d\theta\, d\varphi \Big\{ n_1 n_1 (C_{11} + C_{66} + C_{55}) + 2 n_1 n_2 (C_{16} + C_{26} + C_{45})\\
&+ 2 n_1 n_3 (C_{15} + C_{46} + C_{35}) + n_2 n_2 (C_{66} + C_{22} + C_{44})\\
&+ 2 n_2 n_3 (C_{56} + C_{24} + C_{43}) + n_3 n_3 (C_{55} + C_{44} + C_{33}) \Big\}
\end{aligned}
$$

As a result we get for V_s^2:

$$
\begin{aligned}
V_s^2 = \frac{1}{\Omega}\frac{1}{\rho}\Big(&(C_{11} + C_{66} + C_{55})\, T_1 + (C_{16} + C_{26} + C_{45})\, T_2 + (C_{15} + C_{46} + C_{35})\, T_3\\
&+ (C_{66} + C_{22} + C_{44})\, T_4 + (C_{56} + C_{24} + C_{43})\, T_5 + (C_{55} + C_{44} + C_{33})\, T_6 \Big) - \frac{1}{2} V_p^2,
\end{aligned}
\tag{3.9}
$$

where

$$T_1 = \left\{\frac{1}{2}\left(\varphi_2 - \varphi_1\right) + \frac{1}{4}(\sin 2\varphi_2 - \sin 2\varphi_1)\right\}\left\{-\cos\theta_2 + \cos\theta_1 + \frac{1}{3}(\cos^3\theta_2 - \cos^3\theta_1)\right\},$$

$$T_2 = \left\{\sin^2\varphi_2 - \sin^2\varphi_1\right\}\left\{-\cos\theta_2 + \cos\theta_1 + \frac{1}{3}(\cos^3\theta_2 - \cos^3\theta_1)\right\},$$

$$T_3 = \frac{2}{3}\left\{\sin\varphi_2 - \sin\varphi_1\right\}\left\{\sin^3\theta_2 - \sin^3\theta_1\right\} \tag{3.10}$$

$$T_4 = \left\{\frac{1}{2}\left(\varphi_2 - \varphi_1\right) - \frac{1}{4}(\sin 2\varphi_2 - \sin 2\varphi_1)\right\}\left\{-\cos\theta_2 + \cos\theta_1 + \frac{1}{3}(\cos^3\theta_2 - \cos^3\theta_1)\right\},$$

$$T_5 = \frac{2}{3}\left\{-\cos\varphi_2 + \cos\varphi_1\right\}\left\{\sin^3\theta_2 - \sin^3\theta_1\right\}$$

$$T_6 = \frac{1}{3}\left\{\varphi_2 - \varphi_1\right\}\left\{-\cos^3\theta_2 + \cos^3\theta_1\right\}.$$

Equations (3.6) and (3.9) define the P- and S-wave velocities of the best-fitting isotropic medium for the elastic parameters of the anisotropic medium under consideration and the angles θ_1, θ_2, φ_1 and φ_2 specifying a sector (cone) around a direction of interest. Note that if the sector is the whole unit sphere, namely $\theta_1 = 0$ and $\theta_2 = \pi$, $\varphi_1 = 0$ and $\varphi_2 = 2\pi$, equations (3.6) and (3.9) take the form

$$\begin{aligned} V_p^2 &= \frac{1}{5\rho}\Big(C_{11} + C_{22} + C_{33}\Big) + \frac{2}{15}\Big(C_{12} + C_{13} + C_{23} + 2C_{44} + 2C_{55} + 2C_{66}\Big) \\ V_s^2 &= \frac{1}{15\rho}\Big(C_{11} + C_{22} + C_{33} - C_{12} - C_{13} - C_{23} + 3C_{44} + 3C_{55} + 3C_{66}\Big), \end{aligned}$$

which correspond to Fedorov's best-fitting medium specified by equations (4.9) on page 86, if the tensor c_{iklm} of the elastic parameters is rewritten in terms of the 6×6 matrix $C_{\alpha\beta}$.

3.2 Quality of sectorial approximation

Two media are used to illustrate the quality of sectorial approximation. Anisotropic media with transversely isotropic and orthorombic symmetries are considered. First, a VTI medium is discussed. The elastic parameters are given in Table 5.4 on page 110. Fedorov's formulae for the best-fitting isotropic medium for this medium yield $V_p = 3.51$ km/s and $V_s = 1.77$ km/s. Figure 3.1 shows plots of the VTI exact phase velocities (solid lines) and the corresponding velocities of Fedorov's best-fitting isotropic medium (open circles). One can see the poor agreement between the anisotropic and isotropic velocities in the Z-direction. The agreement can be improved, since two qS-waves have the same phase velocities in this direction. To obtain the best-fitting isotropic medium for a 20° cone around the Z-direction ($\theta_1 = 0$, $\theta_2 = 20$, $\varphi_1 = 0$, $\varphi_1 = 360°$) equations (3.6) and (3.9) are used. The equations yield the velocities $V_p = 3.30$ km/s and $V_s = 1.68$ km/s. In Figure 3.1 plots of the best-fitting velocities for this 20° cone are given by black circles. One can see that the anisotropic and sectorially best-fitting isotropic velocities are in close agreement for the 20° cone around Z-direction for qP- as well as for qS-waves.

The elastic parameters of the orthorombic medium are given in Table 5.4 on page 110. Fedorov's best-fitting medium is given by $V_p = 3.17$ km/s and $V_s = 2.00$ km/s. Figures 3.2 and 3.3 show plots of the qP and qS-wave phase velocities (solid lines) in the orthorombic medium and in Fedorov's best-fitting isotropic medium (unfilled circles). Application of equations (3.6) and (3.9) allows to construct the best-fitting isotropic medium for a 20° cone around the Z-direction. In Figure 3.2 the sectorially best-fitting isotropic velocities ($V_p = 2.93$ and $V_s = 1.95$) are represented by black circles. One can see that the sectorially best-fitting isotropic P-wave velocity is closer to the anisotropic qP-wave velocity within

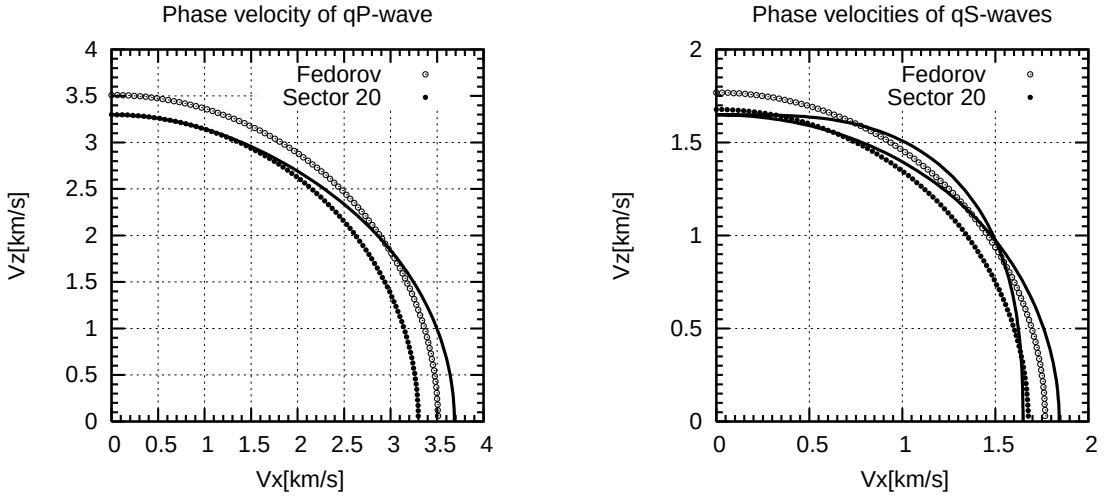

Figure 3.1: Plots of phase velocities for the VTI medium and approximating isotropic media. The phase velocities of the qP- (left) and two qS-waves (right) in the VTI medium are given by solid lines. The velocities in Fedorov's best-fitting isotropic medium are shown by open circles, the best-fitting medium for 20° cone around the Z-axis direction ($\theta_1 = 0$, $\theta_2 = 20°$) by black circles.

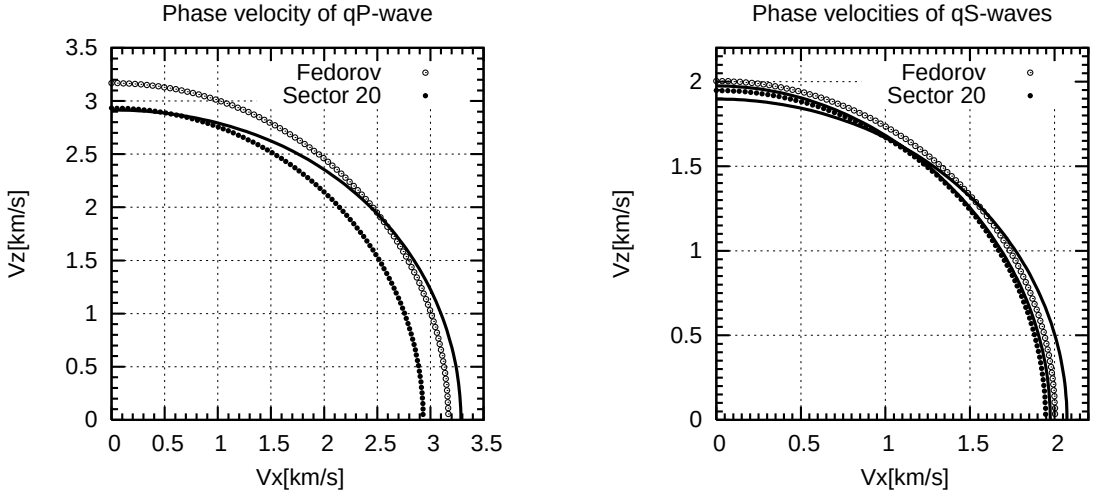

Figure 3.2: Plots of phase velocities for the orthorombic medium and best-fitting isotropic media in the $X - Z$ plane. The phase velocities of the qP- (left) and two qS-waves (right) in the orthorombic medium are given by solid lines. The velocities in Fedorov's best-fitting isotropic medium are shown by open circles, the best-fitting medium for 20° cone around the Z-direction ($\theta_1 = 0$, $\theta_2 = 20°$) by black circles.

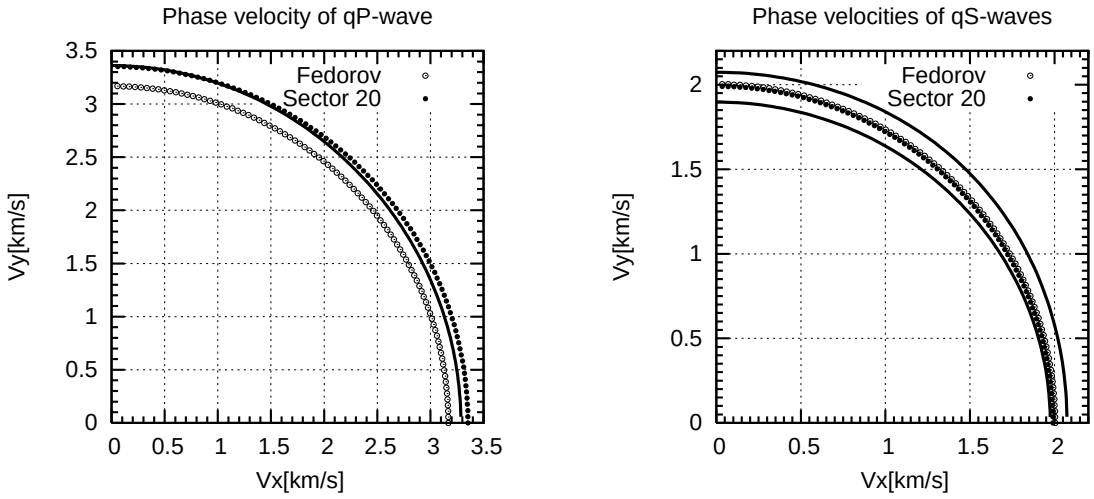

Figure 3.3: Plots of phase velocities for the orthorombic medium and best-fitting isotropic media in the $X-Y$ plane. The phase velocities of the qP- (left) and two qS-waves (right) in the orthorombic are given by solid lines. The velocities in Fedorov's best-fitting isotropic medium are shown by open circles, the best-fitting medium for 20° cone around the Y-direction ($\theta_1 = 80$, $\theta_2 = 100°$, $\varphi_1 = 80$, $\varphi_2 = 100°$) by black circles.

this cone than the corresponding Fedorov velocity. For the qS-waves, the sectorially best-fitting isotropic velocity is situated between the velocities of the two qS-waves. Therefore, it is closer to both qS-wave velocities within this cone compared to Fedorov's velocity.

A similar situation can be observed for a 20° cone around the Y-direction in Figure 3.3. This cone is defined with $\theta_1 = 80$, $\theta_2 = 100°$, $\varphi_1 = 80$ and $\varphi_2 = 100°$. The sectorially best-fitting isotropic velocities are $V_p = 3.35$ km/s and $V_s = 1.99$ km/s. These two velocities are in close agreement with the anisotropic phase velocities for the cone considered.

3.3 Conclusions

Formulae for the sectorially best-fitting isotropic background medium were derived, see equation (3.6) with coefficients from (3.7) and (3.8) for the P-wave velocity, and equation (3.9) with coefficients from (3.10) for the S-wave velocity. They allow to construct an isotropic medium which is in close agreement with the anisotropic medium under consideration for the direction of interest. The sector (cone) around this direction is specified by four phase angles: $[\theta_1, \theta_2]$ and $[\varphi_1, \varphi_2]$. The application of the derived formulae was illustrated by examples of media with VTI and orthorombic symmetries.

Chapter 4

FD perturbation method

Robust and efficient methods for the traveltime computation are important in many seismic modeling and inversion applications. (For example, for migration or traveltime tomography, a large number of traveltime computations with varying source positions must be performed.) These methods are particularly important for anisotropic media where any computations are much more complicated and computationally expensive than for isotropic media.

In this chapter, a finite-difference (FD) perturbation method is discussed. According to this method, first-order perturbation theory is used for fast 3-D computation of qP-wave traveltimes in arbitrary anisotropic media. For efficiency the perturbation approach was implemented into a finite-difference eikonal solver. Traveltimes in an unperturbed background medium are computed with an FD eikonal solver, while perturbed traveltimes are obtained by adding a traveltime correction to the traveltimes of the background medium. The traveltime correction must be computed along the raypath in the background medium. Since the raypath is not determined in FD eikonal solvers, rays are approximated by linear segments corresponding to the direction of the phase normal of plane wavefronts in each cell. An isotropic medium as a background medium works well for weak anisotropy. Using media of ellipsoidal anisotropy as a background medium in the perturbation approach allows to consider stronger anisotropy without loosing the computational speed. The traveltime computation in media with ellipsoidal anisotropy using FD eikonal solver is fast and accurate. The relative error is below 0.5% for the models investigated in this study. Numerical examples show that a background model with ellipsoidal anisotropy allows to compute the traveltime for models of strong anisotropy with an improved accuracy compared to the isotropic background medium.

I begin this chapter with a small introduction followed by a detailed description of the FD perturbation method. Then, applications of the suggested method for traveltime computations in several anisotropic models are shown. The accuracy of the FD perturbation method is estimated using traveltimes computed analytically (for homogeneous ellipsoidally anisotropic models), by ray tracing (homogeneous anisotropic model with arbitrary symmetry) or a wavefront-oriented ray trancing (factorized anisotropic model).

4.1 Introduction

There are two major approaches which can be used for computing traveltimes: ray tracing methods (see, e.g., Červený, 1972; Gajewski and Pšenčík, 1987) and methods which are based on a direct numerical solution of the eikonal equation using finite-differences (see, e.g., Vidale, 1988, 1990; Qin et al., 1992). Ray tracing methods are difficult to implement and time consuming when applied to anisotropic media because for each propagation step an eigenvalue problem must be solved. Similar to the isotropic case the ray methods in anisotropic media fail in shadow zones or in the vicinity of a caustic.

The methods based on numerical solving of the eikonal equation are restricted to the computation of first arrival traveltimes, but they are very fast and work efficiently for shadow and caustic zones. FD eikonal solvers were extended to certain types of anisotropic media by Dellinger (1991), Eaton (1993) and Lecomte (1993). Dellinger (1991) used the upwind scheme of Van Trier and Symes (1991) for transversely isotropic media. Eaton (1993) applied an expanding-wavefront scheme on a hexagonal grid in 2-D anisotropic models. He approximated one component of the slowness vector using FD and found the root of the sixth-order polynomial for the other component numerically. Lecomte (1993) applied the finite difference calculation of traveltimes for P-waves using the method of Podvin and Lecomte (1991) for a 2-D model with elliptical and orthorombic symmetry.

The aim of this work was to compute traveltimes for qP-wave in arbitrary anisotropic media without solving higher order polynomials numerically. Perturbation techniques are suitable tools to describe wave propagation in complex media. The anisotropic medium is considered as a perturbed medium and approximated by a simpler, analytically treat-able background medium. Isotropic or ellipsoidal anisotropic media are used as background media. For the traveltime computation, the perturbation method is combined with the FD eikonal solver. This combined method is called FD perturbation method. The concept of the 2-D FD perturbation method was suggested in a paper by Ettrich and Gajewski (1998). They used the FD perturbation method to compute qP-wave traveltimes in 2-D isotropic and weakly anisotropic media with transversely isotropic symmetry. My work consists of 3-D extension of the FD perturbation method and its implementation for anisotropic models with arbitrary types of symmetry. My implementation is also restricted to qP-waves.

An isotropic medium as a background medium works well for models of weak anisotropy. Using media of ellipsoidal anisotropy as a background medium in the perturbation approach allows to consider stronger anisotropy without loosing the computational speed. The traveltime computation in media of ellipsoidal anisotropy is fast and accurate using the FD eikonal solver. A basic routine for the FD eikonal solver for an elliptically anisotropic medium in the 3-D case was presented by Ettrich (1998). He tested his routine in a medium with identical velocities along two principal axes (ellipsoid with rotational symmetry). The algorithm presented in this paper works for ellipsoidal background media with three different velocities along the principal axes. Therefore it is possible to use a broader class of ellipsoidal media as a background medium. To minimize errors in the perturbation approach, the background medium should be chosen closely to the given anisotropic medium. For the construction of the best-fitting ellipsoidal background medium we use formulae which were derived by Ettrich et al. (2001). They obtained linear relations for the coefficients of the ellipsoidal medium that depend on the elastic

coefficients of the anisotropic medium. Since, it is assumed that the polarization vector coincides with the phase normal vector, only qP-wave anisotropy is approximated.

4.2 Concept of the FD perturbation method

I have already stated that the concept of the 2-D FD perturbation method was suggested in a paper by Ettrich (1998). Here I present the 3-D extension of this method and its implementation for the case of arbitrary anisotropic media for qP-waves. As a background model I consider either isotropic or ellipsoidally anisotropic background media. The arbitrary anisotropic model considered for traveltime computation is also called perturbed model (perturbed with respect to the background model). For the background model as well as for the perturbed model velocities or elastic parameters are given on a regular grid. The background medium is given by the P-wave velocity v_p^{ref} for the isotropic case or by a 3×3 symmetric matrix $\mathbf{R}$ for the ellipsoidal anisotropic case. Elements of the matrix $\mathbf{R}$ are squares of qP-wave velocities in different directions. The parameters of the background medium are determined from the parameters of the considered perturbed, i. e. arbitrary anisotropic medium, given by the density normalized elastic parameters a_{ijkl}. Traveltimes for the isotropic or ellipsoidally anisotropic background model are computed directly using the FD eikonal solver along expanding wavefronts (see Qin et al., 1992). For the perturbed model we perform the traveltime computation using standard perturbation techniques. The traveltime corrections are computed along the ray segments corresponding to plane waves in each grid cell for every step of the FD scheme.

4.2.1 Background medium

To minimize errors in the perturbation approach the background medium should be chosen as close as possible to the given anisotropic medium. For the construction of the ellipsoidal background medium we used formulae for a best-fitting ellipsoidal background medium which were derived by Ettrich et al. (2001) using similar concepts as Fedorov (1968) used for the determination of the best fitting isotropic medium. Ettrich et al. derived linear relations between the velocity parameters of the ellipsoidal medium giving the best fit to the anisotropic medium considered and the elastic parameters of this anisotropic medium. In this study it was assumed that the polarization vector of the qP-wave in the background medium coincides with the phase normal vector. Therefore, only qP-wave anisotropy is considered. To construct the isotropic background model we use formulae for the best fitting isotropic medium derived by Fedorov (1968). All formulae for best-fitting isotropic and ellipsoidal anisotropic background media are given at the appendix in the end of this chapter (see page 86).

4.2.2 FD scheme

Traveltimes in the background medium are computed by a FD eikonal solver along expanding wavefronts (for isotropic media see Qin et al., 1992). The FD eikonal solver for the medium of ellipsoidal anisotropy is based on the eikonal equation for this type of medium,

i.e.,

$$(\mathbf{p}, \mathbf{R}\,\mathbf{p}) = 1, \tag{4.1}$$

where $\mathbf{p}$ is the slowness vector, $\mathbf{R}$ is the 3×3 symmetric matrix of velocity parameters of the ellipsoidal background medium, $(,)$ denotes scalar product. The components of the slowness vector $\mathbf{p}$ are the derivatives of traveltimes with respect to space coordinates x_i:

$$p_i = \frac{\partial \tau}{\partial x_i}, \qquad i = 1, 2, 3.$$

Local problem

The local problem for the ellipsoidal medium is similarly to the isotropic one. Two components of the slowness vector are approximated with finite differences using the grid points where traveltimes are already known. Then, the eikonal equation (4.1) allows for the computation of the third component of the slowness vector, if the medium parameters are known.

For the eikonal equation (4.1) of an ellipsoidally anisotropic medium I use three approximating formulae. The formulae were suggested by Ettrich (1998). The main formula is applied for the following situation: If there are known traveltimes at grid points 0, 3, 4, 5, 6, 7 and 8 (see Fig. 4.1) the unknown traveltime t_9 is obtained from:

$$\begin{aligned} t_9 = t_0 + w_0 + w_1[(t_5 - t_3)^2 + (t_7 - t_8)^2] + w_2[(t_5 - t_4)^2 + (t_6 - t_8)^2] \quad + \\ w_3[(t_6 - t_3)^2 + (t_7 - t_4)^2] + w_4[(t_3 - t_4)^2 + (t_6 - t_7)^2] \quad + \\ w_5[(t_6 - t_5)^2 + (t_8 - t_4)^2] + w_6[(t_7 - t_5)^2 + (t_8 - t_3)^2], \end{aligned} \tag{4.2}$$

where t_i is the traveltime at the corresponding grid point with index i. The grid point with the index 0 is a grid point with minimum traveltime. The weight coefficients $w_0, \ldots, w_6$ are defined as follows:

$$\begin{aligned} w_1 &= 1.5 - \frac{w_0}{4h^2}(2v_4^2 + 2v_6^2 - v_1^2 - v_3^2), \\ w_2 &= 1.5 - \frac{w_0}{4h^2}(2v_4^2 + 2v_5^2 - v_2^2 - v_3^2), \\ w_3 &= 1.5 - \frac{w_0}{4h^2}(2v_5^2 + 2v_6^2 - v_1^2 - v_2^2), \\ w_4 &= \frac{w_0}{4h^2}(2v_4^2 - v_1^2 - v_2^2) - 0.5, \\ w_5 &= \frac{w_0}{4h^2}(2v_6^2 - v_2^2 - v_3^2) - 0.5, \\ w_6 &= \frac{w_0}{4h^2}(2v_5^2 - v_1^2 - v_3^2) - 0.5, \\ w_0 &= \frac{3h^2}{v_7^2}, \end{aligned} \tag{4.3}$$

where h denotes grid spacing. The velocities $v_1, \ldots, v_6$ represent phase velocities in the directions of the X-, Y- and Z-axes ($i = 1, 2, 3$ respectively) and in the directions of the

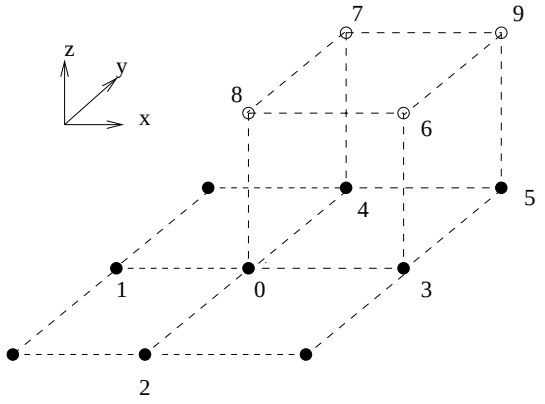

Figure 4.1: Local problem. The grid points with known traveltimes are given by the black circles. Let us assume the grid point 0 is grid point with the minimum traveltime. Then, the computation starts at this point 0. Using traveltimes in points 0, 1, 2, 3 and 4 the traveltime at point 8 can be calculated (*scheme C*). Using traveltimes in points 0, 2, 3, 4 and 8 the traveltime at point 6 can be calculated (*scheme B*). To find the traveltime at point 9 the traveltimes at points 0, 3, 4, 5, 6, 7 and 8 are used (*scheme A*).

diagonals of the XY-, XZ- and YZ-planes ($i = 4, 5, 6$ respectively). These velocities are computed as $v_i^2 = (\mathbf{n}^{(i)}, \mathbf{R}\,\mathbf{n}^{(i)})$, where $\mathbf{n}^{(i)}$ is a unit vector in the corresponding direction.

Equation (4.2) with coefficients (4.3) is analogous to the Vidale's approximating equation (1) for isotropic media called scheme A, see Vidale (1990). I will refer to equation (4.2) as *scheme A*. During traveltime computations, the scheme A is applied at the majority of grid points.

Two additional approximations of the eikonal equation (4.1) are also similar to schemes from Vidale (1990). Let us assume the traveltimes at the grid points 0, 1, 2, 3 and 4 (see Fig.4.1) are known, and traveltime at the grid point 0 is minimum. To compute the traveltime t_8, the slowness components p_x and p_y are approximated by

$$p_x = \frac{t_3 - t_1}{2h}, \qquad p_y = \frac{t_4 - t_2}{2h}.$$

The eikonal equation (4.1) is then solved for the remaining component:

$$p_z = \frac{t_8 - t_1}{h},$$

which leads to traveltime t_8. This computation scheme I will denote as *scheme C*.

A third formulae called *scheme B* makes it possible to compute the traveltime t_6, when traveltime t_0 is minimum and traveltimes at the grid points 0, 2, 3, 4 and 8 are known. The slowness components can then be approximated by

$$p_x = \frac{t_3 - t_0 + t_6 - t_8}{2h}, \qquad p_y = \frac{t_4 - t_2}{2h}, \qquad p_z = \frac{t_8 - t_0 + t_6 - t_3}{2h}.$$

With these expressions the eikonal equation (4.1) is solved for the unknown traveltime t_6.

Global problem

We need to define an order in which traveltimes are assigned to grid points. Vidale (1988) suggested a computational order which corresponds to expanding squares starting from the source. The expanding squares scheme is fast, but for an ellipsoidal medium it is more convenient to use the scheme of expanding wavefronts suggested by Qin et al. (1992). This scheme retains causality and guarantees stability of the traveltime computations.

In the scheme of expanding wavefronts, grid points are timed according to the order in which the wave fronts reaches them. Figure 4.2 illustrates how the scheme of expanding

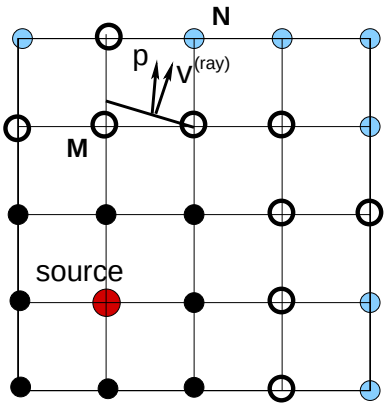

Figure 4.2: Expanding wavefront. The unfilled disks form a perimeter surface of the grid points with already known traveltimes (the inner timed grid points are shown with black filled circles). The gray disks denote the grid points with unknown traveltimes. Traveltime at the point M is minimal among the perimeter surface points. To compute traveltime at point N the slowness $\mathbf{p}$ as well as the ray velocity $\mathbf{v}^{(ray)}$ need to be determined. Since in anisotropic media there are two velocities – phase and ray velocities, the slowness direction and direction of the ray velocity do not coincide.

works. For simplicity the 2D sketch is used. For the initialization of the procedure, several grid points around the source location have to be timed using any method for traveltime computation, for example ray tracing. Then, the grid point with the minimum traveltime (the grid point M in Fig. 4.2) among the timed points of the outer perimeter (unfilled circles on Fig. 4.2) is determined. Because it is the point at which the wavefront first reaches the perimeter surface, the region, where traveltimes for all grid points are founded, should be expanded from this point first. All grid points (the gray discs) with unknown traveltimes next to the grid point with the minimum traveltime are timed using the FD approximating *scheme A*, *B* or *C*. The newly timed points are used to form the update perimeter surface of the grid points with known traveltimes. And the procedure is repeated until traveltimes for all points inside the model are computed.

In isotropic media this procedure provides the causal expansion of the FD scheme. For anisotropic media, however, an additional test has to be performed. In anisotropic media, two types of velocities should be considered: ray velocity and phase velocity. The propagation of energy and, therefore, the causal expansion of the FD scheme is governed by the ray velocity vector. But the eikonal equation controls only the phase velocity. Therefore, for every step of the FD scheme, we need to compare the direction of the scheme of expansion with the direction of the ray velocity. The traveltime at a given grid point has been successfully computed only if the directions coincide, otherwise, the point with minimum traveltime is not a point for a casual expansion and we have to consider the point with the next minimum of traveltime. In the case of arbitrarily anisotropic medium, to calculate of the ray velocity vector, the polarization vector is also required. It entails expensive computations. But, in the case of an ellipsoidally anisotropic medium, the ray velocity vector, $\mathbf{v}^{(ray)}$, depends only on the slowness vector $\mathbf{p}$ determined from the eikonal equation (4.1) and matrix $\mathbf{R}$ of velocity parameters in the cell considered:

$$\mathbf{v}^{(ray)} = \mathbf{R}\,\mathbf{p}. \tag{4.4}$$

4.2.3 Accuracy of the FD scheme

To investigate the accuracy of the traveltime computation by the 3-D FD eikonal solver for an ellipsoidally anisotropic medium a homogeneous model is considered, since for this medium an analytical solution for the traveltimes exists.

Figure 4.3 shows the wavefronts obtained from numerically computed traveltimes for two different ellipsoidally anisotropic models. These ellipsoidally anisotropic models are obtained as the best-fitting ellipsoidal background models for the anisotropic models of triclinic sandstone and orthorombic olivine. The matrices $\mathbf{R}$ of the ellipsoidal media are given in Tables 4.1 and 4.2 (see pages 76 and 80). Because a 3-D model is considered two vertical slices are displayed. One slice includes the source position (on the left-hand side of Fig. 4.3) the other slice has a lateral offset from the source (on the right-hand side of Fig. 4.3). The underlying gray scale images show the relative errors with respect to analytically computed traveltimes. The numerical examples demonstrate, that the traveltimes in elliptically anisotropic media are computed with high accuracy. The maximum error for the examples shown is below 0.5%. This error is entirely attributed to the fact, that the eikonal equation for ellipsoidally anisotropic media is expressed by finite differences. This is similar to the well known errors obtained by expressing the eikonal equation for isotropic media by finite differences.

The computation of traveltimes in ellipsoidally anisotropic media is the first step in the approach for computing traveltimes in arbitrarily anisotropic media. Media of ellipsoidal anisotropy will serve as background models in the perturbation approach to compute traveltimes in media of strong arbitrary anisotropy. The perturbation scheme is discussed in the next section.

4.2.4 Basic perturbation formulae

To compute traveltimes for an arbitrarily anisotropic medium a perturbation scheme is embedded into an FD eikonal solver: traveltimes at every grid point of the background model are computed using a FD eikonal solver for isotropic media (in the case of weak anisotropy) or ellipsoidally anisotropic media (in the case of strong anisotropy). The perturbation method is used for the computation of the traveltime corrections to yield traveltimes in the perturbed (arbitrarily anisotropic) model.

To compute the traveltime correction, the raypath between the source and receivers in the background medium must be known. Rays are not determined in the FD method. In the FD method traveltimes are computed on a discrete grid assuming local plane wavefronts inside the grid cell, therefore, we compute the traveltime correction along the ray segments corresponding to the plane wavefronts in each cell. The ray segment is a straight line between the grid point (see Figure 4.4), where the traveltime needs to be computed (point A7), and the point where the ray crosses the cell boundary (point N) which is defined by the orientation of the ray velocity vector. The ray velocity vector for the background ellipsoidal medium is given by the equation (4.4). The traveltime at the intersection point N of the ray segment with the cell boundary (see Fig. 4.4) is obtained by linear interpolation between the corner points A0 to A3 of the cell of the corresponding background model. Therefore, the traveltime at point A7 for the perturbed model is given by:

$$t_{pert}(A7) = t_{ref}(A7) + \Delta t'(N) + \Delta t(N, A7),$$

where t_{pert} is the traveltime in the perturbed model and t_{ref} is the traveltime in the background model, $\Delta t'(N) = t_{pert}(N) - t_{ref}(N)$ is the difference between the traveltimes at point N in the perturbed and background models, and $\Delta t(N, A7)$ is the traveltime

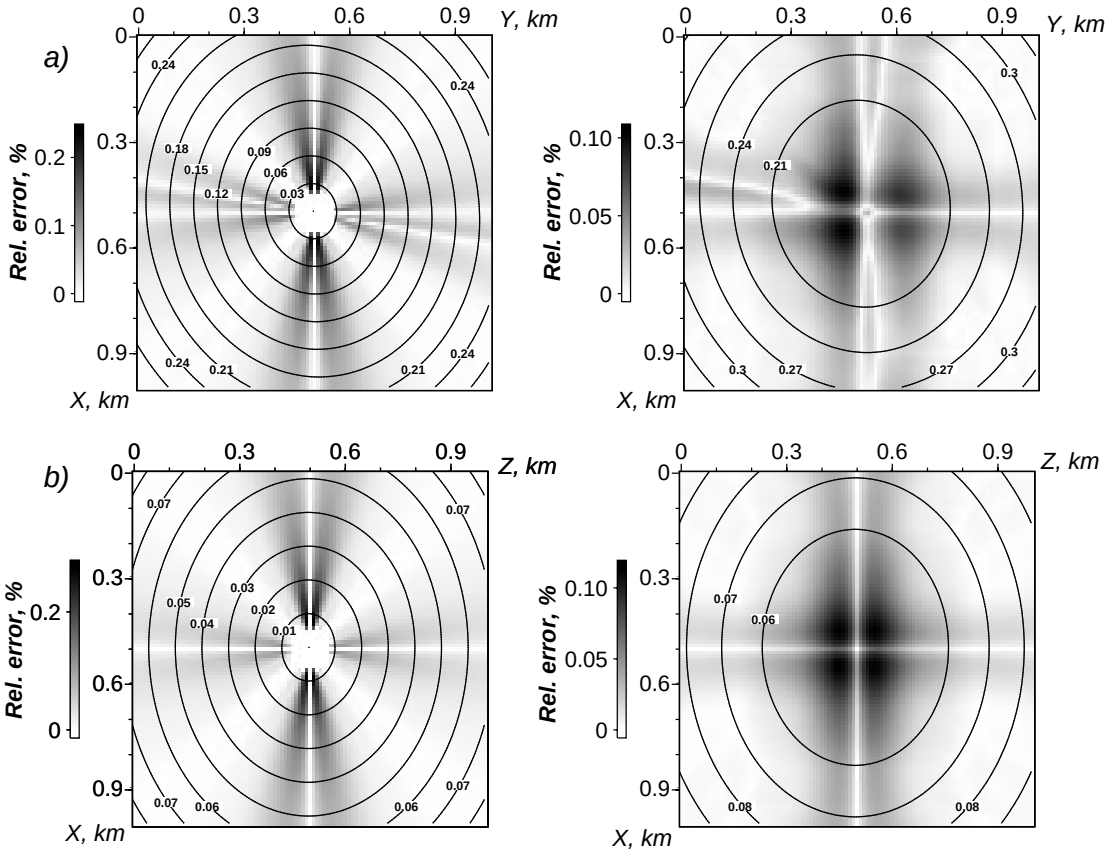

Figure 4.3: Wavefronts in a homogeneous ellipsoidally anisotropic model: (*a)* — in the elliptical background medium for triclinic sandstone, for the parameters, see Tab. (4.2); (*b)* — in the elliptical background medium for olivine, for the parameters, see Tab. (4.1). For each model there are two vertical slices: with offset 0 km (left) and 0.4 km (right) from the source located at (0.5, 0.5 and 0.5 km). Underlying gray scale images shows the relative errors of the traveltime computation with respect to analytically computed traveltimes. The maximum of the relative errors in the 3-D model does not exceed 0.4% for the case (*a)* and 0.5% for the case (*b)*.

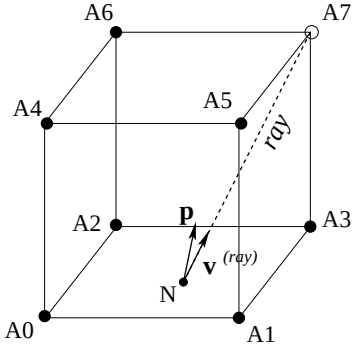

Figure 4.4: Grid cell with already timed points A1 to A6. A locally plane wavefront is assumed to propagate through the cell to compute the traveltime at A7, $\mathbf{p}$ is the slowness vector in the background medium. The raypath in the cell is defined by the direction of the ray velocity $\mathbf{v}^{(ray)}$. The ray segment (dashed line) is a straight line connecting the intersection point, point N, of the ray with the cell boundary and the grid point A7.

correction derived by Červený and Jech (1982):

$$\Delta t(N, A7) = -\frac{1}{2} \int_{t_{ref}(N)}^{t_{ref}(A7)} \Delta a_{ijkl}\, p_i\, p_l\, \mathrm{g}_j\, \mathrm{g}_k\, dt, \tag{4.5}$$

where

$$\Delta a_{ijkl} = a^{pert}_{ijkl} - a^{ref}_{ijkl}.$$

The parameters a^{pert}_{ijkl} are the density normalized elastic coefficients of the anisotropic medium, p_i are the components of the slowness vector, and g_j are the components of the quasi P-wave polarization vector. The vectors $\mathbf{p}$ and $\mathbf{g}$ are taken in the background medium. For isotropic background media the P-wave polarization is a unit vector which is normal to the wavefront and the density normalized elastic coefficients are defined by

$$a^{ref}_{ijkl} = \frac{\lambda}{\rho}\delta_{ij}\delta_{kl} + \frac{\mu}{\rho}\Big(\delta_{ik}\delta_{jl} + \delta_{il}\delta_{jk}\Big),$$

with the Lamé parameters μ and λ.

In the case of the ellipsoidal background medium we substitute the wavefront normal vector $\mathbf{n}$ instead of the unknown polarization vector $\mathbf{g}$ (similar to the approach used in Ettrich et al., 2001), therefore, the traveltime correction reads:

$$\Delta t(N, A7) \approx -\frac{1}{2}\int\limits_{t_{ref}(N)}^{t_{ref}(A7)} \Big(a^{pert}_{ijkl} n_j n_k - R_{il}\Big)\, p_i p_l dt, \tag{4.6}$$

where R_{il} is the 3×3 matrix of the ellipsoidal background medium introduced in equation (4.1). Since the medium inside of the cells is homogeneous the equation (4.6) can be simplified:

$$\Delta t(N, A7) \approx -\frac{t_{ref}(A7) - t_{ref}(N)}{2}\Big(a^{pert}_{ijkl} n_j n_k - R_{il}\Big)\, p_i p_l, \tag{4.7}$$

The assumption that the orientation of the vector of polarization coincides with the orientation of the wavefront normal introduces an additional error, which is quantified by several numerical examples in the following section.

4.3 Numerical examples

To illustrate the traveltime computation by the FD perturbation method in 3-D anisotropic media, two types of symmetries, triclinic and orthorombic, are chosen. To obtain an estimate on the accuracy we consider homogeneous media. For comparison, traveltimes for all models are computed with respect to isotropic and ellipsoidally anisotropic background models. In the figures, traveltimes are displayed as first-arrival wavefronts. Traveltimes in the perturbed medium are called exact traveltimes (exact wavefronts) if they are computed analytically or by the methods which provide higher accuracy then the FD perturbation method. They are considered to be exact with respect to the proved accuracy of the method used.

The traveltime errors in the examples are caused by three sources: (1) the error of the numerical computation of traveltimes in the background ellipsoidal (or isotropic) model using the FD eikonal solver which we already quantified above, (2) the inherent error of the perturbation technique, and (3) the error by approximating the unknown polarization vector $\mathbf{g}$ by the wavefront normal vector $\mathbf{n}$ (in the case of an ellipsoidal background model).

For all examples, a model cube of 101 grid points along each spatial direction is considered. The grid spacing is 10 m. The source is located at the center of the models, at (0.5, 0.5, 0.5 km). A cubic region of 11 grid points around the source is initialized using the exact solution. Since 3-D models are presented I always show two vertical slices: with zero and non-zero offset from the source.

4.3.1 Homogeneous medium with orthorombic symmetry

First, a model with orthorombic anisotropic elastic parameters of olivine (parameters taken from Babuska et al., 1991) is considered. The density normalized parameters (in km^2/s^2) are given in Table 4.1.

$$\begin{pmatrix} 97.77 & 21.62 & 20.05 & 0. & 0. & 0. \\ & 71.0 & 22.83 & 0. & 0. & 0. \\ & & 59.68 & 0. & 0. & 0. \\ & & & 19.51 & 0. & 0. \\ & & & & 23.86 & 0. \\ & & & & & 23.77 \end{pmatrix} \Rightarrow R_{il} = \begin{pmatrix} 91.99 & 0 & 0 \\ & 67.35 & 0 \\ & & 57.25 \end{pmatrix} ; \; V_p = 8.5 \, \frac{km}{s}$$

Table 4.1: The density normalized elastic parameters of orthorombic model of olivine (left). Coefficients for the best-fitting ellipsoid background medium (Ettrich et al., 2001) and the P-wave velocity, V_p for the best-fitting isotropic background medium (Fedorov, 1968) are listed on the right-side. RMSD from the isotropy is 18.7%.

The relative square root deviation (RMSD) of the orthorombic medium considered from the best-fitting isotropic medium is 18.7%. For the qP-wave the difference between velocities along the X- and Z-axes directions totals 22%. To compute traveltimes in this medium with sufficiently strong qP-wave anisotropy I use three types of background media: isotropic, ellipsoidally anisotropic and transversely isotropic with elliptical qP-wavefronts.

The isotropic background medium is constructed using formulae for the best fitting isotropic background medium (Fedorov, 1968). The traveltimes for this isotropic background medium is computed by the FD eikonal solver. Then, to compute the traveltimes in the orthorombic medium, the traveltime corrections are performed. There are no problems to apply equation (4.5) for traveltime corrections. In the isotropic background medium the polarization of the qP-wave, $\mathbf{g}$, is a unit vector in the direction of the slowness vectors. Results of the traveltime computations for the orthorombic olivine model are shown in Figures 4.5 (slices including the source position) and 4.6 (slices with offset from the source position). Figures 4.5a and 4.6a display the exact wavefronts in the olivine model (solid lines) and the circular wavefronts for the best-fitting isotropic background medium (dashed lines). The exact wavefronts in the olivine model are obtained from the traveltimes computed by anisotropic ray shooting. Figures 4.5b and 4.6b show the exact wavefronts and the wavefronts from the traveltimes computed by the FD perturbation method with the best-fitting isotropic background medium. The underlying gray scale images of relative errors between the FD perturbation traveltimes with respect to the exact traveltimes are shown. (Note that the white color box around the source position corresponds to several

grid points where the traveltimes have been computed by the anisotropic ray shooting to start the finite-difference computations.) The errors depend of the directions. The largest relative errors (darker color) between exact (dashed lines) and FD perturbation traveltimes (solid lines) appear in directions where the isotropic background medium gives the worst fit. The maximum relative error for the complete model is 3.9 %. Such large error is expected, because the anisotropy of the perturbed model is too strong to use an isotropic background medium.

The ellipsoidally anisotropic background medium for the perturbation method allows to consider stronger anisotropy. However, for this type of background medium the polarization vector required for the calculation of the traveltime correction is unknown. Since, the qP-polarization vector and the phase normal vector are close. I approximate the polarization vector by the phase normal vector to compute the traveltime correction. The phase normal vector is determined as a unit vector in the slowness direction. Therefore, to compute the traveltime corrections in the perturbed model, an approximate equation (4.6) is used instead of equation (4.5).

Figures 4.5*c* and 4.6*c* show the exact wavefronts in olivine (solid lines) and the wavefronts in the best-fitting ellipsoidally anisotropic background medium (dashed lines). The ellipsoidally anisotropic background medium yields a better fit to the orthorombic medium compared to the isotropic background medium. Figures 4.5*d* and 4.6*d* show that the accuracy of the traveltime computation is higher than in the previous case with the isotropic background medium. The errors depend on the directions. The maximum relative error for the model is 1.9%. This error is mainly due to the approximation of the unknown polarization vector by the phase normal, while the error produced by the traveltime computation using the FD eikonal solver in the background model does not exceed 0.5% (see discussion above and Figure 4.3*b*).

Following Burridge et al. (1993) there are three possibilities to simplify orthorombic symmetry to ellipsoidal symmetry. One of these three possibilities is a transversely isotropic medium with elliptical qP-wavefronts. For this case we can compute the correct polarization vector for the ellipsoidal anisotropic background medium. A transversely isotropic medium with the axis of symmetry along the X-axis has ellipsoidal symmetry if the non-zero elastic parameters satisfy the relations:

$$\begin{aligned} &A_{22} = A_{33}; \quad A_{12} = A_{13}; \quad A_{55} = A_{66}; \\ &A_{44} = \frac{1}{2}(A_{22} - A_{23}); \quad A_{55} = \frac{A_{11}A_{22} - A_{12}^2}{A_{11} + A_{22} + 2A_{12}}. \end{aligned} \tag{4.8}$$

Since, there are non-linear relations between the elastic parameters in equation (4.8), I construct the transversely isotropic background medium in the following manner. Four elastic parameters are determined from the elastic parameters of the olivine model

$$A_{11} = A_{11}^{oliv}; \quad A_{12} = \frac{1}{2}(A_{12}^{oliv} + A_{13}^{oliv}); \quad A_{22} = \frac{1}{2}(A_{22}^{oliv} + A_{33}^{oliv}); \quad A_{23} = A_{23}^{oliv}.$$

and, then, relations (4.8) are used to obtained the elastic parameters A_{44} and A_{55}.

Figures 4.5*e,f* and 4.6*e,f* show results of the traveltime computations by the FD perturbation method with the transversely isotropic background medium. Figures 4.5*e* and 4.6*e*

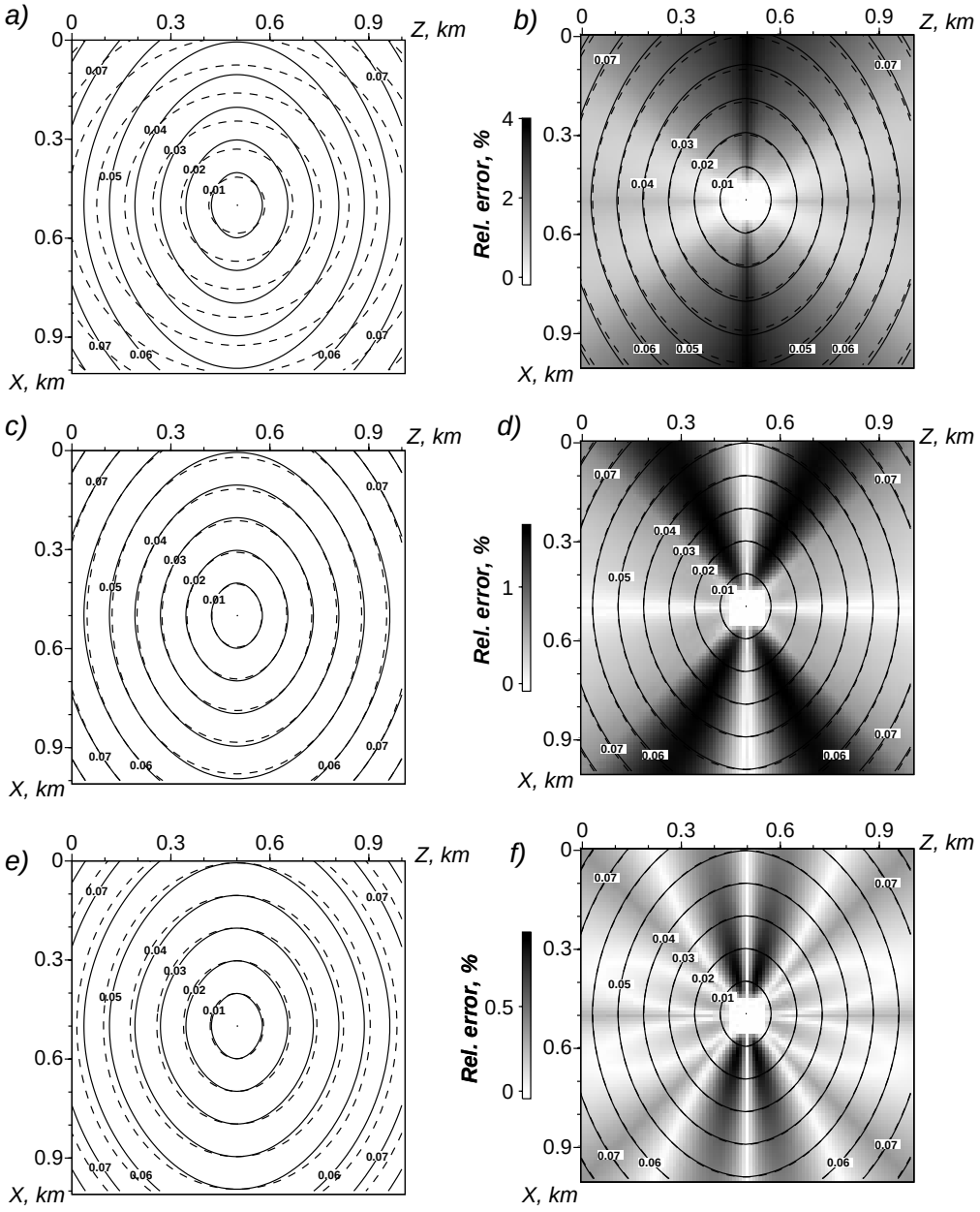

Figure 4.5: Wavefronts in a homogeneous model of olivine; vertical slices including the source at (0.5, 0.5, 0.5 km) are shown. In the left-hand diagrams, solid lines show exact wavefronts and dashed lines show wavefronts in the background models: *(a)* — isotropic model; *(c)* — ellipsoidally anisotropic model; *(e)* — transversely isotropic model. The diagrams on the right-hand side show the FD perturbation method wavefronts (solid) for the corresponding background model and exact wavefronts (dashed) with the underlying gray scale images of relative errors. Note that the error scales are different in *(b)*, *(d)* and *(f)*.

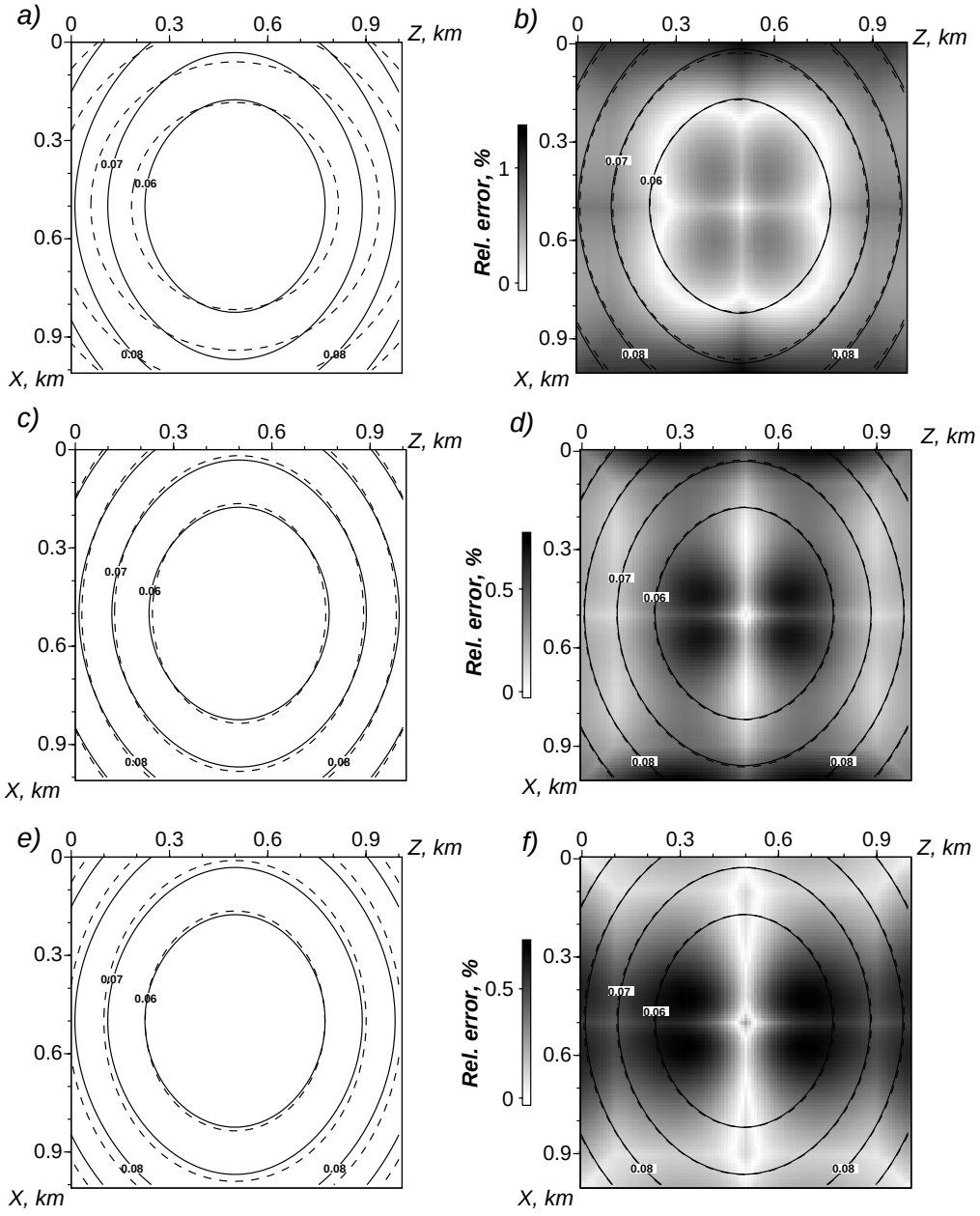

Figure 4.6: Wavefronts in a homogeneous model of olivine; vertical slice with offset 0.4 km from the source at (0.5, 0.5, 0.5 km). In the left-hand diagrams solid lines show exact wavefronts and dashed lines show wavefronts in background models: *(a)* — isotropic model; *(c)* — ellipsoidally anisotropic model; *(e)* — transversely isotropic model. The right-side diagrams show the FD perturbation method wavefronts (solid) for the corresponding background model and exact wavefronts (dashed) with the underlying gray scale images of relative errors. Please note that the error scales are different in *(b)*, *(d)* and *(f)*.

display the exact wavefronts in olivine and the wavefronts in the transversely isotropic background medium. Figures 4.5*f* and 4.6*f* show the exact wavefronts (dashed) in the olivine and the wavefronts constructed from the FD perturbation traveltimes. Underlying gray scale images display the relative errors between the exact and FD perturbation traveltimes. The maximum of the relative errors in the model does not exceeds 1.2%. The errors depend of the directions. The largest relative errors are located where bigger differences of the angle between the wavefront normals in the perturbed and background media occur (in other words, the wavefront curvatures are too different).

4.3.2 Homogeneous medium with triclinic symmetry

Next numerical example is a model of triclinic sandstone. The parameters are taken from Mensch and Rasolofosaon (1997). The density normalized parameters (in km^2/s^2) are given in Table 4.2.

$$\begin{pmatrix} 6.77 & 0.62 & 1.0 & -0.48 & 0. & -0.24 \\ & 4.95 & 0.43 & 0.38 & 0.67 & 0.52 \\ & & 5.09 & -0.28 & 0.09 & -0.09 \\ & & & 2.35 & 0.09 & 0. \\ & & & & 2.45 & 0. \\ & & & & & 2.88 \end{pmatrix} \Rightarrow R_{il} = \begin{pmatrix} 6.88 & 0.27 & 0.27 \\ & 5.10 & -0.05 \\ & & 5.08 \end{pmatrix} ; \; V_p = 2.38 \, \frac{km}{s}$$

Table 4.2: The density normalized elastic parameters of triclinic sandstone (left). Coefficients for the best-fitting ellipsoid background medium and the P-wave velocity, V_p, for the best-fitting isotropic background medium are listed on the right-side.

The RMSD of the triclinic medium considered from the best-fitting isotropic medium is 21%. For the qP-wave the difference between velocities along the X- and Y-axes directions totals 14.5%. The medium has strong qP-wave anisotropy and irregular velocity surfaces caused by the relatively small "non-orthorombic" coefficients.

The left-hand sides of Figure 4.7 and Figure 4.8 display exact wavefronts in the triclinic sandstone (solid lines) and background wavefronts (dashed lines) in the ellipsoidal background model (Fig. 4.7*a* and 4.8*a*) and in the isotropic background model (Fig. 4.7*c* and 4.8*c*). On the right-hand side, these figures display results of the numerical computation by the FD perturbation method using the ellipsoidal background medium (Figures 4.7*b* and 4.8*b*) and the background isotropic background medium (Fig. 4.7*d* and Fig. 4.8*d*). The underlying gray scale images show the relative errors with respect to the exact solutions. The maximum relative error in the model is 2.3% when the ellipsoidal background medium is used and 2.4% for the isotropic background medium. Although the maximum error in traveltimes using the ellipsoidally anisotropic background medium is close to the maximum error in the traveltimes for the isotropic medium for this particular model, as may be seen from Figures 4.7 and 4.8, the accuracy for the ellipsoidal background medium is considerably better for most parts of the model (mostly light gray despite a different gray scale than for the isotropic model).

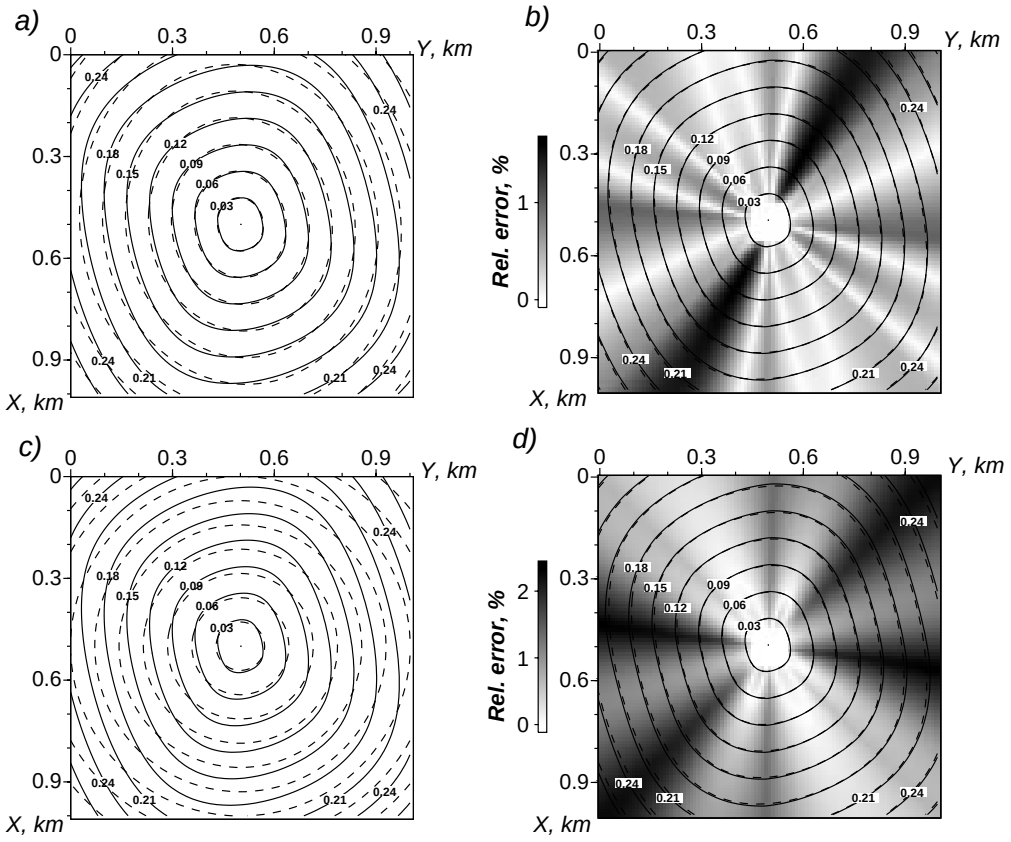

Figure 4.7: Wavefronts in a homogeneous model of triclinic sandstone; vertical slice including the source at (0.5, 0.5, 0.5 km). On the left-hand side diagrams show exact wavefronts (solid) and background wavefronts (dashed): *(a)* — ellipsoidal anisotropic model; *(c)* — isotropic model. The right-hand side diagrams show FD perturbation method wavefronts (solid) for the corresponding background model and exact wavefronts (dashed) with underlying gray scale images of relative errors: *(b)* — ellipsoidal anisotropic background model; *(d)* — isotropic background medium. Please note that the error scales are different in *(b)* and *(d)*.

4.3.3 Factorized anisotropic inhomogeneous medium

The numerical examples presented above were homogeneous in order to validate the method and to investigate the errors, since for heterogeneous arbitrarily anisotropic models no exact solution for the traveltimes are available. The FD eikonal solver combined with the perturbation approach can be used to compute traveltimes in heterogeneous anisotropic media without any change to the technique described above. The only condition is that the model has to be smooth. There are many methods to smooth isotropic inhomogeneous media (see, e.g., Versteeg, 1993). In anisotropic models, smoothing of 21 elastic parameters has to be performed. This complex problem is a topic for special investigation and is not considered here.

Here a factorized anisotropic inhomogeneous (FAI) medium is considered as heterogeneous model. The FAI medium was suggested by Červený and Simões-Filho (1991).

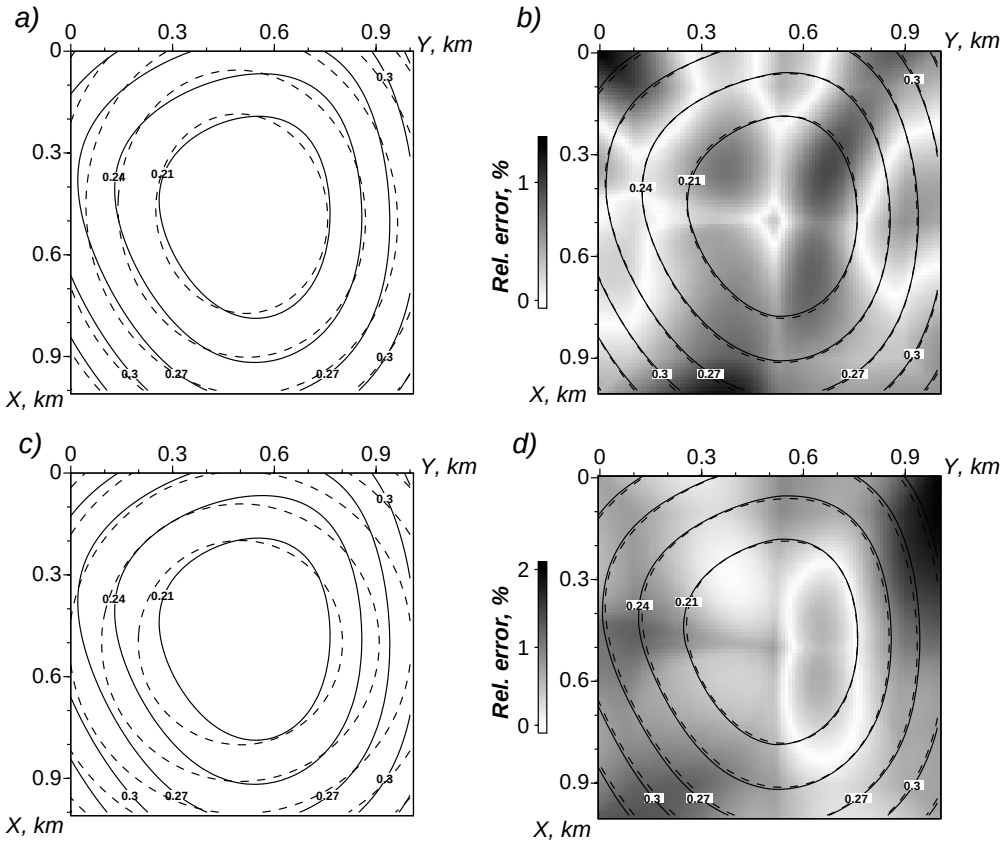

Figure 4.8: Wavefronts in a homogeneous model of triclinic sandstone; vertical slice with offset 0.4 km from the source at (0.5, 0.5, 0.5 km). On the left-hand side diagrams show exact wavefronts (solid) and background wavefronts (dashed) are shown: *(a)* — ellipsoidal anisotropic model; *(c)* — isotropic model. The right-hand side diagrams FD perturbation method wavefronts (solid) for the corresponding background model and exact wavefronts (dashed) with underlying gray scale images of relative errors: *(b)* — ellipsoidal anisotropic background model; *(d)* — isotropic background medium. Please note that the error scales are different in *(b)* and *(d)*.

Use of this type of medium allows us to construct a smooth inhomogeneous anisotropic model. For factorized anisotropic inhomogeneous media, the density normalized elastic parameters a_{iklm} can be described by the relation:

$$a_{iklm}(\mathbf{x}) = f^2(\mathbf{x})\, A_{iklm},$$

where A_{iklm} are elastic constants (in km^2/s^2), independent of coordinates $\mathbf{x}$, and $f^2(\mathbf{x})$ is a continuous smooth function of coordinates $\mathbf{x}$. The types of anisotropy A_{iklm} and inhomogeneity $f^2(\mathbf{x})$ are not restricted.

To construct the FAI medium for the next example the elastic parameters of a transversely isotropic (TI) medium are multiplied in each cell by the corresponding value of the function $f^2(\mathbf{x})$. This value I will call factor. The factors vary smoothly from 1.9 to 4 and form a parabolic lens. In Figure 4.9 the left-hand table displays the elastic parameters for the transversely isotropic medium are presented. (Thomsen's parameters of this medium

are $\varepsilon = 0.143$, $\gamma = 0.508$ and $\delta = 0.202$.) The right-hand side image displays the values of the factors for different cells. The source is at (0.45, 0.45, 0.05 km). The source and the lens center are situated at the same vertical (XZ and YZ) sections.

Since exact traveltimes for the FAI medium can not be determined, I compare traveltimes computed by the FD perturbation method with traveltimes computed by a wavefront-oriented ray tracing (WRT) method for anisotropic media (Kaschwich and Gajewski, 2003). The WRT method is more time consuming in comparison to the FD perturbation method, but it provides higher accuracy. For a homogeneous medium with triclinic symmetry from Table 4.2, the maximum of relative errors following from the WRT method does not exceed 0.3%, while for the homogeneous TI medium from the left-hand side table in Figure 4.9 the maximum of relative errors is only 0.2% for WRT traveltimes. Also in contrast to finite-difference methods, the WRT method does not accumulate the errors with growing distance from the source. In the WRT method errors are mainly located in the small source area. Outside of this area the relative errors are less then 0.01%. All traveltime computations using the WRT method were performed by Tina Kaschwich.

The traveltime computations by the FD perturbation method were performed with respect to the ellipsoidally anisotropic background medium as well as with respect to the isotropic background medium. Since, the medium considered is inhomogeneous, the background media are also inhomogeneous. The parameters for the best-fitting background media are defined in each cell from the corresponding elastic parameters a_{iklm} (see Fig. 4.9) according to equations (4.9) or (4.10).

Figure 4.10 shows the results of the traveltime computation for the FAI model. The solid lines in Figure 4.10 show FD perturbation wavefronts in the FAI medium. The dashed lines display wavefronts for the background media. The underling images show relative errors with respect to traveltimes computed by the WRT method. Similar to

$$a_{iklm} = \text{“}factor\text{''} \cdot A_{iklm},$$

$$A_{iklm} = \begin{pmatrix} 15.96 & 6.99 & 6.06 & 0. & 0. & 0. \\ & 15.96 & 6.06 & 0. & 0. & 0. \\ & & 11.4 & 0. & 0. & 0. \\ & & & 2.22 & 0. & 0. \\ & & & & 2.22 & 0. \\ & & & & & 4.48 \end{pmatrix}$$

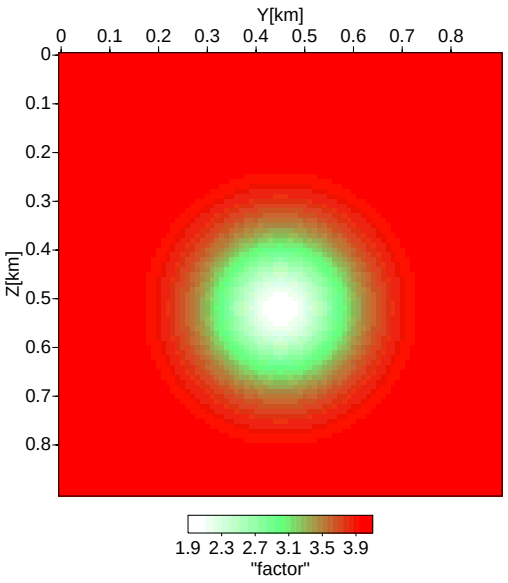

Figure 4.9: FAI medium. The left-hand table presents the elastic parameters A_{iklm} defining a transversely isotropic medium. The right-hand side image displays values of the function of coordinates $f^2(\mathbf{x})$ for different cells. The values vary from 1.9 to 4. and forms a parabolic lens.

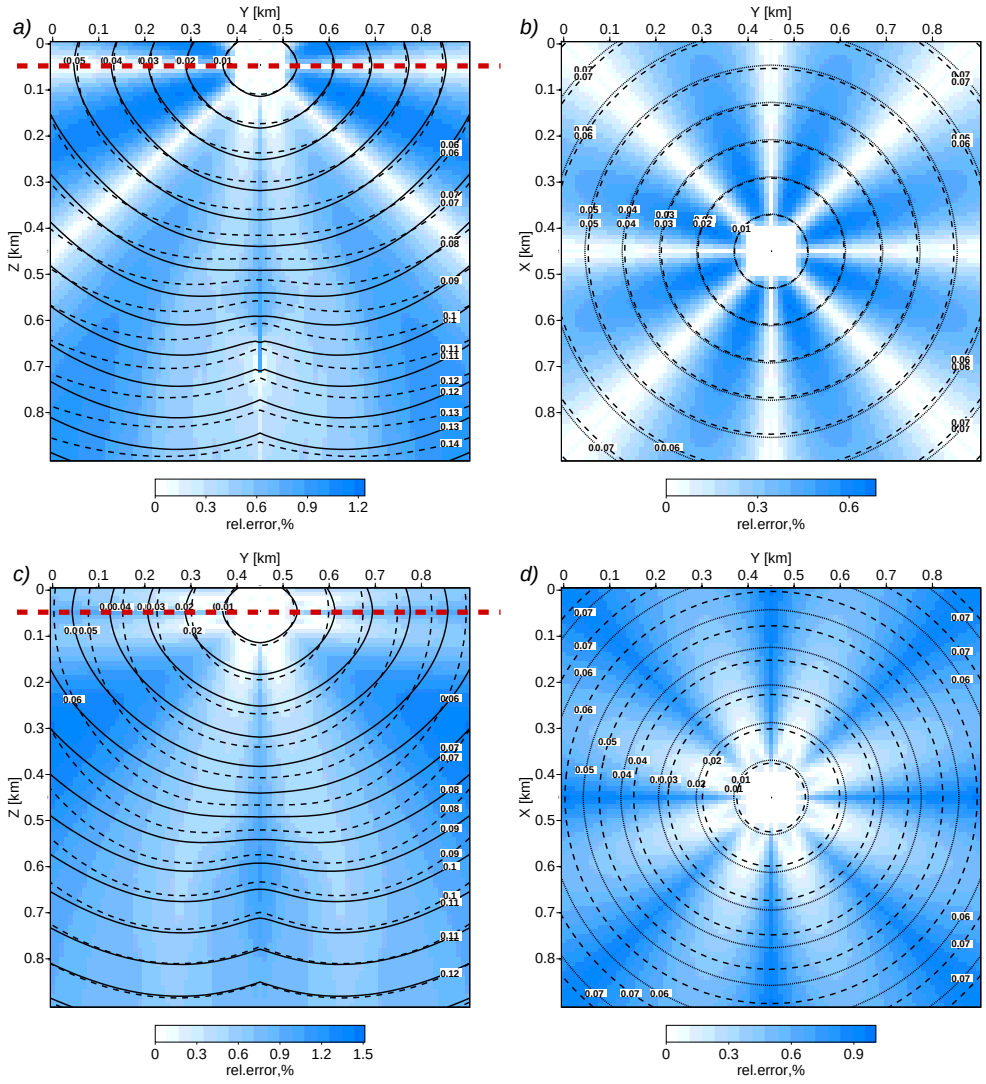

Figure 4.10: Wavefronts in a factorized anisotropic inhomogeneous model from Fig. 4.9; vertical YZ (on the left side) and horizontal XY (on the right side) slices including the source at (0.45,0.45,0.05 km). Bold dashed lines show the position of the horizontal slides. The solid lines show the FD perturbation method wavefronts and thin dashed lines show wavefronts in the background models: *(a)* and *(b)* — ellipsoidally anisotropic model; *(c)* and *(d)* — isotropic model. The underlying gray scale images show relative errors with respect to traveltimes computed by the wavefront-oriented ray tracing method. Please note the different error scales.

the homogeneous examples, the traveltime computation with respect to the ellipsoidally anisotropic background medium provides slightly better accuracy. The maximum of the relative errors is 1.6%. For the traveltime computation with respect to the isotropic background medium the maximum error is 1.8%. The average relative error is 0.6% in the former case and 0.8% in the latter case.

Also, the errors depend on the directions. Due to the perturbation technique, the directions where the curvatures of the wavefronts in the background and perturbed media are close to each other are characterized by smaller errors. Please note, that the errors in Figure 4.10*c* are higher for directions where the FD perturbation wavefronts and the

isotropic wavefronts cross each other. The ellipsoidally anisotropic background medium gives a better fit to the FAI medium, but additional errors are introduced due to the assumption about the polarization vector.

4.4 Conclusions

In this chapter a finite-difference perturbation method for the efficient computation of traveltimes for qP-waves in arbitrarily anisotropic 3-D media was presented. An arbitrarily anisotropic medium was considered as a perturbed model with respect to a simple background medium. Traveltimes in the background medium are computed using an FD eikonal solver which allows fast and accurate computation of traveltimes. Traveltimes in the perturbed medium are obtained by adding traveltime corrections to the traveltimes of the background medium using a perturbation approach. Instead of the raypath between source and a grid point, the ray segments corresponding to plane wavefronts in each grid cell were used.

Models of ellipsoidal symmetry as a background model to compute traveltimes for strongly anisotropic media were discussed. An ellipsoidally anisotropic medium approximates a medium of strong anisotropy better than an isotropic one. The corresponding eikonal equation is only slightly more complex than for the isotropic case. The primary source of errors related to the ellipsoidally anisotropic medium is the unknown polarization vector which is needed to carry out the computation of the traveltime corrections using the perturbation method. The unknown polarization vector was substituted by the phase normal vector to compute the traveltime correction, thus leading to additional errors. The accuracies of the traveltime computations using the different background media were tested. The maximum relative error in the model for an olivine model with respect to the isotropic background model was 3.9%. For the ellipsoidally anisotropic background model it was 1.9%. A transversely isotropic medium possessing elliptical qP-wavefronts was also used as the background medium. The polarization vectors for this medium are known. Therefore, the maximum relative error did not exceeds 1.2%. It is obvious that for the isotropic background model, the deviation between the perturbed and the background model is too large in order to the perturbation method provides good accuracy. In this case the error of the perturbation scheme is larger than the error caused by the approximation of the unknown polarization vectors in the case of an ellipsoidally anisotropic background medium.

The FD eikonal solver combined with the perturbation approach can be used to compute traveltimes in heterogeneous anisotropic media without any change to the technique described above. The only condition is that the model has to be smooth. The accuracy of the traveltime computation for inhomogeneous anisotropic medium was tested for a factorized medium. The computed traveltimes were compared with traveltimes obtained by a wavefront-oriented ray tracing (considered as exact method, since its maximum relative errors did not exceed 0.3% for homogeneous models). The accuracy of the FD perturbation method in the heterogeneous model considered was 1.6% in the case of ellipsoidal anisotropic background medium and 1.8% in the case of isotropic background medium.

The presented FD eikonal perturbation technique can be used for the fast compu-

tation of qP-wave traveltimes in arbitrarily anisotropic media. It provides an efficient tool to compute diffraction surfaces for Kirchoff type of migration of reflection data from anisotropic media.

Appendix

A. Best-fitting isotropic background medium

To construct the background isotropic model the formulae for the best-fitting isotropic medium derived by Fedorov (1968) are used:

$$\begin{aligned} \mu &= \frac{1}{30}\Big(3c_{ikik} - c_{iikk}\Big) \\ \lambda &= \frac{1}{30}\Big(3c_{iikk} - c_{ikik}\Big) - \mu. \end{aligned} \tag{4.9}$$

Here, the λ and μ are Lamé parameters of the isotropic medium, c_{iklm} are the elastic parameters of the anisotropic medium under consideration.

B. Best-fitting ellipsoidal background medium

The linear relation for the coefficients R_{ik} $(i,k = 1,2,3)$ of the best-fitting ellipsoidal medium and the elastic coefficients of the arbitrarily anisotropic medium $A_{\alpha,\beta}$ $(\alpha,\beta = 1,\ldots,6)$ were obtained by Ettrich et al. (2001):

$$\begin{aligned} R_{11} &= \frac{1}{35}\Big(27A_{11} + 8A_{12} + 8A_{13} + 16A_{55} + 16A_{66} - 3A_{22} - 3A_{33} - 4A_{44} - 2A_{23}\Big) \\ R_{22} &= \frac{1}{35}\Big(27A_{22} + 8A_{12} + 8A_{23} + 16A_{44} + 16A_{66} - 3A_{11} - 3A_{33} - 4A_{55} - 2A_{13}\Big) \\ R_{33} &= \frac{1}{35}\Big(27A_{33} + 8A_{13} + 8A_{23} + 16A_{44} + 16A_{55} - 3A_{11} - 3A_{22} - 4A_{66} - 2A_{12}\Big) \\ R_{12} &= \frac{2}{7}\Big(3A_{16} + 3A_{26} + A_{36} + 2A_{45}\Big) \\ R_{13} &= \frac{2}{7}\Big(3A_{15} + 3A_{35} + A_{25} + 2A_{46}\Big) \\ R_{23} &= \frac{2}{7}\Big(3A_{24} + 3A_{34} + A_{14} + 2A_{56}\Big). \end{aligned} \tag{4.10}$$

Chapter 5

Inversion

The tomographic inversion of traveltimes of waves propagating in an elastic medium is a powerful tool to determine the elastic moduli (parameters) of this medium. The presence of anisotropy requires that tomographic methods be generalized to account for anisotropy. In the general case of anisotropy, the tomographic inversion of qP- as well as qS-wave traveltimes are non-linear problems.

The assumption of weak anisotropy allows to simplify the solution of the forward modeling and to obtain relations between perturbations of the elastic parameters with respect to an isotropic background medium and the corresponding traveltime perturbations. With the fixed isotropic background medium the relations are inherently linear for qP-waves and, therefore, are very useful for inversion goals. These relations were already used to solve inversion problems in weakly anisotropic media in many studies. However, applying tomographic inversion in weakly anisotropic media for either qP- or qS-wave traveltimes alone allows to determine a limited number of elastic parameters. Only if qP- and qS-wave traveltimes are jointly inverted, the full elastic tensor of the weakly anisotropic medium can be determined. However, the inversion of qS-wave traveltimes leads to non-linear inversion relations. To linearize these relations, I suggest to use qS-wave polarization vectors which are often available from seismic experiments as well as qS-wave traveltimes. If the observed qS-wave polarization vectors are introduced into the inversion, the tomographic relations for qS-waves can be linearized and are then formally identical to those for qP-waves. An important aspect of these relations is that they do not assume any particular symmetry of the anisotropic medium.

In this chapter, the linear tomographic relations for qP- and qS-waves are applied to develop an inversion procedure for the determination of the elastic parameters of an anisotropic medium. The inversion procedure can be applied to anisotropic layered models where the structure is supposed to be known. The determination of the elastic parameters of homogeneous anisotropic layers is performed in a layer-by-layer manner. The qP- and qS-wave traveltimes and qS-wave polarization vectors recorded at receivers within the layers are used as observed data.

After an introduction, I will review the required perturbation equations, followed by the inversion scheme used in this study. Special emphasis will be given on how the qS-wave polarization vectors are used for the inversion. To demonstrate the applicability of the suggested inversion scheme synthetic data for homogeneous anisotropic models with

different types of symmetry (VTI and triclinic) and a model composed from homogeneous anisotropic layers are inverted.

5.1 Introduction

Since many rocks possess an anisotropic structure resulting from, for example, fine-scale layering, the presence of oriented micro-cracks or fractures, or preferred orientation of non-spherical grains or anisotropic minerals, it requires that tomographic methods be generalized to account for anisotropy. The properties of an anisotropic medium are described by the 21 elastic moduli (parameters) of the elasticity tensor (see eqs. (1.1) and (1.2) on page 14). The number of independent moduli can vary depending on the class of symmetry of the elastic medium. For instance, in the case of transversely isotropic symmetry the elasticity tensor consists of five independent parameters. In the case of an anisotropic medium with orthorombic symmetry there are nine independent parameters. The goal of inversion in the presence of anisotropy is the determination of the elastic parameters from observed traveltimes.

The perturbation method is used for the computation of traveltimes in the anisotropic medium. The traveltime of each wave propagating in the anisotropic medium is represented as a sum of the traveltime in the isotropic background medium and the traveltime perturbation due to the deviation of the elastic parameters of the anisotropic medium from the isotropic ones. The basic relations for traveltime perturbations in weakly anisotropic media were established in 1982 (Červený, 1982; Hanyga, 1982). In the homogeneous case the qP-wave traveltime perturbations $\Delta\tau_{qP}$ due to the perturbations of the elastic parameters Δa_{iklm} read as follows (see, e.g., Jech and Pšenčík, 1989; Červený, 2001):

$$\Delta\tau_{qP} = -\frac{\tau_p}{2}\Delta a_{iklm}\, p_i\, p_m\, n_k\, n_l. \tag{5.1}$$

Throughout this chapter summation over the repeated indices is assumed. Here, p_i and τ_p are the components of the slowness vector and the traveltime of the P-wave, respectively, in the isotropic background medium, and n_k are components of the P-wave normal vector. In isotropic media the normal vector coincides with the P-wave polarization vector. With the known isotropic background medium, the traveltime τ_p and the vectors $\mathbf{p}$ and $\mathbf{n}$ can be calculated by the standard isotropic ray method. As a result, equation (5.1) provides a linear relation between the perturbations of the elastic parameters Δa_{iklm} and the traveltime perturbations $\Delta\tau_{qP}$. On the basis of (5.1) a tomographic system can be constructed: each observation of the qP-wave traveltime adds the corresponding equation to this system. Then, to determine Δa_{iklm} a conventional tomography scheme can be applied.

Application of equation (5.1) for inversion of the elastic parameters of an anisotropic medium was considered by Chapman and Pratt (1992). They inverted the elastic parameters of arbitrary anisotropic media from qP-wave traveltime observations in 2-D cross-borehole tomographic experiments (i.e., the rays remain in a 2-D plane containing the borehole). Of course, only a restricted number of the elastic parameters can be determined in the 2-D experiments.

For quasi-shear waves the relations between the traveltime perturbations $\Delta\tau_{qSM}$ and the perturbations Δa_{iklm} of the elastic parameters

$$\Delta\tau_{qSM} = -\frac{\tau_s}{2}\Delta a_{iklm}\, p_i\, p_m\, \mathrm{g}_k^{(M)}\, \mathrm{g}_l^{(M)}, \qquad M = 1, 2 \tag{5.2}$$

are intrinsically more complicated than for the quasi-compressional waves. First, there are two qS-waves: indices $M = 1$ and 2 correspond to $qS1$- and $qS2$-waves. The structure of equations (5.1) and (5.2) is similar: τ_s and p_i are the traveltime and the slowness components of the S-wave, respectively, and $\mathrm{g}_k^{(M)}$ can be considered as components of the polarization vector of the S-wave in the isotropic background medium (as well as the vector $\mathbf{n}$ can be considered as the P-wave polarization vector). The second problem is that the components n_k are known in the isotropic background medium, whereas $\mathrm{g}_k^{(M)}$ are not. The vectors $\mathbf{g}^{(M)}$ depend on the perturbations of the elastic parameters Δa_{iklm}. Therefore, they can not be obtained until the perturbations Δa_{iklm} are known. This leads to a non-linear behavior of the qS-wave traveltime perturbations with respect to the perturbation of the elastic parameters.

Červený and Jech (1982) suggested linearized equations for quasi-shear waves based on an average value on the traveltime corrections for both quasi-shear waves. Jech and Pšenčík (1992) performed a simultaneous inversion for qP- and qS-waves, but the inversion scheme can only be applied to TI structure.

I suggest to use the observations of qS-wave polarization vectors to estimate the unknown vectors $\mathbf{g}^{(M)}$. With the known vectors $\mathbf{g}^{(M)}$ the relations (5.2) would become linear and formally identical to the relations (5.1) for qP-waves. This would allow to use the same inversion scheme for qP- as for qS-waves.

Observations of qS-wave polarization vectors are available from the three-component seismograms as well as traveltime observations. The polarization data can be used to invert for medium parameters or to improve the resolution of the tomographic image. Several papers using the polarization tomography have been published. For instance, Le Bégat and Farra (1997) inverted qP-wave traveltimes and polarizations of synthetic examples simulating a VSP experiment. Horne and Leaney (2000) inverted qP- and qSV polarization and slowness component measurements obtained from a walk-away VSP experiment using a global optimization method. Horne and MacBeth (1994) developed a genetic algorithm to invert shear-wave observations from VSP data. They used horizontal polarizations and time-delays between two qS-waves to invert for hexagonal and orthorombic symmetry. Farra and Le Bégat (1995) investigated the sensitivity of qP-wave traveltime and polarization vectors to heterogeneity, anisotropy and interfaces.

Borehole seismic data have traditionally been analyzed by inverting traveltimes for velocity structure. The down-hole and cross-hole experiments are ideal for determining seismic anisotropy (see, e.g., Cliet et al., 1991; Williamson, 1993; Le Bégat and Farra, 1997). The angular coverage makes the seismic traveltimes sensitive to any type of anisotropy. In this study, a vertical seismic profiling (VSP) experiment is considered. Wavefields from sources distributed on the Earth's surface are recorded at receivers within a vertical borehole. Traveltimes of transmitted qP- and qS-waves are inverted to determine the elastic parameters of the anisotropic medium between the sources and receivers. I present a joint inversion of qP- and qS-waves in piecewise homogeneous weakly anisotropic media using

a linear inversion formalism for both qP- and qS-waves. Similar to previous studies I assume that each of the two propagating qS-waves are recorded separately, i.e., no qS-wave coupling exists, and that the observations are not close to singular directions.

After this introduction I briefly review the required basic perturbation formulae, followed by a discussion of the linearized equations for the qS-waves. Special emphasis is given to the determination of the vectors $\mathbf{g}^{(M)}$ for the inversion using the measured polarization vectors of qS-waves. Following this, the tomographic system is presented. In the last two sections numerical case studies demonstrate the applicability of the inversion scheme for homogeneous and layered models.

5.2 Basic perturbation formulae

Following the theory described in chapter 2, the elasticity tensor of a weakly anisotropic medium is represented by the sum of the tensor of the density-normalized elastic parameters in an isotropic background medium, $a_{iklm}^{(iso)}$, and small perturbations Δa_{iklm} describing the deviations from isotropy:

$$a_{iklm} = a_{iklm}^{(iso)} + \Delta a_{iklm}. \tag{5.3}$$

For weakly anisotropic media the zeroth-order solution for the wave field of qP- and qS-waves is written in the following form (see Červený, 2001; Zillmer et al., 1998; Pšenčík, 1998):

$$\mathbf{u}^{qP} = \frac{e^{-i\omega\tau_p}}{\sqrt{\rho J_p(\tau,\gamma_1,\gamma_2)}} D(\gamma_1,\gamma_2)\, e^{i\omega\Delta\tau_{qP}}\, \mathbf{n}(\gamma_1,\gamma_2) \tag{5.4}$$

$$\mathbf{u}^{qS} = \frac{e^{-i\omega\tau_s}}{\sqrt{\rho J_s(\tau,\gamma_1,\gamma_2)}} \Big[A(\gamma_1,\gamma_2)\, e^{i\omega\Delta\tau_{qS1}}\, \mathbf{g}^{(1)}(\gamma_1,\gamma_2) + \tag{5.5}$$

$$+ C(\gamma_1,\gamma_2)\, e^{i\omega\Delta\tau_{qS2}}\, \mathbf{g}^{(2)}(\gamma_1,\gamma_2) \Big].$$

Here, $\mathbf{u}^{qP}$ and $\mathbf{u}^{qS}$ are the displacement vectors of the qP- and qS-waves, and τ_p and τ_s are the traveltimes of the P- and S-waves in the isotropic background medium, respectively (bold letters denote vectors); J_p and J_s are the Jacobians of the transformation from ray coordinates (τ,γ_1,γ_2) to Cartesian coordinates. The scalar amplitudes A, C and D are defined by the initial conditions, e.g., by the type of the source (see e.g. Gajewski, 1993).

In equation (5.4), the traveltime perturbation $\Delta\tau_{qP}$ is:

$$\Delta\tau_{qP} = -\frac{\tau_p}{2} \Delta a_{iklm} p_i p_m n_k n_l, \tag{5.6}$$

where $\mathbf{p}$ is the P-wave slowness vector and $\mathbf{n}$ is the wavefront normal vector. Both vectors are tangent to the reference ray of the P-wave in the isotropic background medium.

In equation (5.5), the traveltime perturbations $\Delta\tau_{qS1}$ and $\Delta\tau_{qS2}$ are obtained by the formulae

$$\Delta\tau_{qS1} = -\frac{\tau_s}{2}\,\lambda_1, \tag{5.7}$$

$$\Delta\tau_{qS2} = -\frac{\tau_s}{2}\,\lambda_2, \tag{5.8}$$

where λ_1 and λ_2 are the eigenvalues of the weak-anisotropy matrix $\mathbf{B}$ constructed with help of two arbitrary mutually orthogonal unit vectors $\mathbf{e}^{(1)}$ and $\mathbf{e}^{(2)}$ situated in the plane perpendicular to the reference S-wave ray and the S-wave slowness $\mathbf{p}$ in the isotropic background medium:

$$B_{IM} = \Delta a_{iklm} p_k p_m e_i^{(I)} e_l^{(M)} \qquad (I, M = 1, 2). \tag{5.9}$$

Then, in equation (5.5) the mutually orthogonal unit vectors $\mathbf{g}^{(1)}$ and $\mathbf{g}^{(2)}$ are linear combinations of the vectors $\mathbf{e}^{(1)}$ and $\mathbf{e}^{(2)}$:

$$\mathrm{g}_i^{(1)} = e_i^{(1)} \cos\phi + e_i^{(2)} \sin\phi, \quad \mathrm{g}_i^{(2)} = -e_i^{(1)} \sin\phi + e_i^{(2)} \cos\phi. \tag{5.10}$$

The linear combinations (5.10) are constructed from the eigenvectors $(\cos\phi, -\sin\phi)^{\mathrm{T}}$ and $(\sin\phi, \cos\phi)^{\mathrm{T}}$ corresponding to the eigenvalues λ_1 and λ_2 of the weak-anisotropy matrix (5.9). For more details see the previous chapter 2 and Červený (2001), Jech and Pšenčík (1989), Zillmer et al. (1998), Pšenčík (1998). For the inversion we will use equations (5.7) and (5.8) for the traveltime perturbations in the form

$$\Delta\tau_{qS1} = -\frac{\tau_s}{2} \Delta a_{iklm}\, p_i\, p_m\, \mathrm{g}_k^{(1)}\, \mathrm{g}_l^{(1)}, \tag{5.11}$$

$$\Delta\tau_{qS2} = -\frac{\tau_s}{2} \Delta a_{iklm}\, p_i\, p_m\, \mathrm{g}_k^{(2)}\, \mathrm{g}_l^{(2)}. \tag{5.12}$$

5.3 Linearized equations for qS-wave traveltime perturbations

Equations (5.6), (5.11) and (5.12) relate the traveltime perturbations $\Delta\tau_{qP}$, $\Delta\tau_{qS1}$ or $\Delta\tau_{qS2}$ and the perturbations Δa_{iklm} of the elastic parameters with respect to the isotropic background medium. Since the qP- and qS-wave traveltimes in the weakly anisotropic medium are represented as

$$\tau_{qP} = \tau_p + \Delta\tau_{qP},$$

$$\tau_{qS1} = \tau_s + \Delta\tau_{qS1},$$

$$\tau_{qS2} = \tau_s + \Delta\tau_{qS2},$$

equations (5.6), (5.11) and (5.12) can also be written in the form:

$$\begin{aligned} \tau_{qP} - \tau_p &= -\frac{\tau_p}{2} \Delta a_{iklm}\, p_i\, p_m\, n_k\, n_l, \\ \tau_{qSM} - \tau_s &= -\frac{\tau_s}{2} \Delta a_{iklm}\, p_i\, p_m\, \mathrm{g}_k^{(M)}\, \mathrm{g}_l^{(M)}, \qquad M = 1, 2. \end{aligned} \tag{5.13}$$

The structure of all equations (5.13) is similar: τ_{qP} and τ_{qSM} are the traveltimes of the qP- and qS-waves in the weakly anisotropic medium, τ_p and τ_s are the traveltimes of P- and S-waves, p_i are components of the P- or S-wave slowness, and n_k are components of the wavefront normal vector in the isotropic background medium. The wavefront normal vector can also be considered as the P-wave polarization vector. The components $\mathrm{g}_k^{(M)}$ ($M = 1$ or 2) define the vectors $\mathbf{g}^{(M)}$ from equations (5.10). They are situated into the plane perpendicular to the ray in the isotropic background medium, and, therefore, can

be considered vectors determining S-wave polarization vectors in the isotropic background medium.

The traveltimes in the weakly anisotropic medium τ_{qP}, τ_{qS1}, and τ_{qS2} are supposed to be obtained by observations. With the known parameters of the isotropic background medium, the traveltimes τ_p and τ_s, the slowness vectors of the P- and S-waves and the wavefront normal $\mathbf{n}$ can be calculated by standard isotropic ray method. As a result, in the case of qP-waves, the traveltime perturbation $\tau_{qP} - \tau_p$ and the perturbations of the elastic parameters Δa_{iklm} are linearly related. In the case of qS-waves, the vectors $\mathbf{g}^{(1)}$ and $\mathbf{g}^{(2)}$ depend on the perturbations Δa_{iklm} and, therefore, can not be determined until the perturbations Δa_{iklm} are known (see section 5.2). This leads to a non-linear behavior of the qS-wave traveltime perturbation with respect to the perturbation of the elastic parameters Δa_{iklm}. If the vectors $\mathbf{g}^{(1)}$ and $\mathbf{g}^{(2)}$ were known, the relations between the traveltime perturbations $\tau_{qS1} - \tau_s$ or $\tau_{qS2} - \tau_s$ and the perturbations Δa_{iklm} of the elastic parameters become linear and formally identical to the relations for qP-waves.

How can we find or estimate the vectors $\mathbf{g}^{(1)}$ and $\mathbf{g}^{(2)}$ without a priori knowledge about Δa_{iklm}? For this purpose, let us consider the physical meaning of these vectors. The vectors $\mathbf{g}^{(1)}$ and $\mathbf{g}^{(2)}$ are introduced into the perturbation theory by equations (5.10). They are mutually orthogonal and situated in the plane orthogonal to the ray in the isotropic background medium. For brevity, I will denote this ray reference ray. I have already said that these vectors can be considered as polarization vectors of the shear-waves propagating in the isotropic background medium along the reference ray. Since the isotropic medium itself does not fix the polarization of the shear-wave, it can be described by any unit vector in the plane orthogonal to the ray. In perturbation theory, however, the specification of the vectors $\mathbf{g}^{(1)}$ and $\mathbf{g}^{(2)}$ is unique. It is controlled by the perturbation Δa_{iklm}. Thus, we get different vectors $\mathbf{g}^{(M)}$ for different Δa_{iklm}. Contrary to isotropic media, any anisotropic medium uniquely fixes the qS-wave polarizations (with exception of so-called singular directions). Therefore, even very small perturbations of the isotropic medium lead to an anisotropic medium with fixed qS-wave polarizations. To provide a continuous and smooth transformation from isotropy to anisotropy, the vectors $\mathbf{g}^{(1)}$ and $\mathbf{g}^{(2)}$ must also be close to the qS-wave polarization vectors in the weakly anisotropic medium. Using this reasoning, I suggest to determine the unknown vectors $\mathbf{g}^{(1)}$ and $\mathbf{g}^{(2)}$ from the observed qS-wave polarization vectors.

Although, the observations of the qS-wave polarization vectors are available from the three-component data, picking qS-wave polarization vectors from real data can be a challenging task. However, to obtain traveltimes, the two qS-waves need to be separated in any case. For this separation the difference in qS-wave polarizations is used (see, e.g., Alford, 1986; Li and Crampin, 1993; Dellinger et al., 1998). Therefore, the qS-wave polarization vectors are automatically obtained as a by-product of the qS-wave separation.

To determine the vectors $\mathbf{g}^{(1)}$ and $\mathbf{g}^{(2)}$ from the observed qS-wave polarization vectors, the following procedure is performed (see Fig. 5.1*a*): Let us assume that at a receiver point observations of two polarization vectors $\mathbf{A}_{qS1}$ and $\mathbf{A}_{qS2}$ are available. First, the reference ray in the isotropic background medium connecting the source and the receiver is calculated. The determination of the isotropic background medium is discussed below. Then, at the receiver point, a plane orthogonal to the reference ray is constructed. The observed

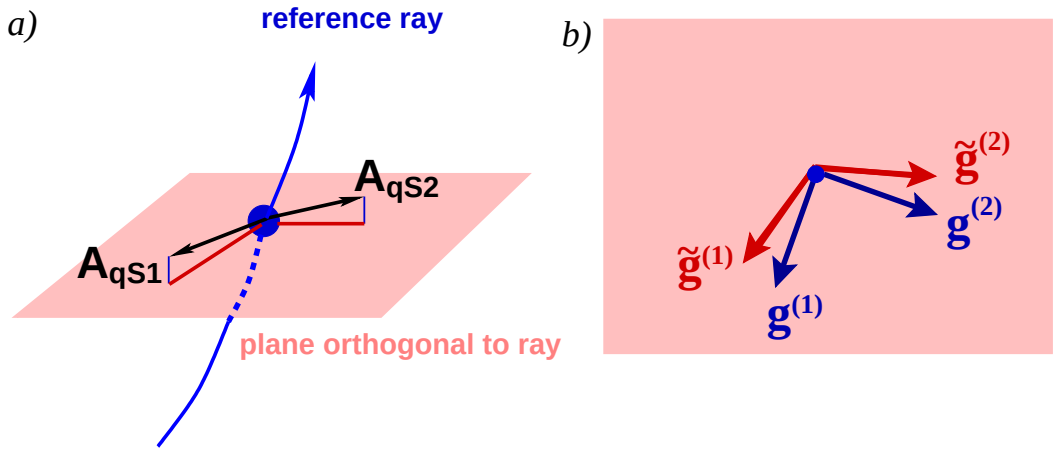

Figure 5.1: Estimation of the vectors $\mathbf{g}^{(1)}$ and $\mathbf{g}^{(2)}$. The observed qS-wave polarization vectors $\mathbf{A}_{qS1}$ and $\mathbf{A}_{qS2}$ are projected into the plane orthogonal to the reference ray *(a)*. The unit vectors corresponding to the projections are denoted by $\tilde{\mathbf{g}}^{(1)}$ and $\tilde{\mathbf{g}}^{(2)}$ *(b)*. These vectors are used in eqs. (5.13) instead of the unknown vectors $\mathbf{g}^{(1)}$ and $\mathbf{g}^{(2)}$.

polarization vectors $\mathbf{A}_{qS1}$ and $\mathbf{A}_{qS2}$ are projected into this plane and their projections are normalized to unit vectors. The normalized projections will be denoted as $\tilde{\mathbf{g}}^{(1)}$ and $\tilde{\mathbf{g}}^{(2)}$. Although these vectors $\tilde{\mathbf{g}}^{(1)}$ and $\tilde{\mathbf{g}}^{(2)}$ are usually not orthogonal, I suggest to use them in equations (5.13) instead of the unknown vectors $\mathbf{g}^{(1)}$ and $\mathbf{g}^{(2)}$ (see Fig. 5.1*b*). The accuracy of this approximation is investigated in section 5.5 on page 96.

As a result, the tomographic system is now composed by the following equations which contain the vectors $\tilde{\mathbf{g}}^{(1)}$ and $\tilde{\mathbf{g}}^{(2)}$ instead of $\mathbf{g}^{(1)}$ and $\mathbf{g}^{(2)}$:

$$\begin{aligned} \frac{\tau_{qP}}{\tau_p} - 1 &= -\frac{1}{2}\, p_i\, p_m\, n_k\, n_l\, \Delta a_{iklm}, \\ \underbrace{\frac{\tau_{qSM}}{\tau_s} - 1}_{y_i} &= \underbrace{-\frac{1}{2}\, p_i\, p_m\, \tilde{g}_k^{(M)}\, \tilde{g}_l^{(M)}}_{X_{ik}}\, \underbrace{\Delta a_{iklm}}_{a_k}, \qquad M = 1, 2, \end{aligned} \tag{5.14}$$

where the traveltimes τ_{qP}, τ_{qS1}, τ_{qS2} and the vectors $\tilde{\mathbf{g}}^{(1)}$ and $\tilde{\mathbf{g}}^{(2)}$ are obtained by observations. The brackets are explained in the next section. For the given isotropic background medium equations (5.14) provide linear relations between the traveltime perturbations and the perturbation of the elastic parameters for both types of waves.

5.4 Statement of the inversion problem

Let us assume that there are N observations of qP- and qS-wave traveltimes $\tau_1, \tau_2, \ldots, \tau_N$ in a weakly anisotropic medium. Each τ_i corresponds to τ_{qP}, τ_{qS1} or τ_{qS2}. On the basis of these observations, the tomographic system is constructed from the equations (5.14). Each traveltime τ_i for either qP- or qS-waves adds the corresponding equation in a tomography system. The system can be written in the form (see also the brackets in eqs. 5.14):

$$y_i = \sum_{k=1}^{L} X_{ik}\, a_k \qquad (i = 1, \ldots N, \quad N > L), \tag{5.15}$$

where the vector $\mathbf{y}$ is specified as

$$y_i = \frac{\tau_i}{\tau_i^{(0)}} - 1. \tag{5.16}$$

The components of the vector $\mathbf{y}$ are formed by the observed traveltimes τ_i of the qP- and qS-waves and the corresponding traveltimes $\tau_i^{(0)}$ of the P- and S-waves computed in the isotropic background medium. The vector $\mathbf{y}$ has a dimension N of the total number of the qP- and qS-wave traveltime observations for all receivers from all sources. The vector $\mathbf{a}$ of the perturbations Δa_{iklm} of the elastic parameters has the dimension L. The maximum value of L is equal to 21. The value of L can be reduced. For example, if the anisotropic medium under consideration is transversely isotropic, L is equal to 5 (see Appendix A at the end of this chapter). The elements of the $N \times L$ matrix $\mathbf{X}$ are composed by components of the P- or S-wave slowness vectors and the vectors $\mathbf{n}$, $\tilde{\mathbf{g}}^{(1)}$ or $\tilde{\mathbf{g}}^{(2)}$. As soon as the reference ray connecting a source and a receiver is constructed, the corresponding element of the matrix $\mathbf{X}$ can be obtained according to section 5.3.

In experiments, the traveltimes τ_i can only be measured with errors ε_i. I denote the measured traveltimes as $\hat{\tau}_i$:

$$\hat{\tau}_i = \tau_i + \varepsilon_i, \qquad i = 1, \ldots, N$$

Let us assume that the traveltime observations $\hat{\tau}_i$ are performed with equal accuracy and the corresponding errors ε_i are independent, unbiased and random with a normal (Gaussian) probability distribution with standard deviation σ_τ:

$$\boldsymbol{\varepsilon} \in \mathcal{N}\Big(\mathbf{0}, \sigma_\tau^2 \mathbf{I}\Big),$$

where $\mathbf{I}$ is the $N \times N$ unit matrix.

Since the traveltime observations $\hat{\tau}_i$ contain errors, the y_i from (5.16) are obtained with errors denoted as $\hat{\varepsilon}_i$:

$$\hat{y}_i = y_i + \hat{\varepsilon}_i, \qquad i = 1, \ldots, N$$

In contrast to the errors ε_i these errors $\hat{\varepsilon}_i$ are of unequal accuracy, but they are also independent, unbiased and random with a normal (Gaussian) probability distribution:

$$\hat{\boldsymbol{\varepsilon}} \in \mathcal{N}\Big(\mathbf{0},\, \mathbf{R}_\mathbf{y}\Big).$$

Because of (5.16), the covariance matrix $\mathbf{R}_\mathbf{y}$ has the form:

$$\mathbf{R}_\mathbf{y} = \sigma_\tau^2\, \mathbf{Q}^{-1}, \tag{5.17}$$

where the weight matrix

$$\mathbf{Q} = \begin{pmatrix} q_1 & 0 & 0 & \ldots & 0 \\ 0 & q_2 & 0 & \ldots & 0 \\ 0 & 0 & q_3 & \ldots & 0 \\ & & & \ddots & \\ 0 & 0 & 0 & \ldots & q_N \end{pmatrix}. \tag{5.18}$$

is composed by

$$q_i = \Big[\tau_i^{(0)}\Big]^2, \qquad i = 1, \ldots, N. \tag{5.19}$$

Now I can rigorously set up the inversion problem. The inverse problem is to find estimates of the L perturbations $\mathbf{a} = (a_1, a_2, \ldots, a_M)$ of the elastic parameters on the basis of the observations $\hat{\mathbf{y}} = (\hat{y}_1, \hat{y}_2, \ldots, \hat{y}_N)$. The search is performed by the method of least squares. According to Linnik (1961) the parameters $\mathbf{a}$ can be found from the condition:

$$\sum_{i=1}^{N} q_i \left(\hat{y}_i - \sum_{k=1}^{M} X_{ik}\, a_k \right)^2 = \min$$

As a result, the least-squares estimate $\hat{\mathbf{a}}$ of the parameters $\mathbf{a}$ has the form (see e.g., Linnik, 1961, eq. 6.3.20)

$$\hat{\mathbf{a}} = \left(\mathbf{X}^T \mathbf{Q} \mathbf{X}\right)^{-1} \mathbf{X}^T\, \mathbf{Q}\, \hat{\mathbf{y}}. \tag{5.20}$$

The covariance matrix of the estimate $\hat{\mathbf{a}}$ is written as

$$\mathbf{R}_{\hat{\mathbf{a}}} = \hat{\sigma}^2 \left(\mathbf{X}^T \mathbf{Q} \mathbf{X}\right)^{-1}, \tag{5.21}$$

where the estimate $\hat{\sigma}^2$ is defined as

$$\hat{\sigma}^2 = \frac{\eta^2}{N - M} \tag{5.22}$$

with the misfit function

$$\eta^2 = \sum_{i=1}^{N} q_i \left(\hat{y}_i - \sum_{k=1}^{M} X_{ik}\, \hat{a}_k \right)^2. \tag{5.23}$$

Note that the diagonal terms of matrix $\mathbf{R}_{\hat{\mathbf{a}}}$ are the variances of the estimated parameters $\hat{\mathbf{a}}$. These terms are used to obtain confidence intervals for the estimated parameters. The confidence intervals give the quality of these parameters. For each parameters $\hat{a}_i$ the confidence interval which covers $\hat{a}_i$ with a probability p_0 (confidence coefficient) can be constructed: (see Linnik, 1961):

$$I^{(i)} = \left[\hat{a}_i - \gamma \sqrt{(\mathbf{R}_{\hat{\mathbf{a}}})_{ii}}\ , \quad \hat{a}_i + \gamma \sqrt{(\mathbf{R}_{\hat{\mathbf{a}}})_{ii}} \right]. \tag{5.24}$$

The value γ is determined from the table of Student's t-distribution by the condition $P\{|t_{N-L}| \le \gamma\} = p_0$, where p_0 is a specified confidence coefficient, and by the number of degrees of freedom, which is equal to $N - L$.

To obtain the solution $\hat{\mathbf{a}}$ from (5.20), the singular value decomposition (SVD) method (see e.g. Menke, 1984) is performed for the matrix $\mathbf{Q}^{1/2}\mathbf{X}$. Additionally, the SVD method gives a good indication for how many parameters $\mathbf{a}$ can be estimated from the observations. The singular values w_i and the associated eigenvectors $\mathbf{W}^{(i)}$ of the matrix $\mathbf{Q}^{1/2}\mathbf{X}$ define the parameter combinations that are well determined or not determined by the data. A parameter $\hat{a}_i$ proportional to $\mathbf{W}^{(i)}$ will be well determined if the corresponding w_i is large.

Note that the condition number of a matrix is defined as the ratio of the largest (in magnitude) of the singular value to the smallest of the singular value. A matrix is singular if its condition number is infinite, and it is ill-conditioned if its condition number is too large. All computations in my thesis were performed for the single machine's precision. Therefore, the condition number larger then 10^4 is considered as too large and the corresponding matrix is ill-conditioned.

Determination of the isotropic background medium

The inverse problem discussed is linear only if the isotropic background medium is known. With an unknown background medium the inversion is non-linear for qP- as well as for qS-waves. In general, the isotropic background medium is unknown as well. We can only make assumptions about the background medium. To overcome this problem the inversion procedure is embedded into an iteration procedure for the determination of the isotropic background medium. Properties of the isotropic background medium are specified by the velocities v_p and v_s of the P- and S-waves propagating in the homogeneous isotropic medium. First, the initial velocities $v_p^{(0)}$ and $v_s^{(0)}$ are defined. For example, they can be estimated for several source-receiver pairs as the distance divided by the corresponding traveltimes. In the next step the elastic parameters of the anisotropic medium determined by the inversion with the isotropic background medium defined by $v_p^{(0)}$ and $v_s^{(0)}$. Then, the inverted elastic parameters of the anisotropic medium are used to construct an updated isotropic background model $v_p^{(\mathrm{new})}$ and $v_s^{(\mathrm{new})}$ using the formulae for the best-fitting isotropic medium derived by Fedorov (1968) (see page 86). The inversion and update of the isotropic background are repeated until the old velocities and the new velocities of the isotropic background differ only by a small value (e.g., 0.01 km/s).

5.5 Accuracy of vectors $\tilde{\mathbf{g}}^{(1)}$ and $\tilde{\mathbf{g}}^{(2)}$

In this section I investigate how close the vectors $\tilde{\mathbf{g}}^{(1)}$ and $\tilde{\mathbf{g}}^{(2)}$ estimated from the qS-wave polarization vectors, $\mathbf{A}_{qS1}$ and $\mathbf{A}_{qS2}$, are to the vectors $\mathbf{g}^{(1)}$ and $\mathbf{g}^{(2)}$ obtained from the perturbation theory (I will call these vectors as exact vectors). For this purpose, the angles, $\tilde{\alpha}_1$ and $\tilde{\alpha}_2$, between the exact and estimated vectors are calculated (see Fig. 5.1*b* on page 93):

$$\tilde{\alpha}_1 = \angle\,(\tilde{\mathbf{g}}^{(1)}, \mathbf{g}^{(1)}), \qquad \tilde{\alpha}_2 = \angle\,(\tilde{\mathbf{g}}^{(2)}, \mathbf{g}^{(2)}). \tag{5.25}$$

For comparison also the angles between the vectors $\mathbf{A}_{qS1}$ and $\mathbf{A}_{qS1}$, and the corresponding vectors $\mathbf{g}^{(1)}$ and $\mathbf{g}^{(2)}$ derived from the perturbation theory are computed:

$$\alpha_1 = \angle\,(\mathbf{A}_{qS1}, \mathbf{g}^{(1)}), \qquad \alpha_2 = \angle\,(\mathbf{A}_{qS2}, \mathbf{g}^{(2)}). \tag{5.26}$$

Calculations of the angles (5.25) and (5.26) are carried out for three homogeneous anisotropic media: an orthorombic medium with 10.6% RMS deviation from isotropy, a VTI medium with 11% RMS deviation from isotropy (Thomsen parameters: $\varepsilon = 0.125$, $\gamma = 0.049$ and $\delta = 0.045$), and a triclinic medium with 8.1% RMS deviation from isotropy. The elastic parameters of the orthorombic and VTI media are given in Table 5.4 on page 110, those of the triclinic medium in Table 5.3 on page 107.

The angles are computed for different ray directions defined by an inclination angle θ and an azimuth angle φ. Each pair (θ, φ) defines a ray connecting a source and a receiver. The $qS1$- and $qS2$-waves propagating along this ray are considered. The qS-wave polarization vectors $\mathbf{A}_{qS1}$ and $\mathbf{A}_{qS2}$ at the receiver are calculated by standard anisotropic ray theory.

The vectors $\mathbf{A}_{qS1}$ and $\mathbf{A}_{qS2}$ are considered as observed qS-wave polarization data and used for the estimation of the vectors $\tilde{\mathbf{g}}^{(1)}$ and $\tilde{\mathbf{g}}^{(2)}$. The background isotropic medium

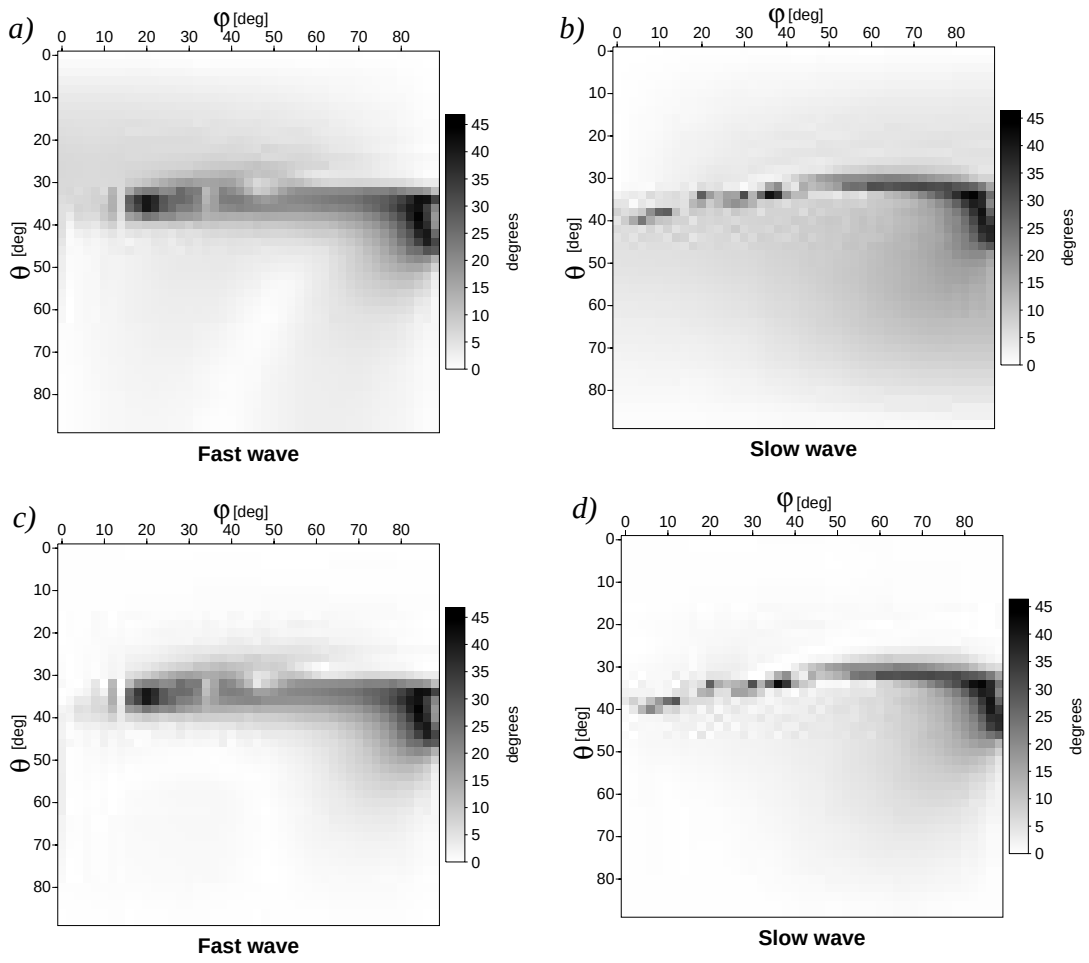

Figure 5.2: Maps of angles α_1, α_2, $\tilde{\alpha}_1$ and $\tilde{\alpha}_2$ in the orthorombic medium from Tab. 5.4. The inclination angle θ and azimuth angle φ define the ray direction. The two upper maps, *(a)* and *(b)*, represent the angles α_1 and α_2 between the vectors $\mathbf{g}^{(1)}$ and $\mathbf{g}^{(2)}$ obtained from perturbation theory and the polarization vectors of the two qS-waves $\mathbf{A}_{qS1}$ and $\mathbf{A}_{qS2}$ computed by standard anisotropic ray theory. The two lower maps, *(c)* and *(d)*, represent the angles $\tilde{\alpha}_1$ and $\tilde{\alpha}_2$ between the vectors $\mathbf{g}^{(1)}$ and $\mathbf{g}^{(2)}$ and the vectors $\tilde{\mathbf{g}}^{(1)}$ and $\tilde{\mathbf{g}}^{(2)}$ estimated from $\mathbf{A}_{qS1}$ and $\mathbf{A}_{qS2}$. Note that the regions with the largest angles (dark) correspond to singular regions in the orthorombic medium (see also Fig. 5.12).

is constructed as a best-fitting isotropic medium, see Appendix A on page 86. In the homogeneous case, the reference ray in the isotropic background medium is a straight line connecting the source and the receiver. The vectors $\mathbf{A}_{qS1}$ and $\mathbf{A}_{qS2}$ are projected into a plane perpendicular to the reference ray. The exact vectors $\mathbf{g}^{(1)}$ and $\mathbf{g}^{(2)}$ are obtained from perturbation theory according to equations (5.9) and (5.10).

Figure 5.2 shows maps of the angles α_1 *(a)*, α_2 *(b)*, $\tilde{\alpha}_1$ *(c)* and $\tilde{\alpha}_2$ *(d)* for the orthorombic medium. Each point on the maps represents a ray direction. The magnitude of the angle corresponding to the ray are shown by a grayscale: The larger the magnitude of the angle, the darker it is presented. One can see that the angles do not exceed 15 degrees (white and light-gray) for most of the ray directions. The largest angles (nearly black) correspond to

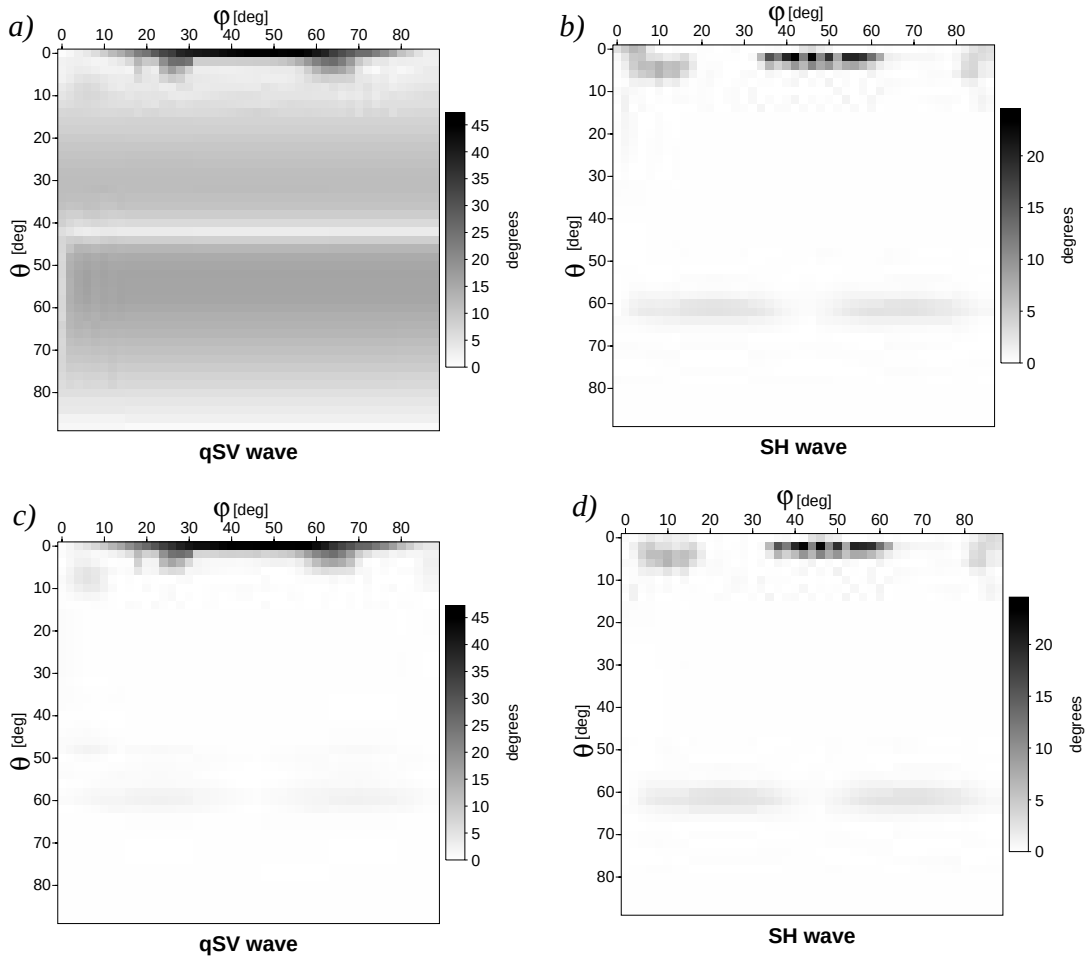

Figure 5.3: Maps of angles α_1, α_2, $\tilde{\alpha}_1$ and $\tilde{\alpha}_2$ in the VTI medium from Tab. 5.4. The inclination angle θ and azimuth angle φ define the ray direction. The two upper maps, *(a)* and *(b)*, represent the angles α_1 and α_2 between the vectors $\mathbf{g}^{(1)}$ and $\mathbf{g}^{(2)}$ obtained from perturbation theory and the polarization vectors of the two qS-waves $\mathbf{A}_{qSV}$ and $\mathbf{A}_{SH}$ computed by standard anisotropic ray theory. The two lower maps, *(c)* and *(d)*, represent the angles $\tilde{\alpha}_1$ and $\tilde{\alpha}_2$ between the vectors $\mathbf{g}^{(1)}$ and $\mathbf{g}^{(2)}$ and the vectors $\tilde{\mathbf{g}}^{(1)}$ and $\tilde{\mathbf{g}}^{(2)}$ estimated from $\mathbf{A}_{qSV}$ and $\mathbf{A}_{SH}$. Note that the regions with the largest angles (dark) correspond to singular regions in the VTI medium (see also Fig. 5.12).

singular directions of the orthorombic medium considered where the two shear wavefronts cross each other (see Fig. 5.12 on page 112). In these directions the perturbation theory fails as well as the standard anisotropic ray theory. Therefore, these directions have to be excepted from our consideration. Comparison of the two upper *(a,b)* and the lower *(c,d)* maps shows that the angles $\tilde{\alpha}_1$ and $\tilde{\alpha}_2$ between the vectors $\tilde{\mathbf{g}}^{(1)}$ and $\tilde{\mathbf{g}}^{(2)}$ obtained by projection of the polarization vectors, $\mathbf{A}_{qS1}$ and $\mathbf{A}_{qS2}$, and the exact vectors $\mathbf{g}^{(1)}$ and $\mathbf{g}^{(2)}$ are smaller than the corresponding angles α_1 and α_2 between the polarization vectors $\mathbf{A}_{qS1}$ and $\mathbf{A}_{qS2}$ and the vectors $\mathbf{g}^{(1)}$ and $\mathbf{g}^{(2)}$.

Figure 5.3 shows similar maps of the angles α_1 *(a)*, α_2 *(b)*, $\tilde{\alpha}_1$ *(c)* and $\tilde{\alpha}_2$ *(d)* for the VTI medium. As in the previous case, the largest angles (dark) correspond to the singular directions of the VTI medium considered. There, qSV- and SH-wavefronts are

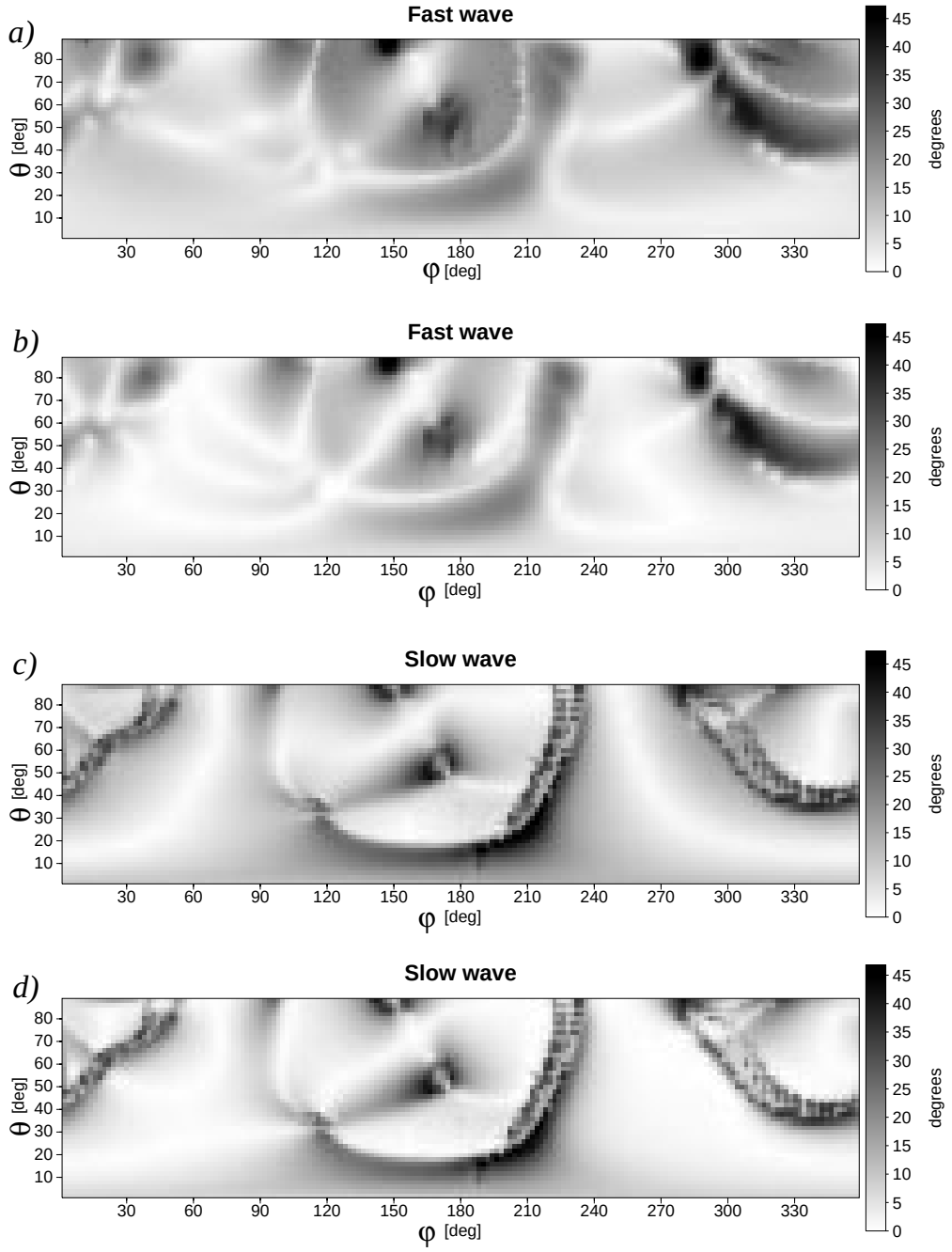

Figure 5.4: Maps of angles α_1, α_2, $\tilde{\alpha}_1$ and $\tilde{\alpha}_2$ in the triclinic medium from Tab. 5.3. The inclination angle θ and azimuth angle φ define the ray direction. The maps *(a)* and *(c)* represent the angles α_1 and α_2 between the vectors $\mathbf{g}^{(1)}$ and $\mathbf{g}^{(2)}$ obtained from perturbation theory and the polarization vectors of the two qS-waves $\mathbf{A}_{qS1}$ and $\mathbf{A}_{qS2}$ computed by standard anisotropic ray theory. The maps *(b)* and *(d)* represent the angles $\tilde{\alpha}_1$ and $\tilde{\alpha}_2$ between the vectors $\mathbf{g}^{(1)}$ and $\mathbf{g}^{(2)}$ and the vectors $\tilde{\mathbf{g}}^{(1)}$ and $\tilde{\mathbf{g}}^{(2)}$ estimated from $\mathbf{A}_{qS1}$ and $\mathbf{A}_{qS2}$. The regions with the largest angles (dark color) correspond to singular regions in the triclinic medium.

tangent to each other around $\theta \approx 0^\circ$ and cross each other around $\theta \approx 60^\circ$ (see Fig. 5.16 on page 116). In the case of qSV-waves, the projections $\tilde{\mathbf{g}}^{(1)}$ of the polarization vectors $\mathbf{A}_{qSV}$ provide a better approximation of $\mathbf{g}^{(1)}$. The angles are smaller on map *(c)* in comparison with map *(a)*. The SH-wave polarization vectors, $\mathbf{A}_{SH}$, are already situated in the plane orthogonal to the reference ray. Therefore, projection does not improve the approximation of $\tilde{\mathbf{g}}^{(2)}$ (see maps *(b)* and *(d)*).

Figure 5.4 shows maps of the angles α_1 (*a*), α_2 (*c*), $\tilde{\alpha}_1$ (*b*) and $\tilde{\alpha}_2$ (*d*) for the triclinic medium. Due to the symmetry of the triclinic medium, the maps represent the ray directions in the range of the azimuth φ from 0 to 360 degrees. The largest angles (dark) correspond to the singular directions of the medium considered. In the regular regions, after projection of the qS-wave polarization vectors into the plane orthogonal to the reference rays, we get slightly better estimate for the vectors $\mathbf{g}^{(1)}$ and $\mathbf{g}^{(2)}$. The maps *(b)* and *(d)* display smaller angles than the maps *(a)* and *(c)*. The angles $\tilde{\alpha}_1$ (*b*) and $\tilde{\alpha}_2$ (*d*) for the regular regions vary from 1 to 20 degrees.

Thus, the angular deviations between $\tilde{\mathbf{g}}^{(1)}$ and $\tilde{\mathbf{g}}^{(2)}$ estimated from the qS-wave polarization vectors and the exact $\mathbf{g}^{(1)}$ and $\mathbf{g}^{(2)}$ vary from 0 till 20 degrees for the regular (non-singular) areas. In the examples considered the maximal deviation does not exceed 5 degrees for the VTI medium and 15 degrees for the orthorombic medium. In the case of the triclinic medium the deviation may be as much as 20 degrees. Are these deviations strong or not? Note that in seismic experiments the accuracy of the observations of the polarization vectors ranges up to about 30 degrees. Nonetheless, the separation based on the difference in qS-wave polarization vectors is possible. Therefore, I do not expect that errors within 5–20 degrees contribute significant errors to the traveltimes in the forward modeling.

5.6 Inversion of homogeneous models

In the following two sections I evaluate the suggested inversion. For this purpose synthetic traveltimes and qS-wave polarization vectors are generated for a VSP observation scheme. The synthetic data are obtained by standard anisotropic ray method (see, e.g., Červený, 2001). Since inversion of an anisotropic medium is a very complex problem, applicability of the inversion scheme is first tested for the simplest, homogeneous models. Three homogeneous models with different types of anisotropic symmetry are inverted: two transversely isotropic media with vertical symmetry axis (VTI) and a triclinic medium. Application of the inversion for a more realistic layered model is discussed in section 5.7.

5.6.1 Synthetic VSP experiment

Synthetic data (traveltimes and qS-wave polarization vectors) for the following observation scheme are computed: The mouth of a borehole is situated at the point $X = 0.5$ km and $Y = 0$ km of a Cartesian coordinate system with horizontal $X-$ and $Y-$axes and a vertical $Z-$axis which is parallel to the borehole. 25 receivers are distributed along the borehole with a spacing of 30 m. The orientation of the receivers in the borehole coincides with the general Cartesian coordinate system, i.e., the two horizontal components are aligned with the $X-$ and $Y-$axes and the vertical component points along the $Z-$axis.

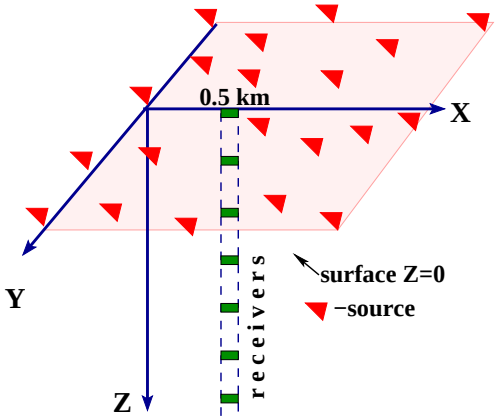

No	X,km	Y,km	No	X,km	Y,km
1	0.	0.	11	1.4	-0.5
2	0.	0.25	12	1.25	0.25
3	0.	0.5	13	1.25	-0.25
4	0.2	0.5	14	0.8	0.25
5	0.4	0.5	15	0.8	-0.25
6	0.25	0.25	16	1.	1.
7	0.4	-0.4	17	1.	-1.
8	0.25	-0.25	18	0.6	-1.
9	1.	0.	19	0.4	-1.
10	1.4	0.5	20	0.55	-0.1

Figure 5.5: The observation scheme of the synthetic VSP experiment. A vertical borehole contains 25 aligned three-component receivers with 30 m spacing until a depth of 750 m. Source positions on the surface are schematically indicated by triangles. The exact source positions are given in Table on the right side. When the VTI medium is considered, the waves are generate at source positions 1–10. The waves in the triclinic medium are generated at all 20 source positions.

Three types of waves propagating in a homogeneous anisotropic (VTI or triclinic) medium are recorded at the receivers. The corresponding qP- and qS-wave traveltimes and qS-wave polarization vectors at the receivers were computed using standard anisotropic ray method. For the VTI media, the waves were generated at 10 different source positions (see coordinates of source positions with numbers from 1 till 10 in Fig. 5.5) on the surface $Z = 0$, where tilted unit forces were used as sources. The tilted forces have a fixed orientation $\mathbf{F}$ for all source positions such that

$$\mathbf{F} = (\sin\vartheta\cos\phi, \sin\vartheta\sin\phi, \cos\vartheta), \quad \text{where} \tag{5.27}$$

For the VTI media I have used $\vartheta = 45°$ and $\phi = 45°$. The tilted force allows to generate both type of qS-waves. In the case of the triclinic model, a vertical unit force was used as a source, i.e. $\vartheta = 0$ and $\phi = 0$ in equation (5.27). To provide sufficient illumination of the triclinic medium the waves were generated for 20 different source positions (see Fig. 5.5).

5.6.2 VTI model

I consider two homogeneous VTI models which differ only in the strength of anisotropy. The relative mean square deviations (RMSD) of these models from isotropy are 5% and 10%. The density-normalized elastic parameters of the VTI medium with 5% deviation from isotropy are given in Table 5.1, and those for the VTI medium with 10% deviation in Table 5.2. For both models there are 225 observations of each wave.

Inversion of noise-free data

Let us first consider noise-free data. For both models the inversion for 21 parameters is performed, meaning that no a priori knowledge on the type of anisotropy is assumed. The inverted elastic parameters, $A_{ik}^{\rm est}(21)$, are shown in the third column of Tables 5.1 and 5.2. The isotropic background models are obtained by the iteration procedure described above on page 96. The final P- and S-wave velocities of the isotropic background medium

were $v_p = 3.592$ km/s and $v_s = 1.805$ km/s for the VTI medium with 5% anisotropy, and $v_p = 3.487$ and $v_s = 1.753$ km/s for the VTI medium with 10% anisotropy. The misfit function η^2 for the VTI medium with 5% anisotropy is equal to 0.0001 s^2. For the VTI medium with 10% anisotropy the misfit function accounts to 0.0018 s^2 for the same number of observations. For either model the condition number of the SVD of the matrix $\mathbf{Q}^{1/2}\mathbf{X}$ from solution (5.20) was 40. This means that both inversion problems for 21 parameters was well-conditioned and, therefore, all parameters are acceptable. The inverted parameters of both models are close to the exact elastic parameters, A_{ik}^{true}. The relative mean square deviation (RMSD) of the inverted elastic parameters from the exact ones is 0.64% for the medium with 5% anisotropy and 1.84% for the medium with 10%

A_{ik}	A_{ik}^{true}	noise-free data		noisy data		noisy data	
		$A_{ik}^{\text{est}}(21)$	$A_{ik}^{\text{est}}(5)$	$A_{ik}^{\text{est}}(21)$	$I_{99\%}$	$A_{ik}^{\text{est}}(5)$	$I_{99\%}$
A_{11}	13.590	13.545	13.549	13.569	±0.256	13.524	±0.093
A_{12}	6.790	6.760	6.752	6.749	±0.135	6.726	±0.093
A_{13}	6.120	6.059	6.044	6.078	±0.191	6.052	±0.052
A_{14}	0.	-0.005	0.	-0.041	±0.062	0.	
A_{15}	0.	0.006	0.	0.007	±0.110	0.	
A_{16}	0.	0.001	0.	0.028	±0.079	0.	
A_{22}	13.590	13.536	13.549	13.503	±0.157	13.524	±0.093
A_{23}	6.120	6.049	6.044	6.039	±0.098	6.052	±0.052
A_{24}	0.	-0.0103	0.	-0.023	±0.052	0.	
A_{25}	0.	-0.009	0.	-0.007	±0.115	0.	
A_{26}	0.	0.000	0.	0.027	±0.077	0.	
A_{33}	12.230	12.229	12.194	12.259	±0.212	12.249	±0.130
A_{34}	0.	0.017	0.	0.006	±0.051	0.	
A_{35}	0.	-0.034	0.	-0.027	±0.110	0.	
A_{36}	0.	0.000	0.	0.024	±0.078	0.	
A_{44}	3.060	3.034	3.036	3.034	±0.024	3.031	±0.011
A_{45}	0.	-0.005	0.	0.004	±0.020	0.	
A_{46}	0.	0.007	0.	0.005	±0.021	0.	
A_{55}	3.060	3.045	3.036	3.039	±0.022	3.031	±0.011
A_{56}	0.	-0.002	0.	-0.001	±0.016	0.	
A_{66}	3.400	3.393	3.398	3.397	±0.021	3.399	±0.011
RMSD		0.64%		0.79%		0.70%	
Misfit, η^2		0.0001 s^2	0.0002 s^2	0.0025 s^2		0.0025 s^2	
Background: v_p		3.593 km/s	3.591 km/s	3.593 km/s		3.591 km/s	
v_s		1.805 km/s	1.805 km/s	1.805 km/s		1.805 km/s	

Table 5.1: Results of inversion of the VTI model with 5% anisotropy. The true model is defined by A_{ik}^{true}. The inversion was performed for 21 as well as for 5 elastic parameters using noise-free and noisy data. The noisy data has a standard deviation of 2 ms of the traveltimes and standard deviations of 10° of the inclination (α) and azimuth (β) angles specifying the qS-wave polarization vectors. The estimated elastic parameters (A_{ik}^{est}) and the corresponding confidence intervals with 99% probability (denoted by $I_{99\%}$) are given.

of anisotropy. The type of symmetry of the inverted parameters is slightly different from VTI. However, the values of the "non-VTI" parameters, i.e., the off-diagonal elements except A_{12}, A_{13} and A_{23} are very small; A_{11} is close to A_{22} and A_{44} is close to A_{55} and A_{13} is close to A_{23}, which indicates a medium of VTI symmetry.

Let us now assume that a priori information on the type of anisotropy and orientation of the symmetry axis is available, i.e., we know that the medium under investigation is a VTI medium. In this case we can restrict the inversion to five independent elastic parameters. The tomographic system (5.15) is specified under the assumptions of a VTI symmetry. Instead of the 21 elastic moduli, only the elastic moduli A_{11}, A_{13}, A_{33}, A_{44} and A_{66} are searched for (see eqs. (5.31) and (5.32) from Appendix at the end of this

A_{ik}	A_{ik}^{true}	noise-free data		noisy data		noisy data	
		$A_{ik}^{\text{est}}(21)$	$A_{ik}^{\text{est}}(5)$	$A_{ik}^{\text{est}}(21)$	$I_{99\%}$	$A_{ik}^{\text{est}}(5)$	$I_{99\%}$
A_{11}	13.591	13.410	13.396	13.437	±0.319	13.376	±0.127
A_{12}	6.795	6.648	6.624	6.631	±0.168	6.594	±0.130
A_{13}	5.436	5.440	5.378	5.449	±0.238	5.389	±0.070
A_{14}	0.	-0.013	0.	-0.038	±0.077	0	
A_{15}	0.	0.012	0.	0.016	±0.138	0.	
A_{16}	0.	0.0011	0.	0.0301	±0.098	0.	
A_{22}	13.591	13.358	13.396	13.332	±0.195	13.376	±0.127
A_{23}	5.436	5.397	5.378	5.384	±0.122	5.389	±0.070
A_{24}	0.	-0.037	0.	-0.049	±0.065	0.	
A_{25}	0.	-0.028	0.	-0.017	±0.144	0.	
A_{26}	0.	-0.000	0.	0.028	±0.096	0.	
A_{33}	10.873	10.810	10.691	10.837	±0.263	10.751	±0.176
A_{34}	0.	0.066	0.	0.055	±0.064	0.	
A_{35}	0.	-0.120	0.	-0.101	±0.137	0.	
A_{36}	0.	-0.003	0.	0.011	±0.097	0.	
A_{44}	2.718	2.637	2.638	2.636	±0.030	2.628	±0.016
A_{45}	0.	-0.021	0.	-0.016	±0.025	0.	
A_{46}	0.	0.017	0.	0.011	±0.026	0.	
A_{55}	2.718	2.664	2.638	2.644	±0.028	2.628	±0.016
A_{56}	0.	-0.005	0.	-0.004	±0.019	0.	
A_{66}	3.398	3.364	3.386	3.375	±0.025	3.391	±0.015
RMSD		1.84%	1.70%	1.88%		1.81%	
Misfit, η^2		$0.0018\,\text{s}^2$	$0.0030\,\text{s}^2$	$0.0045\,\text{s}^2$		$0.0056\,\text{s}^2$	
Background: v_p		3.487 km/s	3.482 km/s	3.487 km/s		3.482 km/s	
v_s		1.753 km/s	1.753 km/s	1.753 km/s		1.753 km/s	

Table 5.2: Results of inversion of the VTI model with 10% anisotropy. The true model is defined by A_{ik}^{true}. The inversion was performed for 21 as well as for 5 elastic parameters using noise-free and noisy data. The noisy data has a standard deviation of 2 ms of the traveltimes and standard deviations of 10° of the inclination (α) and azimuth angles (β) specifying the qS-wave polarization vectors. The estimated elastic parameters (A_{ik}^{est}) and the corresponding confidence intervals with 99% probability (denoted by $I_{99\%}$) are given.

chapter on page 124). The inversion results are also presented in Tables 5.1 and 5.2 in the third columns (see the elastic moduli $A_{ik}^{\rm est}(5)$). The P- and S-wave velocities of the final background isotropic medium hardly differ from the velocities obtained above. The misfit function η^2 is larger than in the previous cases. It amounts up 0.0002 s^2 for the VTI medium with 5% anisotropy and 0.0030 s^2 for the VTI medium with 10% anisotropy. For both models the inversion for 5 parameters was conditioned better than in the inversion for 5 parameters Each condition number was 19. However, the RMSD of the inverted parameters from the exact ones decreases only slightly. It becomes 0.64% in the case of the VTI medium with 5% anisotropy and 1.70% for the VTI medium with 10% anisotropy.

It should be noted that even using noise-free data, I have not reconstructed the exact elastic parameters, but obtained close estimates of the elastic parameters. The reason is the manner in which the traveltimes are computed in the forward modeling. The traveltimes in the forward modeling are computed using the perturbation method and, therefore, they always contain errors. The stronger anisotropy of the medium under consideration, the greater errors are obtained. Thus, the quality of the inversion results depends directly on the assumption of weak anisotropy. Therefore, the model with 5% anisotropy was inverted with higher accuracy than the model with 10% anisotropy in spite of the same observation scheme and the same number of data were used.

Inversion of noisy data

Now I will examine the sensitivity of the inversion results to errors of the traveltimes and the polarization vectors. For this purpose, noise is added to the synthetic traveltimes and qS-wave polarization vectors of both VTI models. The traveltime noise is random with a normal (Gaussian) probability distribution and a mean value equal to zero and standard deviation $\sigma_\tau = 2$ ms. To add the noise to the qS-wave polarization vectors the following procedure was used. Each polarization vector $\mathbf{A}_{qSM}$ is described by two angles, the inclination angle α and the azimuthal angle β as

$$\mathbf{A}_{qSM} = (\sin\alpha\,\cos\beta,\, \sin\alpha\,\sin\beta,\, \cos\alpha), \qquad M = 1, 2. \tag{5.28}$$

In the following examples errors are introduced into these two angles α and β to perturb the orientation of the polarization vectors obtained in the VSP experiment. The errors are random with a normal (Gaussian) probability distribution and a mean value equal to zero and standard deviations $\sigma_\alpha = 10^\circ$ and $\sigma_\beta = 10^\circ$.

For each set of noisy data the inversion was performed for 21 parameters and for 5 parameters as in the previous noise-free examples. The results of the inversions are given in the fourth and fifth columns of Table 5.1 and 5.2. For the VTI medium with 5% anisotropy the misfit function η^2 do not exceed 0.0025 s^2 for the inversion for 21 parameters as well as for the 5 elastic parameters parameters. For the VTI medium with 10% anisotropy, the misfit function η^2 is 0.0045 s^2 and 0.0056 s^2 for the inversion for 21 and 5 elastic parameters, respectively. Note that the same isotopic background media were finally obtained as in the noise-free cases.

For both models, when the inversion for 5 parameters is performed, the condition number (the ratio of the maximal singular value to the minimal singular value) is half as that for the inversion for 21 elastic parameters. The condition number for the inversion for 21 parameters is equal to 40, whereas for the inversion for 5 parameters it is equal

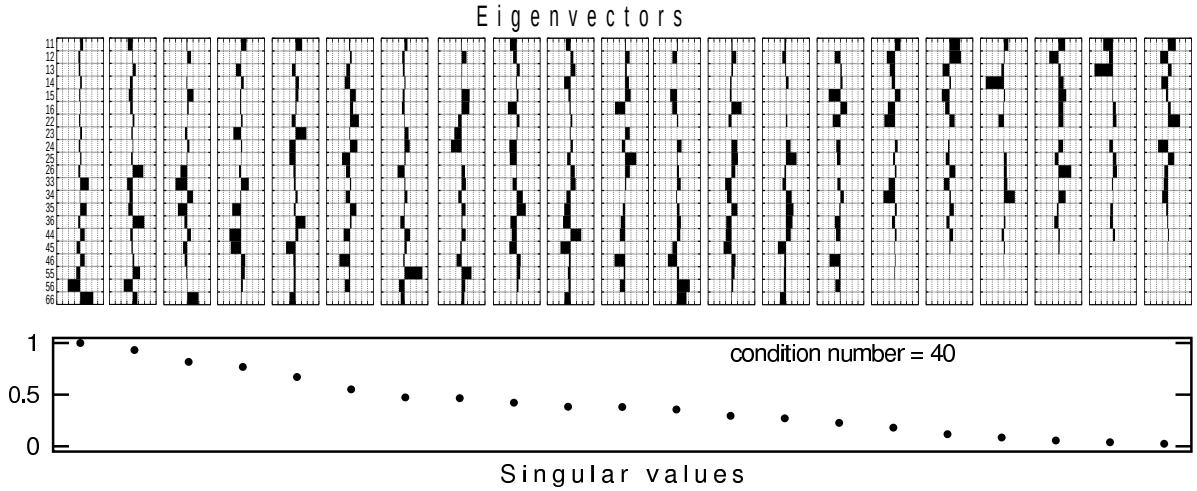

Figure 5.6: Eigenvectors and associated singular values for the inversion procedure for 21 parameters of the VTI medium with 10% anisotropy (see Tab. 5.2). The singular values are normalized to the largest one. The smallest normalized singular value is 0.025. The inversion was performed assuming standard deviations 2 ms of the traveltimes and 10° of the angles α and β of the polarization vectors of the qS-waves (see eq. (5.28)). The singular values are normalized to the largest one. The 21 pairs of numbers to the left of the eigenvectors correspond to indices of 21 parameters A_{ik} inverted.

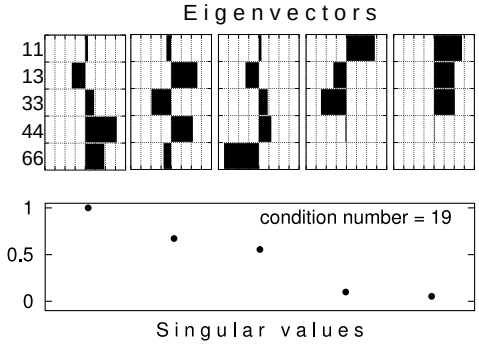

Figure 5.7: Eigenvectors and associated singular values for the inversion procedure for 5 parameters of the VTI medium with 10% anisotropy (see Tab. 5.2). The singular values are normalized to the largest one. The smallest normalized singular value is 0.053. The inversion was performed assuming standard deviations 2 ms of the traveltimes and 10° of the angles α and β used for the polarization vectors of the qS-waves (see eq. (5.28)). The five pairs of numbers to the left of the eigenvectors correspond to indices of five parameters A_{ik} inverted.

to 19. This shows that the inversion for 5 parameters is better conditioned and, therefore, more robust.

Figures 5.6 and 5.7 show the singular values normalized to the largest one for the VTI medium with 10% anisotropy. The corresponding eigenvectors are plotted above. The singular values and eigenvectors are obtained in the SVD of the matrix $\mathbf{Q}^{1/2}\mathbf{X}$ from solution (5.20). In the case of the inversion for 21 parameters, the normalized singular values spread over an interval between 1 and 0.025. The largest singular values correspond to combinations of parameters A_{66}, A_{56}, A_{33}, A_{26} and A_{55}. Therefore, these parameters should be better resolved, then the parameters A_{22}, A_{12}, A_{11}, A_{13} or A_{24} connecting with the smallest singular values. In the case of the inversion for 5 parameters, the largest singular value corresponds to combination of parameters A_{66} and A_{44} and A_{13}, whereas the smallest singular value corresponds to combinations of A_{11} and A_{33}. As the result, the parameter A_{66} and A_{44} are resolved better than A_{11} and A_{33}. Note, for the VTI medium with 5% anisotropy the singular values and the eigenvectors look similar to the

VTI medium with 10% anisotropy.

All these conclusions correlate well with confidence intervals I obtained for each inverted parameters. Each confidence interval corresponds to a probability coefficient of 99% and is calculated according to equation (5.24). The confidence intervals, $I_{99\%}$ are also given in Tables 5.1 and 5.2. For the VTI medium with 5% anisotropy, all confidence intervals of the inverted parameters cover the corresponding exact parameters with the exception of the parameter A_{44}. But for the VTI medium with 10% anisotropy, almost all exact parameters are situated outside of the corresponding confidence intervals. The reason is that the quality of the inversion depends directly on the assumption of weak anisotropy (see the inversion of the noise-free data).

Note that in the case of the VTI medium with 5% anisotropy, the RMSD of the inverted parameters from the exact ones are 0.79% and 0.70% for the inversion for 21 and 5 elastic parameters respectively. In the case of the VTI medium with 10% anisotropy, they are 1.88% and 1.81%.

5.6.3 Triclinic model

The elastic parameters, A_{ik}^{true}, of the triclinic sandstone model are given in the second column of Table 5.3. As in the previous examples, to generate traveltimes and qS-wave polarization vectors a synthetic VSP experiment was carried out (see section 5.6.1). To provide sufficient illumination the waves were generated at 20 different source positions. Each source was a vertical unit force (i.e., $\vartheta = \phi = 0$ in equation (5.27)). The data contains 542 observations of qP-waves (traveltimes), and 401 and 438, respectively $qS1$- and $qS2$-wave observations (traveltimes and the corresponding qS-wave polarization vectors). Note that the different numbers of observations of qP- and qS-waves are caused by failing of the anisotropic ray method to produce qS-wave observations for singular regions.

Noise is added to the synthetic traveltimes and qS-wave polarization vectors. Because the triclinic medium is more complicated than the VTI media from the previous examples, noisier traveltimes were used then for the previous VTI media. The traveltime noise is random with a normal (Gaussian) probability distribution and a mean value equal to zero and a standard deviation $\sigma_\tau = 4$ ms. To perturb the qS-wave polarization vectors, random noise with a normal (Gaussian) probability distribution and a mean value equal to zero was added to the angles α and β from equation (5.28). The standard deviations of the angles were $\sigma_\alpha = 10^\circ$ and $\sigma_\beta = 10^\circ$.

The noisy data were inverted for 21 elastic parameters. The results of the inversion are represented in Table 5.3. The misfit function η^2 was 0.0029 s^2. The final isotropic background medium had $v_p = 3.328$ and $v_s = 1.601$ km/s. The SVD of the matrix $\mathbf{Q}^{1/2}\mathbf{X}$ from the solution of (5.21) had the condition number 25. Therefore, all the 21 inverted parameters are acceptable. The singular values are presented in Figure 5.8. The singular values are normalized to the largest one spread over the interval between 1 and 0.040. The corresponding eigenvectors in the parameter space are plotted above. For each inverted parameter, I obtained a confidence interval with a probability coefficient of 99% according to equation (5.24). The confidence intervals are presented in Table 5.3. Although for half of the inverted parameters, the confidence intervals do not cover the corresponding exact parameters, the RMSD of the inverted parameters, A_{ik}^{est}, from the exact parameters, A_{ik}^{true}, is only 2%.

A_{ik}	A_{ik}^{true}	noisy data	
		$A_{ik}^{\text{est}}(21)$	$I_{99\%}$
A_{11}	11.000	11.001	±0.140
A_{12}	5.340	5.530	±0.078
A_{13}	6.160	6.312	±0.094
A_{14}	-0.230	-0.206	±0.051
A_{15}	0.270	0.281	±0.054
A_{16}	-0.230	-0.218	±0.043
A_{22}	10.730	10.621	±0.092
A_{23}	5.750	5.797	±0.081
A_{24}	-0.090	-0.112	±0.043
A_{25}	0.000	0.107	±0.055
A_{26}	0.500	0.524	±0.041
A_{33}	12.100	12.068	±0.162
A_{34}	0.050	0.042	±0.043
A_{35}	-0.180	-0.097	±0.053
A_{36}	-0.090	-0.124	±0.044
A_{44}	2.690	2.685	±0.014
A_{45}	0.000	0.050	±0.014
A_{46}	0.090	0.072	±0.016
A_{55}	2.370	2.310	±0.023
A_{56}	-0.140	-0.153	±0.015
A_{66}	2.510	2.463	±0.027

Table 5.3: Results of inversion of the triclinic model (RMSD is 8.3% of anisotropy). The true model is defined by A_{ik}^{true}. The inversion was performed for 21 elastic parameters using noisy data. The noisy data has a standard deviation of 4 ms of the traveltimes and standard deviations of 10° of the inclination (α) and azimuth (β) angles specifying the qS-wave polarization vectors. The isotropic background medium obtained from the iteration procedure has $v_p = 3.328$ km/s and $v_s = 1.601$ km/s. The estimated elastic parameters (A_{ik}^{est}) and the corresponding confidence intervals with 99% probability (denoted by $I_{99\%}$) are given. Note that the RMSD of the inverted parameters, A_{ik}^{est}, from the exact parameters, A_{ik}^{true}, is only 2%. The misfit function η^2 is 0.0029.

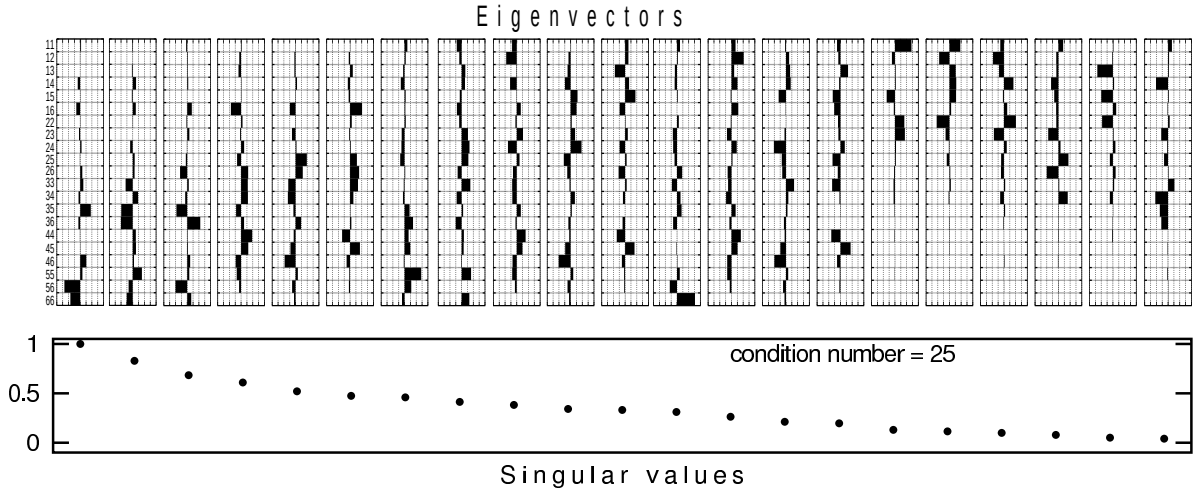

Figure 5.8: Eigenvectors and associated singular values for the inversion procedure for 21 parameters of the triclinic medium with 8.3% anisotropy (see Tab. 5.3). The singular values are normalized to the largest one. The smallest normalized singular value is 0.040. The inversion was performed assuming a standard deviations of 4 ms of the traveltimes and 10° on angles α and β of the polarization vectors of the qS-waves. The 21 pairs of numbers to the left of the eigenvectors correspond to indexes of 21 parameters A_{ik} inverted.

5.7 Inversion of inhomogeneous models

In inhomogeneous anisotropic models the elastic parameters vary from one point in space to the other. The isotropic background model also becomes inhomogeneous. As a result the vectors $\mathbf{g}^{(1)}$ and $\mathbf{g}^{(2)}$ from the perturbation theory rotate along the reference ray due to two reasons: (1) inhomogeneity of the isotropic background medium, and (2) changes of the anisotropic parameters along the reference ray. To estimate the vectors $\mathbf{g}^{(1)}$ and $\mathbf{g}^{(2)}$, the observations of the polarization vectors $\mathbf{A}_{qS1}$ and $\mathbf{A}_{qS2}$ at each point along the reference ray would be needed. However, the information about the polarization vectors $\mathbf{A}_{qS1}$ and $\mathbf{A}_{qS2}$ is available only at the receiver points. In the general case of inhomogeneity, this is not sufficient. But there are at least two types of inhomogeneous models, where the suggested inversion procedure can be applied.

The first type concerns media, where the rotations of the vectors $\mathbf{g}^{(1)}$ and $\mathbf{g}^{(2)}$ along the ray are initiated only by inhomogeneities of the isotropic background medium. An example of such media are the factorized anisotropic inhomogeneous (FAI) media suggested by Červený and Simões-Filho (1991). (A description of FAI media is given on page 81). The inhomogeneity of an FAI medium is specified by a smooth function of coordinates $f^2(\mathbf{x})$, whereas the anisotropic properties are independent of the coordinates. If the parameters of the isotropic background medium are chosen proportional to the function $f^2(\mathbf{x})$, the perturbations of the elastic parameters due to anisotropy are identical in each point. Therefore, the rotations of the vectors $\mathbf{g}^{(1)}$ and $\mathbf{g}^{(2)}$ along the reference ray in the background medium are caused only by the inhomogeneity of the background medium. These rotations then follow the differential equations (2.61) on page 54. If the vectors $\tilde{\mathbf{g}}^{(1)}$ and $\tilde{\mathbf{g}}^{(2)}$ estimated at the receiver points are used as initial conditions for the differential equations (2.61), we get the vectors $\tilde{\mathbf{g}}^{(1)}$ and $\tilde{\mathbf{g}}^{(2)}$ at each point on the ray by solving these equations along the reference ray.

The second type consists of piecewise homogeneous anisotropic media. Piecewise homogeneous media are common in exploration geophysics. For these media a recurrent inversion procedure can be suggested. In this study anisotropic layered models are considered. First, a description of the recurrent inversion procedure is given. Then, the procedure is applied to an anisotropic layered model.

5.7.1 Recurrent inversion scheme

To obtain the elastic parameters of an anisotropic layered model the inversion procedure described above are recurrently applied. The model structure is supposed to be known, i.e., a VSP experiment is assumed. This means that the number of the layers and their depths are known. All receivers are divided into K groups, where K is the number of layers in the model considered. The inversion procedure is performed in K steps in a layer-by-layer manner. Figure 5.9 explains the procedure for an example of a three-layers model.

To estimate the elastic parameters of the first layer, only the observed data at the receivers situated in the first layer are used ($K = 1$). Since the layer is homogeneous, its elastic parameters are determined as in the previous homogeneous examples, see Fig. 5.9*a*. For the following step the elastic parameters of the first layer and the corresponding

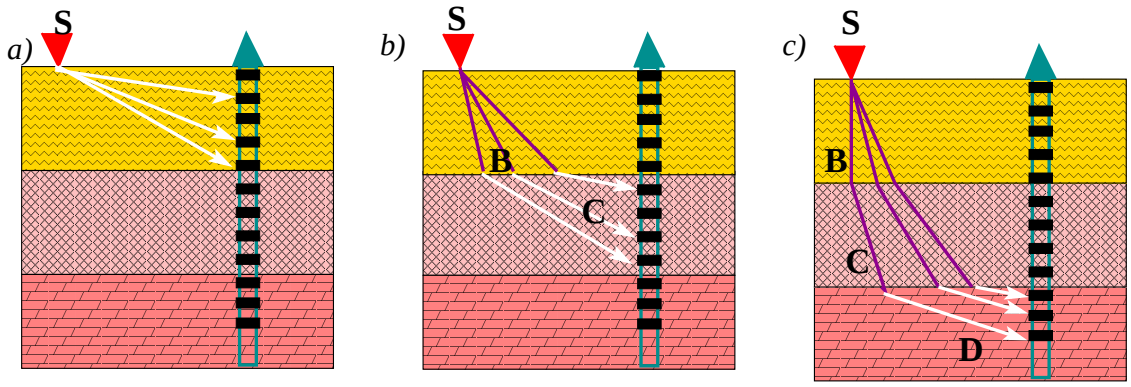

Figure 5.9: Recurrent inversion scheme: The model consists of three layers. The inversion procedure is performed in a layer-by-layer manner. *(a)* The perturbations Δa_{iklm} in the first layer are inverted using the observed data at the receivers situated in the first layer. *(b)* Traveltimes along the rays in the first layer are subtracted from the traveltimes observed at the receivers situated in the second layer. Then, these newly obtained traveltimes are used for inverting for Δa_{iklm} in the second layer. *(c)* To invert Δa_{iklm} in the third layer, traveltimes along the rays in the first and second layers are subtracted from the observed traveltimes.

isotropic background medium are assumed to be known.

In the second step, data observed at the receivers from the second layer is used ($K = 2$). The reference ray paths of all waves recorded at these receivers consist of two parts (see Fig. 5.9*b*) those in the first layer (SB) and in the second layer (BC). The traveltime τ of each wave thus consists of two terms

$$\tau = \tau^{(SB)} + \tau^{(BC)},$$

where $\tau^{(SB)}$ is the traveltime in the first layer and $\tau^{(BC)}$ is the traveltime in the second layer. With the known elastic parameters of the first layer, the traveltimes $\tau^{(SB)}$ in the first layer can easily be calculated by the equations (5.13) with the perturbation method. Then, the calculated traveltime $\tau^{(SB)}$ is subtracted from the whole traveltime τ recorded at the receiver. As a result the traveltime $\tau^{(BC)}$ along the ray path BC in the second layer is obtained. The second layer is homogeneous, therefore, the polarization vector at the receiver can be used to estimate the corresponding vector $\tilde{\mathbf{g}}$ along the ray path BC. With the traveltime $\tau^{(BC)}$ and the vector $\tilde{\mathbf{g}}$ as input data, the inversion of the perturbations Δa_{iklm} in the second layer can be performed in the same manner as in the first layer. Note that the parameters of the isotropic background medium in the first layer are fixed, whereas the parameters of the isotropic background medium in the second layer are searched with help of the iteration procedure described above (see page 96). Therefore, the reference ray paths have to be recalculated as soon as the parameters of the isotropic background medium in the second layer are changed.

In a similar way the elastic parameters of the third layer can be determined, see Fig. 5.9*c*. Now, the elastic parameters of the first and second layer are assumed to be known. Therefore, the traveltimes along the path in the first (SB) and second (BC) layers can be calculated. Then, the calculated traveltimes are subtracted from the observed traveltimes at the receivers of the third layer. The newly obtained traveltimes, $\tau^{(CD)}$,

and polarization vectors at the receivers of the third layer are used to invert for the perturbations Δa_{iklm} in the third layer. Note that the parameters of isotropic background media in the first and second layers are known from the previous steps. Therefore, the iteration procedure for the construction of the isotropic background medium is only applied for the third layer. All the reference ray paths have to be recalculated as soon as the parameters of the isotropic background medium in the third layer are changed.

Thus, the elastic parameters of all layers can be determined in the layer-by-layer manner using the already known elastic parameters in the upper layers and the traveltimes and polarization vectors in the layers under consideration.

5.7.2 Synthetic data for the three layer model

A layered model was used to test the suggested recurrent inversion procedure. The model consists of three layers. The first layer is an anisotropic medium with orthorombic symmetry, the second layer is a transversely isotropic medium with vertical axis of symmetry (VTI); the third layer is isotropic. The density-normalized elastic parameters (in $\mathrm{km}^2/\mathrm{s}^2$) of the anisotropic layers and the P- and S-wave velocities of the isotropic layer are summarized in Table. 5.4. The ray velocity and slowness surfaces are shown in Figure 5.12 for the first orthorombic layer and in Figure 5.16 for the second VTI layer.

orthorombic

$$\begin{pmatrix} 10.8 & 2.2 & 1.9 & 0. & 0. & 0. \\ & 11.3 & 1.7 & 0. & 0. & 0 \\ & & 8.5 & 0. & 0. & 0. \\ & & & 3.6 & 0. & 0. \\ & & & & 3.9 & 0. \\ & & & & & 4.3 \end{pmatrix}$$

VTI

$$\begin{pmatrix} 13.59 & 6.8 & 5.44 & 0. & 0. & 0. \\ & 13.59 & 5.44 & 0. & 0. & 0. \\ & & 10.87 & 0. & 0. & 0. \\ & & & 4.1 & 0. & 0. \\ & & & & 4.1 & 0. \\ & & & & & 4.5 \end{pmatrix}$$

isotropic

$V_p = 3.87\,\mathrm{km/s}$
$V_s = 2.24\,\mathrm{km/s}$

Table 5.4: The density normalized elastic parameters (in $\mathrm{km}^2/\mathrm{s}^2$) of the anisotropic layers and the P- and S-wave velocities of the isotropic layer. See also Fig. 5.12 and 5.16.

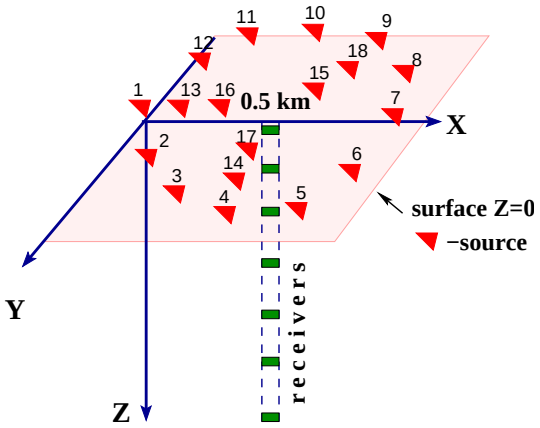

No	X,m	Y,m	No	X,m	Y,m
1	0.	0.	10	500.	-500.
2	67.	250.	11	250.	-433.
3	250.	433.	12	67.	-250.
4	500.	500.	13	100.	0.
5	750.	433.	14	500.	400.
6	933.	250.	15	604.	-386.
7	1000.	0.	16	300.	0.
8	933.	-250.	17	500.	200.
9	750.	-433.	18	552.	-193.

Figure 5.10: The observation scheme of the synthetic VSP experiment. A vertical borehole contains 25 aligned three-component receivers with 30 m spacing until a depth of 750 m. All sources denoted by triangles are vertical forces. The exact source position are given in the Table on the right.

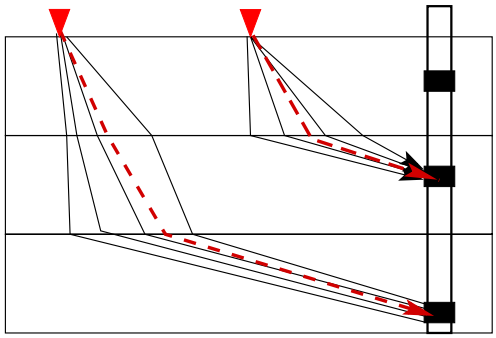

Figure 5.11: Ray paths (solid lines) of four qS-waves arriving at receivers (black boxes) in the second and third layers. Traveltimes of all qS-waves are computed along one reference isotropic ray (dashed lines). Each reference ray approximates four anisotropic rays.

As observed data I used traveltimes and polarization vectors computed in a synthetic VSP experiment. The scheme of the VSP experiment is shown in Figure 5.10. A vertical borehole contains 25 aligned three-component receivers with 30 m spacing until a depth of 750 m. There are 10 receivers in the first layer, 11 receivers in the second layer and 4 in the third isotropic layer. The receivers record the wavefields from 18 sources situated around the borehole on the Earth surface. All sources are vertical forces. In Figure 5.10 these 18 source positions are denoted by triangles. Traveltimes and polarizations are calculated by standard anisotropic ray tracing using the ANRAY package, see Gajewski and Pšenčík (1990). According to the anisotropic ray theory, three waves arrive at each receiver in the first layer: one qP and two quasi-shear waves. Therefore, for each receiver in the first layer there are three traveltimes (qP, $qS1$ and $qS2$ waves).

On the interface between two anisotropic layers each quasi-shear wave produces two quasi-shear waves. One wave is the same type as the incident wave, the other is a converted wave. Therefore, two incident quasi-shear waves produce four quasi-shear waves in the second layer, namely, $qS1$-$qS1$, $qS2$-$qS2$, $qS1$-$qS2$ and $qS2$-$qS1$. As a result for each receiver in the second layer there is one qP-wave traveltime and four quasi-shear wave traveltimes. The converted $qP - qS$ and $qS - qP$ waves are not considered. (Note that these converted waves can also be used in the suggested inversion.) Since the third layer is isotropic, there is one qP-wave traveltime and four qS-wave traveltimes.

Figure 5.11 shows a simple scheme of the ray paths (solid lines) of four shear-waves arriving at the receivers in the second and third layers. Note that each of these four shear-waves has its individual ray path. According to the perturbation theory anisotropic traveltimes are computed along the S-wave ray in the isotropic background medium. Since, there are only S-waves in the homogeneous isotropic medium, to compute the four qS-wave traveltimes in the anisotropic medium only one reference isotropic ray (dashed line) can be used.

5.7.3 Inversion for the first layer

Inversion of the elastic parameters of the first layer is performed just as it is performed in homogeneous anisotropic media. The observed data from the first 10 receivers is used. There are 171 observations of qP-wave traveltimes, 169 and 162 observations of traveltimes and polarization vectors of $qS1$- and $qS2$-waves respectively. Note that here and in the subsequent discussion the different numbers of observations of qP- and qS-waves are due to excluding some observations from the inversion. No observations were used for regions

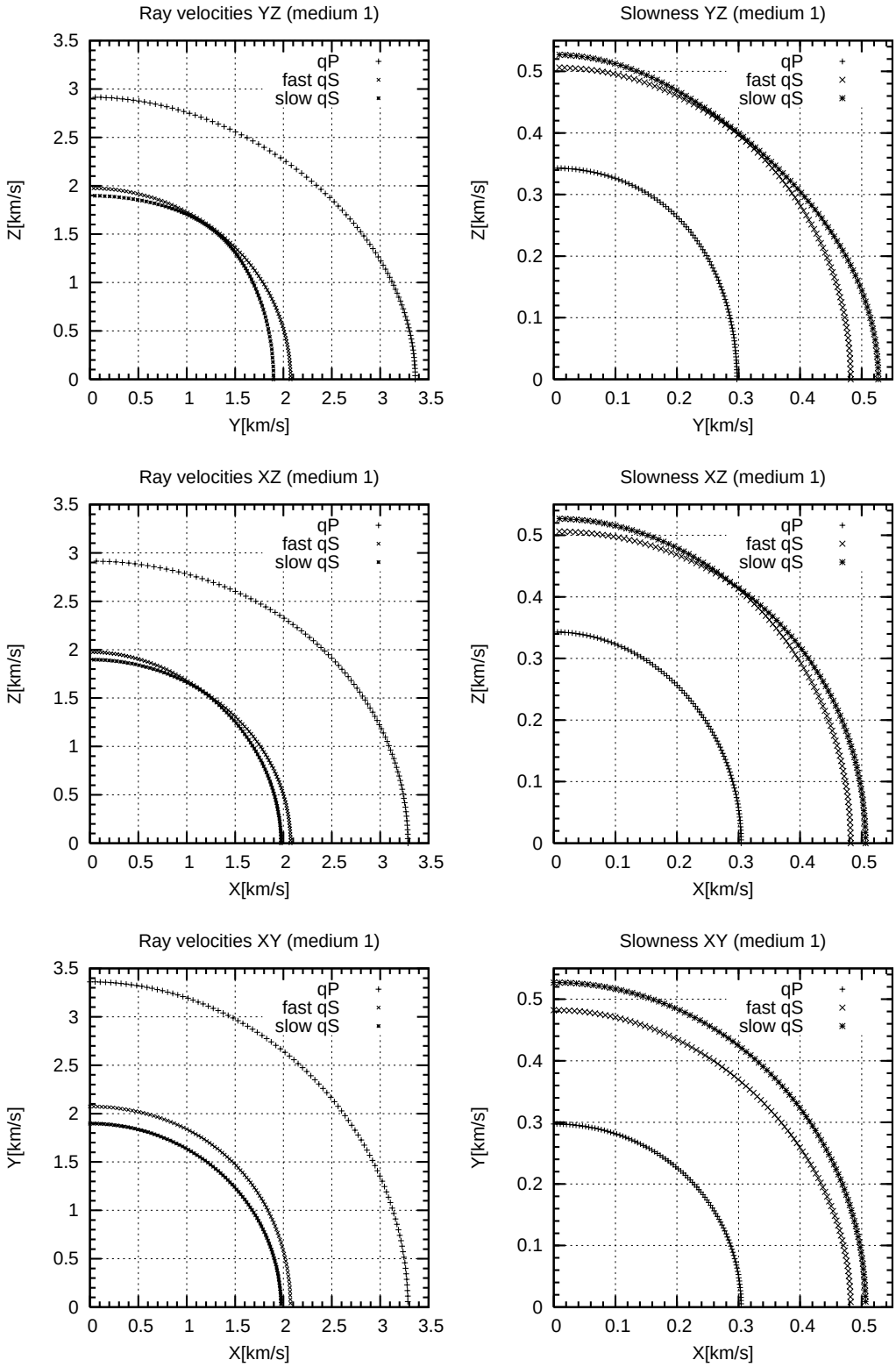

Figure 5.12: Ray velocities and slowness surfaces for the first orthorombic layer. The elastic parameters of the orthorombic medium are given in Tab. 5.4.

where the ray theory fails, e.g., for singular directions. Noise is added to the synthetic traveltimes and qS-wave polarization vectors. The errors have a standard deviation of 2 ms of the traveltimes and standard deviations of 10° on the inclination (α) and the azimuth (β) angles specifying the qS-wave polarization vectors (see eq. (5.28)).

Let us assume that there is no a priori knowledge on the type of anisotropy. Therefore, the inversion for all 21 elastic parameters must be performed. The results of this inversion are given in the third column of Table 5.5. The final isotropic background medium had $v_p = 3.151$ and $v_s = 1.993$ km/s. The misfit function η^2 was 0.002 s^2. The SVD of the matrix $\mathbf{Q}^{1/2}\mathbf{X}$ from the solution (5.21) has the condition number 23. This means that the inversion problem for 21 parameters was well-conditioned. Therefore, all 21 parameters are acceptable. The singular values normalized to the largest one and the corresponding eigenvectors are plotted in Figure 5.13. The singular values spread over an interval between 1 and 0.043. The largest singular values correspond to combinations of the elastic parameters from A_{34} till A_{66}, but the smallest ones correspond to combinations of the elastic parameters from A_{11} till A_{22}, i.e., the parameters A_{34} till A_{66} are best resolved by the inversion for this particular acquisition scheme. For each inverted parameter, I obtained also a confidence interval with a probability coefficient of 99% according to equation (5.24). Note that the inverted parameters, $A_{ik}^{\text{est}}(21)$, are close to the exact ones, A_{ik}^{true}. The RMSD of the inverted parameters from the exact parameters is 1.80%.

The non-orthorombic parameters of $A_{ik}^{\text{est}}(21)$ are relatively small. The corresponding confidence intervals show that these small parameters can not be distinguished from zero. Therefore, we can assume an orthorombic symmetry of the considered medium. In this case we can restrict the inversion to nine independent elastic parameters: A_{11}, A_{12}, A_{13}, A_{22}, A_{23}, A_{33}, A_{44}, A_{55} and A_{66}. The results of the inversion for the 9 parameters are given in the fourth column of Table 5.5. The inverted parameters $A_{ik}^{\text{est}}(9)$ are also

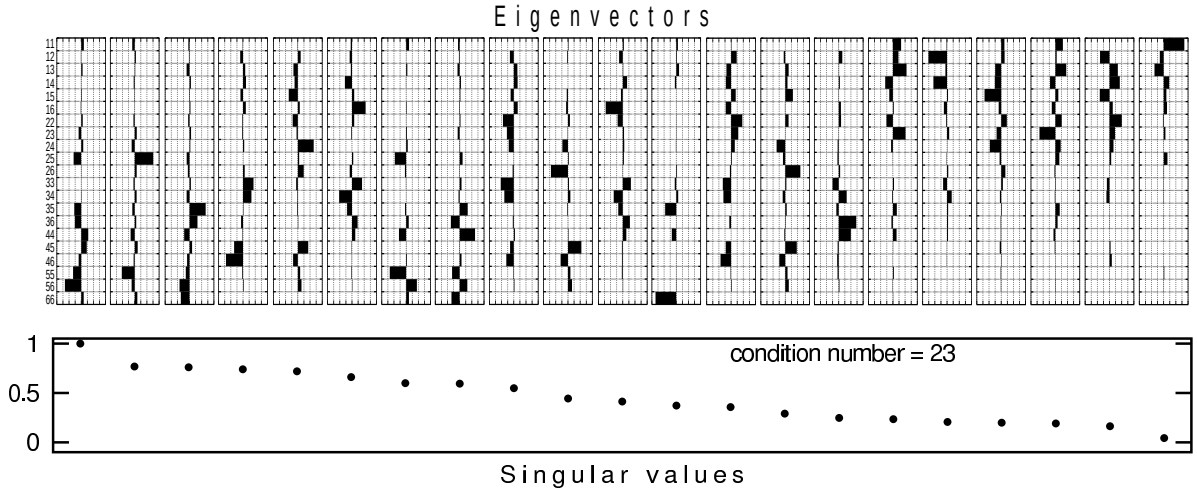

Figure 5.13: Eigenvectors and associated singular values for the inversion procedure for 21 parameters of the first layer (orthorombic anisotropy, see Tab. 5.5). The singular values are normalized to the largest one. The smallest normalized singular value is 0.043. The inversion was performed assuming a standard deviations of 2 ms of the traveltimes and standard deviations $\sigma_\alpha = 10°$ and $\sigma_\beta = 10°$ of the polarization vectors of the qS-waves.

	First layer, σ_τ=2ms, σ_α=10°, σ_β=10°					Second layer, σ_τ=3ms, σ_α=15°, σ_β=15°						
	A_{ik}^{true}	$A_{ik}^{\text{est}}(21)$	$I_{99\%}$	$A_{ik}^{\text{est}}(9)$	$I_{99\%}$	A_{ik}^{true}	$A_{ik}^{\text{est}}(21)$	$I_{99\%}$	$A_{ik}^{\text{est}}(9)$	$I_{99\%}$	$A_{ik}^{\text{est}}(5)$	$I_{99\%}$
A_{11}	10.800	10.766	±0.127	10.763	±0.127	13.590	13.474	±0.895	13.471	±0.895	14.003	±0.786
A_{12}	2.200	2.150	±0.098	2.146	±0.099	6.800	6.893	±0.749	6.882	±0.746	6.031	±0.793
A_{13}	1.900	1.893	±0.209	1.884	±0.208	5.440	5.501	±0.362	5.512	±0.359	5.541	±0.236
A_{14}	0.	-0.004	±0.097	0.		0.	-0.118	±0.185	0.		0.	
A_{15}	0.	-0.017	±0.067	0.		0.	0.058	±0.171	0.		0.	
A_{16}	0.	-0.038	±0.056	0.		0.	0.008	±0.314	0.		0.	
A_{22}	11.300	11.102	±0.124	11.102	±0.124	13.590	13.853	±0.920	13.793	±0.914	14.003	±0.786
A_{23}	1.700	1.775	±0.200	1.775	±0.201	5.440	5.505	±0.343	5.498	±0.341	5.541	±0.236
A_{24}	0.	0.004	±0.062	0.		0.	-0.082	±0.157	0.		0.	
A_{25}	0.	-0.040	±0.085	0.		0.	0.139	±0.190	0.		0.	
A_{26}	0.	0.016	±0.054	0.		0.	0.012	±0.313	0.		0.	
A_{33}	8.500	8.226	±0.450	8.217	±0.452	10.870	10.471	±0.669	10.499	±0.665	10.403	±0.728
A_{34}	0.	0.044	±0.068	0.		0.	-0.018	±0.154	0.		0.	
A_{35}	0.	-0.042	±0.075	0.		0.	0.069	±0.170	0.		0.	
A_{36}	0.	0.006	±0.087	0.		0.	-0.053	±0.313	0.		0.	
A_{44}	3.600	3.557	±0.038	3.559	±0.039	4.100	4.097	±0.099	4.099	±0.095	4.166	±0.082
A_{45}	0.	-0.004	±0.034	0.		0.	0.006	±0.081	0.		0.	
A_{46}	0.	0.006	±0.036	0.		0.	0.027	±0.063	0.		0.	
A_{55}	3.900	3.891	±0.039	3.889	±0.039	4.100	4.118	±0.090	4.125	±0.089	4.166	±0.082
A_{56}	0.	0.008	±0.037	0.		0.	0.003	±0.054	0.		0.	
A_{66}	4.300	4.312	±0.026	4.314	±0.026	4.500	4.481	±0.153	4.485	±0.152	4.486	±0.134
RMSD		1.80%		1.67%			2.32%		1.58%		5.61%	
Misfit, η^2		0.002 s^2		0.002 s^2			0.009 s^2		0.009 s^2		0.011 s^2	
Background: v_p		3.151 km/s		3.151 km/s			3.649 km/s		3.648 km/s		3.640 km/s	
v_s		1.993 km/s		1.993 km/s			1.966 km/s		1.966 km/s		1.971 km/s	

Table 5.5: Results of the inversion of two layers of the three-layer model. The first layer is an orthorombic medium; the second layer is a VTI medium. The true elastic parameters are given in the columns A_{ik}^{true}. Random noise with a normal probability distribution is added to the synthetic data. The standard deviation of errors for the traveltimes is denoted as σ_τ and for the inclination (α) and azimuth (β) angles defining the qS-wave polarization vectors as σ_α and σ_β. For the orthorombic medium the inversion of the noisy data was performed for 21 and 9 parameters (see $A_{ik}^{\text{est}}(21)$ and $A_{ik}^{\text{est}}(9)$). For the VTI medium the inversion of the data with noise was performed for 21, 9 and 5 parameters (see $A_{ik}^{\text{est}}(21)$, $A_{ik}^{\text{est}}(9)$ and $A_{ik}^{\text{est}}(5)$). For each estimated parameter the confidence interval with 99% probability (denoted by $I_{99\%}$) is given.

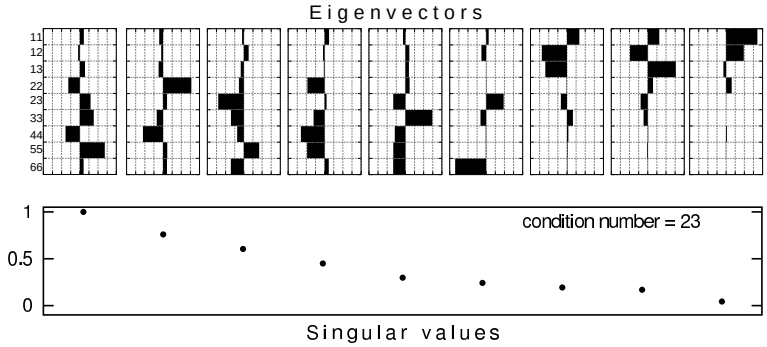

Figure 5.14: Eigenvectors and associated singular values for the inversion procedure for 9 parameters of first layer (orthorombic anisotropy, see Tab. 5.5). The singular values are normalized to the largest one. The smallest normalized singular value is 0.043. The inversion was performed assuming a standard deviation 2 ms of the traveltimes and standard deviations $\sigma_\alpha = 10^\circ$ and $\sigma_\beta = 10^\circ$ of the polarization vectors of the qS-waves.

given with the confidence intervals of 99% probability ($I_{99\%}$). The misfit function η^2 equals to 0.002 s^2. Figure 5.14 shows the normalized singular values and the corresponding eigenvectors obtained for the SVD of the matrix $\mathbf{Q}^{1/2}\mathbf{X}$ from the solution (5.21). As in the previous case, the singular values vary from 1 till 0.043 and, thus, the condition number of the inversion is 23. Therefore all the inverted parameters are acceptable. The RMSD of the inverted parameters $A_{ik}^{\rm est}(9)$ from the exact parameters, $A_{ik}^{\rm true}$, is 1.67%.

Please note that the small confident interval for A_{44} indicates that this parameter is well-resolved. But the exact value of A_{44} is outside of the corresponding confidence interval. The reason is that the inversion is based on the assumption of weak anisotropy, thus, only some estimates of the elastic parameters can be obtained (see the inversion of the noise-free data). The confidence intervals provide the quality of these estimates and depend on the illumination of the observation scheme and the quality of the observed data. The data and the observation scheme considered allow to obtain a well-resolved estimate of A_{44}, but due to the approximation of weakly anisotropy this estimate is found to be shifted with respect to the exact value. The similar situation is observed for the parameter A_{22}.

What happens if we ignore that the medium under consideration is an anisotropic medium? Figure 5.15 shows traveltime residuals for the first layer obtained after the inversion of noise-free data for the 9 elastic parameters (red crosses) and after the inversion for only 2 parameters (isotropic P- and S-wave velocities) (blue stars). The traveltime residuals are given in ms. One can see that the traveltimes for the inverted anisotropic medium differ from the observed traveltimes by 1-3 ms for qP- as well as for two quasi-shear waves. The deviations of the isotropic traveltimes may be as big as 5-13 ms.

5.7.4 Inversion for the second layer

In the second layer there are 11 receivers. The data includes 187 observations of qP-waves, 193 and 144 observations respectively of $qS1-qS1$- and $qS1-qS2$-waves, 183 and 171 observations respectively of $qS2-qS2$- and $qS2-qS1$-waves (see explanations on page 111). As in the previous examples, noise is added to the synthetic traveltimes and

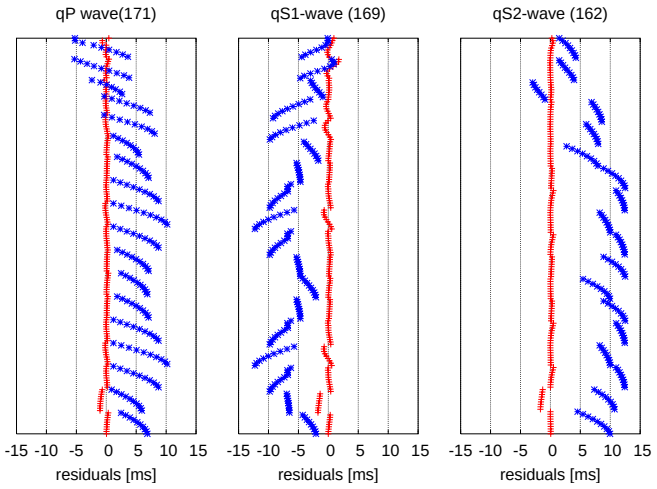

Figure 5.15: Traveltime residuals after inversion of noise-free data in the first orthorombic layer. Gray crosses show traveltime residuals after inversion for 9 different elastic parameters defining the orthorombic medium, black stars show the traveltime residuals after inversion for 2 isotropic parameters. 120 observations of the qP-wave traveltimes, 120 and 115 observations of $qS1$- and $qS2$-waves, respectively, were used.

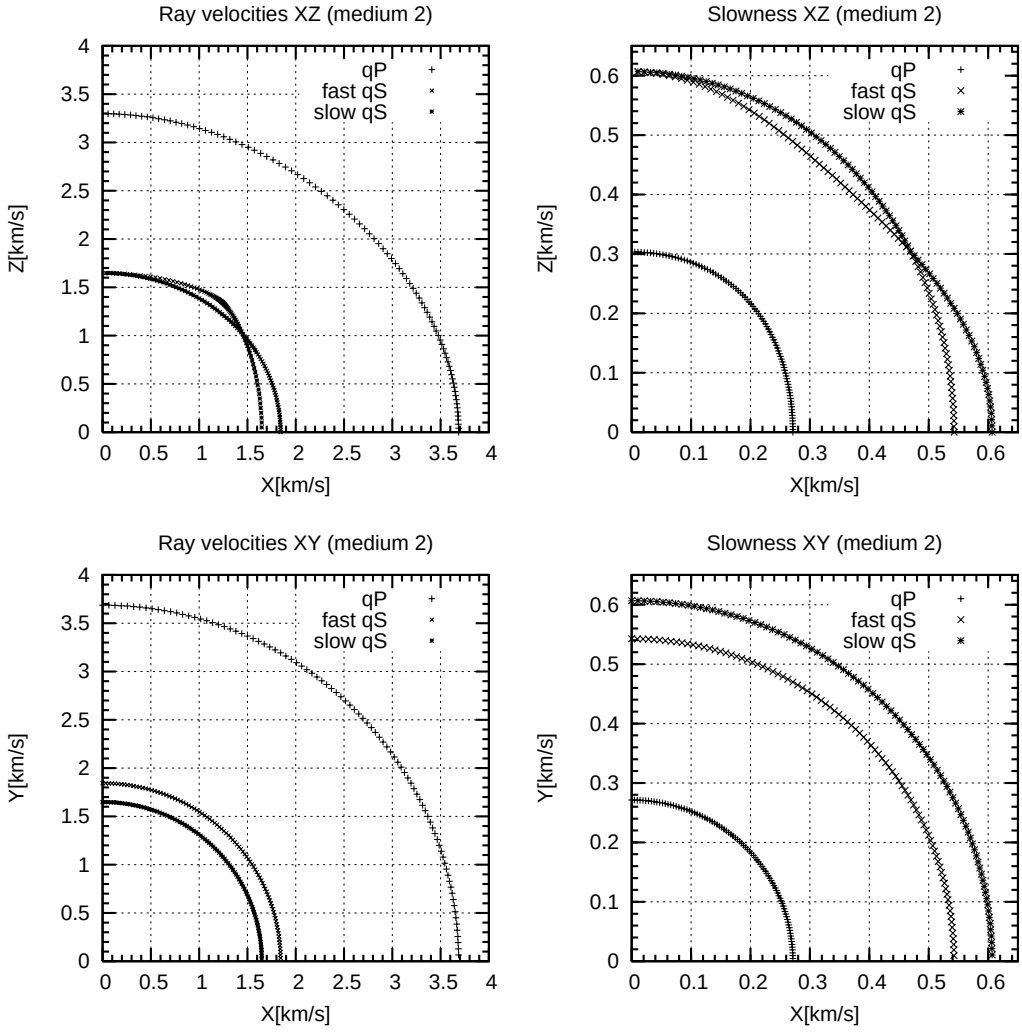

Figure 5.16: The ray velocities and slowness surfaces for the second VTI layer. The elastic parameters of the VTI medium are given in Tab. 5.4.

qS-wave polarization vectors. I assume the data from the second layer are more noisier then from the first layer. Therefore, the errors have a standard deviation of 3 ms of the traveltimes and standard deviations of 15° of the inclination (α) and azimuth (β) angles specifying the qS-wave polarization vectors (see eq. (5.28)).

If there is no a priori knowledge on the type of anisotropy, the inversion must be performed for all 21 elastic parameters. The results of the inversion are given in the sixth column of Table 5.5. The final isotropic background medium has $v_p = 3.649$ km/s and $v_s = 1.966$ km/s. For each inverted parameter, a confidence interval with a probability coefficient of 99% is given (see eq. (5.24)). The misfit function η^2 was 0.009 s^2. Figure 5.17 shows the 21 normalized singular values and the corresponding eigenvectors obtained in the SVD of the matrix $\mathbf{Q}^{1/2}\mathbf{X}$ from the solution (5.20). The normalized singular values spread over an interval between 0.036 and 1. It corresponds to the condition number equals to 28. All 21 inverted parameters are acceptable.

The confidence intervals show that the small non-orthorombic inverted parameters of $A_{ik}^{\rm est}(21)$ can not be distinguished from zero. One could conclude that the considered medium can possess orthorombic symmetry as well as VTI symmetry. The last two columns of Table 5.5 give the results of the inversion for the 9 parameters, $A_{ik}^{\rm est}(9)$, and for the 5 parameters, $A_{ik}^{\rm est}(5)$. One see that A_{11} can not be distinguished from A_{22}, A_{44} from A_{55} and A_{13} from A_{23}. For the inversion for 9 parameters the background isotropic medium was hardly different from the inversion for 21 parameters: $v_p = 3.648$ m/s and $v_s = 1.966$ km/s. But for the inversion for 5 parameters it has $v_p = 3.640$ m/s and $v_s = 1.971$ km/s. The misfit function η^2 is 0.009 s^2 in the first case and 0.011 s^2 in the last case. For each inverted parameter the corresponding confidence interval is obtained. Analysis of these confidence intervals show that the inverted parameters $A_{ik}^{\rm est}(9)$ can not be distinguished from the inverted parameters $A_{ik}^{\rm est}(5)$. Please note that among the inverted

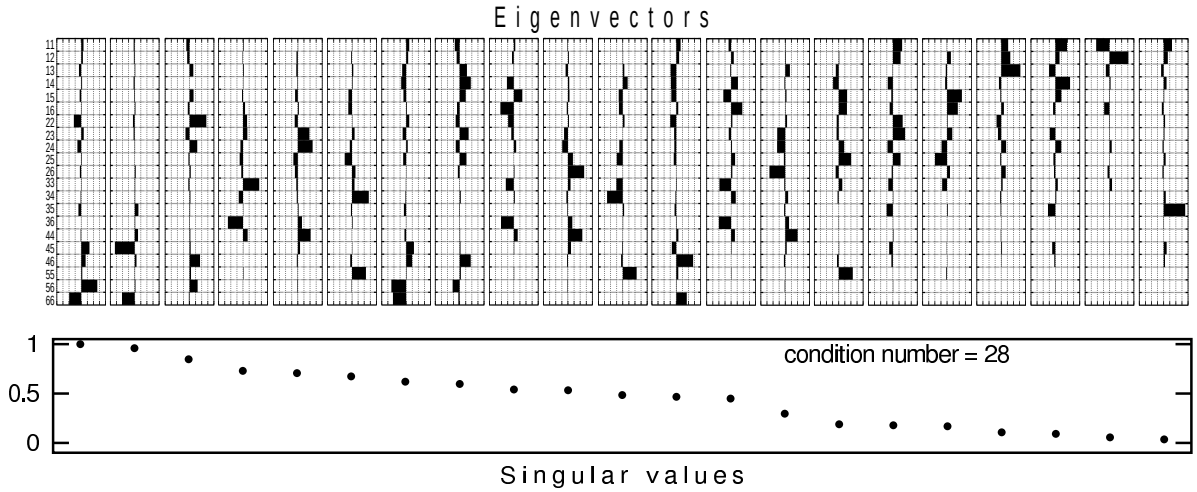

Figure 5.17: Eigenvectors and associated singular values for the inversion procedure for 21 parameters of the second layer (VTI anisotropy, see Tab. 5.5). The singular values are normalized to the largest one. The smallest normalized value is 0.036. The inversion was performed assuming a standard deviation 3 ms of the traveltimes and standard deviations $\sigma_\alpha = 15°$ and $\sigma_\beta = 15°$ of the polarization vectors of the qS-waves.

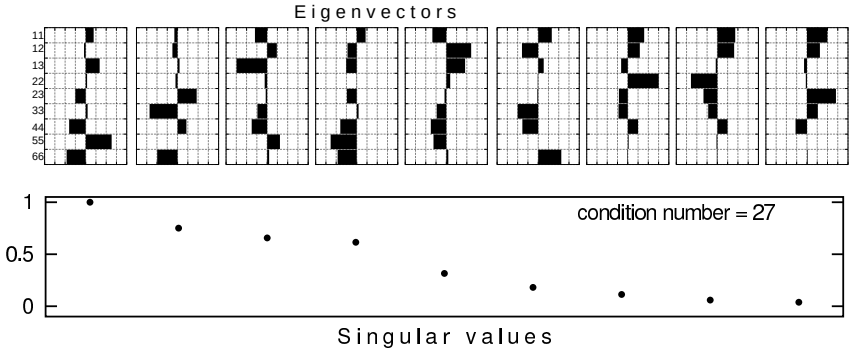

Figure 5.18: Eigenvectors and associated singular values for the inversion procedure for 9 parameters of the second layer (VTI anisotropy, see Tab. 5.5). The singular values are normalized to the largest one. The smallest normalized value is 0.037. The inversion was performed assuming errors with a standard deviation 3 ms of the traveltimes and standard deviations $\sigma_\alpha = 15°$ and $\sigma_\beta = 15°$ of the polarization vectors of the qS-waves.

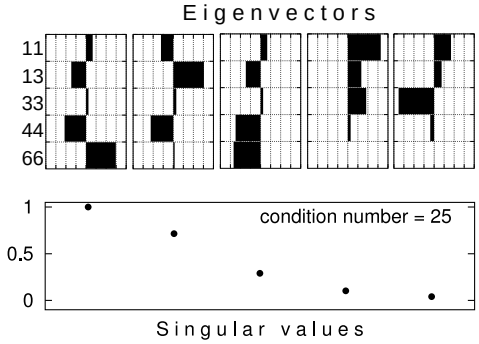

Figure 5.19: Eigenvectors and associated singular values for the inversion procedure for 5 parameters of the second layer (VTI anisotropy, see Tab. 5.5). The singular values are normalized to the largest one. The smallest normalized value is 0.041. The inversion was performed assuming a standard deviation 3 ms of the traveltimes and standard deviations $\sigma_\alpha = 15°$ and $\sigma_\beta = 15°$ of the polarization vectors of the qS-waves.

parameters $A_{ik}^{\rm est}(9)$, the parameter A_{11} can not be distinguished from the parameter A_{22}, A_{44} from A_{55} and A_{13} from A_{23}. This means that the medium of the second layer possesses most likely VTI symmetry. The RMSD of the inverted parameters $A_{ik}^{\rm est}(5)$ from the exact parameters $A_{ik}^{\rm true}$ is 5.9%.

What happens if we ignore that the medium under consideration is an anisotropic medium? Figure 5.20 shows traveltime residuals obtained after the inversion of noise-free data for the 5 elastic parameters (red crosses) and after the inversion for only the 2 parameters (isotropic P- and S-wave velocities) (blue stars). Traveltime residuals are given in ms. One can see that the traveltimes for the inverted anisotropic medium differ from the observed traveltimes by 1–4 ms for the qP- as well as for the two quasi-shear waves. The deviations of the isotropic traveltimes may be as big as 1–15 ms.

5.7.5 Inversion for the third layer

In the third layers 4 receivers are situated. There are 48 observations of the P-waves and 175 observations of S-waves. According to the discussion on page 111, the observations of the S-waves are separated into four groups: $qS1$-$qS1$-S (50 observations), $qS2$-$qS2$-S (36), $qS1$-$qS2$-S (42) and $qS2$-$qS1$-S (47). Noise is added to the traveltimes and qS-wave polarization vectors. The errors have a standard deviation of 3 ms of the traveltimes and

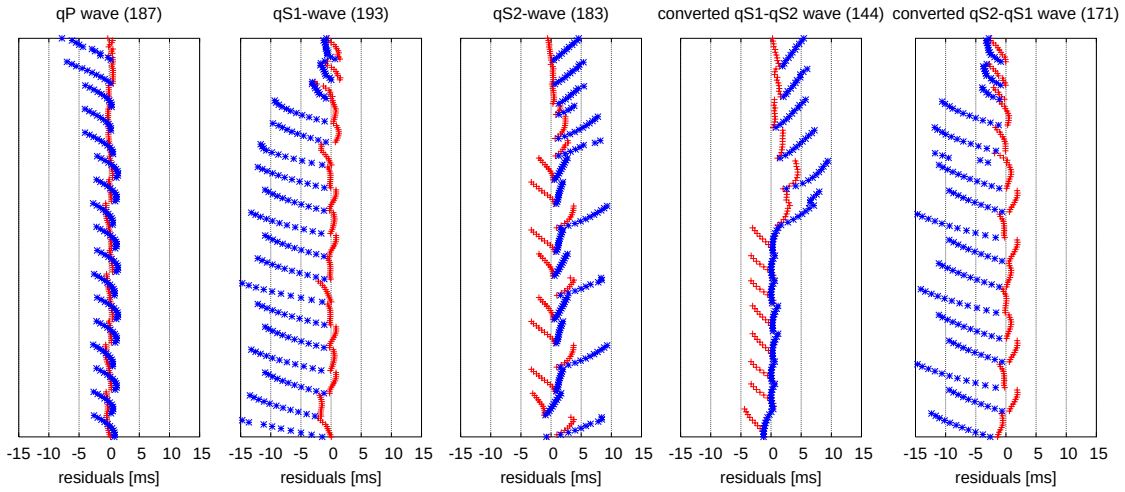

Figure 5.20: Traveltime residuals after the inversion of noise-free data in the second VTI layer. Gray crosses show traveltime residuals after the inversion for 5 elastic parameters defining the VTI medium, black stars show the traveltime residuals after the inversion for 2 isotropic elastic parameters.

standard deviations of 15° of the inclination (α) and azimuth (β) angles specifying the qS-wave polarization vectors (see eq. (5.28)).

The inversion was performed for the 2 elastic parameters (the density-normalized Láme parameters λ/ρ and μ/ρ). The misfit function η^2 was 0.0034 s^2. The condition number of the SVD of the matrix $\mathbf{Q}^{1/2}\mathbf{X}$ from the solution (5.20) is 10. As a result the following P- and S-wave velocities and their confidence intervals with a probability coefficient of 99% were obtained:

$$\begin{aligned} V_p &= 3.88\,\text{km/s} \quad I_{99\%} = 1.56 \\ V_s &= 2.16\,\text{km/s} \quad I_{99\%} = 0.47 \end{aligned}$$

(The exact velocities of the third layer are given in Table 5.4 on page 110.) Note that the RMSD of the inverted parameters from the exact parameters is 5.38%.

Figure 5.21 shows traveltime residuals in the third isotropic layer after the inversion of noise-free data for 2 parameters.

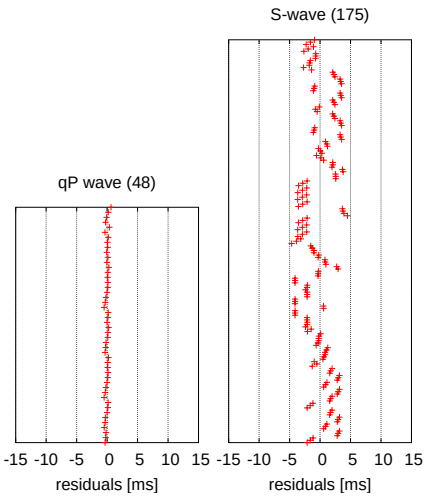

Figure 5.21: Traveltime residuals after the inversion of noise-free data in the third isotropic layer. Black crosses show traveltime residuals after inversion for the isotropic elastic parameters.

5.8 Conclusions

An inversion procedure for weakly anisotropic media using traveltimes of qP- and qS-waves as well as qS-wave polarizations was suggested. The presented inversion procedure allows to use the same linear inversion scheme for qP- as well as for qS-wave data. The joint

inversion of qP- and qS-waves allows to determine the full elastic tensor of the anisotropic medium.

In comparison to a conventional tomographic approach, the suggested inversion scheme requires not only traveltime observations, but also the observed qS-wave polarization vectors. Although the observed qS-wave polarizations are available from three component data, picking qS-wave polarization vectors from real data can be a challenging task. However, to obtain traveltimes, the two qS-waves need to be separated in any case. For this separation the difference in qS-wave polarizations is usually used (see, e.g., Alford, 1986; Li and Crampin, 1993; Dellinger et al., 1998). Therefore, the qS-wave polarization vectors are automatically obtained as a by-product of the qS-wave separation.

The advantage of the presented inversion procedure is that no assumption about any special type of anisotropic symmetry is needed. If there is no a priori information on the type of anisotropy, all 21 elastic parameters can be inverted. Then, analysis of the 21 inverted elastic parameters can be carried out. Based upon the significance and accuracy of each parameter, we can restrict the inversion to a smaller number of the elastic parameters and determine the symmetry of the medium under consideration. In all examples the following strategy was used. First, all 21 elastic parameters were inverted. Then, the inversion for 9, 5 or 2 different elastic parameters was performed.

The main restriction of the suggested inversion procedure is that it is based on perturbation theory which provides a smooth transition from isotropic media to anisotropic media by small perturbations of the elastic parameters. Therefore, the accuracy of the traveltime computations in the forward modeling problem and, as a result, the quality of the inversion depend directly on the assumption of weak anisotropy. This means that the inversion procedure allows to reconstruct the elastic parameters only if the anisotropic medium is weakly anisotropic. According to the examples presented in this study, for the medium with more then 5% anisotropy, the inversion does not reconstruct the elastic parameters, but only gives some estimates of these elastic parameters even when the noise-free data are used. Namely, although some of these estimates were well-resolved, but they were found to be shifted slightly with respect to the exact values.

The inversion procedure was tested using synthetic data. The synthetic data (qP- and qS-wave traveltimes and qS-wave polarizations) was obtained for a VSP experiment by standard anisotropic ray theory. Noise and noise-free synthetic data were considered. The inversion procedure was performed for homogeneous and layered models.

As homogeneous models with transversely isotropic media with a vertical axis of symmetry which differ in strength of anisotropy (5% and 10% anisotropy) were considered. The inversion of noise-free data showed that the VTI model with 5% anisotropy was inverted with higher accuracy then the the VTI model with 10% anisotropy. The relative mean square deviation (RMSD) of the inverted elastic parameters from the exact ones was less than 1% for the VTI model with 5% anisotropy and less than 2% for the VTI model with 10% anisotropy. In the case of a more complicated triclinic medium the RMSD was 2–3% depending on magnitude of data noise.

Piecewise homogeneous media are common in exploration geophysics. For these models the inversion can be applied in a layer-by-layer manner (recurrently). This recurrent inversion was tested in a model consisting of three layers: The first layer was an anisotropic

medium with orthorombic symmetry (10.6% anisotropy), the second layer was a medium with VSP symmetry (11% anisotropy) and the third layer was an isotropic medium. Synthetic data, qP- and qS-wave traveltimes and qS-wave polarization vectors were generated for a VSP experiment by the ANRAY program package (Gajewski and Pšenčík, 1987). Noisy data were used for the inversion. Errors were introduced in the qP- and qS-wave traveltimes as well as in the qS-wave polarization vectors. First the inversion was performed for all 21 parameters. And for each inverted parameter a confidence interval with a probability coefficient of 99% was constructed. Then, the number of parameters was restricted based upon the significance and accuracy of each parameter. The RMSD of the inverted elastic parameters from the exact parameters were less than 2% for the first orthorombic layer, 1–6% for the second VTI layer, and less then 6% for the third isotropic layer. The value of the traveltime residuals in one sample varied from 1–4 ms. These correspond to errors in picking of traveltimes of the different waves from real data.

The presented inversion procedure can be very useful despite of the fact that it does not reconstruct exact values of the elastic parameters. Because the inversion procedure can be performed fast and has no restrictions on the types of anisotropic symmetry, it can be used to construct initial models for non-linear inversion procedures. A good initial model is quite important for any non-linear inversion.

Appendix

The assumption of weak anisotropy allows to obtain relations between perturbations of the elastic parameters with respect to an isotropic background medium and the corresponding traveltime perturbations. These relations are very useful for inversion goals. However, applying tomographic inversion in weakly anisotropic media for either qP- or qS-wave traveltimes alone allows to determine a limited number of elastic parameters. Only if qP- and qS-wave traveltimes are jointly inverted the full elastic tensor of the weakly anisotropic medium can be determined. In this Appendix I give explicit relations between perturbations of the elastic parameters and and the corresponding traveltime perturbations for qP- and qS-waves.

The weakly anisotropic medium is given here in the compressed Voigt-notation $A_{\alpha\beta}$ for the density normalized tensor a_{iklm} with the usual correspondence: $11 \rightarrow 1$, $22 \rightarrow 2$, $33 \rightarrow 3$, $23 \rightarrow 4$, $13 \rightarrow 5$, $12 \rightarrow 6$:

$$A_{\alpha\beta} = A^{(iso)}_{\alpha\beta} + \Delta A_{\alpha\beta}, \quad \alpha, \beta = 1, \ldots, 6 \quad ,$$

where $A^{(iso)}_{\alpha\beta}$ are the elastic parameters of the isotropic reference medium, and $\Delta A_{\alpha\beta}$ characterize the small deviations from the isotropic background medium.

First, **the general case of anisotropy** is considered. The perturbation formula for qP-waves contains only 15 independent elastic parameters (or combinations of them). Equation (5.29) is analogous to the result from Pšenčík and Gajewski (1998) (their equation 17a). I slightly rewrote it for a better correspondence with the results I obtained for qS-waves (see below equation (5.30)):

$$\begin{aligned}\Delta\tau_{qP} = -\frac{\tau_p}{2v_p^2}\Big[& n_1^4\Delta A_{11} + 2n_1^2n_2^2\epsilon_1 + 2n_1^2n_3^2\epsilon_2 + 4n_1^2n_2n_3\epsilon_3 + 4n_1^3n_3\Delta A_{15} \\ & + 4n_1^3n_2\Delta A_{16} + n_2^4\Delta A_{22} + 2n_2^2n_3^2\epsilon_4 + 4n_2^3n_3\Delta A_{24} + 4n_1n_2^2n_3\epsilon_5 \\ & + 4n_1n_2^3\Delta A_{26} + n_3^4\Delta A_{33} + 4n_2n_3^3\Delta A_{34} + 4n_1n_3^3\Delta A_{35} + 4n_1n_2n_3^2\epsilon_6\Big],\end{aligned} \tag{5.29}$$

where v_p is the P-wave velocity, τ_p is the traveltime of the P-wave and $\mathbf{n}$ is the unit vector tangent to the reference ray in the isotropic background medium; $\Delta\tau_{qP}$ is the traveltime perturbation with respect to the traveltime τ_p caused by the perturbations in the elastic parameters $\Delta A_{\alpha\beta}$. In equation (5.29) the following notations are used:

$$\epsilon_1 = \Delta A_{12} + 2\Delta A_{66}, \quad \epsilon_2 = \Delta A_{13} + 2\Delta A_{55}, \quad \epsilon_3 = \Delta A_{14} + 2\Delta A_{56},$$

$$\epsilon_4 = \Delta A_{23} + 2\Delta A_{44}, \quad \epsilon_5 = \Delta A_{25} + 2\Delta A_{46}, \quad \epsilon_6 = \Delta A_{36} + 2\Delta A_{45}.$$

Thus, the qP-wave traveltime perturbations $\Delta\tau_{qP}$ depends on the nine pure parameters $\Delta A_{\alpha\beta}$ and six combinations of the rest twelve parameters.

Similarly, the perturbation formula for qS-waves depends only on 15 elastic parameters (or combinations of them). Based upon equations (5.11) and (5.12) I obtained the following relations between the qS-wave traveltime perturbations and the perturbation of the elastic

parameters:

$$\begin{aligned}\tau_{qS_M} = -\frac{\tau_s}{2}\Big[&p_2^2 g_2^2\delta_1 + 2p_2g_2p_3g_3\delta_2 + 2p_2g_2(p_2g_3 + p_3g_2)\delta_3 + \\ &+2p_2g_2(p_1g_3 + p_3g_1)\delta_4 + 2p_2g_2(p_1g_2 + p_2g_1)\delta_5 + p_3^2g_3^2\delta_6 + \\ &+2p_3g_3(p_2g_3 + p_3g_2)\delta_7 + 2p_3g_3(p_1g_3 + p_3g_1)\delta_8 + \\ &+2p_3g_3(p_1g_2 + p_2g_1)\delta_9 + (p_2g_3 + p_3g_2)^2\Delta A_{44} + \\ &+2(p_2g_3 + p_3g_2)(p_1g_3 + p_3g_1)\Delta A_{45} + \\ &+2(p_2g_3 + p_3g_2)(p_1g_2 + p_2g_1)\Delta A_{46} + \\ &+2(p_1g_3 + p_3g_1)(p_1g_2 + p_2g_1)\Delta A_{56} + \\ &+(p_1g_3 + p_3g_1)^2\Delta A_{55} + (p_1g_2 + p_2g_1)^2\Delta A_{66}\Big], \quad M = 1, 2.\end{aligned} \tag{5.30}$$

Here, τ_s is the traveltime of the S-wave in the isotropic background medium, $\Delta\tau_{qSM}$ is the traveltime perturbation with respect to the traveltime τ_s caused by the perturbations in the elastic parameters $\Delta A_{\alpha\beta}$, g_i is the i-th component of the polarization vector $\mathbf{g}^{(M)}$ of the qS_M wave, see equation (5.10). For simplicity I omit the index M in the following. In equation (5.30) the following notations are used:

$$\begin{aligned}&\delta_1 = \Delta A_{22} + \Delta A_{11} - 2\Delta A_{12}, \qquad \delta_2 = \Delta A_{23} + \Delta A_{11} - \Delta A_{12} - \Delta A_{13}, \\ &\delta_3 = \Delta A_{24} - \Delta A_{14}, \qquad \delta_4 = \Delta A_{25} - \Delta A_{15}, \qquad \delta_5 = \Delta A_{26} - \Delta A_{16}, \\ &\delta_6 = \Delta A_{33} + \Delta A_{11} - 2\Delta A_{13}, \qquad \delta_7 = \Delta A_{34} - \Delta A_{14}, \\ &\delta_8 = \Delta A_{35} - \Delta A_{15}, \qquad \delta_9 = \Delta A_{36} - \Delta A_{16}.\end{aligned}$$

Thus, the qS-wave traveltime perturbations $\Delta\tau_{qS_M}$ depend on six pure parameters $\Delta A_{\alpha\beta}$ and nine combinations of the rest fifteen parameters.

These results show that for the weakly anisotropic medium only three of the 15 independent parameters are present in the perturbation formula if either qP- or qS-waves are considered alone (i.e., in an inversion only 15 parameters can be recovered if only qP- or qS-waves are considered).

It is easily to see that in the case of **an orthorombic medium** the traveltime perturbation of each wave depends on only the six parameters $\delta A_{\alpha\beta}$ or on their combinations instead of nine ones (i.e., in an inversion only 6 parameters can be recovered if only qP- or qS-waves are considered). Formulae (5.29) and (5.30) take the following form:

$$\Delta\tau_{qP} = -\frac{\tau_p}{2v_p^2}\Big[n_1^4\Delta A_{11} + 2n_1^2n_2^2\epsilon_1 + 2n_1^2n_3^2\epsilon_2 + n_2^4\Delta A_{22} + 2n_2^2n_3^2\epsilon_4 + n_3^4\Delta A_{33}\Big],$$

$$\begin{aligned}\tau_{qS_M} = -\frac{\tau_s}{2}\Big[&p_2^2g_2^2\delta_1 + 2p_2g_2p_3g_3\delta_2 + p_3^2g_3^2\delta_6 + (p_2g_3 + p_3g_2)^2\Delta A_{44} \\ &+(p_1g_3 + p_3g_1)^2\Delta A_{55} + (p_1g_2 + p_2g_1)^2\Delta A_{66}\Big], \quad M = 1, 2,\end{aligned}$$

where the same notations are used as in (5.29) and (5.30).

In the case of **a VTI medium** formulae (5.29) and (5.30) take the following form:

$$\tau_{qP} = -\frac{\tau_p}{2v_p^2}\Big[(n_1^4 + n_2^4)\Delta A_{11} + n_3^4\Delta A_{33} + 2(n_2^2 n_3^2 + n_1^2 n_3^2)(\Delta A_{13} + 2\Delta A_{44})\Big] \quad (5.31)$$

$$\tau_{qS} = -\frac{\tau_s}{2}\Big\{ \left[(p_2 g_3 + p_3 g_2)^2 + (p_1 g_3 + p_3 g_1)^2\right] \Delta A_{44} + \quad (5.32)$$

$$+ p_3^2 g_3^2(\Delta A_{11} + \Delta A_{33} - 2\Delta A_{13}) + (p_1 g_2 + p_2 g_1)^2 \Delta A_{66}\Big\}, \quad M = 1, 2,$$

where τ_p and τ_s are the traveltimes of the P- and S-waves in the isotropic background medium; v_p is the P-wave velocity in the isotropic background; $\Delta\tau_{qP}$ and $\Delta\tau_{qSM}$ are the traveltime perturbations with respect to the corresponding traveltime τ_p or τ_s caused by the perturbations in the VTI elastic parameters. These results show that for the VTI medium only three of the 5 independent parameters are present in the perturbation formula if either qP- or qS-waves are considered alone (i.e., in an inversion only 3 parameters can be recovered if only qP- or qS-waves are considered).

Conclusions

The approximation of weakly anisotropic media which is best suited to seismic anisotropy allows to simplify solutions of modeling and inversion in anisotropic media.

For modeling of wavefields in weakly anisotropic media an QI approach was used. The QI approach is based on the kinematic and dynamic ray-tracing differential equations for an isotropic background medium. The asymptotic solution of the elastodynamic equation is searched as an expansion with respect to two small parameters of the same order: the parameter used in the standard ray method, $1/(i\omega)$, and the parameter ε characterizing the deviation of a weakly anisotropic medium from the isotropic background medium. Expression for the calculation of zeroeth- and additional first-order (0+1A) terms of the QI approximation were derived. The equations are applicable to inhomogeneous media of arbitrary but weak anisotropy. For homogeneous weakly anisotropic media the analytical QI solutions for qP- and qS-waves were obtained. Analysis of these analytical solutions revealed drawbacks of the QI approximation. Particularly, in the singular directions the QI approximation method produces distorted results. But in contrast to the standard anisotropic ray theory, in the QI approach this manifests only in the first-order approximation.

The quality of the QI approach used for the modeling in weakly anisotropic media was investigated. Seismograms for a numerical VSP experiment were computed using the (0+1A) terms of the QI approximation and compared with seismograms obtained by ray tracing and by finite-difference numerical forward modeling. The seismograms obtained by the latter method were considered as exact seismograms. Homogeneous weakly anisotropic media with different types of symmetry (VTI, orthorombic) and strength of anisotropy (5%, 8.3%) were used.

For a qP-wave propagating in a homogeneous weakly anisotropic medium, the QI seismograms were very close to the exact ones. The relative error did not exceed 1–3%. For two qS-waves propagating in a weakly anisotropic medium, the quality of the QI approximation strongly depends on the type and strength of anisotropy. In the regular regions, the deviations between the qS-wave polarization vectors resulting from the zeroeth-order QI approximation and the exact ones varied from 1° to about 10–20°. Note that in singular regions, these deviations can range up to 45°. Taking into account the additional first-order terms slightly improved the QI solution, but introduced an additional problem connected with the singular regions.

To minimize errors which are inherent in any perturbation method the background isotropic medium should be chosen to be as close as possible to the true anisotropic medium, with respect to the physical properties to be investigated. Formulae for the

sectorially best-fitting isotropic reference medium were derived. In contrast to Fedorov's best-fitting isotropic formulae, they allow to construct an isotropic medium which is in close agreement with the anisotropic medium under consideration for a sector (cone) of interest. Applications of the derived formulae were illustrated by examples of media with VTI and orthorombic symmetries. The sectorially best fitting reference medium provides an improved fit in the area of interest compared to Fedorov's original results.

The approximation of weakly anisotropic media allows to simplify solution of inversion problem in anisotropic media. For inversion based on Kirchoff type of migration, the assumption of weak anisotropy was used to develop FD perturbation method for fast and efficient computation of traveltimes. The FD perturbation method for the efficient computation of qP-wave traveltimes in arbitrarily anisotropic media as suggested by Ettrich and Gajewski (1998) was extended to 3-D models. The arbitrary anisotropic media were considered as a perturbed model with respect to a simple isotropic background medium. Traveltimes in the background medium are computed using an FD eikonal solver which allows fast and accurate computation of traveltimes. Traveltimes in the perturbed medium are obtained by adding traveltime corrections to the traveltimes of the background medium using a perturbation approach.

I also propose to use background media with ellipsoidal symmetry in order to compute traveltimes for strongly anisotropic media. An ellipsoidally anisotropic medium approximates a medium of strong anisotropy better than an isotropic one. The corresponding eikonal equation is only slightly more complex than for the isotropic case. The accuracy of the traveltime computations using the different background media was tested. For example, the maximum relative error in an olivine model (anisotropic medium with orthorombic symmetry) with respect to the isotropic background model was 3.9%, but with respect to the ellipsoidally anisotropic background model it was only 1.9%.

To compute traveltimes in heterogeneous anisotropic media using the developed FD perturbation approach, the only condition is that the model has to be smooth. The accuracy of the traveltime computation was tested for a factorized medium. The computed traveltimes were compared with traveltimes obtained by wavefront-oriented ray tracing (considered as an exact method). The main restriction of the FD perturbation method lies in the fact that it is based on finite-difference solution of the eikonal equation and, thus, can be used for calculations of first arrivals.

For inversion based on ray tomography the approximation of weakly anisotropic media is used to obtain the linear relations between the elastic parameters and the traveltimes of waves. The relations are inherently linear for qP-waves and can be linearized for qS-waves using qS-wave polarization vectors which are available from a seismic experiment as well as the traveltimes. As the result, the same linear inversion scheme for qP- as well as for qS-wave data can be used. Applying tomographic inversion in weakly anisotropic media for either qP- or qS-wave traveltimes alone allows to determine a limited number of elastic parameters, and only the joint inversion of qP- and qS-waves allows to determine the full elastic tensor.

Although the observed qS-wave polarizations are available from three component data, picking qS-wave polarization vectors from real data can be a challenging task. However, to obtain traveltimes, the two qS-waves need to be separated in any case. For this separation

the difference in qS-wave polarizations is used (see, e.g., Alford, 1986; Li and Crampin, 1993; Dellinger et al., 1998). Therefore, the qS-wave polarization vectors are automatically obtained as a by-product of the qS-wave separation.

The advantage of the presented inversion procedure is that no assumption about any special type of anisotropic symmetry is needed. If there is no a priori information on the type of anisotropy, all 21 elastic parameters can be inverted. Then, analysis of the 21 inverted elastic parameters can be carried out. Based upon the significance and accuracy of each parameter, we can restrict the inversion to a smaller number of the elastic parameters and determine the symmetry of the medium under consideration. In all examples the following strategy was used. First, all 21 elastic parameters were inverted. Then, the inversion for 9, 5 or 2 different elastic parameters depending on the symmetry of the medium was performed.

The main restriction of the suggested inversion procedure is that it is based on perturbation theory which provides a smooth transition from isotropic media to anisotropic media by small perturbations of the elastic parameters. Therefore, the accuracy of the traveltime computations in the forward modeling problem and, as a result, the quality of the inversion directly depend on the assumption of weak anisotropy. This means that the inversion procedure allows to reconstruct the elastic parameters only if the anisotropic medium is weakly anisotropic. According to the examples presented in this study, for the medium with more then 5% anisotropy, the inversion does not reconstruct the elastic parameters, but only gives estimates of these elastic parameters even when noise-free data are used. The following situation may occur. Some well-resolved estimates are found to be slightly shifted with respect to the exact values and the corresponding confidence intervals do not cover the the exact values. This happens due to the errors of traveltime computations in the forward modeling. However, the presented inversion procedure can be very useful despite of the fact it does not reconstruct exact values of the elastic parameters. Because the inversion procedure can be performed fast and has no restrictions on the types of anisotropic symmetry, it can be used to construct initial models for non-linear inversion procedures. A good initial model is quite important for any non-linear inversion.

The quality of the inversion procedure was tested using synthetic data. The synthetic data (qP- and qS-wave traveltimes and qS-wave polarizations) was obtained for a VSP experiment by standard anisotropic ray theory. Noise and noise-free synthetic data were considered. The inversion procedure was performed for homogeneous and layered models.

As homogeneous models transversely isotropic media with a vertical axis of symmetry which differ in strength of anisotropy (5% and 10% anisotropy) were considered. The relative mean square deviation (RMSD) of the inverted elastic parameters from the exact ones was less than 1% for the VTI model with 5% anisotropy and less than 2% for the VTI model with 10% anisotropy. In the case of the more complicated triclinic medium the RMSD was 2–3% depending on the magnitude of noise in the data.

Piecewise homogeneous media are common in exploration geophysics. For these models the inversion can be applied in a layer-by-layer manner (recurrently). This recurrent inversion was tested in a model consisting of three layers. For each layer first the inversion was performed for all 21 parameters. Then, the number of parameters was restricted according to the significance and accuracy of each parameter. The RMSD of the inverted

elastic parameters from the exact parameters were less then 2% for the first orthorombic layer, 1–6% for the second VTI layer, and less then 6% for the third isotropic layer. The value of the traveltime residuals varied from 1–4 ms. These correspond to errors in picking of traveltimes of the different waves from real data.

Bibliography

Alford, R. M. (1986). Shear data in the presence of azimuthal anisotropy. In *Expanded Abstracts*, page S9.6. Soc. Expl. Geophys.

Babuska, V., , and Cara, M. (1991). Seismic anisotropy in the earth. *Modern Approaches in Geophysics*, 10.

Burridge, R., Chadwick, P., and Norric, A. N. (1993). Fundamental elastodynamic solutions for anisotropic media with ellipsoidal slowness surfaces. *Proceedings of the Royal Socity London A*, 440:655–1681.

Červený, V. (1972). Seismic rays and ray intensities in inhomogeneous anisotropic media. *Geophys. J. R astr. Soc.*, 29:1–13.

Červený, V. (1982). Direct and inverse kinematic problems for inhomogeneous anisotropic media – a linearization approach. *Contr. Geophys. Inst. Sov. Acad. Sci.*, 13:127–133.

Červený, V. (1989). Ray tracing in factorized anisotropic inhomogeneous media. *Geophys. J. Int*, 99:91–100.

Červený, V. (2001). *Seismic ray theory*. Cambridge University Press.

Červený, V. and Jech, J. (1982). Linearized solutions of kinematic problems of seismic body waves in inhomogeneous slightly anisotropic media. *Geophys. J. Int*, 51:96–104.

Červený, V. and Simões-Filho, I. A. (1991). The traveltime perturbations for seismic body waves in factorized anisotropic inhomogeneous media. *Geophys. J. Int*, 107:219–229.

Chapman, C. H. and Pratt, R. G. (1992). Traveltime tomography in anisotropic media — I. Theory. *Geophys. J. Int*, 109:1–19.

Cliet, C., Brodov, L., Tikhonov, A., Marin, D., and Michon, D. (1991). Anisotropy survey for reservoir definition. *Geophys. J. Int*, 107:417–427.

Coates, R. T. and Chapman, C. H. (1990). Quasi-shear wave coupling in weakly anisotropic 3-D media. *Geophys. J. Int*, 103:301–310.

Dellinger, J. (1991). Anisotropic finite-difference traveltimes. In *Expanded Abstracts, 61st Annual International Meeting SEG,November 10–14, Houston, Texas*, pages 1530–1533. Soc. Expl. Geophys.

Dellinger, J., Nolte, B., and Etgen, J. (1998). Symmetric Alford diagonalization. In *Expanded Abstracts*, pages 1673–1676. Soc. Expl. Geophys.

Eaton, D. W. S. (1993). Finite difference traveltime calculation for anisotropic media. *Geophysical Journal International*, 114:273–280.

Eisner, L. and Pšenčík, I. (1996). Computation of additional components of the first-order ray approximation in isotropic media. *PAGEOPH*, 148:227—253.

Ettrich, N. (1998). FD eikonal solver for 3-d anisotropic media. In *Expanded Abstracts, 68th Ann. Int. Mtg. SEG*, pages 1957–1960.

Ettrich, N. and Gajewski, D. (1998). Traveltime computation by perturbation with FD-eikonal solvers in isotropic and weakly anisotropic media. *Geophysics*, 63:1066–1078.

Ettrich, N., Gajewski, D., and Kashtan, B. (2001). Reference ellipsoids for anisotropic media. *Geophys. Pros.*, 49:321–334.

Farra, V. (2001). High-order perturbations of the phase velocity and polarization of *qp* and *qs*waves in anisotropic media. *Geophys. J. Int.*, 147:93–104.

Farra, V. and Le Bégat, S. (1995). Sensitivity of qP-wave traveltimes and polarization vectors to heterogeneity, anisotropy and interfaces. *Geophys. J. Int.*, 121:371–384.

Fedorov, F. I. (1968). *Theory of elastic waves in crystals*. Plenum Press, New York.

Gajewski, D. (1993). Radiation from point sources in general anisotropic media. *Geophys. J. Int.*, 113:299–317.

Gajewski, D. and Pšenčík, I. (1987). Computation of hight-frequency seismic wavefields in 3-D laterally inhomogeneous anisotropic media. *Geophys. J. R. astr. Soc.*, 91:383–411.

Gajewski, D. and Pšenčík, I. (1990). Vertical seismic profile synthetics by dynamic tracing in laterally varying layered anisotropic structures. *J.Geophys.Res.*, 95:11301–11315.

Grechka, V., Theophanis, S., and Tsvankin, I. (1999). Joint inversion of P- and PS-waves in orthorombic media: Theory and a physical modeling study. *Geophysics*, 64:146–161.

Hanyga, A. (1982). The kinematic inverse problem for weakly laterally inhomogeneous anisotropic media. *Tectonophysics*, 90:253–262.

Helbig, K. (1994). *Foundations of anisotropy for exploration seismic*. Pergamon.

Horne, S. and Leaney, S. (2000). Short note: Polarization and slowness component inversion for TI anisotropy. *Geophysical Prospecting*, 48:779–788.

Horne, S. and MacBeth, C. (1994). Inversion for seismic anisotropy using genetic algorithms. *Geophysical Prospecting*, 42:953–974.

Jech, J. and Pšenčík, I. (1989). First-order perturbation method for anisotropic media. *Geophys. J. Int*, 99:369–376.

Jech, J. and Pšenčík, I. (1992). Kinematic inversion for qP and qS waves in inhomogeneous hexagonally symmetric structures. *Geophys. J. Int*, 108:604–612.

Kaschwich, T. and Gajewski, D. (2003). Wavefront-oriented ray tracing in 3d anisotropic media. In *Expanded Abstracts, EAGE 65th Conference & Technical Exhibition — Stavanger, Norway, 2 - 5 June 2003*, page P041. EAGE.

Kosloff, D. and Baysal, E. (1982). Forward modeling by a Fourier method. *Geophysics*, 47:1402–1412.

Kravtsov, Y. A. (1968). Quasiisotropic approximation to geometrical optics. *Dokl. AN SSSR*, 183:1,74–77, (in Russian).

Kucher, V. I. and Kashtan, B. M. (1999). *Ray method for isotropic inhomogeneous elastic medium*. St-Petersburg University (in Russian).

Le Bégat, S. and Farra, V. (1997). *P*-wave traveltime and polarization tomography of VSP data. *Geophys. J. Int.*, 131:100–114.

Lecomte, I. (1993). Finite difference calculation of first traveltimes in anisotropic media. *Geophys. J. Int*, 113:318–342.

Li, X. Y. and Crampin, S. (1993). Linear-transform techniques for processing shear-wave anisotropy in four-component seismic date. *Geophysics*, 58:240–256.

Linnik, Y. V. (1961). *Method of least squares and principles of the theory of observations*. Pergamon Press.

Mallick, S. and Frazer, L. N. (1990). Computation of synthetic seismograms for stratified azimuthally anisotropic media. *J. Geophys. Res.*, 86:359–377.

Van Trier, J. and Symes, W. W. (1991). Upwind finite-difference calculation of traveltimes. *Geophysics*, 56:812–821.

Menke, W. (1984). *Geophysical data analysis: discrete inverse theory*. Academic Press, Inc.

Mensch, T. and Farra, V. (1999). Computation of qP-wave rays, traveltimes and slowness vectors in orthorombic media. *Geophysical Journal International*, 138:244–256.

Mensch, T. and Rasolofosaon, P. (1997). Elastic-wave velocities in anisotropic media of arbitrary symmetry — generalization of thomsen's parameters ε, δ and γ. *Geophysical Journal International*, 128:43–64.

Petrashen, I. G., Kashtan, B. M., and Kovtun, A. A. (1984). *Propagation of body waves and methods for wave field calculations in anisotropic elastic media*. Leningrad, Nauka (in Russian).

Podvin, P. and Lecomte, I. (1991). Finite difference computation of traveltimes in very contrasted velocity model: a massively parallel approach and its associated tools. *Geophys. J. Int*, 105:271–284.

Popov, M. M. and Pšenčík, I. (1978). Computation of ray amplitudes in laterally inhomogeneous media with curved interfaces. *Studia Geoph. et Geod.*, 22:248–258.

Pratt, R. G. and Chapman, C. H. (1992). Traveltime tomography in anisotropic media — II. Application. *Geophys. J. Int*, 109:20–37.

Pšenčík, I. (1998). Green's functions for inhomogeneous weakly anisotropic media. *Geophys. J. Int*, 135:279–288.

Pšenčík, I. and Dellinger, J. A. (2001). Quasi-shear waves in inhomogeneous weakly anisotropic media by the quasi-isotropic approach: A model study. *Geophysics*, 66:308–319.

Pšenčík, I. and Gajewski, D. (1998). Polarization, phase velocity, and NMO velocity of qP-waves in arbitrary weakly anisotropic media. *Geophysics*, 63:1754–1766.

Qin, F., Luo, Y., Olsen, K. B., Cai, W., and Schuster, G. T. (1992). Finite-difference solution of the eikonal equation along expanding wavefronts. *Geophysics*, 57:478–487.

Shearer, P. M. and Chapman, C. H. (1988). Ray tracing in anisotropic media with a linear gradient. *Geophys. J.*, 94:575–580.

Soukina, S. M., Gajewski, D., and Kashtan, B. M. (2003). Traveltime computation for 3D anisotropic media by a finite-difference perturbation method. *Geophysical Prospecting*, 51:431–441.

Tessmer, E. (1995). 3-D seismic modelling of general material anisotropy in the presence of the free surface by a chebyshev spectral method. *Geophys. J. Int*, 121:557–575.

Thomsen, L. (1986). Weak elastic anisotropy. *Geophysics*, 51:1954–1966.

Thomsen, L. (2002). *Understanding Seismic Anisotropy in Exploration and Exploitation.* Distinguished Instructor Series N5, SEG/EAGE.

Tsvankin, I. (1997). Anisotropic parameters and P-wave velocity for orthorombic media. *Geophysics*, 62:1292–1309.

Versteeg, R. J. (1993). Sensitivity of prestack depth migration to the velocity model. *Geophysics*, 58:873–882.

Vidale, J. E. (1988). Finite-difference calculation of traveltimes. *Bull. Seis. Soc. Am.*, 78:6, 2062–2076.

Vidale, J. E. (1990). Finite-difference calculation of traveltimes in three dimensions. *Geophysics*, 55:521–526.

Williamson, P. R. (1993). Anisotropic crosshole tomography in layered media. Part II: applications, results and conclusions. *Jrnl.Seismic Explor.*, 2:223–238.

Zillmer, M., Kashtan, B. M., and Gajewski, D. (1998). Quasi-isotropic approximation of ray theory for anisotropic media. *Geophys. J. Int.*, 132:643–653.

Acknowledgements

I wish to thank Prof. Dr. **Dirk Gajewski** and Prof. Dr. **Boris M. Kashtan** as the supervisors of my work. I appreciated their help in development the ideas presented in my thesis.

I enjoyed doing my research work in the Applied Geophysics Group at the University of Hamburg. I particularly thank to **Radu Comman**, **Manfred Elive Menyoli** and **Tina Kaschwich** for their companionship and their support. I would say many thanks to **Claudia Vanelle** for her help to eliminate the major mistakes in the text on my thesis due to my poor knowledge of the English language. I would like to thank **Ekkehart Tessmer** for permission to use his program for numerical forward modeling in anisotropic media.

I thank to **Ivan Pšenčík** for the computation of synthetic data used for inversion in my work. His helpful comments about the QI approximation are gratefully acknowledged.

This work was kindly supported the German Science Foundation,the German Israeli Foundation and the sponsors of the WIT-Consortium.

CURRICULUM VITAE

1989–1995	Undergraduate student at the St-Petersburg State University, Russia, Faculty of Physic, Department of Earth Physics.
February 1995	Diploma (Topic of Diploma: Calculation of interfering elastic waves for models with a high velocity layer)
1995–1998	Research scientist in the Institute of Physics, St-Petersburg State University, Russia (Topic: Calculation of wave-fields for models with non-weld contact conditions on interfaces)
December 1998– –April 1999	Geophysicist in "SEVMORGEO", St-Petersburg, Russia (Topic: Inversion of first arrivals of P- and S-waves using tomography and kinematic modeling package FIRSTOMO)
August 1999– –June 2004	PhD student at the University of Hamburg, Institute for Geophysics, Hamburg, Germany. I worked on the two projects: "Depth Domain Seismic Imaging and Material Parameter Estimation for Anisotropic Media" (GIF98) and "Migration and Tomography in 3D anisotropic media" (GA 350/11-1)
April 2004	PhD (Topic of Dissertation: Modeling and inversion in weakly anisotropic media)